Examining coral reef ecosystem dynamics using microorganisms and metabolites

by

Cynthia Carroll Becker

B.S. and B.A., Ithaca College, 2017

Submitted to the Department of Earth, Atmospheric, and Planetary Sciences in partial fulfillment of the requirements for the degree of

Doctor of Philosophy

at the

MASSACHUSETTS INSTITUTE OF TECHNOLOGY

and the

WOODS HOLE OCEANOGRAPHIC INSTITUTION

June 2023

Authored by: Cynthia C. Becker
Joint Program in Oceanography/Applied Ocean Science and Engineering
Massachusetts Institute of Technology
and Woods Hole Oceanographic Institution
May 3, 2023

Certified by: Dr. Amy Apprill
Department of Marine Chemistry & Geochemistry
Woods Hole Oceanographic Institution
Thesis Supervisor

Accepted by: Dr. Jesús Pineda
Chair, Joint Committee for Biological Oceanography
Massachusetts Institute of Technology/
Woods Hole Oceanographic Institution

Examining coral reef ecosystem dynamics using microorganisms and metabolites

by

Cynthia Carroll Becker

Submitted to the MIT Department of Earth, Atmospheric, and Planetary Sciences on May 5, 2023 in partial fulfillment of the requirements for the degree of Doctor of Philosophy in Biological Oceanography

ABSTRACT

Microorganisms and metabolites are foundational to the success and productivity of biodiverse and economically important coral reef ecosystems and are also tightly connected. Metabolites are small organic compounds produced by reef organisms and are the chemical currencies exchanged by unicellular microorganisms (bacteria and archaea) within the seawater. Although central to reef biogeochemical cycling, we still lack fundamental information on the dynamics of these components of reefs. In this dissertation, I analyzed microorganisms in Caribbean coral reef habitats over temporal, spatial and reef health gradients as well as metabolites in a spatial reef study. In Chapter 2, I applied a rapid sequencing methodology to corals afflicted with the lethal stony coral tissue loss disease and identified specific microorganisms which were biological indicators of the disease. In Chapter 3, I investigated the dynamics of microorganisms over short temporal tidal and diurnal cycles, as well as spatially across US Virgin Island (USVI) coastal habitats. In these habitats, I found tidal cycles were driving changes in microbial communities within mangroves, but diurnal patterns were more important in reef habitats. In Chapter 4, I examined reefs over a longer temporal scale by contributing to the building of a 7-year time-series of USVI reef ecology and found that reef water microorganisms were predictive of hurricane and stony coral tissue loss disease impacts. Finally, in Chapter 5, I combined analyses of untargeted and targeted metabolomics, microbial taxa, and functional genes from metagenomics across 300 km of reefs in Florida, in addition to microorganisms in healthy and diseased corals. With this unprecedented combination of ‘omics datasets, I found that biogeographic zones, environmental features, and underlying habitat characteristics were related to microbial and metabolite features in the reef ecosystem. Further, I identified microorganisms and metabolites which were characteristic of specific reef biogeographic zones. Collectively, my work advances our understanding into the dynamics of microorganisms and metabolites in biodiverse coral reef habitats across natural temporal and spatial gradients and in the face of unprecedented stress and disturbance.

Thesis supervisor: Dr. Amy Apprill
Title: Associate Scientist
Woods Hole Oceanographic Institution

ACKNOWLEDGEMENTS

The work in this dissertation and my graduate training were supported by numerous granting agencies and by the Academic Programs Office at the Woods Hole Oceanographic Institution (WHOI). This research was funded by The Tiffany & Co. Foundation, the Rockefeller Philanthropy Advisors, Dalio Foundation (now "OceanX"), and the Andrew W. Mellon Foundation Endowed Fund for Innovative Research to Amy Apprill. The National Science Foundation funded the research through awards NSF OCE-1928753 to Marilyn Brandt and Tyler Smith, OCE-1536782 to T. Aran Mooney, Joel K. Llopiz, and Amy Apprill, and OCE-1928761, OCE-1938147 and OCE-1736288 to Amy Apprill. This was also funded by NOAA OAR Cooperative Institutes award NA19OAR4320074 to Amy Apprill and Elizabeth Kujawinski, and an Ocean Ventures Fund grant through WHOI to me.

I'd first like to thank my advisor, Amy Apprill. I came to her lab through the Semester at WHOI program and I was immediately hooked. I got to dive right into new analyses, and she even took me on a research expedition to St. John, which has been a part of my research ever since. After that first Fall, I came back for a summer, and then came back full time for my graduate work. Through all of this, Amy has been an excellent advisor. From guiding me in planning field expeditions, to chatting about complex data, to the fun stuff like leaving our 8-hour experiment to go get some drinks and ice cream in Cruz Bay, she has been there. Her determination, level-headedness, and her compassion for her students and lab make her a remarkable person and someone I will look up to long after my graduate work is over.

I'd also like to thank my committee: Harriet Alexander, Tami Lieberman, and Stefan Sievert. Their time and thoughtfulness with respect to my data and projects has made me a better scientist. In addition to my committee, I have been lucky to go into the field with numerous other scientists including Aran Mooney, Joel Llopiz, Marilyn Brandt, Colleen Hansel, and Yogi Girdhar. Working with other scientists and collaborating both on data analysis and field expeditions has been a highlight of my time in graduate school.

The Academic Programs Office (APO) at WHOI deserves a special thank you. Without them and the undergraduate programs they help administer, I wouldn't be here. As an undergrad with no marine science program at her school, I squeezed every ounce of experience I could out of WHOI, participating in the Semester at WHOI, Summer Student Fellowship, and the Guest Student programs. I especially must thank Kama Thieler and Julia Westwater, who always put a smile on my face and made me feel welcome. As a JP Rep during my time as a graduate student, I loved getting to know Kris Kipp, Lea Fraser, and Tricia Nesti, who do so much to make our lives as graduate students better.

I especially thank Mark Hahn, John Stegeman, Diana Franks and all the people in their labs. I first came to WHOI as a Summer Student Fellow and their kind guidance and support helped me get where I am today.

The Apprill Lab is one spectacular group, and I am so thankful to have joined the lab. Firstly, Laura Gray was the first person I met in the lab, and she has been a positive force and unwavering friend to me ever since. From being the best field buddy and singing along to Disney tunes to solving problems that take us Uber-ing all over Miami, I couldn't imagine a better person guiding me when I was a new graduate student. Thank you to Carolyn Miller

whose skill and experience in the lab makes her the “go-to” for all things lab problem solving. And thank you to the countless other Apprill lab members for enriching my life and fostering a culture of support and amazing science.

Field work was central to my PhD and I cherish the long sun-filled days diving, filtering water, and forming friendships with the lovely people I got to work with. Nadège Aoki, Kalina Grabb, Naomi Huntley, Alexis Earl, Jessica Dehn, Justin Suca, Ian Jones, and countless others I am sure I am forgetting, as well as the crews and other scientists aboard vessels like the R/V Walton Smith and M/V Alucia and at the Virgin Islands Environmental Resource Station made this research possible. I also want to send a special shout out to Ed O’brien and Kim Malkoski at the WHOI Dive Office for their patient and supportive training to make me a great scientific diver.

I want to thank my friends at WHOI and beyond for supporting me through graduate school. My Woods Hole friends: Jordan Pitt, Sarah Weiss, Rachel Kahn, Katie Halloran (and Hatch), Bethany Fowler, Nadège Aoki, and Kalina Grabb – you all have enriched my life and I have cherished the times we spent together whether it was walking, camping, going to concerts, or just hanging out. To my music friends, especially Melanie Hayn and Ali Armitage, thank you for our trios and wine and cheese nights. To my college friends: Carrie Lindeman and Cailin Harro, thank you for sending supportive thoughts and texts whenever I needed them throughout my PhD.

To my loving parents, Chris Becker and Juliet Carroll, I love you both so much. I was privileged to grow up with two PhD-parents who were unwaveringly supportive. The excitement and wonder they fostered in me for the natural world and our regular family trips to Swans Island, Maine, are the reasons I am pursuing my PhD in marine science today. To my siblings, Eric Becker and my twin sister, Vivian Becker, I love you both and am so lucky to have you. Words cannot describe what you mean to me.

Finally, to Eric Eichelberger, my soon-to-be husband. The last five years of my life that I have been in graduate school have been the best years of my life because I have had you by my side. From our Covid lockdown time together cooking innumerable cookies and other baked goods, to taking camping trips with our dog, Monty, you make my life whole, and I am so excited for our future together.

I’d like to dedicate my thesis to my grandmother, Fairlee Winfield, who showed me early on what it was to be a strong independent woman, encouraged me to explore, and who received a PhD at a time when it was still rare for women to pursue that path.

Table of Contents

List of Figures

List of Tables

Chapter 1 - Introduction

Coral reefs are one of the most biodiverse ecosystems on the planet, often being referred to as "rainforests of the sea". Estimates of global biodiversity of coral reefs are around 9 million species, but these are likely underestimates due to the challenges of capturing cryptic species, time-consuming collections, and challenges with identifications requiring highly-specialized taxonomists (Reaka-Kudla, 1997; Small *et al.*, 1998; Plaisance *et al.*, 2011). Additionally, these biodiversity estimates are almost entirely focused on visible macroorganisms, and overlook the numerically abundant prokaryotes, viruses, and fungi in reef habitats. Besides the striking biodiversity, humans rely on coral reefs. Coral reefs are highly valuable for recreational activities (Brander *et al.*, 2007). Nearshore fisheries in coral reef environments supply food to millions of people worldwide and these fisheries can be highly valuable. In Hawai'i alone, the nearshore coral reef fishery is valued between $10.3-$16.4 million (Grafeld *et al.*, 2017). Coral reefs protect shorelines from storm surge and sea level rise, and the United States saves approximately $1.8 billion annually that would be spent on economic losses due to flooding (Reguero *et al.*, 2021). Human health also benefits from coral reef biodiversity in the form of compounds used in medical applications (reviewed by Bruckner, 2002).

The high biodiversity of coral reefs is perhaps more astonishing considering it is sustained in seemingly nutrient-poor and pristine seawater environments; an observation made over one hundred years ago and termed "Darwin's Paradox." While the seawater may look like a nutrient desert, reef habitats are locations of intense nutrient recycling (Duarte and Cebrián, 1996). A keystone organism and the namesake of coral reefs, Scleractinia, also called "hard" or "stony" corals, harbor symbiotic photosynthetic microalgae, *Symbiodiniaceae,* that live within coral tissues and fix carbon and contribute to coral growth and overall reef accretion (Tremblay *et al.*, 2012). Any photosynthate left over from primary production within the coral host and other algal reef organisms are exuded into the water column, where it is either quickly incorporated into biomass for higher trophic levels or remineralized into nutrients that are required for growth of reef organisms (reviewed by Nelson *et al.*, 2023). This nutrient and organic matter recycling both sustains the high biodiversity of reefs while also maintaining the classic low-nutrient reef regime.

Microorganisms are the central machines driving remineralization and transfer of organic matter to higher trophic levels within reef ecosystems. With every reef "macroorganism", there are multitudes of microorganisms that make a home out of that animal, in a way creating numerous "nested ecosystems" (Pita *et al.*, 2018). Even within the pristine blue seawater that flushes over the reef crest, there are approximately 750,000 bacterial and archaeal cells within every milliliter, making them one of the most numerous organisms in reef habitats (Chapter 5). In this dissertation, I will pull back the curtain and take a glimpse into the dynamic world of microorganisms that thrive in coral reefs. Bacteria have been visible with microscopy in the ocean for decades (ZoBell, 1946), but it is only in the last few decades with the use of modern molecular methods that knowledge about these reef microorganisms has emerged.

Even smaller than the tiniest microorganisms on a reef are the organic metabolic byproducts of the diverse living beings that make up coral reefs: metabolites. These small dissolved organic molecules are abundant in reef waters, but have only recently gained attention with the advancement in 'omics technologies that can probe and detect thousands of such chemicals at once. Even with limited studies, it is clear these are important in reef habitats. They are the currency that the microorganisms use, consume, and produce on reefs and in the ocean more broadly (Kujawinski, 2011). On reefs, they play a critical role as signaling molecules between animals for settlement, the process in which motile larvae such as coral attach to and transition to a sessile stage, or organisms such as fish identify a suitable habitat and remain there for life (Sweatman, 1988; Sneed *et al.*, 2014). Chemical cues on reefs are also important for communication (Buchinger *et al.*, 2014).

While the vibrant and diverse invisible world of chemicals and microbes within coral reefs is just beginning to be revealed, coral reefs are already declining worldwide. Decades of anthropogenic climate change is increasing the temperature of seawater worldwide. Scleractinian corals, which already live at the upper limit of their thermal range, are bleaching, or expelling their symbiotic algae they rely on for survival, at intervals and severity that is unprecedented (Hughes *et al.*, 2018). Additionally, the threat of overfishing and increasing severity of hurricanes compound these impacts. Even natural disturbances, such as coral

disease, can have devastating impacts. Within the Caribbean, there is an outbreak of stony coral tissue loss disease that is likely the most lethal disease in recorded history (Alvarez-Filip *et al.*, 2022). While coral reefs have been around for millennia, in recent history 50% of the world's reefs have been lost (Eddy *et al.*, 2021). Some estimates even suggest that coral reefs may die off within 100 years if we do not take action (Ainsworth *et al.*, 2016).

While the amount of coral might be declining on reefs, there are innumerable other components to the reef habitat that might hold the keys to reef survival. Microorganisms and chemicals within a reef are one massive group of keys that must be examined to understand how they may unlock new insights into reef health. In the following sections, I will introduce coral reef microorganisms and metabolites, and emphasize how they relate to the reef habitat. Additionally, I will introduce the stony coral tissue loss disease epidemic of the Caribbean as a case study to demonstrate how probing these components of a reef can unlock insights to reef health. Finally, I will summarize how reef "'omics" may further inform reef ecosystem functions and provide an overview of the following dissertation. While coral reefs are well-established as one of the most biodiverse ecosystems, as new methodological techniques become available, we can probe even deeper into just how diverse and unique these charismatic systems truly are.

Coral reef exometabolites: the currency of benthic-pelagic coupling

The seawater habitat is host to innumerable dissolved, organic, extracellular metabolites, or "exometabolites". These metabolites are dissolved organic molecules that are in part exuded by benthic and pelagic fauna on a reef. In considering benthic organisms, hard corals, soft corals, macroalgae, sponges, and other organisms all produce species-specific collections of metabolites. Hard corals, the organisms responsible for coral reef structure, host endosymbiotic photosynthetic algae that fix carbon and translocate approximately 60% of it to the coral host, which uses it for metabolism (Tremblay *et al.*, 2012). Excess organic matter is then released into the surrounding water column as dissolved or particulate (mucus) matter enriched in compounds such as riboflavin and pantothenic acid (Weber *et al.*, 2022), as well as diverse nitrogen and phosphorus compounds (Wegley Kelly *et al.*, 2022a).

Soft corals, or octocorals, are similar to hard corals in that they harbor symbiotic algae, but these organisms are considered mixotrophs, and are more dependent on heterotrophy to supplement their nutrition needs than hard corals (Fabricius and Klumpp, 1995). These soft corals release organic matter of a lower C:N ratio than hard corals (Nakajima *et al.*, 2018). Soft corals release these nitrogen-rich compounds, such as indole-3-acetic acid, inosine, tryptophan, 4-hydroxybenzoic acid, and malic acid (Weber *et al.*, 2022), shifting the pool of exometabolites present in the seawater. Sponges filter huge amounts of water daily, "exhaling" seawater enriched in nucleosides (Fiore *et al.*, 2017). As coral reefs undergo shifts in composition from hard coral dominated to increasing dominance of octocorals and sponges in the Caribbean (Norström *et al.*, 2009; Tsounis and Edmunds, 2017), it is likely that this exometabolite pool in reef seawater will also shift to favor metabolites released by soft corals.

Beyond changes in coral and sponge cover, Caribbean reefs have historically undergone coral-algal phase shifts (e.g. Bruno *et al.*, 2009). This algal cover includes fleshy macroalgae, turf algae, cyanobacterial mats, as well as other encrusting algae like crustose coralline algae. Algae are photosynthetic organisms on reefs that generally exude more labile organic matter than corals (Haas *et al.*, 2011). These exudates are further enriched in sugars such as fucose and galactose, nonnitrogenous compounds, and alkaloids, which are distinct from coral exudates (Nelson *et al.*, 2013; Wegley Kelly *et al.*, 2022a). The encrusting alga, *Ramicrusta textilis,* an invasive algal crust invading Caribbean reefs, exudes a distinct suite of compounds, including the herbivory and pathogen deterrent, caffeine, which may be linked to its success (Edmunds *et al.*, 2019; Weber *et al.*, 2022). As algal crusts, turf algae, and macroalgae continue to dominate reefs, continued investigations into the diverse dissolved organic metabolite pool will offer insight into the mechanisms of algal phase-shifts on reefs.

The collective release of organic compounds from benthic organisms into the surrounding water column is one part of "benthic-pelagic coupling", in which the benthic habitat directly influences the seawater environment that surrounds it. Experimental incubations show the distinct effect that this benthic release of organic matter has on the seawater-bound microbial community. When bulk reef seawater microorganisms are incubated with pools of metabolites exuded from hard corals, the community of bacteria that respond is

distinctly different than when metabolites of soft coral and algae are used (Haas *et al.*, 2011; Nelson *et al.*, 2013; Nakajima *et al.*, 2018; Weber *et al.*, 2022). Soft coral exudates seem to favor growth of heterotrophic bacteria, which were inhibited by hard coral exudates (Weber *et al.*, 2022). Algal exudates favor copiotrophic bacterial lineages, which grow in response to the higher amounts of DOC released compared to hard corals (Nelson *et al.*, 2013). These studies show the direct link between benthic organisms and the pelagic-bound microorganisms within coral reefs, and how shifting baselines in dominant reef fauna may influence such communities.

Reef microorganisms are critical to a functioning reef

Seawater microorganisms: Within 1 milliliter of seawater there can be upwards of 1 million microbial cells, and orders of magnitude more when viruses are counted. These microorganisms include single celled eukaryotic algae, fungi, bacteria, archaea, and viruses. Bacteria and archaea in coral reefs have been studied for decades (ZoBell, 1946), in particular since the recognition of the importance of microorganisms in the "microbial loop" (Azam *et al.*, 1983). Functionally, bacteria and archaea are significant primary producers and consumers of organic matter in marine ecosystems, including coral reefs (Sorokin, 1973; Pomeroy, 1974; Chisholm *et al.*, 1988). As described earlier, seawater microorganisms consume benthic-derived organic matter, but this is not unidirectional. The specific lineages of seawater microorganisms that grow on coral exudates are a food source for corals (Sorokin, 1973; McNally *et al.*, 2017). Microbiome analyses on reef seawater over the past 20-30 years have begun to apply names to the massive group of bacteria and archaea in reef habitats. Common seawater-based groups found in reef habitats include the picocyanobacteria, *Prochlorococcus* and *Synechococcus,* SAR11 and SAR116 clades of Alphaproteobacteria, Bacteroidetes, and Marine Group II Archaea (Apprill *et al.*, 2015; Becker *et al.*, 2020). In nearshore and benthic reef habitats, the seawater is enriched in Rhodobacteraceae, Sphingomonadaceae, Flavobacteriaceae, and Alteromonadaceae families. These seawater bound microorganisms recycle energy within the reef, maintaining highly productive environments, but as coral reef ecosystems change, the microbial community shifts in response (Vanwonterghem and Webster, 2020).

As central members in recycling organic matter in reefs, the microbial community is highly responsive to natural gradients in reef habitats. Commonly, studies have related the seawater microbial community to reef-wide changes, demonstrating the coordinated changes of reef microbes in response to coral cover (Glasl *et al.*, 2019; Apprill *et al.*, 2021), temperature and chlorophyll (Glasl *et al.*, 2019), organic carbon and disease (Laas *et al.*, 2021), overall biogeography (Apprill *et al.*, 2021; Ma *et al.*, 2022a), and disturbances associated with storm events (Yeo *et al.*, 2013). Reefs that are less protected harbor fewer picocyanobacteria, and generally lower species richness compared to reefs that are highly protected and of higher quality (Weber, González-Díaz, *et al.*, 2020). Additionally, as phase-shifts to increasingly algal-dominated reefs occur worldwide, reefs are hypothesized to show "microbialization" (Haas *et al.*, 2016). The microbialization hypothesis is the DDAM model (Dissolved organic carbon, disease, algae, microorganism), in which algal dominance produces higher amounts of dissolved organic carbon, which promotes the growth of potentially pathogenic, copiotrophic microorganisms, reinforcing coral disease, and reinforcing further growth of algae on reefs, creating a positive feedback to increasing organic carbon in the seawater (Haas *et al.*, 2016). Beyond being a mechanism for sustaining reef health and contributing to reef decline, microorganisms also show promise as targets for reef monitoring programs (Glasl *et al.*, 2017). Seawater microorganisms in particular respond to temperature changes, making them predictive of potential coral bleaching events (Glasl *et al.*, 2019). These microorganisms also respond to nutrient and freshwater input in response to storm events (Yeo *et al.*, 2013), suggesting they could be leveraged as a proxy for disturbances. Continued work that evaluates and demonstrates their worth in monitoring programs as well as how they are involved in responding and contributing to reef degradation is warranted.

While studies on bacterial and archaeal members of coral reef communities abound, far less attention has been given to eukaryotic, fungal, and viral partners in coral reef habitats. The microeukaryotic microorganisms include photosynthetic plankton and coral endosymbionts (i.e. *Symbiodiniaceae*), fungi, and other protists that may be beneficial, pathogenic and parasitic to other reef organisms (Ainsworth *et al.*, 2017). Additionally, in the planktonic environment, phagotrophic microeukaryotes are a critical link in the microbial loop as consumers of bacteria

(Weisse, 2016). Viruses outnumber all other microbial groups by at least an order of magnitude in reef seawater, and play a role in the microbial loop in the form of the "viral shunt", in which mortality of pelagic microeukaryotes and prokaryotes contributes to the organic matter pool in the seawater (Thurber *et al.*, 2017). Through the "kill-the-winner" and "piggyback-the-winner" hypotheses, they also impact the community composition of microbes on coral reefs (Thingstad, 2000; Silveira and Rohwer, 2016). Collectively, microeukaryotes and viruses far outnumber their prokaryotic counterparts, and continued work will shed light on the importance of these diverse microbes in reefs.

Within the water column, the near-coral seawater that is within and just beyond the coral-seawater boundary layer is a unique microbial habitat, referred to as the "ecosphere" (Weber *et al.*, 2019) or the "aurabiome" (Walsh *et al.*, 2017). This area has been shown to foster microbes with more virulent-like and surface-associated genes, and may be a recruitment zone for pathogens (Weber *et al.*, 2019). Comparisons of this habitat between corals and algae also show mechanisms in which increased algal growth may select for more pathogenic taxa and microbial taxa adapted to low oxygen concentrations, reinforcing coral-algal phase shifts (Walsh *et al.*, 2017). Within this habitat, water flow across the reef also impacts microbial community structure (Silveira *et al.*, 2017). In the context of coral disease, microbial bioindicator taxa, or taxa that are enriched in diseased tissue, are also sometimes detected in the near-coral seawater habitat, supporting hypotheses that this area may selectively recruit coral pathogens (Becker *et al.*, 2021). From the near-coral seawater to the surrounding seawater habitat which extends to the surface, microorganisms form dynamic and diverse communities that respond to the changing reef environment.

Coral microorganisms and nested ecosystems: Scleractinian coral are foundational in the reef ecosystem, but within the coral organism is a dynamic nested ecosystem. Corals are host to innumerable microorganisms including their symbiotic eukaryotic algae, bacteria, archaea, fungi, and viruses. Together, these microorganisms and coral host create a "holobiont" (Margulis, 1991; Rohwer *et al.*, 2002; Baedke *et al.*, 2020). The most well-characterized symbionts are the eukaryotic algae of the family *Symbiodiniaceae*, which provide nutrients and energy and are thus essential to tropical coral survival (reviewed in Stat *et al.*, 2006). While less

well-characterized than *Symbiodiniaceae*, the increasing accessibility and usage of 'omics tools have uncovered an incredible diversity of bacteria and archaea within coral hosts that are increasingly respected for their beneficial roles to host fitness (Bourne *et al.*, 2016; Peixoto *et al.*, 2017).

Within the coral, there are different compartments (skeleton, tissue, and mucus), where distinct communities of microorganisms reside (Sweet *et al.*, 2011; Apprill *et al.*, 2016; Bourne *et al.*, 2016). The skeleton harbors a diverse array of microbes, including bacteria, archaea, fungi, and filamentous *Ostreobium* algae, and we are only just beginning to understand the potential beneficial roles this endolithic community has on the coral host (Pernice *et al.*, 2020). The tissue compartment has generally lower microbial abundances than other compartments, but these are likely due to the presence of more specific symbiotic associations (Bourne *et al.*, 2016). Clusters of coral-associated microbial aggregates (CAMAs) often containing *Endozoicomonas* bacteria are found globally in the tissues of corals (Neave *et al.*, 2017). These CAMAs sequester and cycle phosphate between coral holobiont partners (Wada *et al.*, 2022). Finally, the surface mucus layer is the most dynamic and microbe-rich habitat, harboring approximately 10^6 bacteria per milliliter (Garren and Azam, 2012). The mucus layer is directly in contact with the surrounding seawater and serves as a barrier to the coral, assisting with sediment shedding, feeding, and removal of potential pathogens (Bourne *et al.*, 2016). As the surface mucus layer is in direct contact with the seawater, but also is regularly shed by the host coral, the microbial communities within that layer are dynamic and show predictable cyclical shifts as the mucus ages (Glasl *et al.*, 2016). As a transient layer produced by the host, the coral surface mucus may harbor microbes that are related to host health. The surface mucus layer microbiome may even be an ideal candidate for early diagnosis for coral health (Huntley *et al.*, 2022). With multiple microhabitats, the coral holobiont is truly an ecosystem residing within and influencing the already complex reef ecosystem.

The concept of the coral holobiont can be expanded to any other individual organism residing within the complex reef, making coral reefs a collection of many nested ecosystems. Sponges are a perfect example of another nested ecosystem (Pita *et al.*, 2018). Sponges are increasingly abundant and common on Caribbean reefs, and up to 40% of their biomass can be

microbes (Webster and Taylor, 2012). Within the water column, fish host diverse communities of bacteria on the mucus layer directly on top of their scales (Chiarello *et al.*, 2018). Additionally, some fish, such as cleanerfish, have skin microbes that are influenced by other fish, as they interact and 'clean' parasites from numerous client fish, and may foster hotspots of microbial transfer on reefs (Pereira *et al.*, 2022). Whether it is corals, sponges, fish, or other macrofauna on a reef, all of them harbor persistent microbial associations that reside within the reef ecosystem. The reef seawater and its microorganisms are the common denominator that interacts with and is influenced by those nested ecosystems to create the thriving and diverse coral reef.

Stony coral tissue loss disease

In 2014, a new coral disease sprouted up near Miami, Florida. Although the disease presented like so many other "white plague like" coral diseases, with a white band that quickly moved across coral colonies, it was clear from the high rates of mortality, fast pace, and widespread nature, that it was something new and potentially devastating (Precht *et al.*, 2016). The disease was soon termed "stony coral tissue loss disease" and in a matter of years, spread both north and south along Florida's Coral Reef, exhibiting a highly contagious epidemiology (Muller *et al.*, 2020). By late 2019, the disease had reached down to the Marquesas, and two years later, it spread across the wide divide to the historically high-quality reefs of Dry Tortugas National Park (Dobbelaere *et al.*, 2022). The disease did not stop there. Before it reached Dry Tortugas, disease with the same ecology sprouted up along the Mexican Caribbean, the Virgin Islands, and numerous other islands within the Caribbean (Kramer *et al.*, 2021). As one example, the disease first reached the United States Virgin Islands in January 2019. Within another 2 years, it was detected on the reefs surrounding all three Virgin Islands (Brandt *et al.*, 2021).

Scientists were quickly motivated to begin to understand how such a lethal and contagious disease spread like an underwater version of the coronavirus pandemic. In some cases, the spread followed natural currents, but even moved against some currents, pointing to a likely neutrally-buoyant pathogenic particle transferring between different corals (Dobbelaere *et al.*, 2020). Other research pointed to ballast water as a likely spreader, in which release of

ballast water too close to a reef could release the contagion into the seawater of an uninfected area (Rosenau *et al.*, 2021; Studivan *et al.*, 2022). Even within a reef, corallivorous fish seem to preferentially feed on diseased tissue and may aid in either transmission or recovery of the disease (Noonan and Childress, 2020; Titus *et al.*, 2022). Regardless, multiple tank-based experiments show that within weeks of residing in proximity to a diseased colony, susceptible coral species will succumb to the disease (Aeby *et al.*, 2019; Meiling *et al.*, 2021; Huntley *et al.*, 2022).

Caribbean coral reefs harbor up to approximately 40-60 species of hard corals responsible for building the reef habitat. As many as half of these coral species on a reef are susceptible to the disease (Florida Keys National Marine Sanctuary, 2018). More concerning, of those that do get the disease, up to 100% of colonies on a reef may experience mortality and this has led to up to 60% of live coral tissue on a given reef to die (Precht *et al.*, 2016; Walton *et al.*, 2018). This is particularly concerning for highly susceptible species and endangered species like the visually stunning pillar coral, *Dendrogyra cylindrus*, that is now functionally extinct in Florida after 93% of colonies died from stony coral tissue loss disease (Neely *et al.*, 2021). With disease prevalence that exceeds “normal” low-levels of disease on a reef, and unprecedented tissue loss rates, the disease is clearly a force to be reckoned with (Meiling *et al.*, 2020; Brandt *et al.*, 2021).

If unprecedented speed and mortality weren’t already challenging enough, stony coral tissue loss disease has no confirmed pathogen, much like the majority of other coral diseases (Mera and Bourne, 2018; Vega Thurber *et al.*, 2020). There is evidence for potential pathogens across the tree of life. Microeukaryotic Ciliophora (ciliates) were associated with disease lesions in both sequence- and microscopy-based work (Landsberg, 2020; Rosales, Huebner, Clark, *et al.*, 2022). Microscopy points to a potentially viral infection within the endosymbiotic *Symbiodiniaceae* corals rely on, but these viral particles are also visible in apparently healthy coral (Landsberg, 2020; Work *et al.*, 2021). Metagenomic evidence of alphaflexivirus-like viral strains in diseased coral tissue, support a potential viral role in infection (Veglia *et al.*, 2022). At the chemical level, endosymbiont-specific lipids that are differentially present between healthy and diseased colonies, shows how metabolomics could hold the key to potential changes

leading to this disease (Deutsch *et al.*, 2021). As further research continues, genomic and metabolomic methods have and will continue to be important in disentangling the chemical and microbial mechanisms of stony coral tissue loss disease.

While some research points to viral infections, most research, and by extension, mounting evidence, points to bacterial infections of the coral host. Antibiotic pastes containing amoxicillin seem to cease lesion progression, though they do not stop lesions from popping up elsewhere on the colony (Aeby *et al.*, 2019; Neely *et al.*, 2020). While broad-spectrum antibiotics do not stop the disease altogether or point to a specific pathogen, they reduce disease incidence and offer a method, albeit time-consuming, of intervention for local reef managers and stakeholders that rely on reef habitats for recreation, fisheries, and more (Walker *et al.*, 2021). Culture-based studies targeting bacteria have identified *Vibrio coralliilyticus,* which exacerbates the disease, but does not cause the disease in isolation (Ushijima *et al.*, 2020). Culture-independent tools in the form of sequencing of the bacterial and archaeal 16S ribosomal RNA (rRNA) gene have been applied many times to stony coral tissue loss disease (Meyer *et al.*, 2019; Iwanowicz *et al.*, 2020; Rosales *et al.*, 2020; Becker *et al.*, 2021; Clark *et al.*, 2021; Thome *et al.*, 2021). Although this survey-type research is unable to identify specific pathogens associated with this disease, these studies are able to point to groups of bacteria that might be common associates of the disease, influencing potential further cultivation or isolation work that could narrow down the window of potential pathogens or opportunistic taxa. The earliest works identified groups of microorganisms including *Fusibacter, Vibrio, Algicola,* Clostridiales and multiple microorganisms from Rhodobacterales and Rhizobiales associated with the disease (Meyer *et al.*, 2019; Rosales *et al.*, 2020; Clark *et al.*, 2021). A new meta-analysis that incorporates thousands of samples also implicates Rhodobacterales groups with the disease, in addition to Peptostreptococcales-Tissierellales (Rosales *et al.*, 2023). These approaches are widespread and able to provide significant information to the disease, but they require increased speed and deployability. Efforts that leverage smaller DNA sequencing machines on-site could increase the turnaround time for results and may even help to inform future efforts to understand new disease outbreaks (Apprill, 2019; Becker *et al.*, 2021). Although a specific pathogen or pathogens remains elusive

for stony coral tissue loss disease, the continued effort and research that integrates multiple tools from microscopy, genomics, and metabolomics, to field-based sampling and experimentation is sure to assist in understanding and curtailing this devastating coral pandemic.

Dissertation overview - A place for 'omics in examining reef ecosystem dynamics

Central to the decline of Caribbean reefs are threats such as climate change, eutrophication, overfishing, hurricanes and diseases like stony coral tissue loss disease. Climate change has led to increasing incidents and severity of coral bleaching events worldwide (Hoegh-Guldberg *et al.*, 2007) and in the Caribbean leading to chronic stress on reefs (McWilliams *et al.*, 2005). Overfishing is a pervasive and sustained pressure on coastal environments, including coral reefs, which has led to trophic shifts and ecosystem collapses (Jackson, 2001). Severe hurricane events in the Caribbean historically cause 17% loss in coral cover, which often takes years to recover (Gardner *et al.*, 2005). Natural pressures like disease, which are common in the Caribbean, have completely restructured some reefs (Green and Bruckner, 2000; Weil, 2004; Bruckner, 2015). Hurricane impacts and the emergence of the recent stony coral tissue loss disease epidemic are threats of particular relevance in this thesis, which focuses on two regions in the Caribbean: Florida's Coral Reef and the United States Virgin Islands (USVI).

Florida's Coral Reef extends over 550 km from St. Lucie Inlet to Dry Tortugas National Park and is the largest barrier reef in North America. *Acropora* spp of corals were once the dominant hard coral members of Floridian reefs that contained multiple species of hard corals. Today, though, the diversity of coral communities is increasingly homogeneous (Burman *et al.*, 2012). Indeed, over the last several millennia, the reefs in Florida have geologically shut down, meaning they are no longer accruing calcium carbonate, leaving the hard coral tissue "veneer" as the last line of defense preventing reef erosion (Toth *et al.*, 2018). A suite of regular stressors and disturbances in Florida have removed that veneer. Bleaching events caused by both cold water and increasingly regular events associated with global warming have led to coral mortality (Davis, 1982; Manzello, 2015). A suite of diseases have led to die-offs of corals, including the white diseases of acroporids (Aronson and Precht, 2001; Williams and Miller,

2012) and more recent multi-species die-offs due to stony coral tissue loss disease (Precht *et al.*, 2016). Die-offs of the *Diadema antillarum* urchin, a major algal grazer, also likely exacerbated loss in corals, leaving increased algae and decreased space for larval coral to settle (Carpenter, 1988; Chiappone *et al.*, 2008). On top of these disturbances, Florida reefs experience approximately one hurricane every 7-8 years, leaving limited time for these already stressed and degraded systems to recover (Gardner *et al.*, 2005; Blake *et al.*, 2011). Hurricanes, die-offs of herbivores, coral disease, and coral bleaching have all led to the degradation of America's largest barrier reef system.

The United States Virgin Islands (USVI) encompass three islands, St. Croix, St. Thomas, and St. John. These islands are surrounded by fringing reefs and have been well-monitored by the Territorial Coral Reef Monitoring Program (TCRMP), which has been quantifying coral and fish abundances since 2002 (Ennis *et al.*, 2019). Additionally, the reefs of St. John are largely protected by the Virgin Islands National Park and the Virgin Islands Coral Reef National Monument, and have been the focus of three decades of research on coral communities, making it one of the longest-studied regions of Caribbean reefs (Edmunds, 2013). While coral cover on St. John is declining slowly overall, there are some reefs, such as Tektite, that could be "oases" that resist decline (Guest *et al.*, 2018). Additionally, compared to the neighboring island of St. Thomas, corals are not declining as quickly on St. John (Edmunds and Smith, 2022). Despite some resilience, historic disturbances such as hurricanes, bleaching, and coral disease have impacted the reefs, leaving them with lower coral cover than in the 1980's (Rogers *et al.*, 2008; Edmunds, 2013). More recently, these reefs were impacted by category five hurricanes, Irma and Maria, in September 2017. Despite being the most intense storms in over a century, the already degraded hard coral communities experienced little change (Edmunds, 2019). A few years later, stony coral tissue loss disease ravaged the reefs, exceeding previous losses due to coral bleaching (Brandt *et al.*, 2021). Although these reefs have declined slowly over time, severe threats to USVI reefs have not abated, and may continue to threaten what little is remaining in these reef ecosystems.

The quintessential monitoring metric for change in coral reefs is the percentage of the reef habitat that is coral, or "coral cover" (Gardner *et al.*, 2003). This metric, in concert with the

changes in other components of the reef benthos, are important for understanding the nature of change in the underlying reef habitat. But as I've introduced here, coral reefs are a collection of nested ecosystems, within a dynamic and complex seawater habitat. At the foundation of this ecosystem are the dissolved organic compounds and microbial players that are often overlooked, yet play important roles in the reef habitat. Water quality monitoring for nutrients and organic carbon, are included in some monitoring programs, and are important additions (Briceño and Boyer, 2018). Continued efforts to develop water quality monitoring programs to also include specific metabolites, compounds, and especially microbiological parameters will be critical as the value of the standard "coral cover" metric erodes with the reef. Beyond value in coral reef dynamics, these parameters may provide further insight into ecosystem dynamics that may have eluded previous detection.

In the following thesis, I leverage microbial communities and metabolites to understand coral reef dynamics. Figure 1-1 presents an overview of the scope of the different chapters within this thesis. In each chapter, I use field-based sampling to characterize the natural variability of microorganisms in these habitats and relate them to environmental characteristics. First, in chapter 2, titled "microbial bioindicators of Stony Coral Tissue Loss Disease identified in corals and overlying waters using a rapid field-based sequencing approach.", I address the coral disease epidemic by developing and applying an in-the-field microbiome processing pipeline to four coral species. Microbiome processing can often take much longer than the few weeks to months it takes for stony coral tissue loss disease to kill individual coral colonies on a reef. By shortening the turnaround time of generating microbiome data to only two weeks, the majority of time could be spent on analysis and generating results to communicate to fellow scientists and stakeholders. In this chapter, I identified 25 bioindicators in coral tissue and the near-coral seawater overlying the colonies and related them to known coral microorganisms, adding to the growing body of work on bacteria and archaea associated with stony coral tissue loss disease.

In chapter 3, titled "Microbial and nutrient dynamics in mangrove, reef, and seagrass waters over tidal and diurnal time scales", I focus on the effect on seawater microorganisms of two of the most fundamental rhythmicities in marine habitats: tides and sunlight. Coastal

biomes including mangroves, seagrass beds, and coral reefs are critically important and distinct despite being near one another in the study area of the southern shore of St. John in the U.S. Virgin Islands. Outside of reef stressors, there is a need to understand fundamental shifts in physicochemical and microbiological parameters across these habitats if we are to leverage them for monitoring reef threats. This chapter explores the especially drastic changes in mangrove habitats due to the tidal cycle and the comparatively muted tidal and more prominent diurnal changes apparent in the reef and seagrass habitats.

In chapter 4, titled "Microorganisms uniquely capture and predict stony coral tissue loss disease and hurricane disturbances on US Virgin Islands reefs", I expand the short temporal work of chapter 3 to a longer timescale of opportunistic sampling events over seven years at eight reefs on St. John, U.S. Virgin Islands. In addition to collecting seawater microbial community data at each reef over this time period, collections of organic and inorganic nutrients, cell abundances, temperature and salinity, benthic composition, and coral recruits allow for a comprehensive investigation into the changes these reefs faced over this time period, that is likely the longest dataset of its kind in coral reef research. It showcases what can be learned if water monitoring programs in reefs were expanded to include microbiological parameters. In the context of two major disturbances, category 5 hurricanes in September 2017, and the devastating stony coral tissue loss disease in 2020, this chapter evaluates ways in which disturbances may enhance reef microbialization, contributing to a positive feedback loop of reef decline.

Finally, in chapter 5, titled "Microorganisms and dissolved metabolites distinguish Florida's Coral Reef habitats", I use a cruise of opportunity to eight different zones spanning over 300 km of Florida's Coral Reef to understand the smallest components of the reef: dissolved metabolites and microorganisms. As described earlier, 'omics techniques to measure these components are gaining traction in reef research, but the extent to which they reflect reef environments and are informative for reef monitoring is unclear. The 'omics strategies I used included targeted and untargeted metabolomics, taxonomic microbiome analysis via 16S ribosomal RNA sequencing of bacteria and archaea, and functional microbiome analysis via shotgun sequencing. These were applied to either reef seawater or coral hosts impacted by

stony coral tissue loss disease. By integrating these ‘omics data with a suite of habitat characteristics, I demonstrate the strong biogeographic influence of reef habitat zones on these parameters. Additionally, I demonstrate how ‘omics strategies may be useful for reef monitoring.

Each chapter individually assesses a reef habitat and the response of the smallest components of coral reefs to some of the most fundamental gradients (i.e. tides, biogeography) and devastating stressors (i.e. hurricanes, disease) causing change in reef habitats. As coral reefs continue to degrade worldwide, this research demonstrates the utility of ‘omic strategies to lend insight into important microbial and chemical players that may be indicators of and contributors to changes in threatened coral reef habitats.

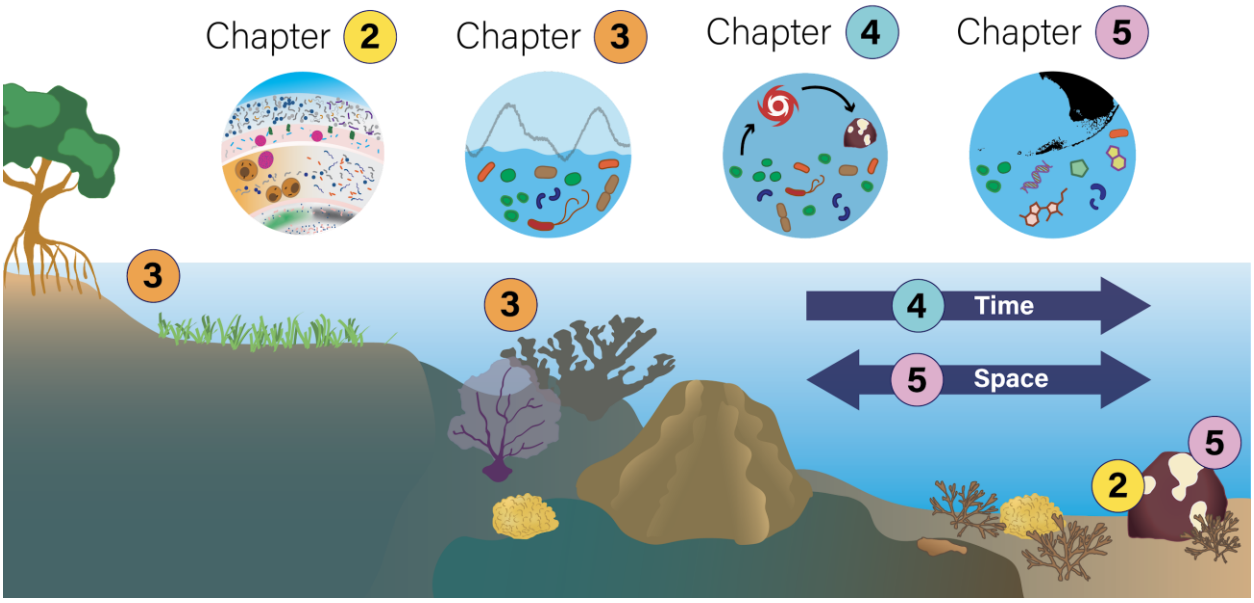

Figure 1-1. Overview of dissertation.

This dissertation investigates the dynamics of microorganisms and metabolites in coral reef ecosystems. Chapter 2 focuses on host-associated and near-coral seawater microbial communities associated with apparently healthy and stony coral tissue loss disease-impacted corals. Chapter 3 investigates tidally-influenced seawater microbial community dynamics in mangrove, seagrass, and coral reef environments. Chapter 4 uses a seven-year time series to show how disturbances (hurricanes, disease) impact coral reef habitats and seawater microbial communities. Chapter 5 combines analyses of microorganisms, metabolites, and coral-associated microbial communities to identify signatures of reef zones and habitat characteristics over 300 km of Florida's Coral Reef.

Chapter 2 - Microbial bioindicators of Stony Coral Tissue Loss Disease identified in corals and overlying waters using a rapid field-based sequencing approach[1]

[1] This chapter was originally published as:

Becker, C.C., Brandt, M., Miller, C.A., and Apprill, A. (2021) Microbial bioindicators of Stony Coral Tissue Loss Disease identified in corals and overlying waters using a rapid field-based sequencing approach. *Environ Microbiol* 1462-2920.15718.

CB, MB, CAM, and AA took part in the research expedition to collect and process the samples. CB and AA designed the study. CB analyzed the data and wrote the manuscript. All authors contributed edits to the final manuscript and approved of the content.

ABSTRACT

Stony Coral Tissue Loss Disease (SCTLD) is a devastating disease. Since 2014, it has spread along the entire Florida Reef Tract and into the greater Caribbean. It was first detected in the United States Virgin Islands in January 2019. To more quickly identify microbial bioindicators of disease, we developed a rapid pipeline for microbiome sequencing. Over a span of 10 days we collected, processed, and sequenced coral and near-coral seawater microbiomes from diseased and apparently healthy *Colpophyllia natans*, *Montastraea cavernosa*, *Meandrina meandrites* and *Orbicella franksi*. Analysis of bacterial and archaeal 16S ribosomal RNA gene sequences revealed 25 bioindicator amplicon sequence variants (ASVs) enriched in diseased corals. These bioindicator ASVs were additionally recovered in near-coral seawater (<5 cm of coral surface), a potential reservoir for pathogens. Phylogenetic analysis of microbial bioindicators with sequences from the Coral Microbiome Database revealed that *Vibrio, Arcobacter,* Rhizobiaceae, and Rhodobacteraceae sequences were related to disease-associated coral bacteria and lineages novel to corals. Additionally, four ASVs (*Algicola*, *Cohaesibacter*, *Thalassobius* and *Vibrio*) were matches to microbes previously associated with SCTLD that should be targets for future research. Overall, this work suggests that a rapid sequencing framework paired with specialized databases facilitates identification of microbial disease bioindicators.

Originality-Significance Statement

We developed and integrated a rapid, field-based pipeline for microbiome characterization that uses the smallest Illumina platform, the iSeq 100 System, and applied it to an unprecedented coral disease, Stony Coral Tissue Loss Disease. Here, we present work on microbial bioindicators of this coral disease in the United States Virgin Islands, an area not previously represented in microbial studies of this disease. We also sample for and detect signatures of this coral disease in near-coral seawater (<5 cm of the coral surface), a microbial microenvironment not commonly sampled which may serve as a disease reservoir. By additionally presenting the disease bioindicators in a phylogenetic context, we identify both potential pathogens of the disease and likely novel coral-associated microbes. In addition to identifying specific targets for

future work on SCTLD, our framework could be a powerful tool for studying both existing and future marine disease outbreaks.

INTRODUCTION

Stony Coral Tissue Loss Disease (SCTLD) is a rapidly progressing, persistent, and widespread coral disease that affects at least 24 reef-building coral species in the Caribbean (Florida Keys National Marine Sanctuary, 2018). Since 2014, when it was first detected off Miami-Dade county, FL, it has devastated Floridian reefs, where loss in live coral has been as high as 60% (Precht *et al.*, 2016; Walton *et al.*, 2018). In the following years, the disease spread over the entire Florida Reef Tract and in 2018, the disease had appeared in disparate areas of the Caribbean (Kramer *et al.*, 2021). The SCTLD outbreak is one of the longest and most widespread coral disease outbreaks ever to be recorded (Rosales *et al.*, 2020). The extended duration, widespread occurrence, and high species susceptibility associated with SCTLD make this an unprecedented and devastating coral disease.

When SCTLD first emerged on Floridian reefs, it initially impacted species including *Meandrina meandrites, Dichocoenia stokesii, Dendrogyra cylindrus* (an Endangered Species Act-listed coral), and the brain corals (i.e. *Colpophyllia natans, Pseudodiploria strigosa*). In ensuing months after the initial outbreak, other species began to show signs of SCTLD, including bouldering-type corals such as *Montastraea cavernosa,* and *Orbicella* spp. (Florida Keys National Marine Sanctuary, 2018). Similar assemblages of affected species and disease ecology confirmed the emergence of SCTLD on reefs off of Flat Cay, an unoccupied island off of St. Thomas, U.S. Virgin Islands (USVI), in January 2019. Tissue loss on USVI corals progress at rates up to 35-fold higher than other common coral diseases and leads to complete mortality of over half of afflicted colonies (Meiling *et al.*, 2020). Throughout 2019, and until the time of sampling in February 2020, the disease spread around the island of St. Thomas and east to the island of St. John (VI-CDAC, 2021).

The causative agent(s) responsible for SCTLD remain elusive, a common feature of the majority of coral diseases (Mera and Bourne, 2018; Vega Thurber *et al.*, 2020). Further, the lack

of correlation between SCTLD severity and ambient temperature or chlorophyll concentrations, suggests that a novel, yet highly contagious, pathogen may be responsible (Muller *et al.*, 2020). Successful cessation of lesion progression following application of amoxycillin paste to afflicted colonies suggests that either the pathogen(s) are of bacterial origin or that bacteria play a role in disease progression and virulence as opportunistic microbes (Aeby *et al.*, 2019; Neely *et al.*, 2020). To detect disease bioindicators, 16S ribosomal RNA (rRNA) gene sequencing approaches that target bacteria and archaea were employed on field-collected coral samples from the Florida Reef Tract, where the disease originated (Meyer *et al.*, 2019; Rosales *et al.*, 2020). Meyer and colleagues (2019) found bacteria from five genera, including *Vibrio, Arcobacter, Algicola, Planktotalea,* and one unclassified genus that were consistently enriched in the lesion tissue of three species (*Montastraea cavernosa*, *Diploria labyrinthiformis* and *Dichocoenia stokesii*). In a separate study (Rosales *et al.*, 2020), Rhodobacterales and Rhizobiales sequences were associated with lesions in *Stephanocoenia intersepta*, *D. labyrinthiformis*, *D. stokesii* and *Meandrina meandrites*. It remains to be seen if these same microbial taxa are associated within SCTLD lesions across the greater Caribbean, especially in the geographically distant USVI, as well as in other coral species affected by the disease.

With such a widespread occurrence, it is important to understand the ways in which SCTLD is transmitted. It is hypothesized that transmission of this disease is through the water column, as evidenced by tank-based experiments (Aeby *et al.*, 2019) and modeling of likely dead coral material and sediments within neutrally buoyant water parcels (Dobbelaere *et al.*, 2020). Additionally, disease-associated microbial taxa were recovered in water and sediment of diseased-afflicted coral reefs, indicating that sediment may also play a role in transmission (Rosales *et al.*, 2020). Disease-associated taxa or putative pathogens have yet to be examined in seawater directly surrounding diseased coral colonies using a targeted sampling method, such as syringe-based water sampling over corals (Weber *et al.*, 2019).

The seawater directly overlying coral, here termed “near-coral seawater”, is an important reef environment. Compared to surrounding reef seawater, this environment is characterized by microbes with unique metabolisms and more virulent-like and surface-associated lifestyles (Weber *et al.*, 2019). Also, this near-coral seawater environment is

hypothesized to be a recruitment zone for both symbiotic microorganisms and potential pathogens (Weber *et al.*, 2019). While coral physiology may influence the microbes living in this environment, water flow and surrounding currents also play a role (Silveira *et al.*, 2017). Given existing evidence and hypotheses that the SCTLD pathogen or pathogens are water-borne (Aeby *et al.*, 2019; Dobbelaere *et al.*, 2020; Rosales *et al.*, 2020), directly targeting the zone of potential pathogen recruitment is important for supporting these claims.

The rapid spread, persistence, and virulence of SCTLD make it imperative to develop speedier response procedures for understanding this disease. While microbial community profiling cannot verify candidate pathogens, it is one step in the process of elucidating SCTLD causation through identification of microbial indicators that can be tested further for their role in disease etiology. Additionally, these methods offer a breadth of information, but can fall short in processing time. Typical microbiome pipeline procedures involve weeks to months of sample processing, sequencing, and data analysis. Combined with the requirement for specialized equipment, these procedures are often difficult to conduct in remote island reef locations. Field-based sequencing circumvents these challenges and offers additional benefits, such as working immediately with fresh samples, and in the case of marine disease studies, the quickly processed data could even inform sampling strategies during the timeline of the project (Apprill, 2019). Recently, Illumina Inc. developed the iSeq 100 System, a portable sequencing platform. The platform uses sequencing by synthesis chemistry combined with complementary metal-oxide semiconductor (CMOS) technology and produces 8 million reads, with greater than 80% of reads passing a quality score of Q30 (99.9% base call accuracy) in each run (Illumina, Inc., 2020). Additionally, the CMOS technology allows the sequencing to occur all in a small, single-use cartridge, contributing to its ease of use in mobile (e.g., ship) laboratory settings. More portable sequencing technology and the increasing availability of portable thermocycler machines and centrifuges have made it possible to set up molecular laboratories in almost any environment with an electrical connection.

Here, we developed and applied a rapid coral microbiome sequencing pipeline designed to more quickly gather data on the effects of SCTLD currently affecting numerous nations and reefs across the Caribbean. By setting up small, portable molecular biology tools in a home

rental, we successfully collected, processed, and sequenced diseased and apparently healthy coral and near-coral seawater samples at two reefs in St. Thomas, USVI (Figure 2-1). We were interested in answering the following questions regarding the implementation of this rapid pipeline to more broadly understand the etiology of SCTLD: (1) How effective is a portable sequencing approach for coral disease studies, and potentially other marine diseases, (2) What microbial taxa are differentially distributed in healthy and diseased coral, and which may be bioindicators of the disease, (3) Can we identify SCTLD bioindicator microbes in the seawater directly overlying healthy and diseased corals, and (4) To what extent are these SCTLD bioindicators phylogenetically related to known or unknown coral-associated bacteria?

METHODS

Sample collection

Coral colonies showing active Stony Coral Tissue Loss Disease (SCTLD) and nearby completely healthy colonies were sampled on February 11 and 13, 2020 on Buck Island (18.27883°, −64.89833°), and Black Point (18.3445°, −64.98595°) reefs, respectively, in St. Thomas, USVI (Figure 2-1, Table 2-1). Buck Island was considered a recent outbreak site where disease first emerged in January 2020, whereas Black Point had SCTLD since at least January 2019. Coral species sampled were *Montastraea cavernosa* (Buck Island and Black Point; SW n = 20, Coral n = 18)*, Colpophyllia natans* (Buck Island and Black Point, n = 16)*, Meandrina meandrites* (Buck Island, n = 9)*,* and *Orbicella franksi* (Buck Island, n = 6) (Table 2-1)*.* SCTLD was identified by single or multi-focal lesions of bleached or necrotic tissue with epiphytic algae colonizing the recently dead and exposed skeleton (Figure 2-2). At both reefs, some paling of colonies was apparent, especially on *Orbicella* spp., as a result of a recent bleaching event in October 2019. Due to this, it was challenging to distinguish SCTLD from white plague-type diseases, which generally occur following bleaching events (Miller *et al.*, 2009). As a result, we avoided sampling *Orbicella* spp*.,* except when it was clear the colony had regained full coloration and the disease lesion was consistent with SCTLD infection.

To investigate if putative pathogens were recoverable from seawater surrounding diseased colonies, near-coral seawater was sampled 2-5 cm away from each coral colony prior to tissue sampling via negative pressure with a 60 ml Luer-lock syringe (BD, Franklin Lakes, NJ, USA). Two seawater samples were collected over each colony displaying SCTLD lesions: one sample was taken directly above healthy tissue approximately 10 cm away from the lesion, when possible, and a second sample over diseased tissue. Syringes were placed in a dive collection bag for the duration of the dive. Once on board the boat, the seawater was filtered through a 0.22 μm filter (25 mm, Supor, Pall, Port Washington, NY, USA) and the filter with holder was placed in a Whirl-pak bag and kept on ice until returning to the shore. While on shore, filters were placed in sterile 2 ml cryovials (Simport, Beloeil, QC, Canada) and frozen in a liquid nitrogen dry shipper.

After near-coral seawater sampling, samples of tissue and mucus mixed together (referred to as coral samples) were collected. One sample was collected from each healthy colony and two from each diseased colony. For the two samples collected from each diseased colony, one was collected from the interface between healthy and newly bleached tissue (Figure 2-2), and the other from healthy tissue approximately 10 cm away from the disease interface. When limited healthy tissue remained on a diseased colony, the coral sample was collected approximately 3 to 5 cm away from the disease lesion interface. The coral samples were collected with 10 ml non-Luer lock syringes (BD) by agitating and disrupting a small area of the tissue surface with the syringe tip while simultaneously aspirating the resulting suspended tissue and mucus into the syringe. To control for the significant amount of seawater and seawater-associated microbiota unavoidably captured during the collection of the coral samples, a total of nine 10 ml syringes of ambient reef seawater were collected from approximately 1 m off the reef benthos, (hereafter referred to as “Syringe Method Control” samples). Immediately after collection, the syringes were placed in a Whirl-pak bag to prevent the loss of sample while underwater. Once back on board the boat, samples were transferred to 15 ml sterile conical tubes and placed in a 4°C cooler. Upon returning to the laboratory, samples were frozen to −20°C until analysis.

The physical and chemical environment of the surrounding seawater was characterized by measuring temperature, salinity, dissolved oxygen, pH, and turbidity using an Exo2 multiparameter sonde (YSI, Yellow Springs, OH, USA) (Table 2-S1). The sonde probes were calibrated following manufacturer's protocols on the day before sampling (February 10, 2020).

DNA extraction, PCR, and sequencing

Protocols for preparing samples for sequencing were specifically designed for the Illumina iSeq 100 System (Illumina Inc., San Diego, CA, USA), a portable, high-quality sequencing technology. In an approximately 1 cu. ft. size, the Illumina iSeq 100 System produces 4 million paired-end 150 bp sequence reads of high quality (<1% error rate) that can be offloaded and processed on a standard laptop without the need for Wi-Fi, making it an attractive technology to adapt for field-based microbiome studies. We brought the iSeq 100 System to a home rental in the USVI, which we transformed into a remote laboratory where we successfully conducted all DNA extractions, Polymerase Chain Reaction (PCR) and subsequent sequencing.

DNA was extracted from seawater, coral, and syringe method control samples, along with associated extraction controls, using the DNeasy PowerBiofilm Kit (Qiagen, Germantown, MD, USA). Modifications at the beginning of the extraction protocol were applied based on the sample type. For filtered seawater samples, the 0.22 μm filter was placed directly into the bead tube, and then manufacturer instructions were followed. For coral and syringe method control samples, samples were thawed at room temperature, then immediately transferred to 4°C prior to extraction. Samples then were vortexed for 10 seconds and 1.8 ml of each sample was transferred to a bead tube. Samples were centrifuged at 12,045 rcf (maximum rcf available on centrifuge) for 10 min to concentrate tissue, mucus, and the associated microorganisms at the bottom of the tube, and supernatant was removed. For samples that were very clear (very little tissue collected via syringe) and for syringe method control samples, a second aliquot of 1.8 ml of sample was centrifuged on top of the existing pellet to capture more microorganisms. The extraction proceeded by following the manufacturer's protocol. Six DNA extraction controls, three for each sample type, were generated by following the manufacturer's protocol using: blank bead tubes for coral and syringe method control samples (named D1-D3) and unused 0.22 μm filters placed in bead tubes for seawater samples (named D4-D6).

A two-stage PCR process was used to prepare the samples for sequencing. In the first stage, PCR was used to amplify the V4 region of the small sub-unit ribosomal RNA (SSU rRNA) gene of bacteria and archaea. The amount of DNA added and the total reaction volume of this first PCR varied by sample type. For each PCR, 2 μl of coral and syringe method control template DNA was added to a final volume of 50 μl. 1 μl template in a 25 μl total reaction volume was used for seawater samples. For negative PCR controls, 1 or 2 μl of sterile PCR-grade water was used in 25 or 50 μl (total volume) reactions, respectively. One Human Microbiome Project mock community, Genomic DNA from Microbial Mock Community B (even, low concentration), v5.1L, for 16S rRNA Gene Sequencing, HM-782D was included as a sequencing control using 1 μl DNA in a 25 μl reaction. 50 μl reactions contained 0.5 μl polymerase (GoTaq, Promega, Madison, WI, USA), 1 μl each of 10 μM forward and reverse primers, 1 μl of 10 mM dNTPs (Promega), 5 μl $MgCl_2$ (GoTaq), 10 μl 5X colorless flexi buffer (GoTaq), and 29.5 μl UV-sterilized, PCR-grade water. 25 μl reactions used the same proportions of reagents as 50 μl reactions. Earth microbiome project primers revised for marine microbiomes, 515F and 806R, targeted bacteria and archaea and were used with Illumina-specific adapters (Apprill *et al.*, 2015; Parada *et al.*, 2016). Two small, portable thermocyclers were used for the PCRs: the mini8 (miniPCR, Cambridge, MA, USA), which contained 8 wells and connected to a laptop for programming and initiation of the run, and the BentoLab (Bento Bioworks Ltd, London, UK), which contained 32 wells and was programmable as a unit. Using both machines was ideal because our targeted number of samples per iSeq 100 sequencing run was 40. The thermocycler program for the first stage PCR was: 2 min at 95°C, 35 cycles (coral and syringe method control) or 28 cycles (seawater) of 20 sec at 95°C, 20 sec at 55°C, and 5 min at 72°C, followed by 10 min at 72°C and a final hold at 12°C. The final hold at 12°C was used due to the limitations of the BentoLab termocycler; samples were removed within an hour of the completed PCR program and stored at 4°C until purification. The resulting PCR products from coral and syringe method control samples were purified as follows: 30 μl of PCR product per sample was mixed with 6 μl 5X loading dye (Bioline, London, UK) and separated using a 1.5% agarose gel stained with SYBR Safe DNA gel stain (Invitrogen, Thermo Fisher Scientific, Waltham, MA, USA). Bands of approximately 350 bp were excised by comparing to a 50 bp

ladder (Bioline), and subsequently purified using the MinElute Gel Extraction Kit (Qiagen) following manufacturer protocols. For seawater PCR products, 5 μl of product mixed with 1 μl 5X loading dye was visualized on a 1% agarose gel to verify successful amplification, and the remaining PCR product was purified with the MinElute PCR Purification Kit (Qiagen).

The second stage PCR procedure attached unique index primers to each sample using the Nextera XT v2 set A kit (Illumina). Purified DNA (5 μl) from stage one PCR products was added to a 50 μl reaction with the following: 5 μl Nextera index primer 1, 5 μl Nextera index primer 2, 5 μl $MgCl_2$ (GoTaq), 10 μl 5X colorless buffer (GoTaq), 0.5 μl Taq polymerase (GoTaq), 1 μl of 10 mM dNTPs (Promega), and 18.5 μl UV-sterilized, PCR-grade water. The PCR was run on the BentoLab or mini8 thermocyclers with the following program: 3 min at 95°C, 8 cycles of 30 sec at 95°C, 30 sec at 55°C, 30 sec at 72°C, followed by 5 min at 72°C and a final hold at 12°C. A subset of PCR products were visualized on a 1% agarose gel stained with SYBR Safe DNA gel stain (Invitrogen) using 5 μl product with 1 μl 5X loading dye (BioLine) to verify bands of approximately 450 bp, indicating successful attachment of sample-specific indexes. The stage two PCR products were purified with the MinElute PCR purification kit (Qiagen) following manufacturer protocols. Purified products were quantified using the Qubit 2.0 fluorometer dsDNA high sensitivity (HS) assay (Invitrogen) following manufacturer protocols to obtain stock concentrations in ng/μl. Concentrations were then converted to nM assuming average amplicon length of 450 bp and average nucleotide mass of 660 g/mol. Samples were diluted to 5 nM and pooled. Pooled samples were quantified via Qubit HS assay as before, and diluted to 1 nM, quantified again, and diluted to a loading concentration of 90 pM. A 10% spike-in of 90 pM PhiX Control v3 (Illumina, Inc.) was added to the pooled 90 pM library and 20 μl of the resulting library was run on the iSeq 100 System using paired-end 150 bp sequencing with adapter removal. Samples were sequenced over three sequencing runs.

Data analysis

All R scripts used for generating ASVs and producing figures were uploaded to GitHub. Forward reads were exclusively used for the downstream processing and data analysis due to minimal overlap between forward and reverse reads. The DADA2 pipeline (v.1.17.3; with parameters: *filterAndTrim* function: trimLeft = 19, truncLen = 145, maxN = 0, maxEE = 1, rm.phix = TRUE,

compress = TRUE, multithread = TRUE) was used to remove the 515F and 806R primers from all sequence reads, filter the reads for quality and chimeras, and generate amplicon sequence variants (ASVs) for each sample (Callahan *et al.*, 2016). This resulted in 17,190 ASVs of the same length (126 bp) across all samples. Taxonomy was assigned using the SILVA SSU rRNA database down to the species level where applicable (v.132) (Quast *et al.*, 2012). ASVs that classified to mitochondria, chloroplast, eukaryote, or an unknown Kingdom were removed from the analysis, resulting in 7,366 remaining ASVs. We further filtered our dataset to remove possible contaminants introduced by DNA extraction reagents and introduced by seawater into coral samples. The R package *decontam* (v. 1.6.0) was used to identify and remove DNA extraction contaminants in all samples (seawater, coral, and syringe method control) by using a combined frequency and prevalence method employing default parameters (Davis *et al.*, 2018). The method identified 26 ASV contaminants, of which only 11 contained enriched frequency in DNA extraction controls so those 11 ASVs were removed (DNA extraction contaminants summarized in Supporting Information Appendix S1, found online at https://doi.org/10.1111/1462-2920.15718). Because the syringe method by nature collects a significant portion of seawater, the coral samples were, in essence, "contaminated" by seawater and thus, the microorganisms most likely derived from seawater rather than coral tissue were removed. To do this, the coral samples were compared with the nine syringe method controls (seawater collected approximately a meter off of the benthos) using the prevalence model in *decontam,* which compares the presence/absence of ASVs within the syringe method controls to the coral samples. After applying the prevalence method, analysis of the distribution of the decontam score, *P*, was conducted to determine an appropriate threshold for identifying whether an ASV was a "contaminant" (i.e. seawater-derived) or an ASV that was tissue-associated. A threshold of 0.1 was chosen in order to be most conservative. While this conservative approach did not remove all ASVs typical of oligotrophic seawater taxa (e.g. *Synechococcus, Prochlorococcus*), a conservative approach here was necessary given the study goals of identifying potential SCTLD-associated ASVs residing in the surrounding seawater. The 184 ASVs identified as most prevalent in the nine syringe method controls (typically oligotrophic bacteria such as SAR11, *Prochlorococcus*, OM60 clade, *Synechococcus*, "*Candidatus* Actinomarina", AEGEAN-169 clade,

etc.) were generally found at low relative abundance in the coral samples (max relative abundance = 0.0074%) and were removed from the coral sample ASV table (contaminants summarized in Supporting Information Appendix S2). After the ASVs identified as contaminants were removed, the coral samples and the near-coral seawater samples were re-merged into one large dataset. The re-merged dataset then was filtered to remove sparse ASVs (present at a count of 0 in the majority of samples) by removing ASVs with a count less than 0.5 when averaged across all samples. This left 2,010 ASVs, which were used for all downstream analyses.

Count data were transformed to relative abundance and coral microbial communities were visualized using stacked bar charts. Data were then further log transformed following the addition of a pseudo count of one in preparation for beta diversity analyses. Bray-Curtis dissimilarity between samples was calculated using the R package *vegan* (v.2.5.7) and the resulting dissimilarities were presented in a Principal Coordinates Analysis (PCoA) (Oksanen *et al.*, 2020). Permutational Analysis of Variance (PERMANOVA) with 999 permutations, using the *adonis* function in *vegan* (Oksanen *et al.*, 2020), compared the Bray-Curtis dissimilarity of healthy and diseased corals to test the hypothesis that coral microbiomes are significantly different between healthy and SCTLD-afflicted samples. PERMANOVA was also used to test the hypotheses that species, reef location, and health state nested within species significantly structure the coral microbial community. We tested the same hypotheses on the near-coral seawater directly overlying the coral colony to determine if species, reef location, or health drove microbiome community structure in near-coral seawater. Dispersion of beta diversity within coral samples was calculated by measuring the distance to centroid within the PCoA as grouped by health state (HH and HD compared to DD) by implementing the *betadisper* function in *vegan* (Oksanen *et al.*, 2020). Significant differences in dispersion by health state was determined by an independent Mann-Whitney U test. Additionally, variability of beta diversity was measured by extracting the Bray-Curtis dissimilarity values calculated within a coral condition (diseased or healthy).

To detect ASVs enriched in diseased coral compared to healthy coral, we employed the R package, *corncob* (v.0.1.0) (Martin *et al.*, 2020). ASV raw counts for each sample were input into the corncob model, which models the relative abundances for each ASV with a logit-link for

mean and dispersion. Differential abundance of each ASV was modeled as a linear function of health state. Health state was defined as either healthy (healthy tissue from either apparently healthy or diseased coral) or diseased (lesion from diseased coral). The hypotheses that the relative abundance of a given ASV changed significantly with respect to coral health state were tested with the parametric Wald test. The multiple comparisons were accounted for by using a Benjamini-Hochberg false discovery rate correction with a cutoff of 0.5. Each test was conducted on the set of coral samples from an individual coral, then results were compared across corals. Following analysis of significantly differentially abundant ASVs in corals, we hypothesized that disease-associated ASVs would be recoverable in the near-coral seawater and graphed relative abundances of each disease-associated ASV in the near-coral seawater. We then employed corncob to test each identified disease-associated ASV using the differential abundance method described above to see if it was enriched at significantly higher abundances in seawater over diseased coral compared to healthy coral or apparently healthy colonies. Disease-associated ASVs were considered SCTLD bioindicators if they were enriched in diseased coral. Further, we searched for exact sequence matches between the 126 bp sequences of disease-associated ASVs reported here to the same sequence region from existing SCTLD-associated ASVs of longer lengths (approx. 253 bp) reported in other studies that also used the DADA2 pipeline. This pipeline allowed for sequences to be reported along with each ASV, enabling cross-study comparison (Callahan *et al.*, 2017).

Sequences of SCTLD bioindicator ASVs, were identified to the species level, when possible, as part of the DADA2 pipeline. To obtain better genus and species-level identification of SCTLD bioindicator ASVs and to relate these ASVs to other studies of coral disease-associated bacteria, we constructed phylogenetic trees for disease-associated ASVs classifying to *Vibrio, Arcobacter,* Rhizobiaceae, and Rhodobacteraceae. *Vibrio* and *Arcobacter* were targeted due to their increased representation in SCTLD-associated ASVs in this study and their previous association with SCTLD (Meyer *et al.*, 2019) and coral disease in general (Ben-Haim *et al.*, 2003; Ushijima *et al.*, 2012). Rhizobiaceae and Rhodobacteraceae were targeted for phylogenetic tree analysis given their previous association with SCTLD (Rosales *et al.*, 2020). Phylogenetic trees of coral-associated *Vibrio* and Rhodobacteraceae bacteria previously constructed from the Coral

Microbiome Database (Huggett and Apprill, 2019) were used as reference trees for the insertion of SCTLD-associated ASVs that classified as *Vibrio* or Rhodobacteraceae. Insertion of our short SCTLD-associated sequence reads was achieved using the 'quick add marked' tool in ARB (version 6.0.6.rev15220) (Ludwig, 2004). Trees produced from ARB were exported using xFig. Phylogenetic trees for *Arcobacter* and Rhizobiaceae were constructed de novo using tools from the CIPRES Science Gateway (Miller *et al.*, 2010). For each tree, long-read (~1,200 bp) 16S rRNA gene sequences from closely-related (>90% sequence similarity) culture collection type strains, strains isolated from the marine environment, or clone sequences from corals were recovered via BLAST searches of SCTLD-associated ASVs from the present study or previous studies (Meyer *et al.*, 2019; Rosales *et al.*, 2020) to the non-redundant nucleotide collection, compiled into a FASTA file, and used for a sequence alignment in MAFFT (v7.402) (Katoh, 2002). This sequence alignment was then used to generate a reference tree using RAxML-HPC (v.8) (Stamatakis, 2014) with the following commands to produce a bootstrapped maximum-likelihood best tree: raxmlHPC-HYBRID -T 4 -f a -N autoMRE -n [output_name] -s [input_alignment] -m GTRGAMMA -p 12345 -x 12345. Next, SCTLD-associated short sequence reads were compiled into a FASTA file and added to the long-read sequence alignment in MAFFT using the "--addfragments" parameter. The sequence alignment with both short and long reads and the reference tree were then used as inputs for the Evolutionary Placement Algorithm, implemented in RAxML (Berger *et al.*, 2011). RAxML was called as: raxmlHPC-PTHREADS -T 12 -f v -n [output_name] -s [long_and_short_read_alignment] -m GTRGAMMA -p 12345 -t [reference_tree]. The output tree including short read sequences (RAxML_labelledTree.[output_name]) was visualized and saved using the interactive tree of life (iTOL v5.6.3) (Letunic and Bork, 2016).

RESULTS

Output of field-based sequencing in a portable microbiome laboratory

Three field-based sequencing runs with the Illumina iSeq 100 system each generated about 2 GB of paired-end, 150 bp sequencing data. In total, 12,997,634 sequencing reads were

produced and used for subsequent data analysis. Each sequencing run lasted approximately 17 hours, and the runs were conducted on sequential days from February18th to 20th, 2020. The three days of sequencing produced high quality reads, with the forward reads containing 89.6%, 94.8%, and 89.8% of reads having a Q30 score or better, respectively. Following filtration of forward sequencing reads, the number of reads for the 49 coral samples ranged from 60,105 to 128,036, with an average of 99,177 (± 14,511) while the range for the 51 seawater samples was 68,527 to 119,141, with an average of 96,933 (± 10,218) (Table 2-S2). Thus, all samples were successfully sequenced with sufficient sequence reads for downstream analysis (60,000+ sequences). The average numbers of sequences recovered from the controls were as follows (average ± 1SD, n): Syringe method control samples (96,290 ± 7,542, n = 9), DNA extraction control samples (19,418 ± 11,672, n = 6), and PCR negative control samples (9,930 ± 904, n = 3) (Table 2-S2). Over the course of the three sequencing runs, the same mock community of 20 known bacteria was sequenced to verify consistency and success of sequencing and ASV generation over the three individual runs. Successful identification of all 20 exact amplicon sequence variants within the mock community was achieved from all three runs, though for each, additional sequence variants were also recovered.

Health state determines coral microbiome structure while near-coral seawater microbiomes change according to site

Visualization of microbial beta diversity in corals using Principal Coordinates analysis (PCoA) of Bray-Curtis dissimilarity revealed significant changes in the coral microbiota associated with health condition, coral species, and reef site (Figure 2-3a, Figure 2-S1, Figure 2-S2, Table 2-1). Permutational Analysis of Variance (PERMANOVA) tests comparing diseased (“DD”; n = 21) to healthy pooled from two sample types (healthy from diseased colonies, “HD”, and healthy from healthy colonies, “HH”; pooling occurred because samples from apparently healthy colonies from all species was not available; n = 28) revealed disease state as having a significant effect on coral microbiome composition (Figure 2-3a, $R^2 = 0.25$, $p < 0.001$). The effect of health state, irrespective of species, was slightly higher when split up by all three conditions (“HH”, “HD”, “DD”, Figure 2-3a, PERMANOVA, $R^2 = 0.26$, $p<0.001$). The effect of species on structuring coral microbial communities was also significant, though the effect size was smaller

than between healthy and diseased corals (Figure 2-3a, Figure 2-S1 to 2-S3, PERMANOVA, R^2 = 0.15, p<0.001). Interestingly, a PERMANOVA with disease state nested within coral species exerted an even greater effect, explaining 36% of microbiome structure (Figure 2-3a, R^2 = 0.36, p<0.001). Together, disease state, species, and the nested designation exerted a larger effect on the microbial community composition compared to site-based changes between Buck Island (n = 30) and Black Point (n = 19), though site did significantly structure the coral microbial communities (Figure 2-3a, Figure 2-S2 to 2-S3, Table 2-1, PERMANOVA, R^2 = 0.041, p = 0.031). Only two coral species, *C. natans* and *M. cavernosa,* were sampled at both Buck Island and Black Point. A PCoA of Bray-Curtis dissimilarity and subsequent PERMANOVA test on only those two species revealed site to be an insignificant factor in structuring the microbiome (Fig S2, PERMANOVA, R^2 = 0.04, p = 0.166), compared to health state (“HH” and “HD” vs. “DD”)(Fig S2, PERMANOVA, R^2 = 0.31, p<0.001).

Analysis of dispersion of beta diversity revealed significant differences between coral health states (healthy vs. diseased) (Figure 2-3b). The distance to centroid of all healthy corals (HH and HD) was significantly lower, though more variable, than that of diseased corals (independent Mann-Whitney U Test, p < 0.001, Figure 2-3b). Diseased microbiome beta diversity dispersion was higher and more consistent compared to healthy microbial beta diversity (Figure 2-3b). Healthy coral microbiomes were generally less dispersed (more closely clustered in the PCoA) except for a few samples, which were dispersed farther from the other healthy samples (Figure 2-3a,b). Furthermore, the range in raw Bray-Curtis dissimilarity values within each coral sample (healthy vs. diseased), reinforced the finding of increased beta diversity dispersion of diseased compared to healthy corals (Mann-Whitney U Test p < 0.001, Figure 2-S4).

The effect of disease state was also visible in the stacked bar plot of coral microbiomes (Figure 2-S5). Notably, *M. cavernosa* contained increased relative abundances of Deltaproteobacteria in diseased corals (Figure 2-S5b). *Clostridia* and *Campylobacteria* relative abundances were increased in diseased corals, though *Clostridia* was most prominent in diseased *M. cavernosa* and *C. natans*, while *Campylobacteria* was most prominent in diseased

O. franksi. (Figure 2-S5). Interestingly, Oxyphotobacteria (predominantly *Prochlococococcus* and *Synechococcus*) decreased in relative abundance in diseased coral (Figure 2-S5).

Near-coral seawater microbiomes (n = 51, Table 2-1) taken within 5 cm of the coral surface were clearly distinct from coral microbiomes (n = 49, Table 2-1), but structured according to site (PERMANOVA $R^2 = 0.67$, $p < 0.001$) and not disease state (PERMANOVA $R^2 = 0.005$, $p = 0.921$) (Figure 2-3c, Figure 2-S1). Coral species also significantly affected the composition of the overlying seawater (Figure 2-3c, PERMANOVA, $R^2 = 0.22$, $p = 0.004$).

Coral disease bioindicators

To detect potential bioindicators of SCTLD, we used the beta-binomial regression model of the *corncob* R package (Martin *et al.*, 2020) to test for differentially abundant ASVs between healthy (HH and HD) and diseased (DD) corals individually for each species (Table 2-1 for sample replication). The model recovered 25 ASVs that were significantly more abundant, i.e. enriched and herein referred to as bioindicators, in the diseased sample of at least one of the coral species (Figure 2-4, Table 2-S3, Figure 2-S6 to 2-S9). Ten of those 25 ASVs were enriched in diseased samples of more than one coral species but none were enriched in all species (Table 2-S3, Figure 2-S6 to 2-S9). Nonetheless, some ASVs, such as ASV44 (*Fusibacter*), were enriched in diseased coral from all species, though the trend was not always significant. The 25 bioindicator ASVs classified as belonging to 12 Families and 14 genera. Families with multiple bioindicator ASVs were Arcobacteraceae, Desulfovibrionaceae, Family XII of the order Clostridiales, Rhodobacteraceae, and Vibrionaceae (Table 2-S3). Within these, four ASVs belonged to the genera *Arcobacter*, five to *Vibrio*, and three to *Fusibacter*.

In addition to identifying ASVs enriched in diseased coral, the differential abundance analysis revealed other ASVs that were depleted in diseased relative to healthy samples, and were therefore healthy coral-associated (coefficient < 0, Figure 2-S6 to 2-S9). *M. meandrites* had only one ASV enriched in healthy samples (Family Terasakiellaceae from Rhodospirillales; Figure 2-S9). Healthy samples of *C. natans* (Figure 2-S6) and *M. cavernosa* (Figure 2-S7) were enriched with ASVs belonging to Clades Ia, Ib, and unclassified Clade II of SAR11, the NS4 Marine Group and NS5 Marine Group of Flavobacteriaceae, *Prochlorococcus* MIT9313*, Synechcococcus* CC9902, and unclassified SAR116. Healthy *C. natans* also was enriched in ASVs

belonging to unclassified Rhodobacteraceae, Clade 1a Lachnospiraceae, and OM60 (NOR5) clade of Halieaceae. Unique healthy-associated ASVs in *M. cavernosa* included 11 diverse taxa (Figure 2-S7). Healthy coral-associated ASVs from *O. franksi* largely represented taxa found in healthy corals from at least one of the other species targeted in this study (Figure 2-S8). One unclassified Arcobacteraceae ASV was associated with healthy *O. franksi*, as well as two *Endozoicomonas* ASVs (ASV99, ASV108).

Disease bioindicator taxa recovered within near-coral seawater

Previous studies indicated that seawater may be a vector for the SCTLD pathogen(s); therefore, we hypothesized that the seawater within 5 cm of coral lesions would harbor the 25 SCTLD bioindicator ASVs we identified from corals. A differential abundance test of the 25 bioindicator ASVs in seawater overlying disease lesions (DD, n = 22, Table 2-1) compared to healthy corals (HH and HD, n = 29, Table 2-1) did not find significant enrichment of those ASVs in seawater over diseased lesions. We further tested the 25 bioindicator ASVs in near-coral seawater over apparently healthy colonies compared to disease lesion colonies of *M. cavernosa,* the only species for which we had sufficient replication of apparently healthy colonies and found no ASV significantly enriched in waters overlying diseased corals. Despite the lack of significant enrichment of putative pathogens within near-coral lesion seawater, we did observe all 25 bioindicator ASVs in the near-coral seawater over diseased corals, except for two ASVs (*Cohaesibacter* ASV226 and *Desulfovibrio* ASV185). Several of the SCTLD-associated ASVs were present in seawater overlying all four diseased coral species, including *Algicola* (ASV52), *Arcobacter* (ASV21, ASV101), *Halodesulfovibrio* (ASV13), *Marinifilum* (ASV39), and *Vibrio* (ASV20) (Figure 2-5). Interestingly, ASV34, an unclassified Rhodobacteraceae, was found only in near-coral seawater directly overlying disease lesions, but not over healthy corals across all species (Figure 2-5). Overall, disease-enriched bacteria were identified at low levels (<1.5% relative abundance) in near-coral seawater, though there was no significant enrichment of these taxa over diseased coral.

Phylogenetic analysis of SCTLD-enriched taxa

Given the high representation of *Arcobacter*, *Vibrio,* Rhizobiaceae and Rhodobacteraceae ASVs in the bioindicator ASVs, we produced phylogenetic trees to better

predict species-level identifications and to relate the ASVs to other sequences associated with coral disease, sequences from the Coral Microbiome Database (Huggett and Apprill, 2019) and SCTLD-associated ASV sequences reported from two previous studies (Meyer *et al.*, 2019; Rosales *et al.*, 2020). Phylogenetic analysis of the Campylobacterota (formerly Epsilonbacteraeota) genus *Arcobacter* spp. indicated no close relationship of the SCTLD-associated ASVs to described *Arcobacter* isolates. Instead, all SCTLD-associated ASVs grouped in clades with coral-associated or coral disease sequences (Figure 2-S10).

Phylogenetic analysis of the SCTLD bioindicator ASVs from the gammaproteobacterial genus *Vibrio* leveraged a reference tree previously constructed using existing coral-associated sequences found in the Coral Microbiome Database (Huggett and Apprill, 2019), *Vibrio* type strains and a SCTLD-associated *Vibrio* ASV by Meyer and colleagues (2019). ASV20 displayed high sequence identity to *V. harveyi* ATCC 35084, an isolate obtained from a brown shark kidney following a mortality event (formerly known as *V. carchariae* (Grimes *et al.*, 1984; Pedersen *et al.*, 1998) (Figure 2-S11). Interestingly, *Vibrio* ASV54 in the present study was an exact sequence match to a longer (253 bp) SCTLD-associated ASV reported previously (Meyer *et al.*, 2019), and this sequence is novel to corals (Table 2-2, Figure 2-S11). The remaining bioindicator ASVs 96, 67, and 25 all displayed high sequence identity to other coral-associated *Vibrio* sequences (Figure 2-S11).

We produced a phylogenetic tree with all known SCTLD-associated ASVs that classified to Rhizobiaceae, sequences from other coral disease studies, and other related sequences (Figure 2-S12). One bioindicator ASV from the present study (ASV226) was identical in the 126 bp overlapping region to a previous SCTLD-associated ASV11394 (Rosales *et al.*, 2020), and both grouped with *Cohaesibacter marisflavi*, a bacterium that has been isolated from seawater (Table 2-2, Figure 2-S12). ASV18209 and ASV19474 also fell within the *Cohaesibacter* genus, close to sequences isolated from White Plague-affected corals (Figure 2-S12). SCTLD-associated ASV19959, ASV30828, and ASV16110 from Rosales *et al.* (2020) were most closely related to *Pseudovibrio denitrificans* NRBC 100300 (Figure 2-S12). Finally, the unclassified Rhizobiaceae ASV34211 and ASV24311 (Rosales *et al.*, 2020) were closely associated to isolates of *Hoeflea* spp. and *Filomicrobium* spp., respectively (Figure 2-S12).

Phylogenetic analysis of SCTLD bioindicators that classified as Rhodobacteraceae using a reference tree generated from the Coral Microbiome Database (Huggett and Apprill, 2019) revealed close classification to bacteria associated with coral hosts that were distinct from existing isolates (Figure 2-S13). Several SCTLD-associated ASVs from Rosales and colleagues (2020) (ASV15252, ASV24736, ASV13497, ASV3538, and ASV29944) were related to sequences from ballast water and hypersaline mats rather than coral sequences (Figure 2-S13). In contrast, the SCTLD bioindicator ASV60 from the present study had high sequence identity to other coral-associated Rhodobacteraceae sequences with no definitive classification, though related to *Phaeobacter* (Figure 2-S13). Several Rhodobacteraceae ASVs classified to *Thalassococcus* sequences (ASV29894, ASV25482, ASV29283 from Rosales *et al.* (2020)) and ASV111 from the present study (exact sequence match to ASV29283 from Rosales *et al.* (2020)). Finally, SCTLD-associated ASV34 classified within the likely *Marinovum* genus alongside many coral-associated sequences (Figure 2-S13).

DISCUSSION

To better understand the effect of Stony Coral Tissue Loss Disease on coral reefs in the U.S. Virgin Islands, an area with an active and detrimental SCTLD outbreak (VI-CDAC, 2021), we developed and integrated a rapid, field-based 16S rRNA gene sequencing approach to characterize microbiomes of coral and near-coral seawater of SCTLD-infected colonies. St. Thomas, USVI does not have a molecular ecology laboratory or sequencing facility; therefore, we transformed a home rental on the island to a molecular laboratory, and in the span of two weeks, we carried out a complete microbiome workflow, from sample collection to sequencing. This short timeline enabled us to process fresh samples, gather data more quickly, and begin data analysis in the following months, which revealed significant differences between healthy and diseased coral, regardless of coral species or reef location. Differential abundance analysis identified 25 SCTLD bioindicators, all of which were present in the seawater directly overlying coral. Furthermore, these bioindicator ASVs represented sequences with high sequence identity

to the 16S sequence of the *Vibrio harveyi* pathogen, as well as sequences previously identified in diseased corals.

SCTLD lesion microbial communities are unique from healthy microbial communities

We identified clear and consistent differences between healthy and diseased coral microbiomes, regardless of location and species of coral. In addition, the dispersion of beta-diversity was consistently higher among the diseased corals, compared to all healthy corals, which had reduced, yet more variable dispersion of beta diversity. This greater beta diversity across diseased coral microbiomes could be indicative of some level of microbial dysbiosis associated with disease (MacKnight *et al.*, 2021). Alternatively, the syringe-based collection method results in a homogenate of newly compromised, diseased tissue, as well as necrotic or sloughed off tissue that likely captures potential pathogen(s), organisms involved in secondary infections, or even saprophytic microorganisms proliferating off the exposed skeleton and dead coral tissue (Burge *et al.*, 2013; Egan and Gardiner, 2016). For example, the finding of increased Deltaproteobacteria in diseased samples of *M. cavernosa,* and the significant enrichment of *Halodesulfovibrio,* known sulfate-reducing bacteria, may have been a signature of the exposed coral skeleton (Y.-H. Chen *et al.*, 2019), or perhaps anaerobic degradation of coral tissue (Viehman *et al.*, 2006). Overall, the finding that disease impacts coral microbiome structure in the USVI is supported by previous findings that show shifts in coral microbiomes between healthy and diseased corals in Florida, USA (Meyer *et al.*, 2019; Rosales *et al.*, 2020).

While this study did not identify causative agents of SCTLD, the differential abundance analysis between healthy and diseased coral microbial communities revealed 25 disease bioindicator ASVs, which may represent potential pathogens or opportunistic bacteria relevant for future experimental work. Of these, we identified one ASV (ASV20), with 100% similarity in the overlapping region to *V. harveyi* (EU130475.1), a pathogen isolated from a shark mortality event, and shown to be virulent for spiny dogfish (*Squalus acanthias*) (Grimes *et al.*, 1984). This ASV was consistently detected in diseased coral (DD samples), including all *C. natans, M. meandrites* and *O. franksi* colonies, and two-thirds of the *M. cavernosa* colonies, at relative sequence abundances of 5% or lower. Additionally, this ASV was frequently recovered in the HD and HH colonies, and most near-coral seawater samples, indicating its broad prevalence in

these diseased reefs. Interestingly, *V. harveyi* has been suggested as the causative agent of white syndrome disease in aquaria and field-based corals (Luna *et al.*, 2010). Despite the prevalence of *V. harveyi* sequences in the present SCTLD study, this was not a SCTLD-associated bacterium identified in the Florida-based studies. Still, it seems relevant to examine pathogenicity of *V. harveyi* in future coral disease experiments.

Four of our SCTLD bioindicator ASVs were identical to ASVs identified in Florida-based SCTLD studies. *Algicola* ASV52 and *Vibrio* ASV54 were identical to ASVs identified in Florida by Meyer *et al.* (2019). These sequences have been associated with coral disease in the past (black band disease or white plague disease type II; reviewed by Meyer *et al.* 2019), but were phylogenetically distinct from other known coral-associated lineages (Figure 2-S11). Furthermore, although not significant in all coral species, the noticeable enrichment in abundance of both ASV52 (*Algicola*) and ASV54 (*Vibrio*) in corals may be biologically relevant, given their association with SCTLD-affected corals sampled in Florida approximately 1,800 km away (Meyer *et al.*, 2019).

Two other bioindicator ASVs in the present study, *Cohaesibacter* (ASV226) and *Thalassobius* (ASV111), matched identical regions of ASVs enriched in a study of Florida-based SCTLD-associated microbiomes by Rosales et al. (2020). In our study, *Cohaesibacter* ASV226 was enriched in diseased *O. franksi,* but barely detected in other corals. Rosales *et al.* (2020) detected the same ASV in *S. intercepta, D. labyrinthiformis,* and *M. meandrites* affected by SCTLD. Phylogenetic analysis placed those two similar sequences (ASV226 and ASV11394, Figure 2-S12) with *Cohaesibacter marisflavi*, a species not currently known to be a pathogen (Qu *et al.*, 2011). Although no *Cohaesibacter* species are known pathogens, *C. intestini* was isolated from the intestine of an abalone (Liu *et al.*, 2019). Two *Cohaesibacter* sequences identified by Rosales *et al.* (2020) were related to sequences previously isolated in cases of coral disease, indicating *Cohaesibacter* may be an important target for future study. Additionally, *Thalassobius* (ASV111) was an exact match to one of eight Rhodobacteraceae ASVs enriched in diseased corals in the Rosales *et al.* (2020) study. In the present study, this ASV was significantly enriched only in *C. natans,* but was generally present in all diseased corals. Furthermore, these ASVs, and two other disease-associated ASVs (ASV29894 and ASV25482)

from Rosales *et al.* (2020) classified as unique unclassified coral bacteria and coral white plague disease afflicted, respectively. Interestingly, several of the SCTLD-associated ASVs added into the Rhodobacteraceae phylogenetic tree were more closely associated to sequences from hypersaline mat or ballast water environments than coral-associated sequences. Despite variability in putative identity of the diverse Rhodobacteraceae sequences associated with SCTLD, exact sequences recovered from diseased corals across geographic regions in the Caribbean (Florida, USA, and USVI) may indicate some concordance in the effect of this disease on different coral species regardless of geography.

It should be noted that there are some methodological differences between the SCTLD studies, which could impact the microbial sequences recovered and compared. The studies all utilized the same primers, but the sequencing platforms differed in read length; the previous studies used merged reads, enabling a total read length of approximately 253 bp, whereas this study used 126 bp forward reads due to sequencing of primers. Although our amplicons are shorter and we only used forward reads, classification and taxonomic certainty does not decrease linearly with amplicon size, and may be between 71.1-83.2% accurate at the genus level compared to full length small subunit rRNA sequences (Wang *et al.*, 2007) and even up to 99% confident at the phylum level compared to the approximately 253 bp V4 region targeted by the 515F and 806R primers (Liu *et al.*, 2020). Despite this, it should be noted that identical 16S rRNA sequences do not always indicate identical species or genera, when analyzed at the whole genome level (Stackebrandt and Goebel, 1994). All three studies compared here employed the DADA2 analysis pipeline, resulting in sequences published alongside ASV identifiers, allowing for comparison of amplicon sequence variants across studies, a significant benefit of the DADA2 pipeline (Callahan *et al.*, 2017). Lastly, we did take care to insert the shorter amplicon sequences into a phylogenetic framework based on longer read sequences. Overall, the placement of the ASVs appear robust, but additional marker genes or genomes are necessary to confirm the taxonomies affiliated with the ASV-based sequences.

Similar to previous reports for white plague disease, it could be that both bacteria and viruses play a role in SCTLD onset and virulence. Antibiotic pastes containing amoxicillin have been shown to be effective at slowing and halting progression of SCTLD (Aeby *et al.*, 2019;

Neely *et al.*, 2020). Despite this, we cannot rule out the role of viruses in this disease, which have been shown to play a role in white-plague-like diseases (Soffer *et al.*, 2014). We did not investigate viruses in our study, but metagenomic and microscopic techniques that investigate holobiont components, such as bacteria, archaea, DNA and RNA-based viruses, and fungi, should be employed in the future. Finally, due to limited availability, this study lacks replication of samples from apparently healthy colonies ("HH") and future work could aim to prioritize collection of samples from apparently healthy colonies, as it would serve as an important baseline for comparison.

Signals of SCTLD infection in near-coral seawater

Bioindicator microbes identified as SCTLD-enriched were broadly recoverable in near-coral seawater (<5 cm) surrounding the coral colonies, in agreement with a current hypothesis that seawater is the disease vector (Aeby *et al.*, 2019). However, seven ASVs were found in fewer than five of the nine samples. According to the differential abundance comparison, none of the disease bioindicator ASVs were significantly enriched in seawater overlying diseased compared to healthy areas of the corals, though the relative closeness (<30 cm) between healthy and diseased seawater samples may have mixed this signal. The largest driver of differences in near-coral seawater microbial communities was location. The two reefs we sampled were distinct reefs approximately 12 km away from each other and featured overall similar environmental conditions (Table 2-S1).

Beyond seawater, recent evidence suggests that sediments surrounding coral may play an important role as a reservoir of SCTLD pathogens (Rosales *et al.*, 2020) though that was not sampled here. Future investigations into SCTLD vectors should aim to sample both near-coral sediments and seawater, both *in situ* and in isolated mesocosm tanks to provide further information on the likely modes of transmission of SCTLD pathogens.

Rapid and portable microbiome profiling is feasible and applicable to marine diseases

Here we successfully implemented an in-the-field microbiome protocol to rapidly gather data on microbiome composition associated with the destructive coral disease, SCTLD. Illumina launched the iSeq 100 System only recently, in 2018. It is the smallest (1 foot cube), cheapest, and most portable Illumina technology to date and features a single-use cartridge that houses

all sequencing reagents, further contributing to its ease of use. Following three sequencing runs, the number of reads generated by the iSeq per sample was comparable to those recovered in a previous study of SCTLD microbiomes that used MiSeq sequencing for the same region of DNA and the same sample collection method (Meyer *et al.*, 2019). Overall, the Illumina iSeq 100 System could be an ideal target for future studies on marine disease outbreaks, when there is a need for rapid information and results to better inform remediation and management of such disease outbreaks.

The present workflow could be applied again to SCTLD research, with some improvements. Although the data were gathered within 10 days of the project start, data analysis still took months. To circumvent this, all data analysis scripts are saved and easily accessible on GitHub, so future data could be easily processed and compared to the present findings. Additional work could focus on producing data analysis scripts that incorporate predictive, machine-learning algorithms to analyze the microbial communities in coral mucus or tissue and identify microbial predictors of SCTLD, similar to work that identified microbial predictors of environmental features within reef seawater microbiomes (Glasl *et al.*, 2019). This could allow scientists the potential to identify corals afflicted with SCTLD before entire colonies are killed, and within the timeline of fieldwork or research cruises. Additionally, as more is learned about the identity of individual marine pathogens, then targeted pathogen identification approaches in novel systems may become more straightforward.

Conclusion

Stony Coral Tissue Loss Disease has collectively affected hundreds of kilometers of coastal and offshore reefs in the Caribbean, with no present indication of stopping. This study developed and implemented a field-based, rapid microbiome characterization pipeline in the USVI, an area more recently affected by the SCTLD outbreak. Following successful sequencing on the Illumina iSeq 100, we identified 25 SCTLD bioindicator ASVs that may represent putative pathogens, including, *V. harveyi*, a bacterium known to be pathogenic in other marine systems. Many of the 25 bioindicator ASV sequences enriched in diseased coral were recovered in near-coral seawater, a potential reservoir for pathogens and the hypothesized vector for SCTLD. Interestingly, four of the SCTLD bioindicator ASVs identified in our study exactly matched

sequences previously reported as enriched in SCTLD lesion samples. Phylogenetic analysis revealed that many of the disease bioindicator ASVs were related to likely novel coral or coral-associated disease bacteria. Future investigations aimed at isolating and characterizing those microorganisms and other SCTLD bioindicator bacteria would better determine if these organisms are pathogens or opportunists, and how they potentially target and grow around or within coral hosts. In the present study, the successful integration of a rapid pipeline for studying coral disease generated data more quickly, and subsequent analysis revealed differences in microbiome structure associated with the SCTLD outbreak in the USVI. This contributes to the growing body of literature on SCTLD that is largely focused in Florida, USA. Finally, we found that this rapid microbiome characterization approach worked well for identifying microbial bioindicators of coral disease, and it may have useful applications to marine diseases more broadly.

ACKNOWLEDGEMENTS

The authors would like to thank Lei Ma, Joseph Townsend, Kathryn Cobleigh, Sonora Meiling, and Kelsey Beavers for field assistance and Illumina Inc. for technical assistance. Additionally, we would like to thank Laura Weber for assistance with iSeq protocol development and field assistance. This work was funded by The Tiffany & Co. Foundation, NSF OCE-1928753, OCE-1928761 and OCE-1938147, the Rockefeller Philanthropy Advisors, Dalio Foundation, and other generous donors of the Oceans 5 project. Samples were collected under permit DFW19057U. We would also like to thank Stefan Sievert, Harriet Alexander, and Tami Lieberman for helpful comments on the manuscript.

DATA AVAILABILITY

Raw sequence reads were deposited into the NCBI GenBank under BioProject accession number PRJNA672912. Metadata associated with the study are also found at BCO-DMO under dataset 833133 (https://www.bco-dmo.org/dataset/833133). All R scripts used to generate

figures and statistical tests are saved and publicly available on GitHub at https://github.com/CynthiaBecker/SCTLD-STT. Supplementary information in the form of Appendix S1 and Appendix S2 can be found online at the publisher's website at: https://doi.org/10.1111/1462-2920.15718

FIGURES AND TABLES

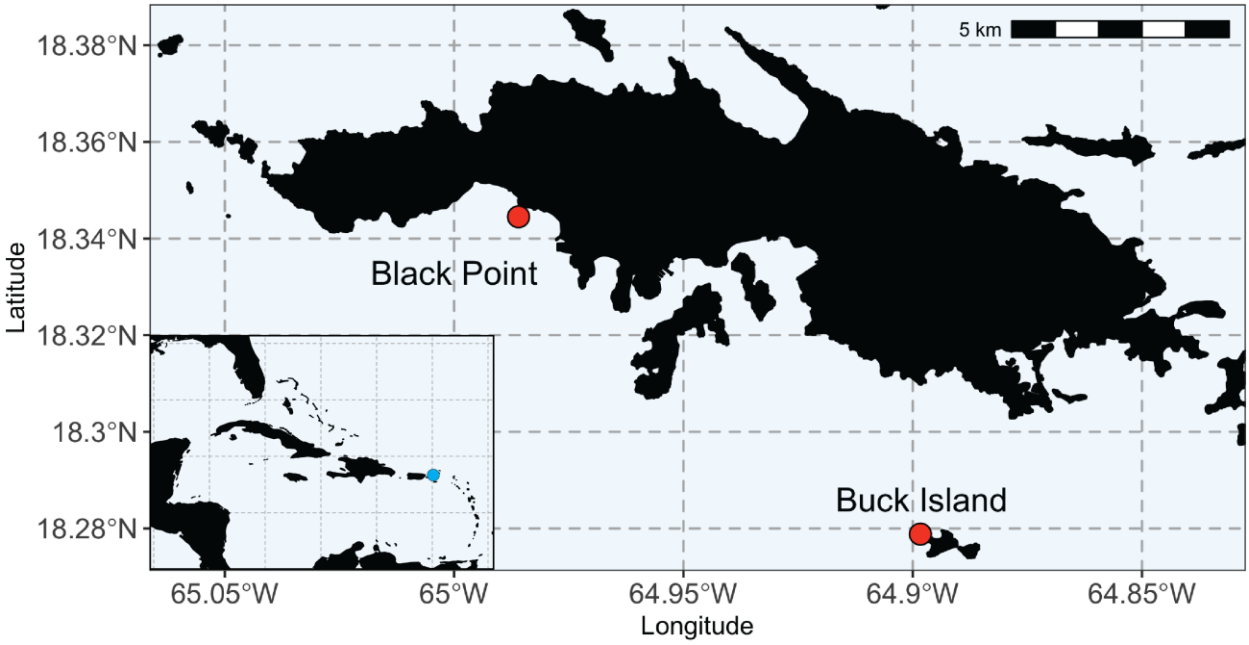

Figure 2-1. Sampling locations
Sampling locations at Black Point and Buck Island reefs in St. Thomas, U.S. Virgin Islands. St. Thomas sampling locations included a reef at Black Point, which was experiencing SCTLD for 13 months prior to sampling and a reef at Buck Island, in which SCTLD broke out in the month prior. Scale bar is 5 km with marks at every kilometer. Inset map shows the greater Caribbean with the blue dot noting the location of the U.S. Virgin Islands.

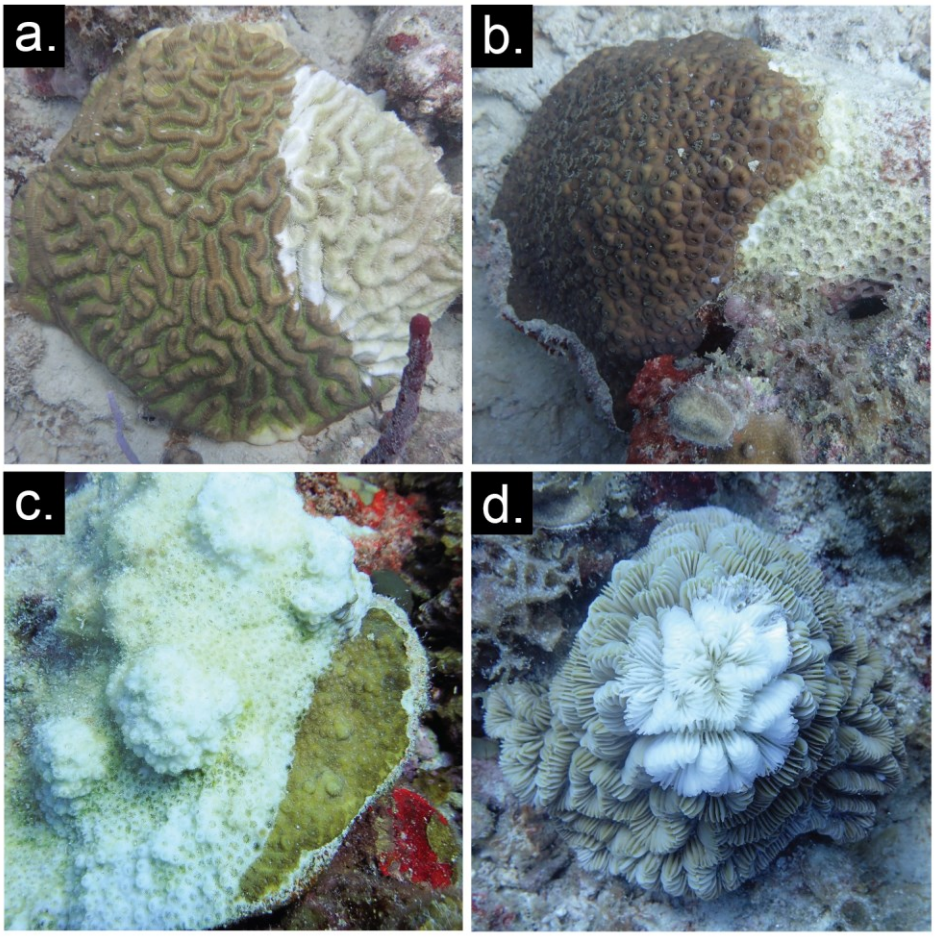

Figure 2-2. Stony coral tissue loss disease lesions progress across healthy tissue.
Photos represent typical disease appearance on the following corals included in the present study: (a) *Colpophyllia natans,* (b) *Montastraea cavernosa,* (c) *Orbicella franksi,* (d) *Meandrina meandrites*. Seawater and coral were sampled at the lesion front and 10 cm away from the lesion, or as far as possible from the lesion, when possible.

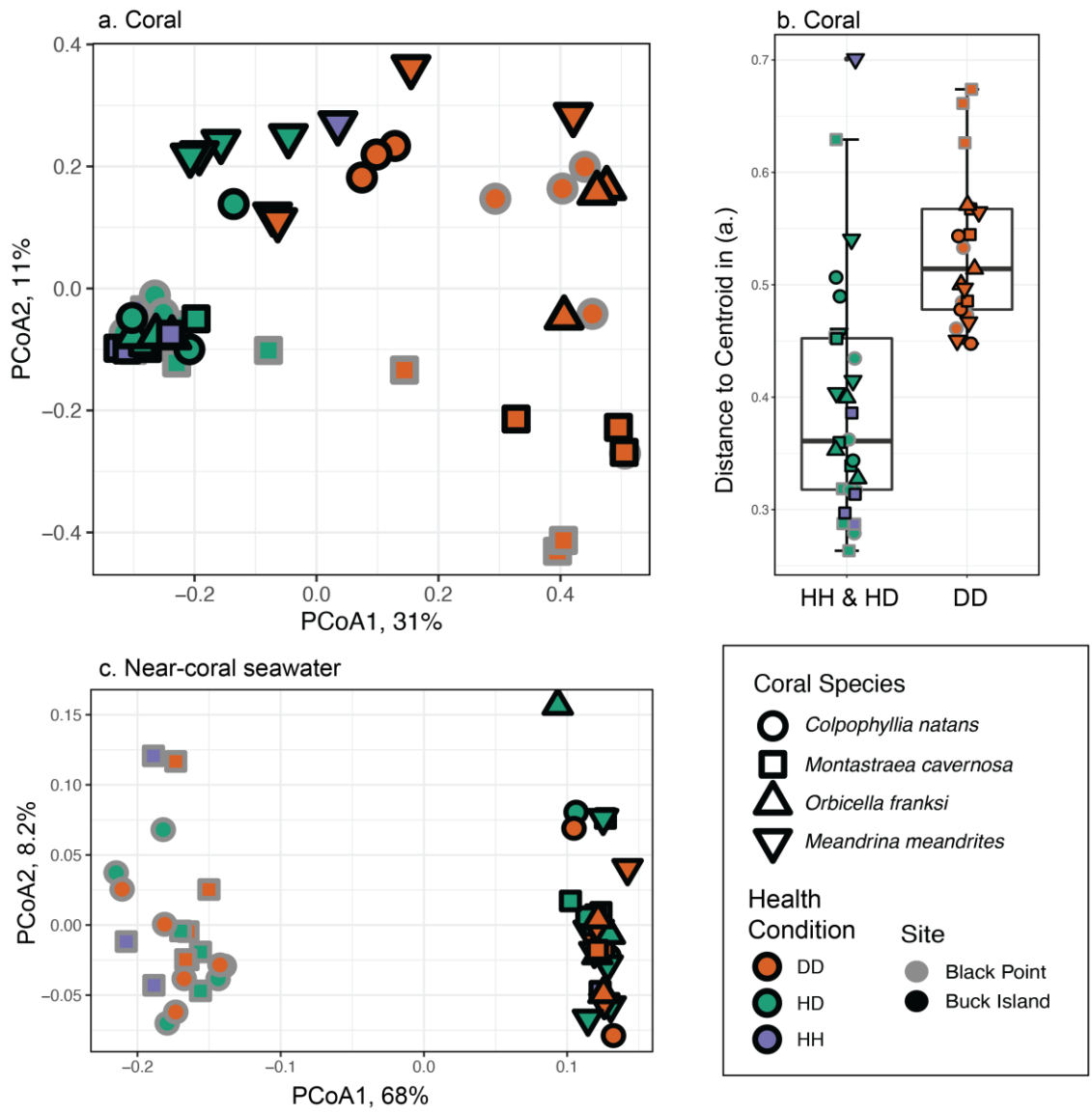

Figure 2-3. PCoA and beta dispersion

Coral microbiomes differed according to health condition and near-coral seawater microbiomes differed according to site. (a) Principal coordinate analysis (PCoA) displays Bray-Curtis dissimilarity of coral microbial communities, (b) beta diversity dispersion of coral microbiomes represented by boxplots of the distance to centroid in (a), and (c) PCoA of Bray-Curtis dissimilarity in near-coral seawater microbiomes. Fill color represents health condition of the sample as diseased (DD, orange), healthy sample from a diseased colony (HD, green), or healthy sample from an apparently healthy colony (HH, purple). Outline color indicates the reef where the sample was taken, which had either existing SCTLD infection (Black Point, gray), or was experiencing a recent (<1 month) outbreak of SCTLD (Buck Island, black). Shape represents species of coral sampled: *Colpophyllia natans* (circle), *Montastraea cavernosa* (square), *Orbicella franksi* (up triangle), and *Meandrina meandrites* (down triangle).

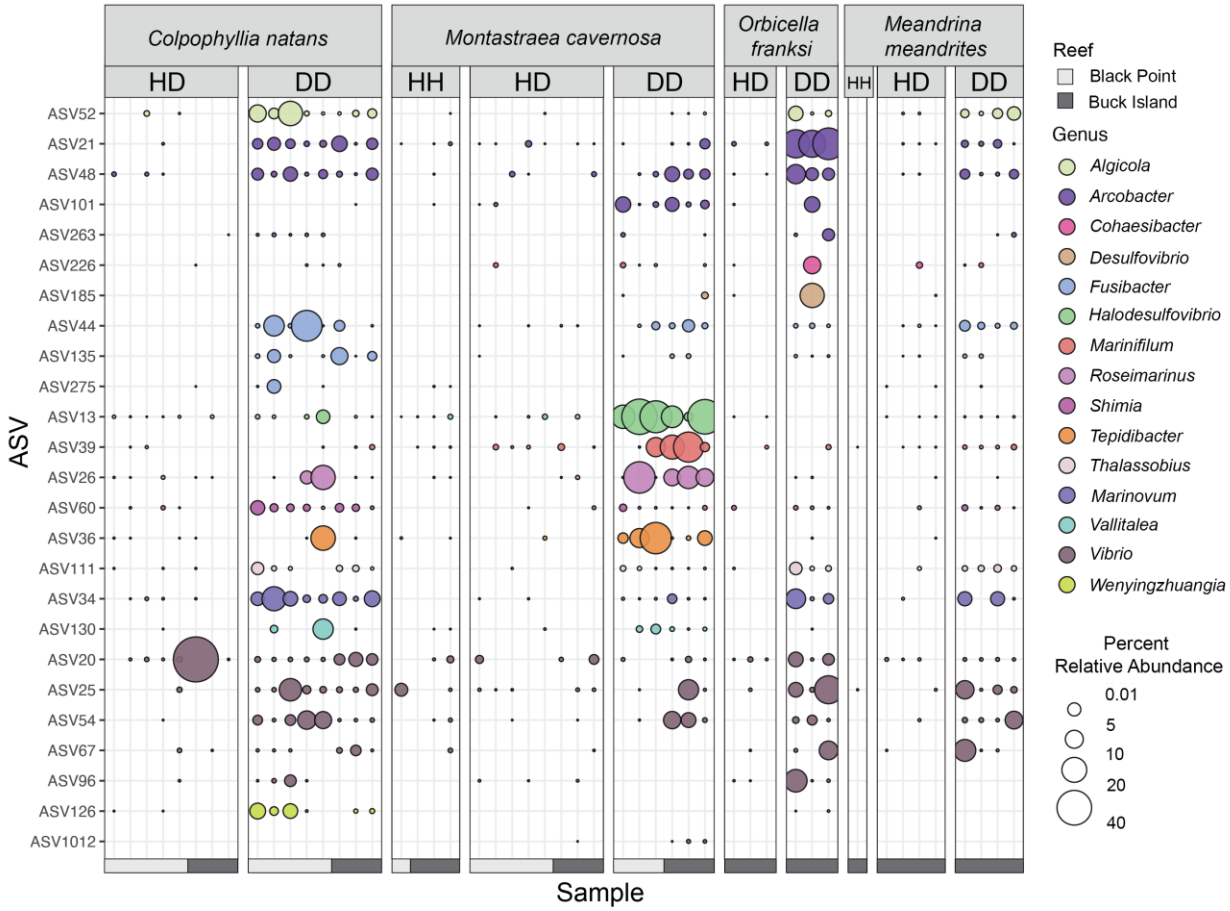

Figure 2-4. SCTLD bioindicator ASVs

Relative abundances of 25 SCTLD bioindicator ASVs significantly differentially enriched (FDR corrected p-value < 0.05) in diseased coral of at least one coral species. Samples on the x-axis are organized by coral species (*Colpophyllia natans*, *Montastraea cavernosa*, *Meandrina meandrites*, and *Orbicella franksi*), health state of the coral (healthy sample from apparently healthy colony = "HH", healthy sample from diseased colony = "HD", disease lesion = "DD"). Additionally, a color bar at the bottom indicates the coral was collected at the Black Point (light gray) or at the Buck Island (dark gray). ASVs on the y-axis are organized and colored by Genus. Percent relative abundance of each ASV is represented by the size of the colored circle, with a percent relative abundance of zero represented by the absence of a circle or dot. The relative abundances were calculated after removing common seawater bacteria and archaea, which were determined using the syringe method control samples containing ambient reef seawater and with the R-package *decontam* (see methods).

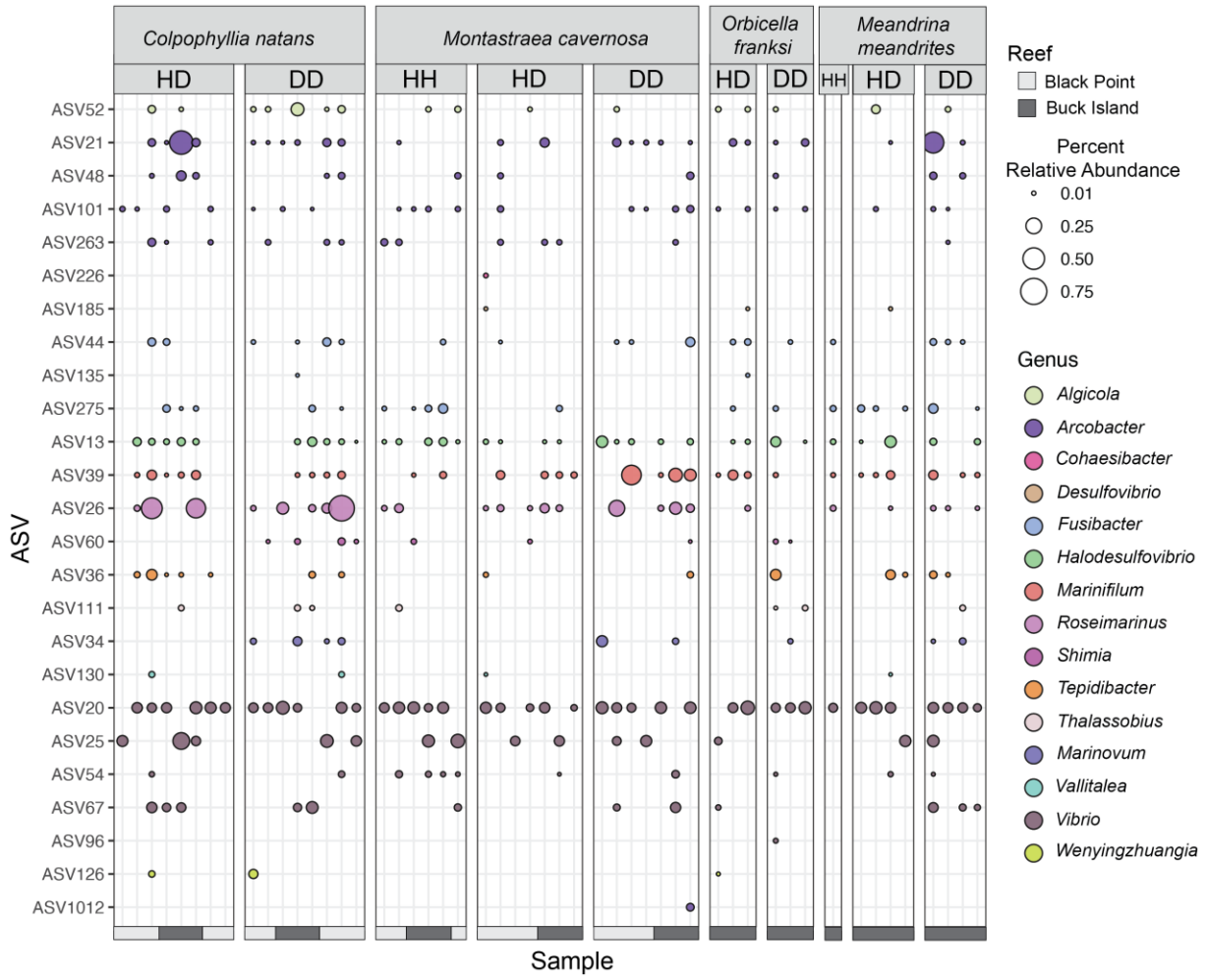

Figure 2-5. SCTLD bioindicator ASVs in near-coral seawater

SCTLD bioindicator ASVs identified in coral were found in near-coral seawater. Samples on the x-axis are organized by coral species (*Colpophyllia natans*, *Montastraea cavernosa*, *Meandrina meandrites*, and *Orbicella franksi*), and health state of the coral (healthy sample from apparently healthy colony = "HH", healthy sample from diseased colony = "HD", disease lesion = "DD"). Additionally, a color bar at the bottom indicates whether the coral was collected at Black Point (light gray) or at Buck Island (dark gray). ASVs on the y-axis are organized and colored by Genus. Percent relative abundance of each ASV is represented by the size of the colored circle, with a percent relative abundance of zero represented by the absence of a circle or dot. ASVs graphed are those identified by differential abundance analysis as significantly enriched in diseased coral (FDR corrected p-value < 0.05) of at least one coral species.

Table 2-1. Number of near-coral seawater (SW) and coral samples collected from Buck Island or Black Point reefs on St. Thomas, USVI.

	Buck Island			Black Point		
	HH	HD	DD	HH	HD	DD
Colpophyllia natans	0	3	3	0	5	5
Montastraea cavernosa	3	3	3	3 SW* 1 Coral*	4 SW* 5 Coral*	4 SW* 3 Coral*
Orbicella franksi	0	3	3	0	0	0
Meandrina meandrites	1	4	4	0	0	0

*Sample sizes from *M. cavernosa* from the Existing disease reef were different between seawater and coral due to sampling and processing constraints.

Table 2-2. Bioindicator ASVs in the present study with 100% sequence similarity over 126 bp to SCTLD-associated ASVs of a longer length (~253 bp) identified by previous studies.

Family	Genus	ASV ID in present study	Enriched in diseased coral (Rosales et al. 2020)	Enriched in diseased coral (Meyer et al. 2019)
Pseudoalteromonadaceae	*Algicola*	52	no	**Yes**
Rhizobiaceae	*Cohaesibacter*	226	**Yes**	no
Rhodobacteraceae	*Thalassobius*	111	**Yes**	no
Vibrionaceae	*Vibrio*	54	no	**Yes**

SUPPLEMENTARY INFORMATION

Table 2-S1. Environmental conditions present at Buck Island or Black Point reefs

Reef	Buck Island	Black Point
Lat (dd)	18.27883	18.34450
Lon (dd)	−64.89833	−64.98595
Depth (m)	14.1	5.2
Temperature (°C)	26.88	26.98
Salinity	35.98	36.04
Dissolved Oxygen (% sat.)	102.5	105.0
pH	7.98	8.09
Turbidity (NTU)	−0.05	0.12

Table 2-S2. Summary statistics of sequencing reads produced by three sequencing runs on the Illumina iSeq 100 System, outlined by sample type.

Sample Type	Average	Standard Deviation	Minimum	Maximum
Seawater (n = 51)	96,933	10,218	68,527	119,141
Coral (n = 49)	99,177	14,511	60,105	128,036
Syringe Method Control (n = 9)	96,290	7,542	85,728	113,293
DNA Extraction Control (n = 6)	19,418	11,672	1,908	34,118
PCR Negative Control (n = 3)	9,930	904	8,928	10,683
Mock Community (n = 3)	74,735	12,494	61,401	86,172

Table 2-S3. Summary of coral species featuring significant enrichment (FDR corrected p-value < 0.05) of SCTLD bioindicator ASVs in disease lesion (DD) compared to healthy coral (HH and HD combined). White cells indicate no significant difference in the relative abundance of the ASV between healthy and diseased corals. Differential abundance of ASVs was calculated using the beta-binomial regression model of the R-package *corncob* and ASVs were considered significant at an FDR corrected p-value <0.05.

Family, Genus	ASV ID	*Colpophyllia natans*	*Montastraea cavernosa*	*Orbicella franksi*	*Meandrina meandrites*
Arcobacteraceae, *Arcobacter*	21				
Arcobacteraceae, *Arcobacter*	48				
Arcobacteraceae, *Arcobacter*	101				
Arcobacteraceae, *Arcobacter*	263				
Arcobacteraceae, *Arcobacter*	1012				
Desulfovibrionaceae, *Desulfovibrio*	185				
Desulfovibrionaceae, *Halodesulfovibrio*	13				
Family_XII, *Fusibacter*	44				
Family_XII, *Fusibacter*	135				
Family_XII, *Fusibacter*	275				
Flavobacteriaceae, *Wenyingzhuangia*	126				
Lachnospiraceae, *Vallitalea*	130				
Marinifilaceae, *Marinifilum*	39				
Peptostreptococcaceae, *Tepidibacter*	36				
Prolixibacteraceae, *Roseimarinus*	26				
Pseudoalteromonadacea, *Algicola*	52				
Rhizobiaceae, *Cohaesibacter*	226				
Rhodobacteraceae, *Shimia*	60				
Rhodobacteraceae, *Thalassobius*	111				
Rhodobacteraceae, unclassified	34				
Vibrionaceae, *Vibrio*	20				
Vibrionaceae, *Vibrio*	25				
Vibrionaceae, *Vibrio*	54				
Vibrionaceae, *Vibrio*	67				

Vibrionaceae, *Vibrio*	96				

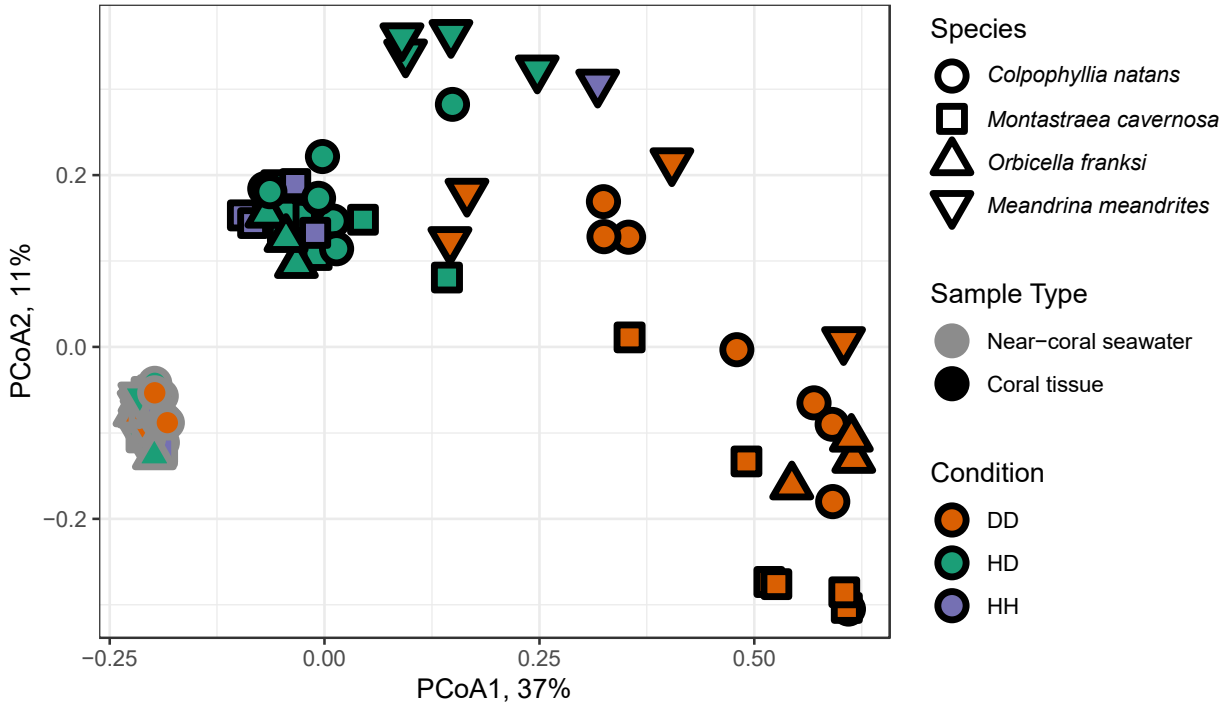

Figure 2-S1. Principal coordinates analysis (PCoA) of Bray-Curtis dissimilarity between all coral and seawater samples. Seawater (gray outline) and coral (black outline) samples are shaped by the coral species, *C. natans* (circle), *M. cavernosa* (square), *O. franksi* (up triangle), and *M. meandrites* (down triangle). Colors indicate health condition where DD = SCTLD lesion sample, HD = healthy sample on diseased colony, HH = healthy sample from apparently healthy colony.

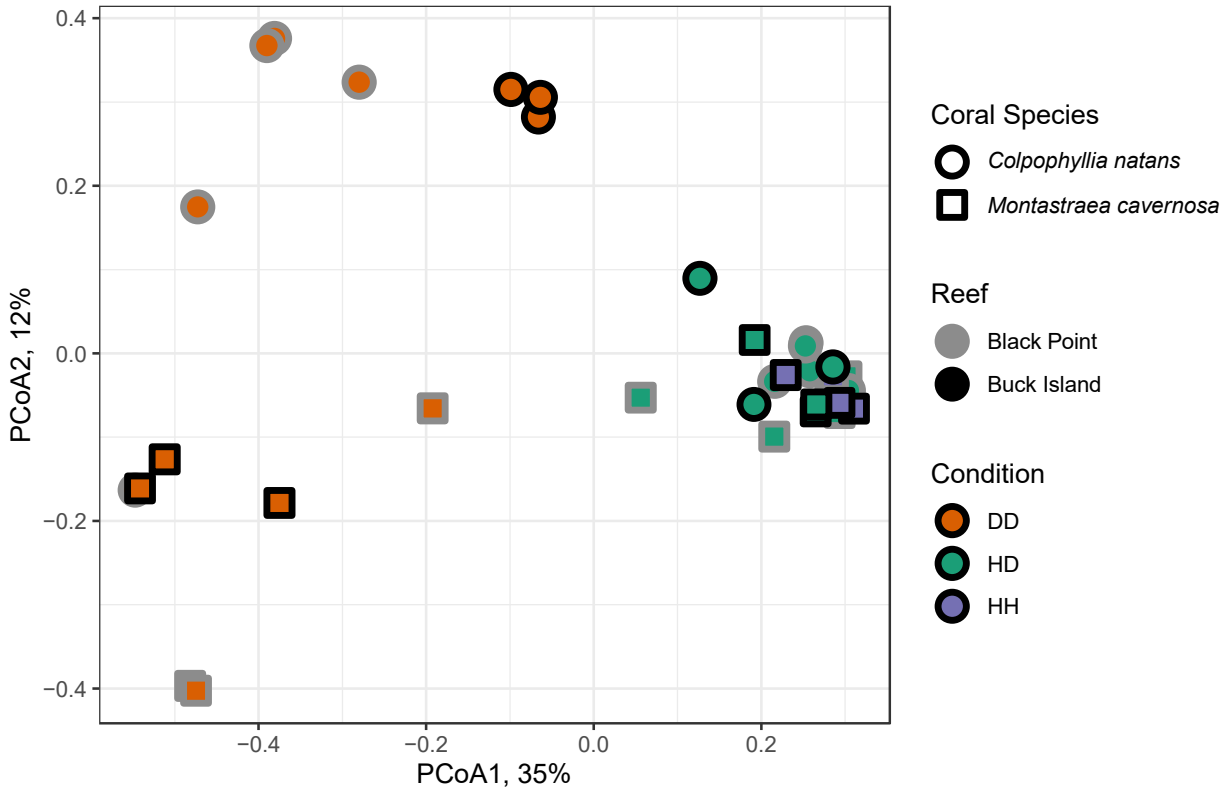

Figure 2-S2. Principal coordinates analysis (PCoA) of Bray-Curtis dissimilarity between all coral samples from *C. natans* and *M. cavernosa*. Outline color denotes whether the corals originated from the Black Point or Buck Island reef. Samples are shaped by the coral species, *C. natans* (circle), *M. cavernosa* (square). Colors indicate health condition where DD = SCTLD lesion sample, HD = healthy sample on diseased colony, HH = healthy sample from apparently healthy colony.

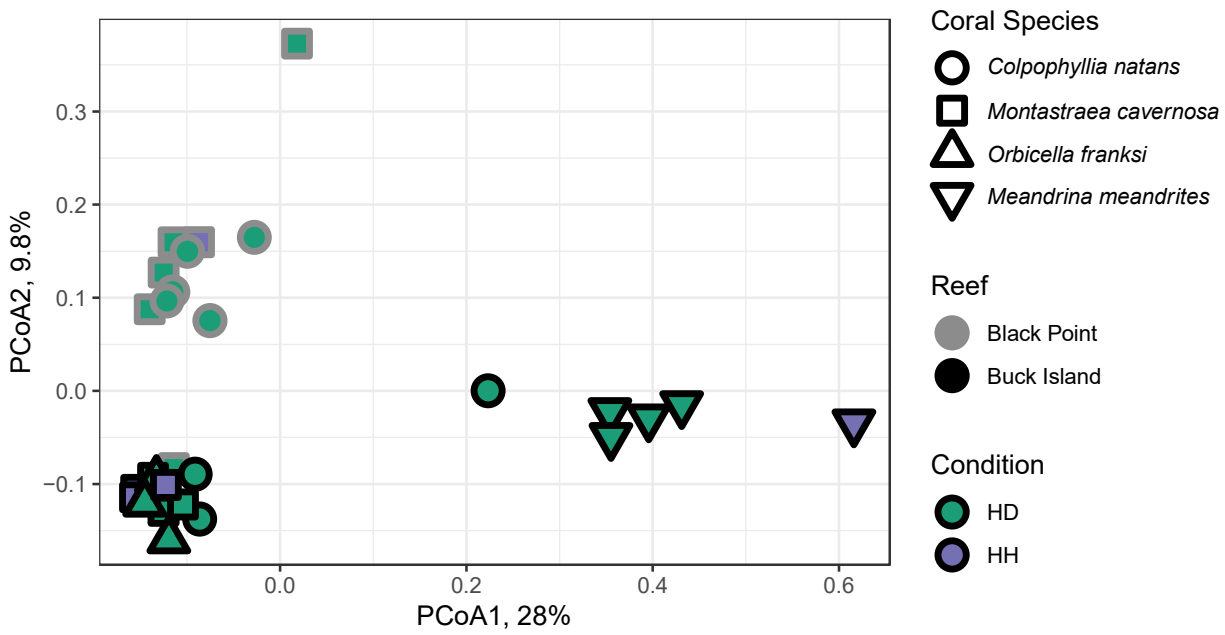

Figure 2-S3. **Principal coordinates analysis (PCoA) of Bray-Curtis dissimilarity within healthy coral samples only**. Outline color denotes whether the corals originated from the Black Point or Buck Island reef. Fill color represents whether the healthy sample was from a diseased colony (HD, green) or apparently healthy colony (HH, purple). Shape denotes the following coral species: *C. natans* (circle), *M. cavernosa* (square), *O. franksi* (up triangle), and *M. meandrites* (down triangle).

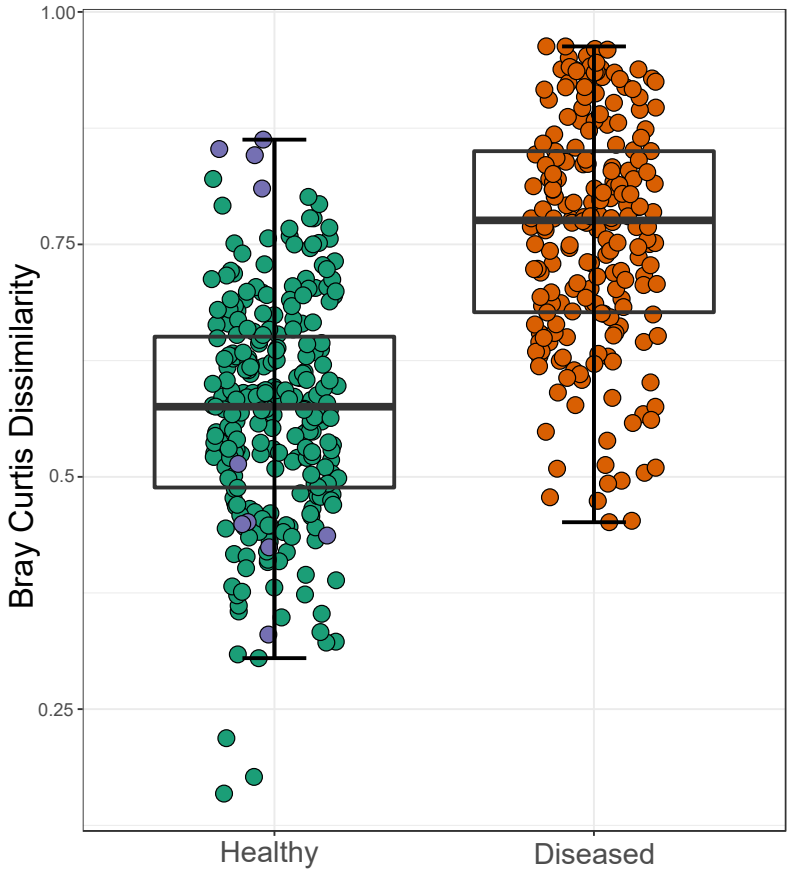

Figure 2-S4. **Boxplots denoting range in Bray-Curtis Dissimilarity values within healthy (HH = purple and HD = green) and diseased (DD = orange) coral microbiomes**. Difference between healthy and diseased Bray-Curtis dissimilarity values is significant by independent Mann-Whitney U Test ($p < 0.001$).

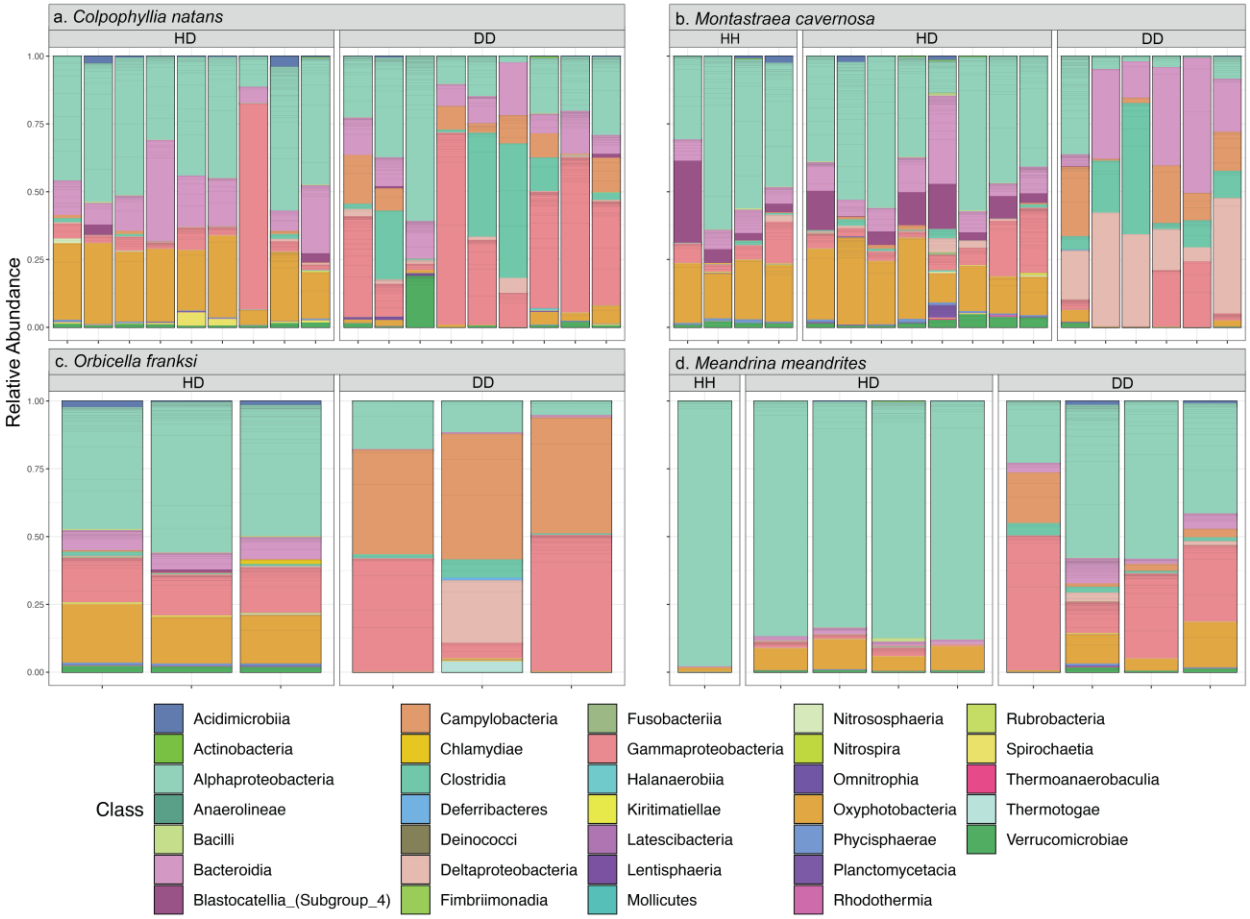

Figure 2-S5. Stacked bar chart of microbial relative abundances within corals in (a) *C. natans*, (b) *M. cavernosa*, (c) *O. franksi*, and (d) *M. meandrites*. Stacked bar charts are organized by coral health condition (HH = healthy sample from a healthy colony, HD = Apparently healthy sample from a diseased colony, DD = Disease lesion).

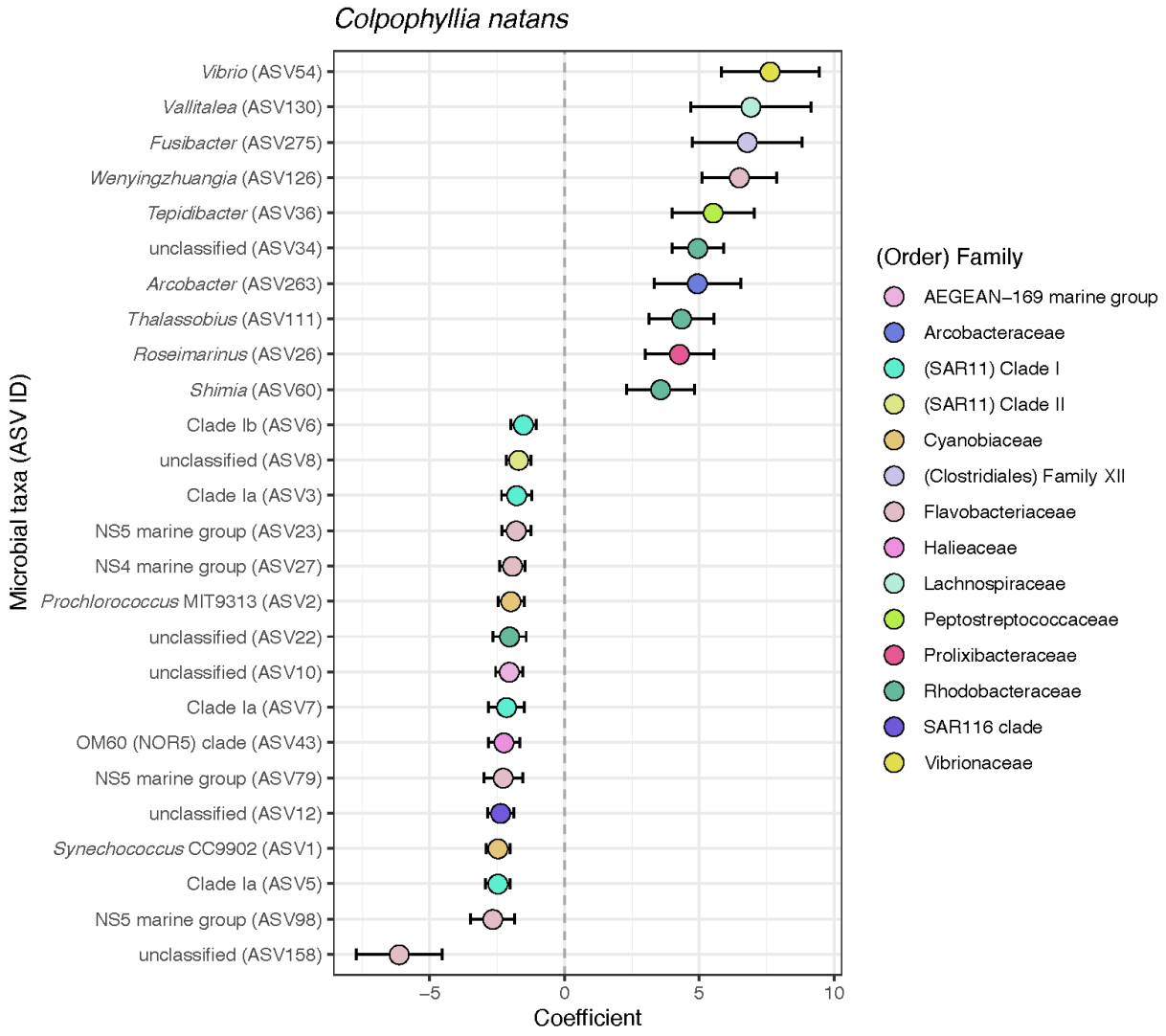

Figure 2-S6. Significantly differentially abundant ASVs between diseased and healthy coral in *Colpophyllia natans*. Positive coefficients indicate ASV relative abundance was enriched in diseased coral relative to healthy coral. Points are labeled by genera and ASV number, and colored by Family.

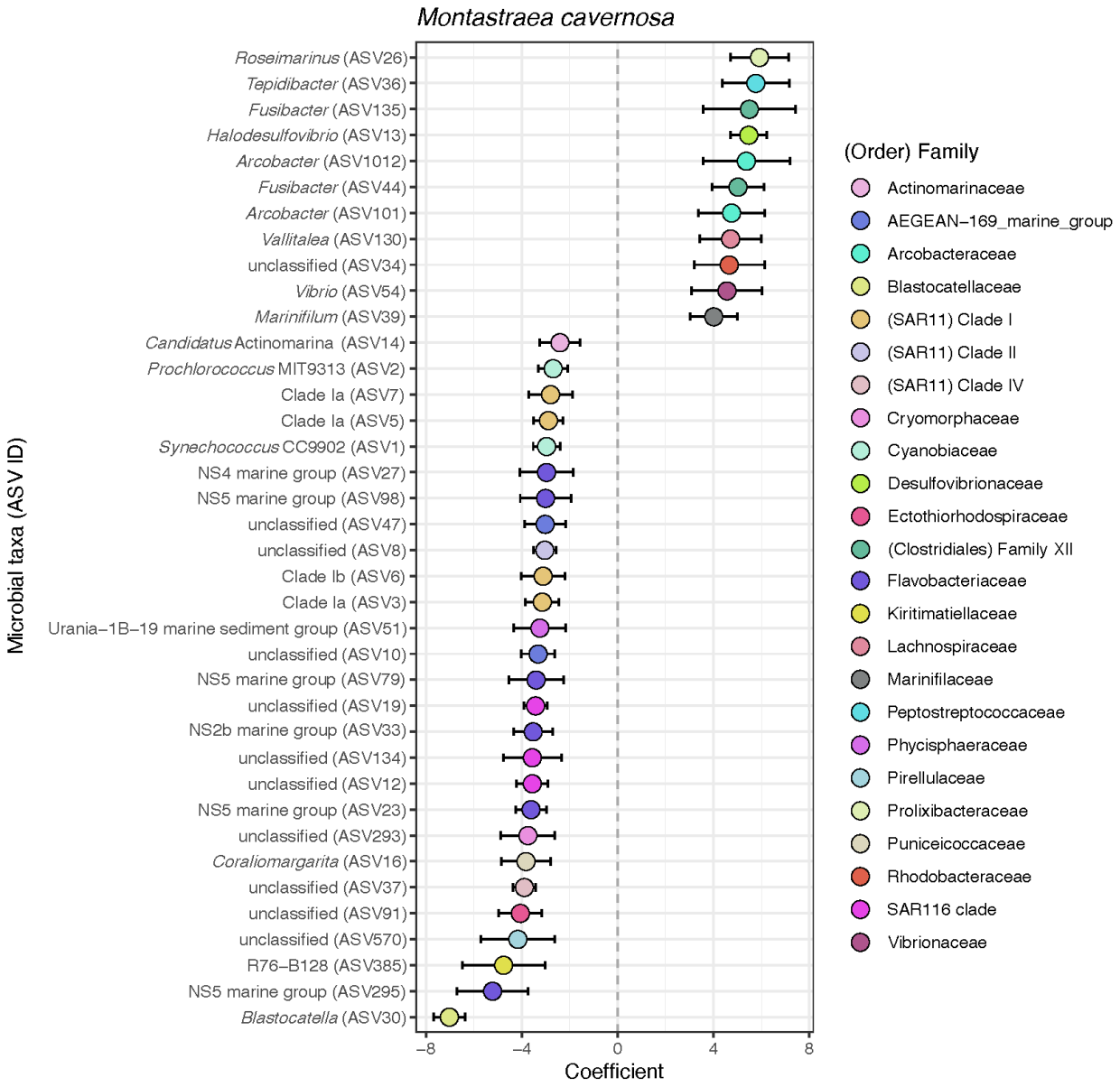

Figure 2-S7. Significantly differentially abundant ASVs between diseased and healthy coral in *Montastraea cavernosa*. Positive coefficients indicate ASV relative abundance was enriched in diseased relative to healthy coral. Points are labeled by genera and ASV number, and colored by Family.

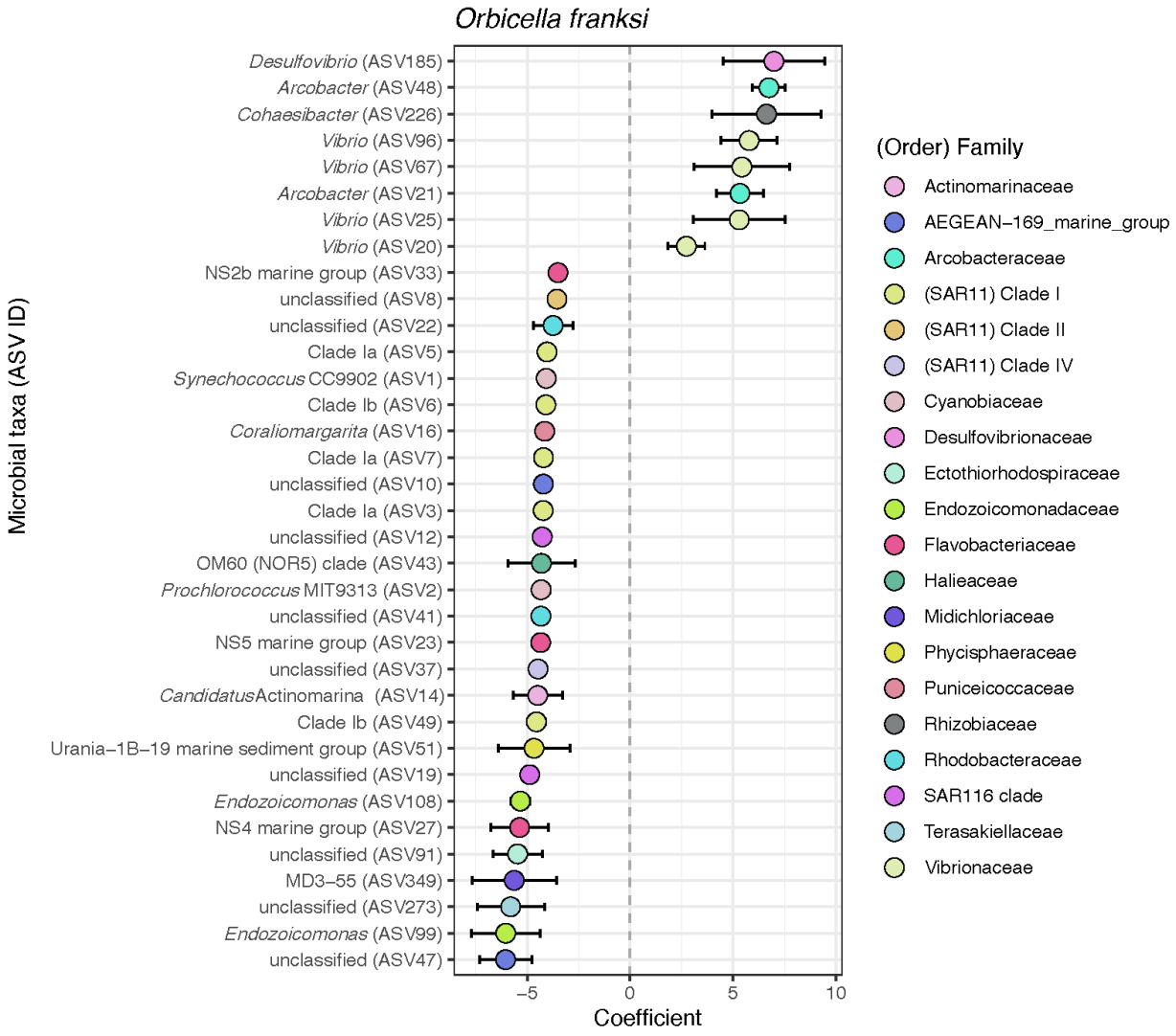

Figure 2-S8. Significantly differentially abundant ASVs between diseased and healthy coral in *Orbicella franksi*. Positive coefficients indicate ASV relative abundance was enriched in diseased relative to healthy coral. Points are labeled by genera and ASV number, and colored by Family.

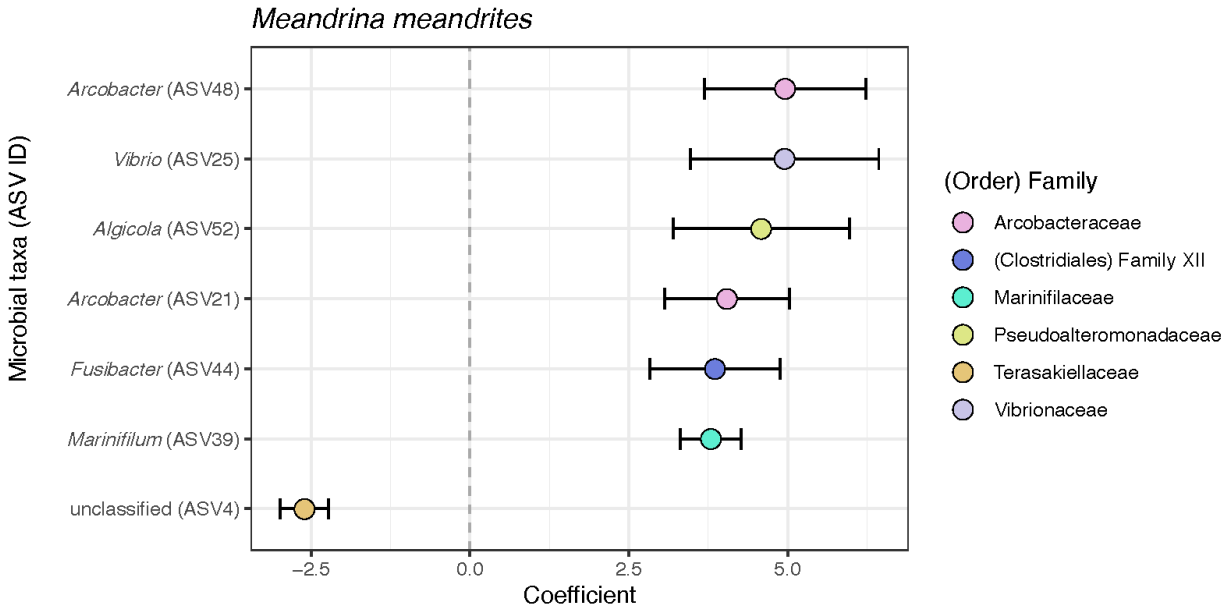

Figure 2-S9. Significantly differentially abundant ASVs between diseased and healthy coral in *Meandrina meandrites*. Positive coefficients indicate ASV relative abundance was enriched in diseased relative to healthy coral. Points are labeled by genera and ASV number, and colored by Family.

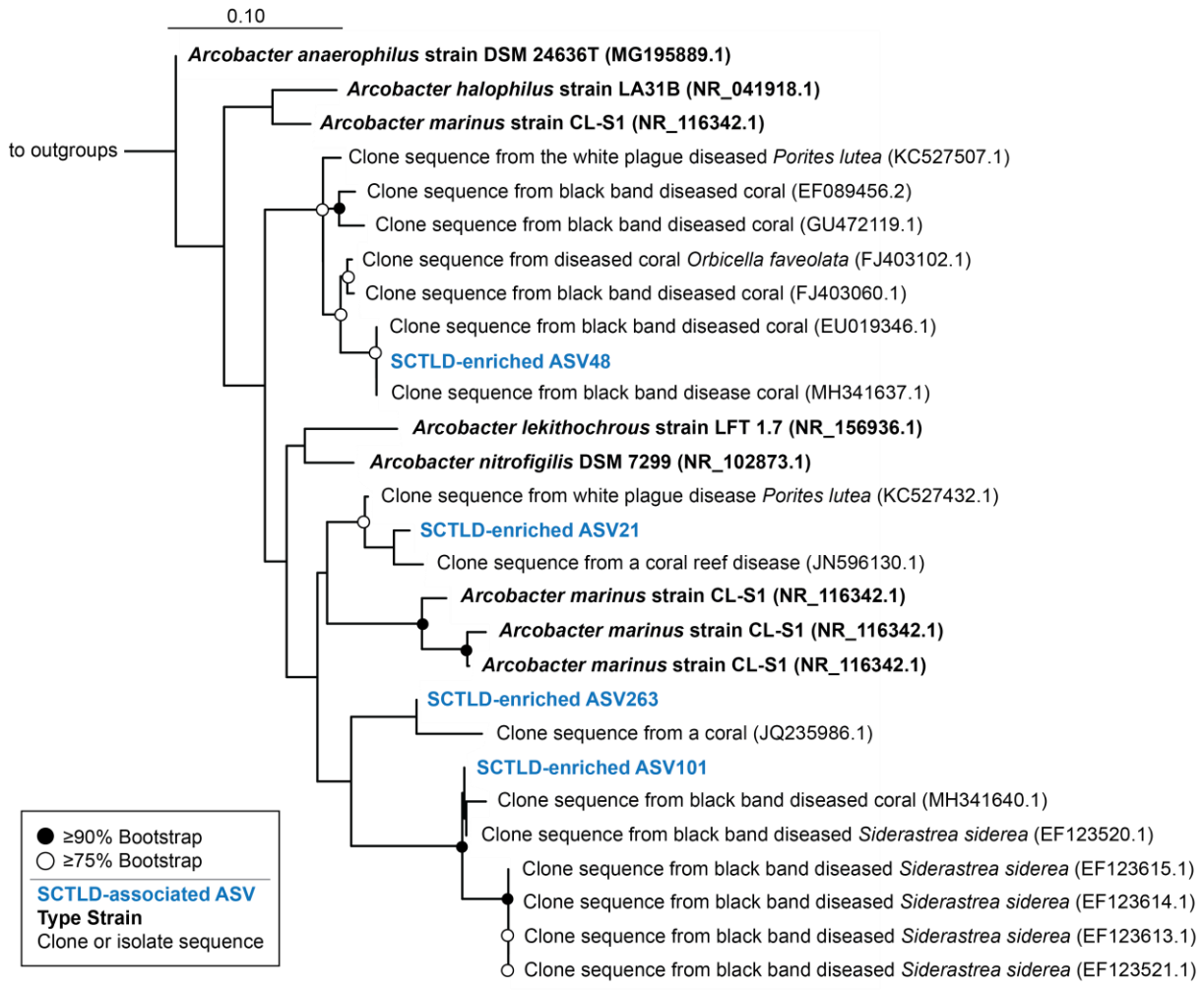

Figure 2-S10. Bioindicator ASVs from the genus *Arcobacter* closely related to isolates and clone sequences from diseased corals. Reference phylogenetic tree was produced using RAxML rapid bootstrapping with an automatic bootstrapping approach to produce the highest-scoring maximum likelihood tree using only longer-length sequences (black). SCTLD-associated ASVs (blue) identified by differential abundance analysis or by previous studies were added to the tree using the Evolutionary Placement Algorithm in RAxML. Colors represent qualitative information about the sequences as follows: Blue = SCTLD-associated ASVs from the present study, black bold = bacterial type strains, black = clone or bacterial isolate/strain sequences. GenBank accession numbers are located in parentheses following each taxa label. Circles at node represent bootstrap values of ≥ 90% (filled-in circle) or ≥ 75% (empty circle). Bar indicates 10% sequence divergence. Tree was rooted using the 16S rRNA gene of *Streptococcus mutans* strain ATCC 25175 (NR_115733.1).

Figure 2-S11. Bioindicator *Vibrio* ASVs from the present study and a recent study related to *Vibrio* pathogens, type strains, and sequences obtained from the Coral Microbiome Database. Maximum likelihood and bootstrapped phylogenetic tree was produced using RAxML based on long (>1200 bp) sequences only, with the shorter coral associated sequences (dashed lines) and SCLTD-associated sequences (blue text) added using the Quick-add Parsimony tool in ARB. Colors represent qualitative information about the sequences as follows: Blue = SCTLD-associated ASVs from the present or previous study (Meyer *et al.*, 2019), Black bold = bacterial type strains, Black = clone or bacterial isolate/strain sequences. GenBank accession numbers are located in parentheses following each taxa label, when available. Circles at node represent bootstrap values of ≥ 90% (filled-in circle) or ≥ 75% (empty circle). Bar indicates 10% sequence divergence. Tree was rooted with *Thalassospira xianhensis* (EU017546) and *Thalassospira tepidiphila* (AB265822).

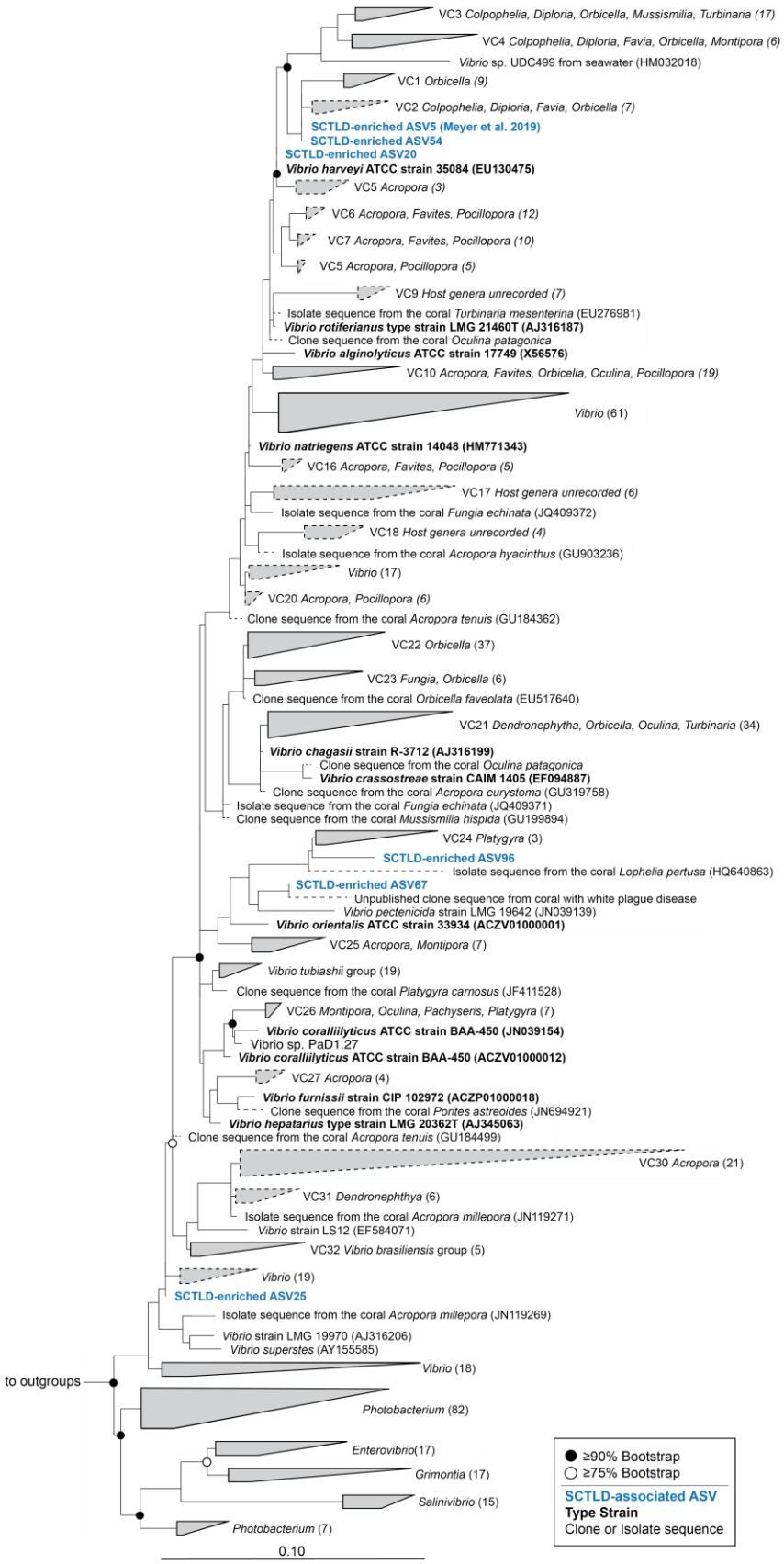
VC3 Colpophelia, Diploria, Orbicella, Mussismilia, Turbinaria (17)
VC4 Colpophelia, Diploria, Favia, Orbicella, Montipora (6)
Vibrio sp. UDC499 from seawater (HM032018)
VC1 Orbicella (9)
VC2 Colpophelia, Diploria, Favia, Orbicella (7)
SCTLD-enriched ASV5 (Meyer et al. 2019)
SCTLD-enriched ASV54
SCTLD-enriched ASV20
Vibrio harveyi ATCC strain 35084 (EU130475)
VC5 Acropora (3)
VC6 Acropora, Favites, Pocillopora (12)
VC7 Acropora, Favites, Pocillopora (10)
VC5 Acropora, Pocillopora (5)
VC9 Host genera unrecorded (7)
Isolate sequence from the coral Turbinaria mesenterina (EU276981)
Vibrio rotiferianus type strain LMG 21460T (AJ316187)
Clone sequence from the coral Oculina patagonica
Vibrio alginolyticus ATCC strain 17749 (X56576)
VC10 Acropora, Favites, Orbicella, Oculina, Pocillopora (19)
Vibrio (61)
Vibrio natriegens ATCC strain 14048 (HM771343)
VC16 Acropora, Favites, Pocillopora (5)
VC17 Host genera unrecorded (6)
Isolate sequence from the coral Fungia echinata (JQ409372)
VC18 Host genera unrecorded (4)
Isolate sequence from the coral Acropora hyacinthus (GU903236)
Vibrio (17)
VC20 Acropora, Pocillopora (6)
Clone sequence from the coral Acropora tenuis (GU184362)
VC22 Orbicella (37)
VC23 Fungia, Orbicella (6)
Clone sequence from the coral Orbicella faveolata (EU517640)
VC21 Dendronephytha, Orbicella, Oculina, Turbinaria (34)
Vibrio chagasii strain R-3712 (AJ316199)
Clone sequence from the coral Oculina patagonica
Vibrio crassostreae strain CAIM 1405 (EF094887)
Clone sequence from the coral Acropora eurystoma (GU319758)
Isolate sequence from the coral Fungia echinata (JQ409371)
Clone sequence from the coral Mussismilia hispida (GU199894)
VC24 Platygyra (3)
SCTLD-enriched ASV96
Isolate sequence from the coral Lophelia pertusa (HQ640863)
SCTLD-enriched ASV67
Unpublished clone sequence from coral with white plague disease
Vibrio pectenicida strain LMG 19642 (JN039139)
Vibrio orientalis ATCC strain 33934 (ACZV01000001)
VC25 Acropora, Montipora (7)
Vibrio tubiashii group (19)
Clone sequence from the coral Platygyra carnosus (JF411528)
VC26 Montipora, Oculina, Pachyseris, Platygyra (7)
Vibrio coralliilyticus ATCC strain BAA-450 (JN039154)
Vibrio sp. PaD1.27
Vibrio coralliilyticus ATCC strain BAA-450 (ACZV01000012)
VC27 Acropora (4)
Vibrio furnissii strain CIP 102972 (ACZP01000018)
Clone sequence from the coral Porites astreoides (JN694921)
Vibrio hepatarius type strain LMG 20362T (AJ345063)
Clone sequence from the coral Acropora tenuis (GU184499)
VC30 Acropora (21)
VC31 Dendronephthya (6)
Isolate sequence from the coral Acropora millepora (JN119271)
Vibrio strain LS12 (EF584071)
VC32 Vibrio brasiliensis group (5)
Vibrio (19)
SCTLD-enriched ASV25
Isolate sequence from the coral Acropora millepora (JN119269)
Vibrio strain LMG 19970 (AJ316206)
Vibrio superstes (AY155585)
Vibrio (18)
to outgroups
Photobacterium (82)
Enterovibrio(17)
Grimontia (17)
Salinivibrio (15)
Photobacterium (7)
0.10
≥90% Bootstrap
≥75% Bootstrap
SCTLD-associated ASV
Type Strain
Clone or Isolate sequence

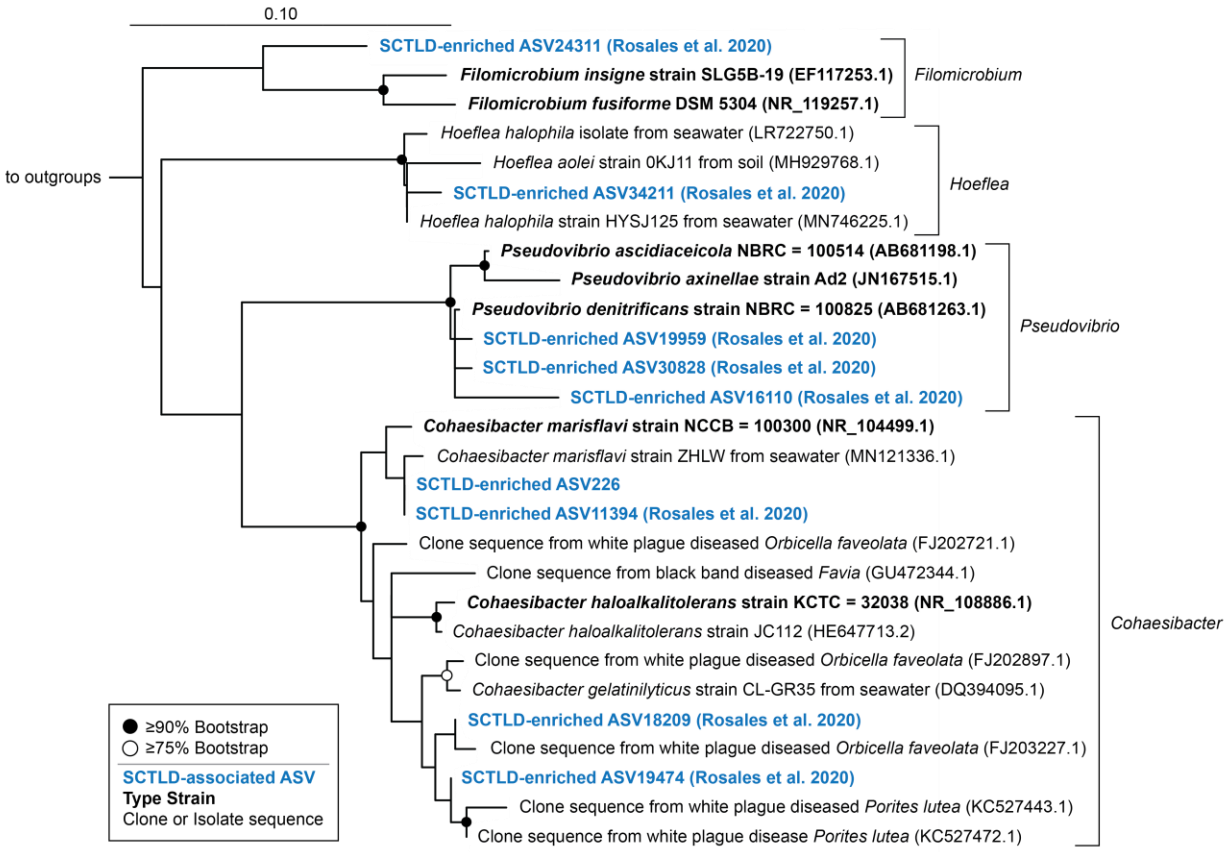

Figure 2-S12. One SCTLD bioindicator Rhizobiaceae ASV from the present study and several from a previous study related to other Rhizobiaceae sequences associated with corals and coral diseases. Reference phylogenetic tree was produced using RAxML rapid bootstrapping with an automatic bootstrapping approach to produce the highest-scoring maximum likelihood tree using only longer-length sequences (black). SCTLD-associated ASVs (blue) identified by differential abundance analysis or in a previous study (Rosales *et al.*, 2020) were added to the tree using the Evolutionary Placement Algorithm in RAxML. Colors represent qualitative information about the sequences as follows: Blue = SCTLD-associated ASVs from the present or a previous study (Rosales *et al.*, 2020), Black bold = bacterial type strains, Black = clone or bacterial isolate/strain sequences. GenBank accession numbers are located in parentheses following each taxa label. Circles at node represent bootstrap values of ≥ 90% (filled-in circle) or ≥ 75% (empty circle). Bar indicates 10% sequence divergence. Tree was rooted using the 16S rRNA gene of *Streptococcus mutans* strain ATCC 25175 (NR_115733.1).

Figure 2-S13. Two SCTLD bioindicator Rhodobacteraceae ASVs from the present study and several from a previous study related to sequences from the Coral Microbiome Database encompassing several genera within the Rhodobacteraceae Family. Maximum likelihood and bootstrapped phylogenetic tree was produced using RAxML based on long (>1200 bp) sequences only, with the shorter coral associated sequences (dashed lines) and SCLTD-associated sequences (blue text) added using the Quick-add Parsimony tool in ARB. Colors represent qualitative information about the sequences as follows: Blue = SCTLD-associated ASVs from the present or a previous study (Rosales *et al.*, 2020), Black bold = bacterial type strains, Black = clone or bacterial isolate/strain sequences. GenBank accession numbers are located in parentheses following each taxa label, when available. Circles at node represent bootstrap values of ≥ 90% (filled-in circle) or ≥ 75% (empty circle). Bar indicates 10% sequence divergence. Tree was rooted with *Alteromonas* (AACY023784545) and *Methylophilaceae* (HM856564 and EU795249).

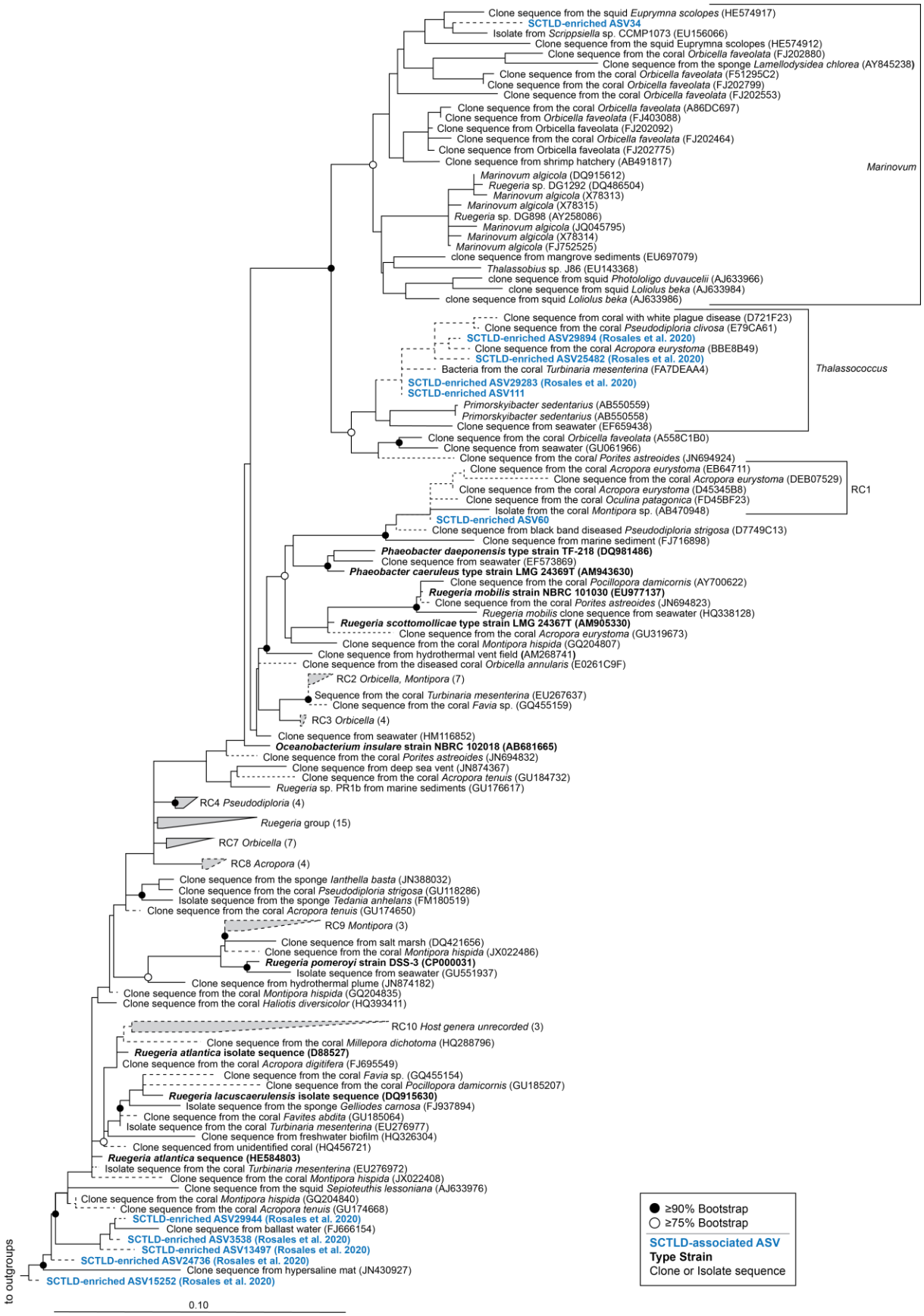
Clone sequence from the squid Euprymna scolopes (HE574917)
SCTLD-enriched ASV34
Isolate from Scrippsiella sp. CCMP1073 (EU156066)
Clone sequence from the squid Euprymna scolopes (HE574912)
Clone sequence from the coral Orbicella faveolata (FJ202880)
Clone sequence from the sponge Lamellodysidea chlorea (AY845238)
Clone sequence from the coral Orbicella faveolata (F51295C2)
Clone sequence from the coral Orbicella faveolata (FJ202799)
Clone sequence from the coral Orbicella faveolata (FJ202553)
Clone sequence from the coral Orbicella faveolata (A86DC697)
Clone sequence from Orbicella faveolata (FJ403088)
Clone sequence from Orbicella faveolata (FJ202092)
Clone sequence from the coral Orbicella faveolata (FJ202464)
Clone sequence from Orbicella faveolata (FJ202775)
Clone sequence from shrimp hatchery (AB491817)
Marinovum algicola (DQ915612)
Ruegeria sp. DG1292 (DQ486504)
Marinovum algicola (X78313)
Marinovum algicola (X78315)
Ruegeria sp. DG898 (AY258086)
Marinovum algicola (JQ045795)
Marinovum algicola (X78314)
Marinovum algicola (FJ752525)
clone sequence from mangrove sediments (EU697079)
Thalassobius sp. J86 (EU143368)
clone sequence from squid Photololigo duvaucelii (AJ633966)
clone sequence from squid Loliolus beka (AJ633984)
clone sequence from squid Loliolus beka (AJ633986)
Marinovum
Clone sequence from coral with white plague disease (D721F23)
Clone sequence from the coral Pseudodiploria clivosa (E79CA61)
SCTLD-enriched ASV29894 (Rosales et al. 2020)
Clone sequence from the coral Acropora eurystoma (BBE8B49)
SCTLD-enriched ASV25482 (Rosales et al. 2020)
Bacteria from the coral Turbinaria mesenterina (FA7DEAA4)
SCTLD-enriched ASV29283 (Rosales et al. 2020)
SCTLD-enriched ASV111
Primorskyibacter sedentarius (AB550559)
Primorskyibacter sedentarius (AB550558)
Clone sequence from seawater (EF659438)
Thalassococcus
Clone sequence from the coral Orbicella faveolata (A558C1B0)
Clone sequence from seawater (GU061966)
Clone sequence from the coral Porites astreoides (JN694924)
Clone sequence from the coral Acropora eurystoma (EB64711)
Clone sequence from the coral Acropora eurystoma (DEB07529)
Clone sequence from the coral Acropora eurystoma (D45345B8)
Clone sequence from the coral Oculina patagonica (FD45BF23)
Isolate from the coral Montipora sp. (AB470948)
RC1
SCTLD-enriched ASV60
Clone sequence from black band diseased Pseudodiploria strigosa (D7749C13)
Clone sequence from marine sediment (FJ716898)
Phaeobacter daeponensis type strain TF-218 (DQ981486)
Clone sequence from seawater (EF573869)
Phaeobacter caeruleus type strain LMG 24369T (AM943630)
Clone sequence from the coral Pocillopora damicornis (AY700622)
Ruegeria mobilis strain NBRC 101030 (EU977137)
Clone sequence from the coral Porites astreoides (JN694823)
Ruegeria mobilis clone sequence from seawater (HQ338128)
Ruegeria scottomollicae type strain LMG 24367T (AM905330)
Clone sequence from the coral Acropora eurystoma (GU319673)
Clone sequence from the coral Montipora hispida (GQ204807)
Clone sequence from hydrothermal vent field (AM268741)
Clone sequence from the diseased coral Orbicella annularis (E0261C9F)
RC2 Orbicella, Montipora (7)
Sequence from the coral Turbinaria mesenterina (EU267637)
Clone sequence from the coral Favia sp. (GQ455159)
RC3 Orbicella (4)
Clone sequence from seawater (HM116852)
Oceanobacterium insulare strain NBRC 102018 (AB681665)
Clone sequence from the coral Porites astreoides (JN694832)
Clone sequence from deep sea vent (JN874367)
Clone sequence from the coral Acropora tenuis (GU184732)
Ruegeria sp. PR1b from marine sediments (GU176617)
RC4 Pseudodiploria (4)
Ruegeria group (15)
RC7 Orbicella (7)
RC8 Acropora (4)
Clone sequence from the sponge Ianthella basta (JN388032)
Clone sequence from the coral Pseudodiploria strigosa (GU118286)
Isolate sequence from the sponge Tedania anhelans (FM180519)
Clone sequence from the coral Acropora tenuis (GU174650)
RC9 Montipora (3)
Clone sequence from salt marsh (DQ421656)
Clone sequence from the coral Montipora hispida (JX022486)
Ruegeria pomeroyi strain DSS-3 (CP000031)
Isolate sequence from seawater (GU551937)
Clone sequence from hydrothermal plume (JN874182)
Clone sequence from the coral Montipora hispida (GQ204835)
Clone sequence from the coral Haliotis diversicolor (HQ393411)
RC10 Host genera unrecorded (3)
Clone sequence from the coral Millepora dichotoma (HQ288796)
Ruegeria atlantica isolate sequence (D88527)
Clone sequence from the coral Acropora digitifera (FJ695549)
Clone sequence from the coral Favia sp. (GQ455154)
Clone sequence from the coral Pocillopora damicornis (GU185207)
Ruegeria lacuscaerulensis isolate sequence (DQ915630)
Isolate sequence from the sponge Gelliodes carnosa (FJ937894)
Clone sequence from the coral Favites abdita (GU185064)
Isolate sequence from the coral Turbinaria mesenterina (EU276977)
Clone sequence from freshwater biofilm (HQ326304)
Clone sequenced from unidentified coral (HQ456721)
Ruegeria atlantica sequence (HE584803)
Isolate sequence from the coral Turbinaria mesenterina (EU276972)
Clone sequence from the coral Montipora hispida (JX022408)
Clone sequence from the squid Sepioteuthis lessoniana (AJ633976)
Clone sequence from the coral Montipora hispida (GQ204840)
Clone sequence from the coral Acropora tenuis (GU174668)
SCTLD-enriched ASV29944 (Rosales et al. 2020)
Clone sequence from ballast water (FJ666154)
SCTLD-enriched ASV3538 (Rosales et al. 2020)
SCTLD-enriched ASV13497 (Rosales et al. 2020)
SCTLD-enriched ASV24736 (Rosales et al. 2020)
Clone sequence from hypersaline mat (JN430927)
SCTLD-enriched ASV15252 (Rosales et al. 2020)
to outgroups
0.10
≥90% Bootstrap
≥75% Bootstrap
SCTLD-associated ASV
Type Strain
Clone or Isolate sequence

Chapter 3 - Microbial and nutrient dynamics in mangrove, reef, and seagrass waters over tidal and diurnal time scales [2]

[2] This chapter was originally published as:

Becker, C., Weber, L., Suca, J.J., Llopiz, J.K., Mooney, T.A., and Apprill, A. (2020) Microbial and nutrient dynamics in mangrove, reef, and seagrass waters over tidal and diurnal time scales. *Aquat Microb Ecol* **85**: 101–119. https://doi.org/10.3354/ame01944

CB, LW, JJS, and AA took part in the research expedition to collect the samples. CB and AA designed the study. CB analyzed the data and wrote the manuscript. All authors contributed edits to the final manuscript and approved of the content.

ABSTRACT

In coral reefs and adjacent seagrass meadow and mangrove environments, short temporal scales (i.e. tidal, diurnal) may have important influences on ecosystem processes and community structure, but these scales are rarely investigated. This study examines how tidal and diurnal forcings influence pelagic microorganisms and nutrient dynamics in three important and adjacent coastal biomes: mangroves, coral reefs, and seagrass meadows. We sampled for microbial (Bacteria and Archaea) community composition, cell abundances and environmental parameters at nine coastal sites on St. John, U.S. Virgin Islands that spanned 4 km in distance (4 coral reefs, 2 seagrass meadows and 3 mangrove locations within two larger bays). Eight samplings occurred over a 48-hour period, capturing day and night microbial dynamics over two tidal cycles. The seagrass and reef biomes exhibited relatively consistent environmental conditions and microbial community structure, but were dominated by shifts in picocyanobacterial abundances that were most likely attributed to diel dynamics. In contrast, mangrove ecosystems exhibited substantial daily shifts in environmental parameters, heterotrophic cell abundances and microbial community structure that were consistent with the tidal cycle. Differential abundance analysis of mangrove-associated microorganisms revealed enrichment of pelagic, oligotrophic taxa during high tide and enrichment of putative sediment-associated microbes during low tide. Our study underpins the importance of tidal and diurnal time scales in structuring coastal microbial and nutrient dynamics, with diel and tidal cycles contributing to a highly dynamic microbial environment in mangroves, and time of day likely contributing to microbial dynamics in seagrass and reef biomes.

INTRODUCTION

Short temporal rhythmicities resulting from daily sunlight cycles and lunar-influenced tidal cycles have governed the dynamics of living organisms throughout evolutionary history. Light is a fundamental source of energy for the photosynthetic cells that dominate in the surface ocean worldwide and produce approximately 46% of global net primary production (Field *et al.*, 1998). Tidal elevation directs the zonation of intertidal flora and fauna along coastlines, influencing local community processes (Alongi, 1987; Peterson, 1991). Coastal ecosystems must cope with the interaction of both diurnal and tidal forcings, and the effect of these cycles are apparent on microbial scales. The tidal cycle influences virus-microbe interactions in estuaries (X. Chen *et al.*, 2019), bacterial abundances in salt marshes (Kirchman *et al.*, 1984), and even the presence of enterococci, fecal bacteria used as a metric for water quality, on beaches (Boehm and Weisberg, 2005). Diurnal cycles, on the other hand, govern microbial nitrogen fixation on mangrove root systems (Toledo *et al.*, 1995), bacterial production rates in seagrass meadows (Moriarty and Pollard, 1982), and coral reef microbial community changes (Kelly *et al.*, 2019; Weber and Apprill, 2020). Together, tidal and diurnal forces play major roles in shaping microbial life in coastal environments.

Seawater bacterial and archaeal communities are fundamental to ocean ecosystems. These prokaryotic microbes form the basis of the marine food web because they cycle organic matter, remineralize nutrients, and take part in all major elemental cycles in the ocean (reviewed by Moran, 2015). Extensive study of microbial communities in the ocean has primarily focused on seasonal changes and shown that communities vary predictably with environmental factors, such as temperature (Fuhrman *et al.*, 2006; Gilbert *et al.*, 2009; Kim and Ducklow, 2016; Bunse and Pinhassi, 2017). The dynamics of microbial communities over short temporal scales (hours to days) are less studied. Studies from estuarine and coastal environments showed that tidal mixing and salinity are major drivers of microbial community structure (Lu *et al.*, 2015; Neubauer *et al.*, 2019; X. Chen *et al.*, 2019). In the case of open ocean environments with more stable physical and chemical features, observed changes in microbial communities may be due to biological interactions. For example, a study centered off the coast

of California over three weeks and following a spring bloom showed that the microbial community composition correlated more closely to biological variables than physical and chemical variables (Needham and Fuhrman, 2016). Short-term microbial dynamics likely play a role in structuring seawater microbial communities within coastal tropical marine environments (mangrove, seagrass and coral reef), but these dynamics are largely unstudied.

Mangrove, seagrass, and coral reef biomes dominate the coast of many tropical and subtropical islands and coastlines. Together, these ecosystems protect coastlines from devastating tropical storms and hurricanes, and sustain local economies that rely on tourism and seafood. Mangroves are halophytic plants that thrive in the transition zone between estuarine and marine environments, tolerating a wide range of physicochemical conditions. Collectively, these trees make up mangrove forests, which are critically important coastal biomes. They sequester carbon (Donato *et al.*, 2011), provide nursery grounds for fish (Aburto-Oropeza *et al.*, 2008), and insulate coastlines from storms and erosion (Duke *et al.*, 2007). At the micro-scale, mangrove ecosystems are important for remineralization as they harbor microorganisms in sediments, roots, and seawater that include denitrifying and nitrogen-fixing bacteria (Reef *et al.*, 2010; Liu *et al.*, 2012). Mangrove sediment microbial community dynamics are well-studied and have been shown to respond to tidal changes, which affect ecosystem processes such as rates of nitrogen fixation and denitrification (Lee and Joye, 2006; Chen *et al.*, 2016; Gong *et al.*, 2019). Given the influence of tide on sediment microbial communities, there may be a concomitant shift in the overlying seawater microbial communities with respect to the tidal forcing of seawater. However, the extent of tidal influence on the microbial dynamics within the overlying seawater remains to be elucidated in mangrove environments.

Seagrass meadows are often found deeper than mangroves, where they are constantly submerged, yet within the photic zone. These environments serve as nursery grounds and habitat for diverse fishes and invertebrates, and contribute significantly to primary production in tropical ecosystems (reviewed in Ugarelli *et al.*, 2017). Sediment-associated microbial communities in seagrasses are important for nitrogen cycling and carbon sequestration (Moriarty *et al.*, 1985; Sun *et al.*, 2015; Ugarelli *et al.*, 2018). The seawater microbial community is far less studied, but has been shown to be important for carbon cycling and the ultimate

transfer of primary production to the marine food web (Blum and Mills, 1991; Peduzzi and Herndl, 1991). Ugarelli et al. (2018) recently examined the spatial variability in seawater microorganisms across three seagrass locations and found quite consistent patterns in the taxa recovered across sites, but small changes in relative abundances of those taxa. Short temporal scales do appear to exert an effect on the microbial communities in seagrass environments. The bacterial production rates within sediment and seawater in seagrass meadows have been shown to change on a diurnal cycle in response to the photosynthetic output of the underlying plants, but this did not relate to the tidal cycle (Moriarty and Pollard, 1982). The extent that the composition of overlying seawater bacterial and archaeal communities changes over similar short temporal cycles remains to be described.

High biodiversity from macro- to micro-organisms and low nutrient concentrations of overlying seawater are hallmarks of coral reef environments. The diverse assemblage of microorganisms is particularly important in reef seawater for recycling organic metabolites and nutrients in these apparent nutrient "deserts" (Gast *et al.*, 1998; Bourne and Webster, 2013; Haas *et al.*, 2013). The fundamental role microbes play in coral reef biogeochemical cycling has made them bioindicators of changing reef environments in the face of climate change (Glasl *et al.*, 2018). While it is established that seawater microbial communities on reefs alter predictably with seasonal shifts in environmental parameters (Bulan *et al.*, 2018; Glasl *et al.*, 2019), much less is known on how short temporal scales, on the orders of hours and days, impact reef seawater communities. Existing studies suggest that seasonal and diurnal changes could be more significant than tidal changes in reef systems (Sweet *et al.*, 2010; Kelly *et al.*, 2019; Weber and Apprill, 2020). While diurnal changes may be more significant than tidal changes in reef ecosystems, at present no data exist in the Caribbean on the effect of tidal changes on reef and other coastal marine seawater microbial communities, precluding a complete assessment of major temporal drivers in reef and other coastal tropical systems.

The objectives of our study were to (1) provide an initial understanding of the variability in the physicochemical environment over two tidal and diurnal cycles at three tropical biomes simultaneously in St. John, USVI, (2) capture the changes in microbial communities at those same locations and time points, and (3) examine the influence of tidal level and time of day on

structuring bacterial and archaeal community composition in these environments. We sampled the seawater at nine sites on the southern shore of St. John, USVI over two full spring tidal cycles in July 2017, which extended over 48 hours and included day and night measurements. Much of this study took place in Virgin Islands National Park, which extends from land into the surrounding waters, protecting mangrove, seagrass, and reef biomes in close proximity to each other. We hypothesized that the mangrove habitats, which reside closest to the intertidal zone, would experience a physicochemical environment that varied in concert with the tide, leading to a more dynamic microbial community compared to reef and seagrass biomes. We hypothesized that any tidal-based changes in the reef and seagrass biomes would be subtler compared to the mangroves, and that these environments would show some evidence of diurnal-based microbial community alterations.

METHODS

Sampling

The study took place on the southern coast of St. John, USVI, in two comparable bays, Lameshur Bay and Fish Bay during summer of 2017 (prior to hurricanes Irma and Maria). In total, three tropical biomes were sampled: coral reef (4 sites), seagrass meadow (2 sites) and mangrove (3 sites; 2 within the same mangrove system) (Figure 3-1). The Lameshur Bay mangrove location included two distinct sampling sites. The “Lameshur Mangrove inland” area was at the upper range of the intertidal zone and was dominated by black mangroves (*Avicennia germinans*) and white mangroves (*Laguncularia racemosa*). The Lameshur Mangrove inland environment was only flooded and sampled during high tide (Figure 3-1). The second Lameshur Bay mangrove area was named “Lameshur mangrove subtidal” because it was located below the mean low low water level. This habitat was dominated by red mangroves (*Rhizophora mangle*) and its subtidal location caused it to be constantly submerged and enabled sampling at each time point (Figure 3-1). The Fish Bay mangrove site was also a subtidal mangrove habitat surrounded by red mangroves that were sampled throughout the study. The seagrass meadows were dominated by turtle grass (*Thallassia testudinum*), but also

included manatee grass (*Syringodium filliforme*) and shoal grass (*Halodule wrightii*). The majority of sites were within the boundaries of the Virgin Islands National Park, which is undeveloped except for a small research station. The Fish Bay mangrove, Fish Bay seagrass, and Ditliff reef sites were outside the boundary of the park, and the land surrounding Fish Bay was inhabited.

Sampling occurred from July 22-24, 2017 and coincided with the spring tides and natural diel cycles. A new moon occurred on July 23 at 05:45 (EST). St. John tidal cycles exhibit a combination of mixed semidiurnal tides, which occur typically during neap tides, and diurnal tides, which occur around the spring tides (Figure 3-1b). Sampling time points coincided with the diurnal tidal cycle at low, flood, high, and ebb tides over a 48 hr window, resulting in 8 total sampling time points (gray dots, Figure 3-1b). Due to the nature of the diurnal tide, over the 48 hrs, low and flood tide only occurred during the day to dusk time period, while high and ebb tide only occurred during night and dawn, respectively. Samples were collected ±1 hr from the designated time point, placed on ice, and processed within two hours of collection.

At all sites, a CTD (Castaway, SonTek, San Diego, CA, USA) was deployed from surface to the bottom depths in reef and seagrass seawater, and single point measurements were collected from mangrove seawater to capture the temperature and salinity at each time point. Only temperature and salinity at the surface of the cast were used for analysis. Water samples were collected from the surface (within 0.5 m) after triplicate rinsing of each respective container. Water for inorganic nutrients (30 ml) was transferred into acid-washed and seawater-rinsed bottles (HDPE, Nalgene, ThermoFisher Scientific, Waltham, MA, USA), which were frozen to $-20°C$. Samples for microbial abundances (875 µl) were transferred from nutrient bottles to a 2 ml cryovial (Corning, Corning, NY, USA), which was fixed to a final concentration of 1% paraformaldehyde (Electron Microscopy Sciences, Hatfield, PA, USA), refrigerated in the dark for 20 min at 4°C, then flash-frozen in a liquid nitrogen (LN_2) dry shipper. Samples were collected for total organic carbon and nitrogen, but were contaminated during sample storage due to improper orientation of the cap seals, unfortunately preventing the incorporation of organic substrates in this study. To capture seawater microbial communities, water was collected into acid-washed, 4 l Nalgene bottles (LDPE plastic,

ThermoFisher Scientific) and 1 l of seawater was pumped using a Masterflex L/S peristaltic pump (Cole-Palmer, Vernon Hills, IL, USA) through Masterflex silicone tubing (L/S, platinum-cured, #96410-24 size, Cole-Parmer) to rinse the tubing. The remaining 2 l of seawater was filtered through a 0.22 µm Supor filter (25 mm; Pall, Ann Arbor, MI, USA). For the mangrove and seagrass sites, 2 l could not always be filtered completely and therefore 0.3 – 2 l and 1.2 – 2 l of water was filtered through the membrane, respectively. For the coral reef sites, 1.5 – 2 l passed through the filter membrane. All filters were placed into 2 ml cryovials using sterile forceps (Corning) and flash-frozen in an LN_2 dry shipper until returned to Woods Hole, MA and stored at −80°C.

Flow cytometry and nutrient analyses

Samples collected for microbial abundance were analyzed at the University of Hawaii SOEST Flow Cytometry Facility with a Beckman-Coulter Altra flow cytometer (Beckman Coulter Life Sciences, Inc, Indianapolis, IN) that was attached to a Harvard Apparatus syringe pump for quantitative sample delivery (50 µl min^{-1}). Samples were stained with Hoechst 33342 DNA stain (1 µg ml^{-1} final concentration), and excited co-linearly by 488 nm (1W) and UV (~350 nm, 200 mW) lasers (Campbell and Vaulot, 1993; Monger and Landry, 1993). Signals were collected as FCS 2.0 listmode files using Expo32 software for scatter (forward and side) and fluorescence (chlorophyll, phycoerythrin and Hoechst-bound DNA). Data were analyzed offline using FlowJo software (Tree Star, Inc., Ashland, OR, USA). Populations and abundances (cells ml^{-1}) of cyanobacteria (*Prochlorococcus* and *Synechoccocus*), eukaryotic phytoplankton and non-pigmented bacteria were distinguished based on their characteristic scatter, chlorophyll, phycoerythrin, and DNA signals. Non-pigmented bacteria were used as a proxy for heterotrophic Bacteria and Archaea (Monger and Landry, 1993; Marie *et al.*, 1997).

Samples collected for nutrient analysis were analyzed at Oregon State University using a Technicon AutoAnalyzer II (SEAL Analytical) and an Alpkem RFA 300 Rapid Flow Analyzer. Ammonium was measured with the indophenol blue method (US Environmental Protection Agency, 1983). Phosphate was measured with an adjusted molybdenum blue method (Bernhardt and Wilhelms, 1967), and nitrite + nitrate and silicate were measured using standard methods in Armstrong et al. (1967).

DNA extraction, PCR amplification, and sequencing

DNA was extracted from the 0.22 µm filters using a sucrose-EDTA lysis method similar to Santoro et al. (2010) that combines lysis with filter column purification. Three DNA extraction controls were included by proceeding with the following DNA extraction procedure on unused 0.22 µm filters identical to those used for sample collection. Briefly, the 25 mm filter was subjected to physical and chemical lysis using 0.1 mm glass beads (Lysing Matrix B, MP Biomedicals, Irvine, CA, USA), sucrose-EDTA lysis buffer (0.75 M Sucrose, 20 mM EDTA, 400 mM NaCl, 50 mM Tris) and 10% sodium dodecyl sulfate (Teknova, Hollister, CA, USA), followed by a proteinase-K digestion (20 mg ml^{-1} Promega, Madison, WI, USA). Lysate was then purified using the DNeasy Blood and Tissue Kit (Qiagen, Germantown, MD, USA) spin column filters following manufacturer protocols. Purified DNA was fluorometrically quantified using a high sensitivity (HS) dsDNA assay on a Qubit 2.0 fluorometer following manufacturer protocols (ThermoFisher Scientific).

Sample as well as extraction control DNA were diluted 1:100 in UV-sterilized PCR-grade H_2O and 1 µl was used in a PCR reaction. One PCR negative control sample was included by adding 1 µl of PCR-grade H_2O to a PCR reaction. Two Human Microbiome Project mock communities, (1) Genomic DNA from Microbial Mock Community B (Even, Low Concentration), v5.1L, for 16S rRNA Gene Sequencing, HM-782D and (2) Genomic DNA from Microbial Mock Community B (Staggered, Low Concentration), v5.2L, for 16S rRNA Gene Sequencing, HM-783D (BEI Resources, ATCC, Manassas, VA, USA) were included as additional controls. 1 µl of each mock community was used in a PCR reaction. Barcoded primers recommended by the Earth Microbiome Project, 515F (Parada *et al.*, 2016) and 806R (Apprill *et al.*, 2015), were used to amplify the V4 region of the small subunit (SSU) rRNA gene in bacteria and archaea. Triplicate 25 µl reactions contained 1.25 units of GoTaq DNA Polymerase (Promega, Madison, WI, USA), 0.2 µM forward and reverse primers, 0.2 mM deoxynucleoside triphosphate (dNTP) mix (Promega), 2.5 mM $MgCl_2$, 5 µl GoTaq 5X colorless flexi buffer (Promega), and nuclease-free water. The reactions were run on a Bio-Rad Thermocycler (Hercules, CA, USA) using the following criteria: denaturation at 95°C for 2 min; 28 cycles at 95°C for 20 s, 55°C for 15 s, and 72°C for 5 min; and extension at 72°C for 10 min. Successful amplification was verified by

running 5 µl of product on a 1% agarose-Tris-Borate-EDTA (TBE) gel stained with SYBR Safe gel stain (Invitrogen, Carlsbad, CA, USA). Triplicate PCR products per sample were pooled and purified using the MinElute PCR purification kit (Qiagen). The concentrations of purified products were quantified using the HS dsDNA assay on the Qubit 2.0 fluorometer (ThermoFisher Scientific). Barcoded PCR products were diluted to equal concentrations and pooled for sequencing. Samples were shipped to the Georgia Genomics and Bioinformatics Core at the University of Georgia for sequencing on an Illumina MiSeq using paired-end 250 bp sequencing.

Data analysis

All sequence processing and data analysis was performed in R Studio (v 1.1.463) running R (v 3.4.0, 2017-04-21). All code and data used for recreating figures is publicly available on GitHub (https://github.com/CynthiaBecker/USVItide). Sequence reads were inspected for quality, filtered, trimmed, and dereplicated in the DADA2 R package (v.1.10.0) (Callahan *et al.*, 2016). Specific filtering parameters used included the following: truncLen = c(240, 200), maxN = 0, maxEE = c(2,2), rm.phix = TRUE, and compress = TRUE. The parameter truncLen was used to truncate forward reads at 240 bp and reverse reads at 200 bp where observed quality began to drop significantly, or below a Q30 of 25. maxN was set to zero and and maxEE was set to two for both forward and reverse reads, which were not changed from default values because they did not lead to drastic losses in sequence read data. The parameters rm.phix = TRUE and compress = TRUE were included as default parameters. DADA2 was also used to remove chimeras and generate amplicon sequence variants (ASVs) which are of finer resolution and more tractable than standard operational taxonomic units (Callahan *et al.*, 2017). Each ASV in the following analyses contains a corresponding DNA sequence that is provided in Table S1 of the Supplement (available at www.int-res.com/articles/suppl/a085p101_supp.xlsx). ASV generation in DADA2 retained between 75.9% and 87.6% of input sequence reads in non-control samples while control samples (DNA extraction controls and sequenced PCR negative controls) retained only 5.1 – 46.0% of input sequences (Table S2 in the Supplement, link above). Taxonomy was assigned in DADA2 using the SILVA SSU rRNA database down to the species level where applicable (v.132) (Quast *et al.*, 2012). Two mock community samples from the Human

Microbiome Project (Even and Staggered) were used to check accuracy of DADA2. DADA2 inferred 29 ASVs in the Even mock community and 21 ASVs in the Staggered mock community, and of those, 22 and 18 ASVs were exact matches to the reference sequences, respectively. This indicated that DADA2 accurately recovered ASVs representative of the input strains.

To understand the variability in microbial communities over time at all sites, ASV counts in each sample were transformed to relative abundance, and then Bray-Curtis dissimilarity was calculated between each sample using the R package vegan (v2.5.4) (Oksanen *et al.*, 2020). The resulting dissimilarity values were illustrated using non-metric multidimensional scaling (NMDS) with the R package, ggplot2 (v3.2.1) (Wickham, 2016a). Environmental vectors that significantly associated (cutoff $p < 0.01$) with the ordination were produced using the function *envfit* in the vegan R package. Pairwise dissimilarity was plotted to represent the range of dissimilarity in microbial communities over 48 hr at each site. A Kruskal-Wallis test was used to examine if there was a significant difference in dissimilarity between sites (significance level $p < 0.05$). To determine which pairs of locations had significantly different dissimilarities, a pairwise Wilcoxon Rank Sum test was used with a Benjamini-Hochberg correction for multiple testing and a cutoff of 0.05.

Differential abundance (DA) of ASVs in relation to the tide was only evaluated for select samples (Fish Bay Mangrove and Lameshur Mangrove subtidal) using the corncob R package (v 0.1.0) (Martin *et al.*, 2020). All ASV counts per sample were input into the corncob program, which modeled relative abundances using a logit-link for mean and dispersion. DA was modeled as a linear function of tide height (a continuous covariate that is representative of the tidal level) while controlling for differential variance and the effect of site and day or night on DA. Controlling for the effect of day or night was imperative because over the 48 hr period low and flood tide occurred during the day, and high and ebb tide occurred during night and dawn, respectively. The parametric Wald test was used to test the hypotheses that the relative abundance of a given ASV changed significantly with respect to tide height and the Benjamini-Hochberg false discovery rate (FDR) correction was applied to account for multiple comparisons, with the cutoff at 0.05.

RESULTS

Environmental characteristics

Temperature and salinity of surface seawater fluctuated more at the mangroves (Fish Bay and Lameshur mangrove subtidal) compared to the seagrass and reef habitats (Figure 3-2a,b). At all sites, temperature was generally highest at flood or low tide. This pattern coincided with a daylight warming period (black and white bar, Figure 3-2). While the temperature tracked with the diel cycle, salinity did not fluctuate more than 2.0% (0.69 psu) of the average salinity over the 48 hr window at reef and seagrass locations (Figure 3-2b). In contrast, salinity at mangrove sites fluctuated much more, and in concert with the tidal cycle. Fish Bay and Lameshur mangrove salinities increased above the average minimum salinities (35.5 and 34.9, respectively) by as much as 5.3% (1.88) and 4.8% (1.70), respectively (Figure 3-2b). The lowest mangrove salinity was observed during high tide at the Lameshur mangrove subtidal area, which reached on average 34.9 and matched average reef water salinity. The highest mangrove site salinity was measured at Fish Bay mangrove, during low or ebb tide, and was on average 37.2 (4.8% higher, Figure 3-2b). In general, Fish Bay mangrove and seagrass habitats were more saline than those in Lameshur Bay (Figure 3-2b).

Nutrient concentrations for phosphate (PO_4^{3-}), ammonium (NH_4^+), silicate, and nitrite + nitrate ($NO_2^- + NO_3^-$) were generally lower and more stable at all reef and seagrass habitats in comparison to the mangroves (Figure 3-3). Reef and seagrass habitats were oligotrophic, with all reefs experiencing average nutrient concentrations of 0.18 µM PO_4^{3-}, 0.16 µM NH_4^+, 2.32 µM silicate, and 0.17 µM $NO_2^- + NO_3^-$. Nutrient concentrations at seagrass locations measured on average 0.20 µM PO_4^{3-}, 0.23 µM NH_4^+, 2.58 µM silicate, and 0.10 µM $NO_2^- + NO_3^-$. Mangrove nutrient concentrations were higher on average compared to reef and seagrass habitats, and measured 0.30 µM PO_4^{3-}, 1.05 µM NH_4^+, 4.27 µM silicate, and 0.39 µM $NO_2^- + NO_3^-$. Nutrient concentrations were also more variable at the mangroves. PO_4^{3-}, NH_4^+, and silicate concentrations were lowest in the mangroves during flood and high tide, when they approached typical reef and seagrass site concentrations (Figure 3-3a,b,c). In contrast, the highest concentrations of PO_4^{3-}, NH_4^+, and silicate at the mangroves were generally sampled

during ebb and low tide (Figure 3-3a,b,c). One exception was the Lameshur mangrove inlet, which was located near the top of the intertidal zone and could only be sampled at high tide when it was flooded. That site contained generally high concentrations of PO_4^{3-}, NH_4^+, and silicate. The Fish Bay mangrove had lower average nitrogen concentrations (0.08 µM NO_2^- + NO_3^-) compared to those at both Lameshur mangrove sites (0.68 µM NO_2^- + NO_3^-, Figure 3-3d). At Lameshur mangrove subtidal, concentrations of NO_2^- + NO_3^- were lowest during high tide (Figure 3-3d).

Microbial cell abundances

While reef sites exhibited predominantly stable nutrient and physical characteristics, picocyanobacterial abundances (*Prochlorococcus* and *Synechococcus*) were highly variable and exhibited dynamics that coincided with both diel and tidal cycles (Figure 3-4). Abundances of *Prochlorococcus* and *Synechococcus* decreased during the day and increased during the night. At reef sites, excluding Ditliff, the concentrations of *Prochlorococcus* increased up to a factor of two between dusk and later in the evening (between flood and high tide) on July 22 (Figure 3-4a). One exception to this trend was at the Ditliff reef (yellow line, Figure 3-4a), where *Prochlorococcus* abundance decreased by 50% between flood and high tide on July 22. This changed on July 23, when abundances of *Prochlorococcus* at Ditliff and all other reefs increased between dusk (flood tide) and night (high tide). In general, *Prochlorococcus* cells were greatest at night and before dawn during high or ebb tide, and lowest in abundance during the day at low and flood tide (Figure 3-4a). Abundances of *Prochlorococcus* were low at Fish Bay seagrass (average 15,333 cells ml^{-1}) and nonexistent at Fish Bay mangrove. In contrast to *Prochlorococcus, Synechococcus* abundances could be measured at all sites, where they exhibited cyclical changes. At all sites, a clear change in abundance was present between dusk and night over both days (flood to high tide). During that time period on July 22nd, *Synechococcus* abundances increased by a factor of 1.70 - 9.30, and on July 23rd the cells increased by a factor of 1.45 - 17.3 (Figure 3-4b). *Synechococcus* abundances also tracked closely to the tidal cycle, with increased cell abundances during flood tide and decreased abundances during ebb tide. The highest abundances coincided with high tide on both days.

Synechococcus abundances were low during ebb or flood tide on both days (Figure 3-4b). A sudden increase in photosynthetic picoeukaryotes between dusk and night time points was also observed at reef and seagrass habitats, which also coordinated with tidal cycle, where the lowest abundances occurred during flood tide, followed by a sharp increase until high tide (Figure 3-4d). Picoeukaryotes in the mangroves exhibited higher variability that was not coordinated with tidal or diel cycles over 48 hrs. Abundances of heterotrophic Bacteria and Archaea were greatest at both mangroves (Fish Bay and Lameshur Bay subtidal) during low tide, and at the Lameshur mangrove inland site that was only sampled at high tide. Fish Bay seagrass and mangroves contained more heterotrophic Bacteria and Archaea compared to Lameshur Bay seagrass and mangrove locations (Figure 3-4c). At the Lameshur mangrove subtidal area during flood and high tide, the abundance of heterotrophic Bacteria and Archaea decreased to 635,646 cells ml^{-1} on average, similar to abundances at Lameshur seagrass and all coral reef sites. Coral reef and seagrass biomes exhibited stable heterotrophic bacterial and archaeal abundances compared to both mangrove biomes (Figure 3-4c).

Variability in microbial communities with tides

Non-metric multidimensional scaling (NMDS) of Bray-Curtis dissimilarity revealed that reef and seagrass seawater microbial community compositions were distinct from those at mangrove habitats (Figure 3-5a). The overlaid environmental vectors indicated that mangroves featured increased nutrient concentrations, salinity, heterotrophic bacterial and archaeal abundances, and picoeukaryote abundances compared to reef and seagrass habitats (Figure 3-5a). Fish Bay sites (mangrove and seagrass), located outside of the National Park, clustered separately from all other reef, mangrove, and seagrass sites, which corresponded with increased temperature at those sites (Figure 3-5a, black and light blue dots). Conversely, dissimilarity of Fish Bay seagrass microbial communities was significantly different than all other sites (Figure 3-5c, Table A2). Reef sites generally clustered together with Lameshur seagrass sites in the NMDS plot (Figure 3-5a) and a bar chart representation of the within-site Bray-Curtis dissimilarity at each site (beta diversity) revealed similar trends between reef and Lameshur seagrass sites (Figure 3-5c, Table 3-S2). Vectors associated with increased depth and

Prochlorococcus cell abundances pointed in the direction of the reef and Lameshur Bay seagrass sites, which verified cell abundance trends captured earlier (Figure 3-4a, 3-5a). Fish Bay seagrass, Lameshur seagrass, Yawzi reef, and Tektite reef samples clustered tightly within site, which suggested little change in community composition over 48 hrs (Figure 3-5a). Ditliff and Cocoloba reef microbial community compositions did not cluster as tightly, which indicated greater variability over 48 hrs (Figure 3-5a).

Microbial community composition at the Fish Bay and Lameshur mangrove sites exhibited a pattern of organization that represents a tidally-influenced shift (Fig 5b). The spread of points in the NMDS was organized with high tide samples (squares) farthest from low tide samples (crosses), and flood and ebb samples in between. Overlaid vectors revealed that tide height and silicate were significantly associated with the ordination of mangrove microbial community composition (Figure 3-5a,b). In the mangrove microbial communities, high tide microbial composition (squares) were oriented in the direction of highest tide height and lowest silicate concentrations, while low tide community composition (crosses) were in the direction of the lowest tide height and highest silicate concentrations (Figure 3-5b). In the NMDS, the Lameshur mangrove inland microbial communities sampled at high tide only were positioned closest to the low tide Lameshur mangrove subtidal communities. The overlaid vectors also revealed that the Fish Bay mangrove site had increased salinity and heterotrophic bacteria and archaea, especially at low tide (Figure 3-5b). The Lameshur mangrove subtidal site, on the other hand, was deeper and contained high abundances of *Synechococcus* at high tide, had more *Prochlorococcus*, and featured higher nitrogen concentrations (Figure 3-5b). Furthermore, tidal changes in Fish Bay mangrove featured cycles in the relative abundances of Bacteroidetes, Epsilonbacteraeota, and Proteobacteria while Lameshur mangrove subtidal exhibited cycles in the relative abundances of Bacteroidetes, Cyanobacteria, and Proteobacteria (Figure 3-S1).

To further investigate the variability in microbial community structure at each site over 48 hrs, we examined pairwise Bray-Curtis dissimilarity of communities within each site (Figure 3-5c). Higher pairwise dissimilarity overall indicated a more variable microbial community composition while a lower, and less variable within-site dissimilarity indicated greater stability

in the microbial community composition. Within-site dissimilarity was significantly different across sites (Kruskal-Wallis test, $p < 0.05$). Pairwise Wilcoxon rank sum tests revealed that within-site dissimilarity was significantly lower at all sites compared to mangrove sites ($p < 0.05$, Table A2), but not significantly different between mangrove sites ($p = 0.9805$, Table A2). All pairwise comparisons are summarized in Table A2.

Differential abundance of ASVs at mangrove sites with tide height

To investigate which taxa were changing with respect to tide height in the mangroves, we tested for significantly differentially abundant (DA) ASVs in relation to tide height, and found 87 DA ASVs (Figure 3-6). DA ASVs were classified into 24 taxonomic orders (ASV68 was unclassified at the Order level). The majority of DA ASVs (82.8%; 72 ASVs) had a positive coefficient and 17.2% (15 ASVs) had a negative coefficient. This indicated that most DA ASVs were enriched with a one unit increase in tide height, and were therefore enriched during high tide. Some of these significantly enriched high tide ASVs were classified to Proteobacteria, including SAR11, SAR86, and AEGEAN-169 marine group, '*Candidatus* Actinomarina' (phylum Actinobacteria), and NS5 marine group (phylum Bacteroidetes) (Figure 3-6). Many ASVs of Flavobacteriales (phylum Bacteroidetes), SAR116 (phylum Proteobacteria), and Cyanobacteria (*Prochlorococcus* and *Synechococcus*) were also significantly associated to a high tide height in mangrove environments (Figure 3-6).

The ASVs with a negative coefficient decreased in relative abundance with a one-unit increase in tide height, and therefore were enriched during low tide heights in the mangrove environment. Significant low tide associated ASVs were classified to phyla that changed dramatically in mangroves as visualized in the stacked bar chart, and included Epsilonbacteraeota (*Arcobacter*), Proteobacteria (OM27 clade of Bdellovibrionaceae, *Marinobacterium, Micropepsis* and *Rhodobacteraceae*), and Bacteroidetes (*Draconibacterium*) (Figure 3-S1, Figure 3-6). The bacteria significantly enriched during low tide were distinct from the bacteria that were significantly enriched during high tide, and included unique Orders such as Bacteroidales (genus *Draconibacterium*) and Micropepsales (genus *Micropepsis*) (Figure 3-6). Differentially abundant ASVs revealed a shifting microbial community with tidal cycle,

specifically as it pertained to changes in tide height, which confirmed trends seen in the NMDS analysis (Fig 5b, 6).

DISCUSSION

We used a combination of genomic and environmental measurements to determine the extent of tidally-influenced microbial dynamics in three important and spatially related tropical biomes: mangroves, seagrass meadows, and coral reefs. Not all bays and areas offered the same biome structure but Lameshur and Fish Bays offered comparable biome patterns of mangroves, seagrasses and coral reefs as we moved southward, allowing for biome replication. We found a significant tide-mediated change in environmental and microbial parameters in mangrove environments. Furthermore, differential abundance analysis identified microbial taxa that were significantly associated with changing tidal elevation. In contrast, seawater overlying reefs and seagrass meadows exhibited strong cyclic changes in picocyanobacterial abundances, despite muted changes in physicochemical variables, nutrient concentrations and microbial community composition. Overall, our findings underpin how short-term tidal and likely also diel cycles influence the microbial dynamics of coastal tropical ecosystems.

Mangrove regions sampled in this study (Fish Bay mangrove and Lameshur mangrove subtidal) were surrounded by red mangroves. Red mangroves are characterized by prop roots that extend into the seawater and sediment and are constantly immersed in seawater. The Lameshur Bay mangrove inland site at the upper intertidal zone was surrounded by black and white mangroves and only flooded during high tide. Over the course of our study, these biomes were characterized by variable salinity, nutrient concentrations, and heterotrophic bacteria and archaea that coincided with different parts of the tidal cycle, a common finding that has previously been reported (Dittmar and Lara, 2001; Sánchez-Carrillo *et al.*, 2009). While seawater flux was not measured here, the data suggest that the tidal flow of seawater from the oligotrophic reef and seagrass biomes into the more eutrophic mangrove ecosystem during flood and high tide promoted depression of salinity, nutrient, and heterotrophic microbial regimes. During ebb and low tide, higher nutrients and heterotrophic bacteria and archaea in

the mangroves may have been caused by the seawater flushing out from the upper intertidal black and white mangrove forest that was enriched in heterotrophic bacteria and archaea as well as some nutrients to the fringing and subtidal red mangrove forest. In contrast, the higher salinity was likely more due to evaporation of seawater during the day than due to tidal mixing.

Compared to mangroves, reef and seagrass meadows were characterized by consistent physicochemical parameters and heterotrophic bacterial and archaeal cell abundances. Despite this, picocyanobacterial (*Prochlorococcus* and *Synechococcus*) abundances were variable over the 48 hr sampling window, which appeared to be related to both tidal and diurnal cycles. Blanchot et al. (1997) noted a similar pattern in *Prochlorococcus* and picoeukaryotes in the equatorial Pacific, where cell abundances increased from dusk to 02:00, then began to decrease until dusk the following day over five consecutive days. This study was not coastal, and therefore unrelated to tides. Additionally, diel-influenced abundances of picocyanobacteria were recently identified on a coral reef just east of the reefs sampled in this study, with *Prochlorococcus* doubling and *Synechococcus* increasing each night, and not in relation to the tides (Weber and Apprill, 2020). These daily cycles were a result of cell growth, where cells divided in late afternoon or evening, resulting in a doubling of the community for well-synchronized populations (Vaulot and Marie, 1999; Binder and DuRand, 2002). Given the photosynthetic capability of these cells, the changes we note in our study were most likely due to growth resulting from changes in light or diel rhythms rather than changes in tide. However, because low and flood tide coincided with daytime and high and ebb tide coincided with night, we were unable to fully disentangle the effects of tide compared to light in our study. We noted the complete absence of *Prochlorococcus* cells at the Fish Bay mangrove, but not at Lameshur Bay mangrove subtidal. This may have been due to the higher temperature, salinity and phosphate concentrations in Fish Bay compared to Lameshur Bay, which may collectively make this environment inhospitable for *Prochlorococcus* (Partensky *et al.*, 1999).

The tidal variability in seawater microbial communities within the mangrove biomes mirrored trends seen in the physicochemical environment. Lu et al. (2015) found that over diurnal periods in a coastal estuarine to reef transition zone, the changes in microbial communities were more likely due to tidal mixing of the seawater rather than growth due to

altered environmental conditions. While Lu and colleagues (2015) did not find tidal changes in environmental variables to correlate well with microbial community composition in estuarine environments, other studies did find that environmental variables such as salinity and inorganic nutrients can impact the structure of microbial communities (Bouvier and del Giorgio, 2002; Campbell and Kirchman, 2013). Our study showed both biological and physical processes to be related to observed changes in microbial communities over short, tidal time scales within the mangroves. In our study, tidal mixing likely exerted the greatest impact on microbial communities within mangrove environments, and was additionally responsible for the changes in the environmental parameters. However, it was challenging to disentangle whether altered microbial communities were a growth response to changing environmental conditions or due to tidally-advected communities reflective of the environment of origin.

Regardless, the observed short-term changes (several hrs and over the course of day) highlight the limitation of snapshot (e.g. once-daily) sampling. All sites showed some daily or tidal-based variation. Thus, long-term sampling schemes aimed at characterizing the nutrient and microbial diversity of a location should consider the importance of short temporal variation and at least sample over a few diel cycles to account for this variability and evaluate its consistency (or lack thereof) over time. Sampling schemes designed to characterize microbial communities and biogeochemistry may be particularly important for monitoring the health and stability of the region within marine reserves; a concept that has had success in coral reef environments (Glasl *et al.*, 2017, 2018). To alleviate misleading results that may stem from sampling design, we suggest that accounting for tidal or diurnal forces is important in these coastal areas. In our study of coral reef and seagrass meadow seawater, the striking changes in picocyanobacteria over two days underpin the importance of sampling at the same time each day, when possible. In contrast, the dramatic tidally-induced changes in the coastal mangrove seawater complicate monitoring efforts. In this case, efforts to sample mangrove environments during a consistent part of the tide cycle (especially ebb or low tide) would allow for a more controlled study of the mangrove seawater. In this way, the temporal microbial community dynamics of the seawater ecosystem would be both controlled for and well-characterized.

Beyond tide-related changes in mangrove seawater microbial communities, there were site-specific changes that may be explained by differences in the environmental variables at each mangrove environment. A study of soil microbiomes at a protected and unprotected mangrove area also noted distinct site-specific changes that were explained by strikingly different environmental factors (Yun *et al.*, 2017). That study was similar to ours because it sampled a protected and unprotected mangrove area. The Lameshur mangrove in our study was within the Virgin Islands National Park, with minimal coastal development. In contrast, the Fish Bay coast and watershed area is considered impacted by human development, and has been a target of management due to erosion and sedimentation from such development and bay contamination from septic systems, household pollutants, and pesticides (Hodge *et al.*, 2001). Both Yun et al. (2017) and the present study included only one protected and unprotected site, so it remains to be seen if the environmental and microbial changes between regions were explained by protective status. Yet the reproducibility across studies suggests there may be some actual differences in microbial communities between human-influenced and more pristine mangrove habitats that could be a target for future studies of mangrove ecosystems. These changes across bays may also illustrate the natural heterogeneity of mangrove habitats (Leung, 2015). For instance, Fish Bay mangrove contains a habitat of red mangroves that surround the sandy shoreline, while Lameshur Bay mangrove extends from a rocky outlet to an inland mangrove swamp with multiple species of mangrove in muddy sediment. How human influence and natural heterogeneity together influence the structure of microbial communities or how microbes play a role in mangrove habitat health and potential recovery are outstanding questions for target in future studies.

Our analysis of differentially abundant (DA) ASVs at mangroves indicated that tidal mixing may be bringing in microbial cells from the reef and seagrass environments, causing significant changes in community composition especially during flood and high tide. SAR11, SAR86, '*Candidatus* Actinomarina', NS5 marine group, AEGEAN-169 marine group, and Rhodobacteraceae were enriched at higher tides within coastal mangrove seawater. These taxa were also shown to be significantly associated with reef seawater by a study that compared seawater microbiomes near and far from corals on Caribbean reefs (Weber et al. 2019). In the

mangroves during high tide, we also identified other microbes that were typical of reef seawater or open ocean microbial communities, including *Prochlorococcus* and *Synechcococcus,* several Proteobacteria, including OM60 clade, SAR116 clade, Oceanospirillales, and Rickettsiales, many Bacteroidetes including Cryomorphaceae, NS9 marine group, Flavobacteriaceae (NS4 marine group and NS2b marine group), NS11-12 marine group, and the archaea Marine Group II (Euryarchaeota) (Nelson *et al.*, 2011; Kelly *et al.*, 2014; Apprill *et al.*, 2015; Choi *et al.*, 2015; Lindh *et al.*, 2015; Polónia *et al.*, 2016; Becker *et al.*, 2017; Kim *et al.*, 2018; Glasl *et al.*, 2019).

Tidal elevation appeared to exert a mixed effect on Bdellovibrionaceae, a family of Proteobacteria that was significantly enriched at both low and high tides. Bdellovibrionaceae are bacterial predators and have been previously found at increased abundance in mangrove ecosystems compared to coral reef environments, which was likely due to the heightened prey available in the mangrove environment (Sutton and Besant, 1994). In our study, the increased heterotrophic bacteria and archaea during ebb and low tide may have provided an environment with abundant prey that fostered growth of Bdellovibrionaceae. In contrast, the presence of a high tide-associated Bdellovibrionaceae ASV (ASV522) may have indicated the influx of a coral reef or seagrass-associated strain with different environmental growth tolerances and prey preferences (Sutton and Besant, 1994). While confirming the exact specific Bdellovibrionaceae strains within the OM27 clade was not possible here, the presence of differentially abundant Bdellovibrionaceae cells within the mangrove habitat underlines a potentially important role of Bdellovibrionaceae within mangrove ecosystems that warrants further investigation.

While tidal mixing exerted varied influences on Bdellovibrionaceae taxa, during low tide height, enrichment of microbial cells likely derived from mangrove seawater and sediment was apparent. For example, three DA ASVs classified as *Marinobacterium,* a gammaproteobacterial genus that has previously been associated with estuarine or mangrove ecosystems (Chen *et al.*, 2010; Alfaro-Espinoza and Ullrich, 2014; Park *et al.*, 2016). Two low tide-associated ASVs were classified as *Arcobacter* (ASV6, ASV454), a genus of the Order Campylobacteria that has been found enriched in intertidal sediment (Wang *et al.*, 2012). While most *Arcobacter* species have

been isolated using aerobic or microaerobic conditions (Collado and Figueras, 2011), some, such as a species isolated from estuarine sediment, grew anaerobically (Sasi Jyothsna *et al.*, 2013). *Micropepsis* (ASV2079) is a recently identified genus of Alphaproteobacteria, with one obligatory anaerobic isolate originating from an oligotrophic bog-like environment (Harbison *et al.*, 2017). The anaerobic lifestyles of *Micropepsis* and potentially *Arcobacter* suggest they may have been derived from anoxic mangrove sediment. *Draconibacterium* (phylum Bacteroidetes) is another genus that contains marine sediment-derived bacteria, providing merit to the detection of this bacterium when water was shallowest (Du *et al.*, 2014; Gwak *et al.*, 2015). The Rhodobacteraceae (Alphaproteobacteria) are some of the most widely spread bacteria in the ocean and a study analyzing distribution and classification of Rhodobacteraceae found that one third of the detected Rhodobacteraceae correlated to sediment parameters, indicating there are specific sediment-associated Rhodobacteraceae (Pohlner *et al.*, 2019). Rhodobacteraceae strains have been isolated from mangrove sediments (Yu *et al.*, 2018; Ren *et al.*, 2019). Overall, these data suggest that during low tide, the mangrove seawater becomes enriched in microbial cells likely derived from the mangrove sediment within the inland tidal flat and mangrove forest.

This work is the first to characterize tide-influenced seawater microbial community variability at three distinct coastal biomes simultaneously, and provides new insights into coastal microbial community dynamics over short temporal scales. Mangrove seawater microbial communities exhibited surprising variability over 48 hours, which was associated with tidal elevation. This was contrasted by the relative consistency in coral reef and seagrass meadow microbial communities sampled over the same time period. All biomes characterized in this study did show some level of short temporal changes associated with tidal or diurnal effects. While we incorporated and repeatedly sampled 8 sites, this was only conducted for 48 hrs, preventing our analysis from fully disentangling the tidal and diurnal effects. Addressing this variability over longer timescales, such as several days, would help elucidate the consistency of these patterns among mangrove versus seagrass and reef seawater microbial communities. Additionally, this study lacks inclusion of organic carbon and nitrogen concentrations and dynamics. These measurements should be included in future studies, and

could provide additional important insights into heterotrophic microbial population dynamics. Another future area of investigation that is relevant to monitoring practices is how the benthic microbial communities (associated with the sediments, seagrass, reef life, and surrounding reef-depth waters) may change during tidal cycles. To this end, some studies have shown evidence for short-term changes in near-coral and reef seawater microbial communities (Kelly *et al.*, 2019; Weber and Apprill, 2020), and seagrass and mangrove sediment microbial parameters (Moriarty and Pollard, 1982; Lee and Joye, 2006). The investigation of microbial community changes over short-term scales in these coastal environments is still rare, and a coordinated study including multiple sample types (seawater, sediment, flora, and fauna) over such timescales would be an important target for future work. Regardless, this study provides a basis for future studies, which could investigate how shifting microbial regimes in mangrove environments impact microbial productivity and habitat processes over short temporal scales in these dynamic and critically important coastal ecosystems. Additionally, this work reinforces the importance of accounting for tidal and diurnal scales within the context of long-term investigations, especially in dynamic and protected coastal biomes.

ACKNOWLEDGEMENTS

We thank the Virgin Islands Environmental Resource Station and University of the Virgin Islands for field support. Thanks to Karen Selph from the University of Hawai'i School of Ocean and Earth Science and Technology (SOEST) for flow cytometry support, Joe Jennings of Oregon State University for measurement of inorganic nutrient concentrations, and the Georgia Genomics and Bioinformatics Core, which provided the sequencing support. This research was supported by NSF awards OCE-1536782 to T.A.M., J.K.L., and A.A. and OCE-1736288 to A.A., NOAA Cooperative Institutes award NA19OAR4320074 to A.A. and E. Kujawinski and the Andrew W. Mellon Foundation Endowed Fund for Innovative Research to A.A.

DATA AVAILABILITY

All raw sequence files used in this study were uploaded to the NCBI Sequence Read Archive under accession number PRJNA578400, and data are also available at BCO-DMO under dataset 783679 (https://www.bco-dmo.org/dataset/783679). R scripts for recreating all figures included in this paper are available on GitHub (https://github.com/CynthiaBecker/USVItide). Supplement tables are also provided on the GitHub page for reference as well as at www.int-res.com/articles/suppl/a085p101_supp.xlsx

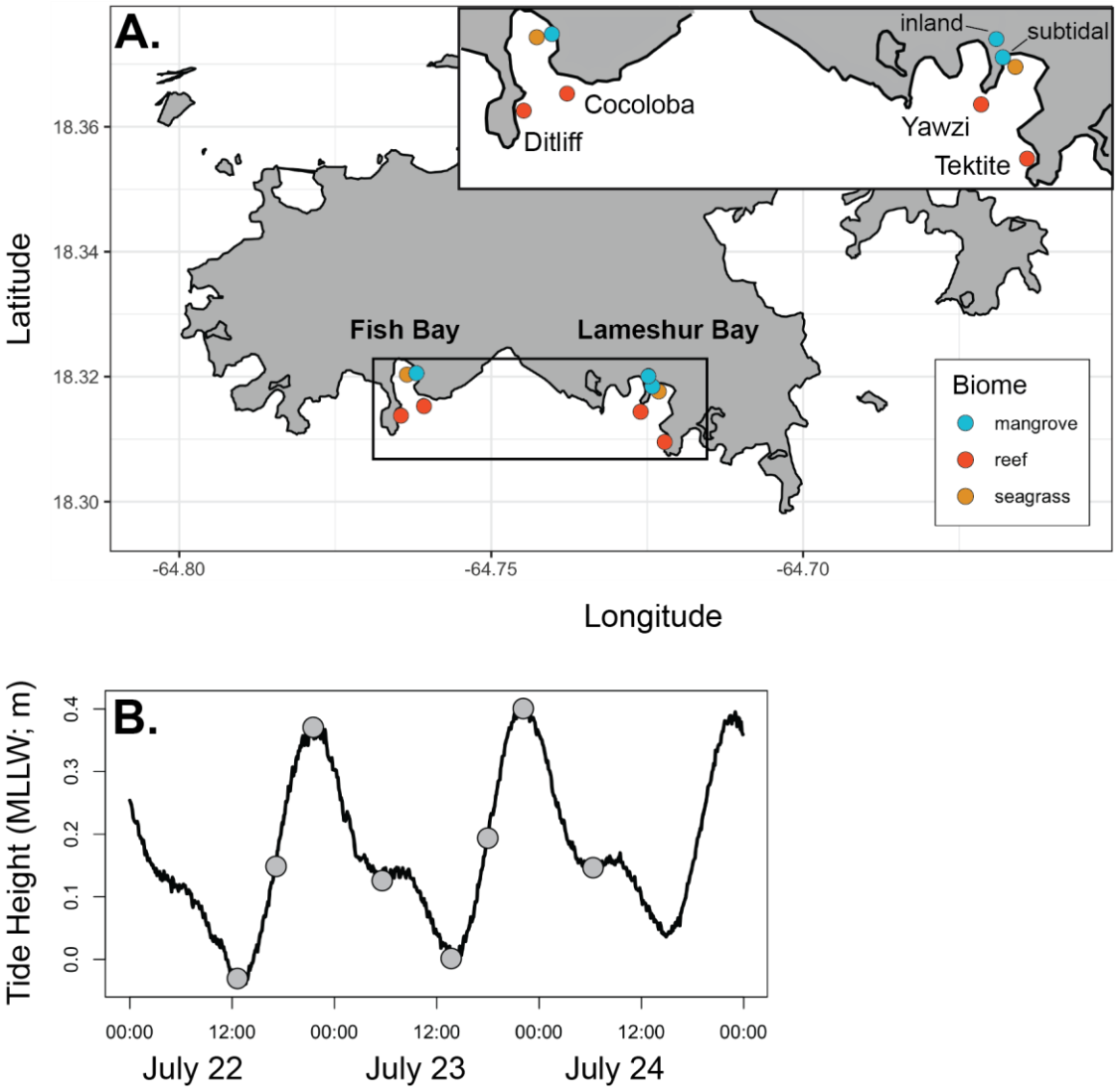

Figure 3-1. Map of sampling area and tide height over the course of the sampling period. A) Map of St. John, United States Virgin Islands (USVI) depicts mangrove (blue dots), reef (red dots), and seagrass (orange dots) sites in Lameshur Bay and Fish Bay with inset provided for greater detail in orientation of sampling locations. Reef sites are labeled by name (Ditliff, Cocoloba, Yawzi, Tektite). B) Tide height relative to mean low low water (MLLW, m) plotted as a function of time with sampling time points indicated with gray dots. Tide height data were collected from NOAA/NOS/CO-OPS Station ID 9751381 in Lameshur Bay, St. John, USVI.

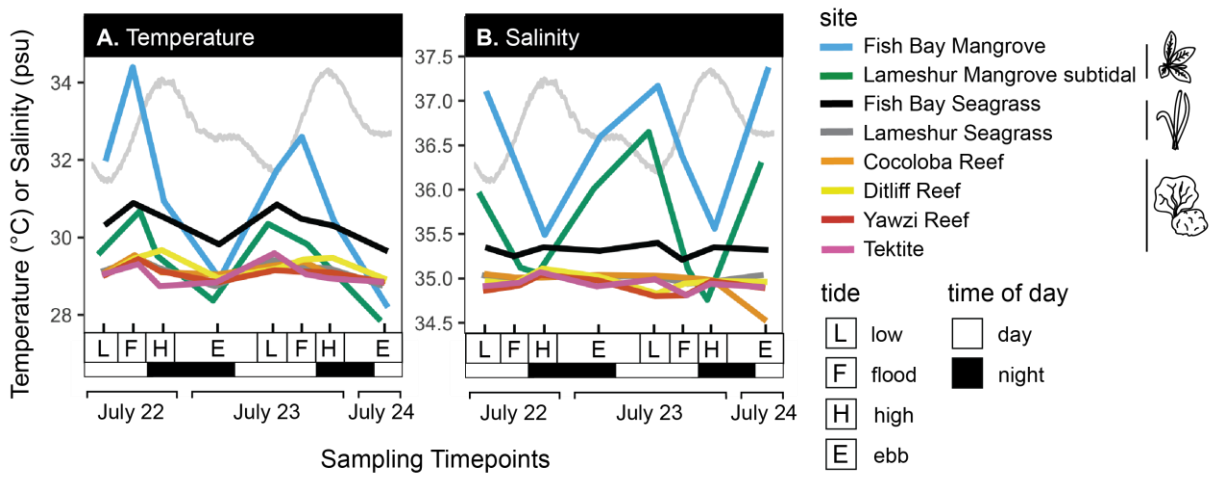

Figure 3-2. Temperature and salinity over 48 hours at each site

Line graphs of (A) temperature (°C) and (B) salinity (psu) in the seawater over the course of the study at each site. Sample time points on the x-axis coincide with low (L), flood (F), high (H), and ebb (E) tide. A representation of the tide height over the sampling period is in the background of each box (light gray line in top half of graph). Night and day are represented by black and white, respectively, in the bar at the bottom of each graph.

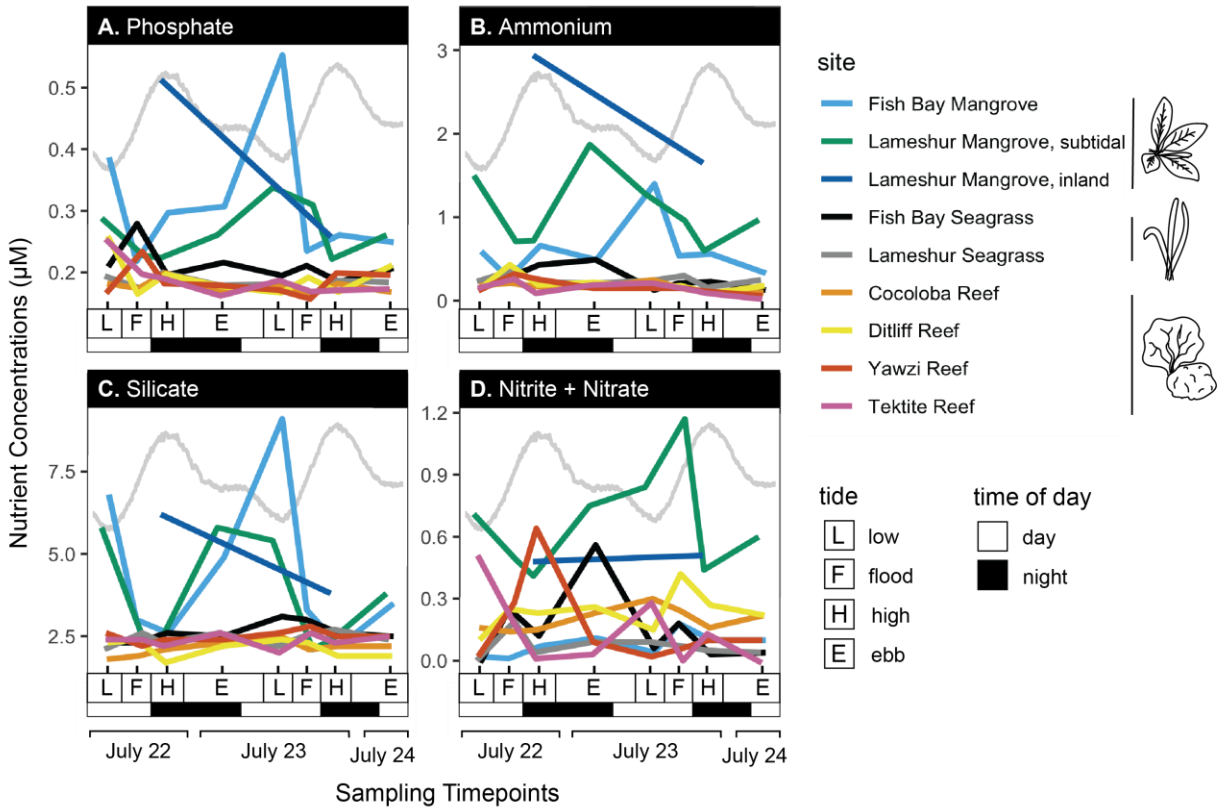

Figure 3-3. Inorganic nutrient concentrations over 48 hours at each site.
Line graphs of (A) phosphate (PO_4^{3-}), (B) ammonium (NH_4^+), (C) silicate, and (D) nitrite + nitrate (NO_2^-+NO_3^-) in the seawater over the course of the study at each site. Sample time points on the x-axis represent low (L), flood (F), high (H), and ebb (E) tide. A representation of the tide height over the sampling period is in the background of each box (light gray line in top half of graph). Night and day are represented by black and white, respectively, in the bar at the bottom of each graph.

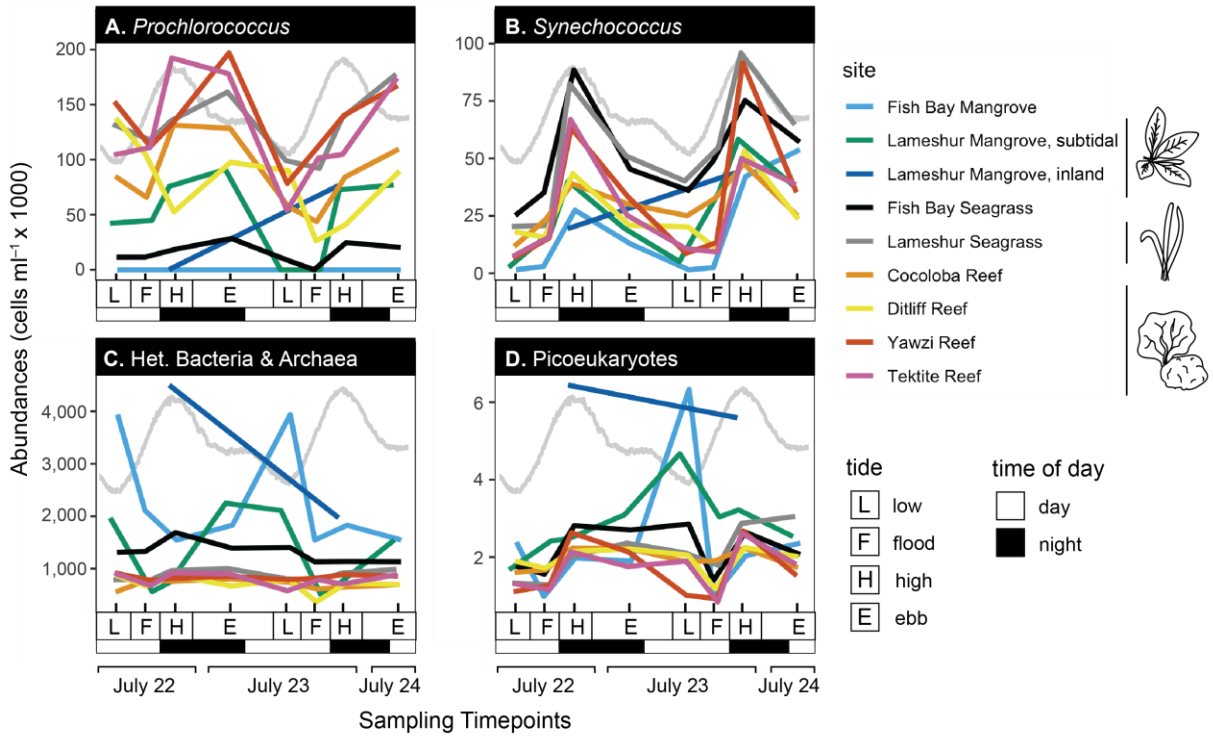

Figure 3-4. Cell abundances from flow cytometry over 48 hours at each site.
Line graphs of (A) *Prochlorococcus*, (B) *Synechococcus*, (C) heterotrophic (unpigmented) bacteria and archaea, and (D) picoeukaryotes over the course of the study at each site. Sample time points on the x-axis represent low (L), flood (F), high (H), and ebb (E) tide. A representation of the tide height over the sampling period is in the background of each box (light gray line in top half of graph). Night and day are represented by black and white, respectively, in the bar at the bottom of each graph.

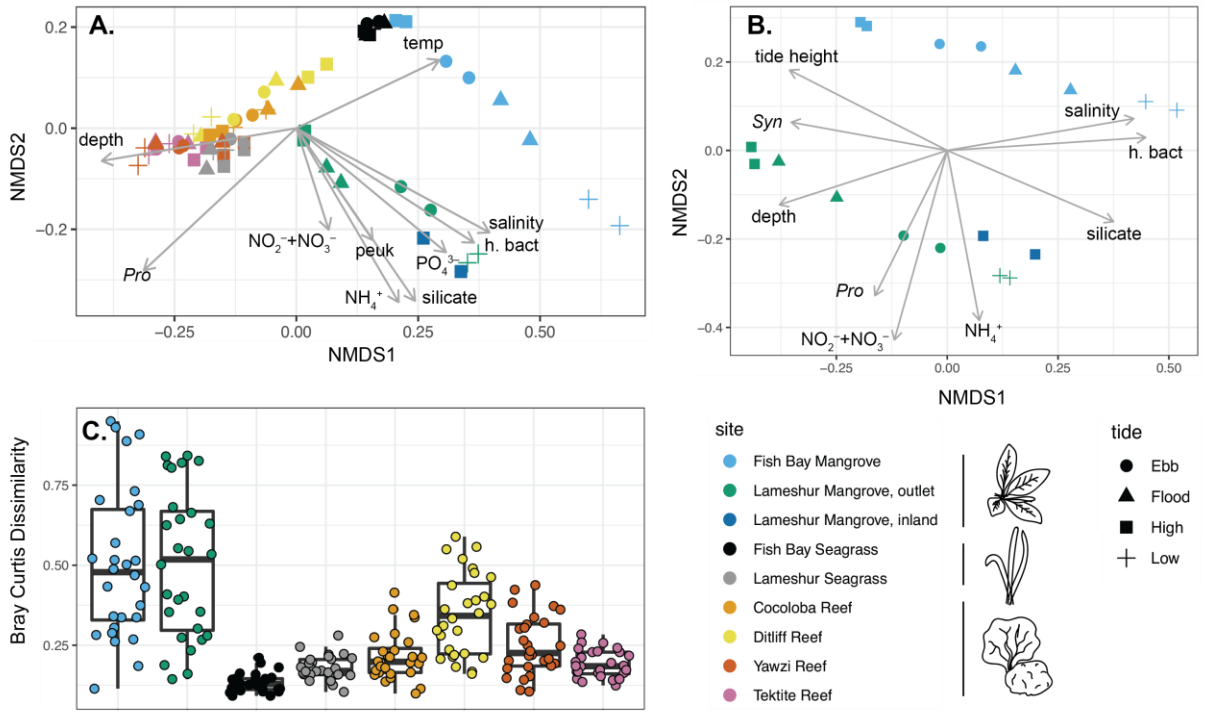

Figure 3-5. Beta diversity

Non-metric multidimensional scaling (NMDS) and boxplots representing Bray-Curtis dissimilarity between microbial communities, obtained from SSU rRNA gene sequencing. Bray-Curtis dissimilarity between samples represented by NMDS with vectors of environmental variables overlaid either (A) all samples collected at each site over 48 hr or (B) mangrove samples collected over 48 hr. Vectors point in the direction of the greatest change in the variable or gradient it represents and the length of the vector is proportional to the strength of the gradient. Only vectors with a $p < 0.01$ are represented. C) Boxplots represent pairwise Bray-Curtis dissimilarity for samples within each site. Boxes in the boxplot represent the interquartile range (IQR), or the area between the 25% and 75% quantiles with the median as the line in the center. Lines extend beyond the box to 1.5×IQR. Points beyond the lines are outliers. *Pro* = *Prochlorococcus, Syn* = *Synechococcus,* peuk = picoeukaryotes, h. bact = heterotrophic bacteria and archaea, temp = temperature.

Figure 3-6. Differential abundance with tide in mangrove habitats.
Differentially abundant (DA) amplicon sequence variants (ASVs) as a function of tide height at Fish Bay and Lameshur Bay subtidal mangrove sites. The relative abundance of each ASV was modeled as a linear function of tide height, a measure of tidal level, and significantly DA ASVs at a cutoff of $p < 0.05$ are shown (see methods). The coefficient is represented on the x-axis and indicates the change in ASV relative abundance with a one unit increase in tide height. ASVs are grouped within positive or negative coefficients on the y-axis by their taxonomic association, "Order_Family_Genus". If classification was not fine enough, only the "Order" or "Order_Family" is shown. ASV68 was not classified to order level, so it is labeled to the phylum level.

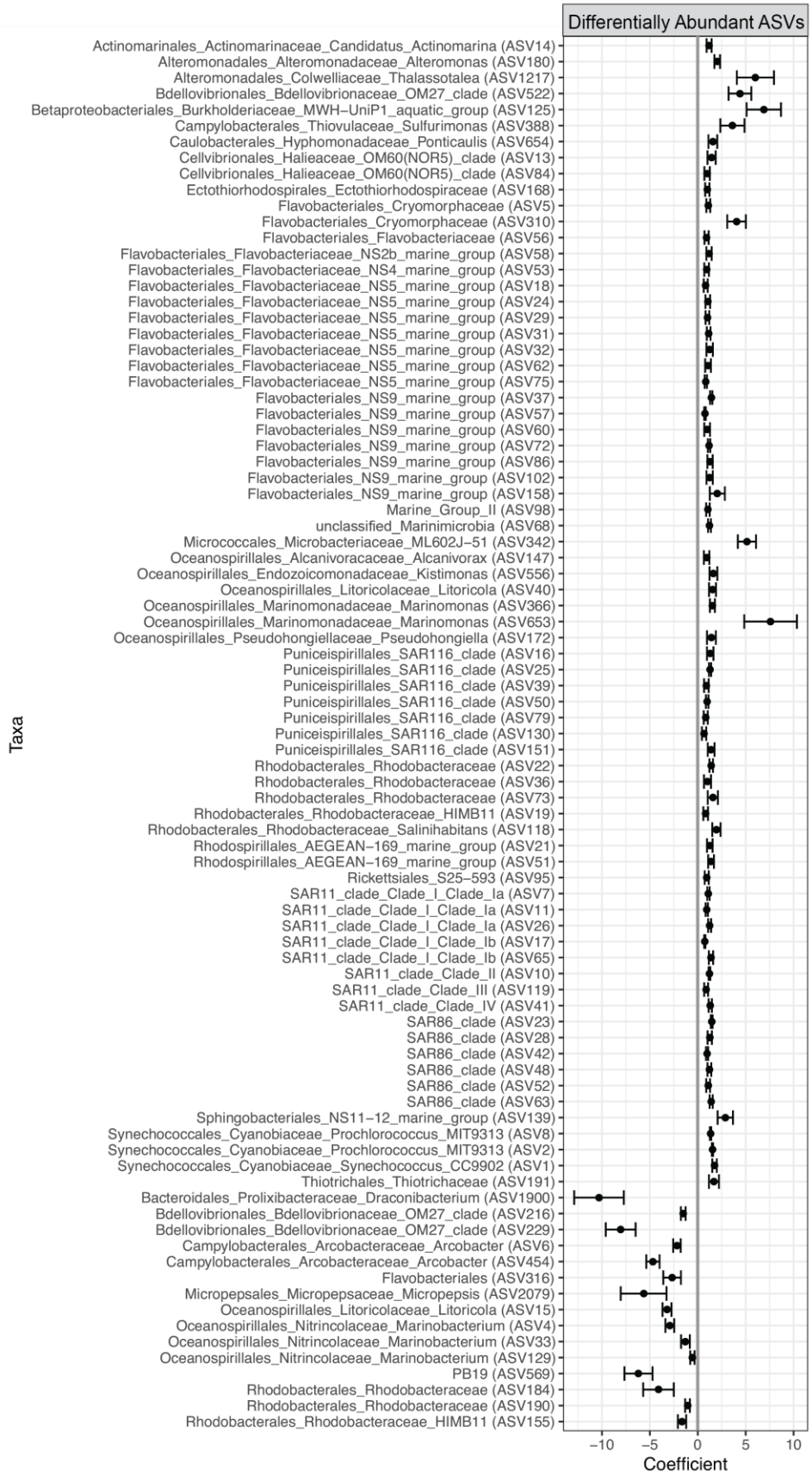
Differentially Abundant ASVs
Actinomarinales_Actinomarinaceae_Candidatus_Actinomarina (ASV14)
Alteromonadales_Alteromonadaceae_Alteromonas (ASV180)
Alteromonadales_Colwelliaceae_Thalassotalea (ASV1217)
Bdellovibrionales_Bdellovibrionaceae_OM27_clade (ASV522)
Betaproteobacteriales_Burkholderiaceae_MWH−UniP1_aquatic_group (ASV125)
Campylobacterales_Thiovulaceae_Sulfurimonas (ASV388)
Caulobacterales_Hyphomonadaceae_Ponticaulis (ASV654)
Cellvibrionales_Halieaceae_OM60(NOR5)_clade (ASV13)
Cellvibrionales_Halieaceae_OM60(NOR5)_clade (ASV84)
Ectothiorhodospirales_Ectothiorhodospiraceae (ASV168)
Flavobacteriales_Cryomorphaceae (ASV5)
Flavobacteriales_Cryomorphaceae (ASV310)
Flavobacteriales_Flavobacteriaceae (ASV56)
Flavobacteriales_Flavobacteriaceae_NS2b_marine_group (ASV58)
Flavobacteriales_Flavobacteriaceae_NS4_marine_group (ASV53)
Flavobacteriales_Flavobacteriaceae_NS5_marine_group (ASV18)
Flavobacteriales_Flavobacteriaceae_NS5_marine_group (ASV24)
Flavobacteriales_Flavobacteriaceae_NS5_marine_group (ASV29)
Flavobacteriales_Flavobacteriaceae_NS5_marine_group (ASV31)
Flavobacteriales_Flavobacteriaceae_NS5_marine_group (ASV32)
Flavobacteriales_Flavobacteriaceae_NS5_marine_group (ASV62)
Flavobacteriales_Flavobacteriaceae_NS5_marine_group (ASV75)
Flavobacteriales_NS9_marine_group (ASV37)
Flavobacteriales_NS9_marine_group (ASV57)
Flavobacteriales_NS9_marine_group (ASV60)
Flavobacteriales_NS9_marine_group (ASV72)
Flavobacteriales_NS9_marine_group (ASV86)
Flavobacteriales_NS9_marine_group (ASV102)
Flavobacteriales_NS9_marine_group (ASV158)
Marine_Group_II (ASV98)
unclassified_Marinimicrobia (ASV68)
Micrococcales_Microbacteriaceae_ML602J−51 (ASV342)
Oceanospirillales_Alcanivoracaceae_Alcanivorax (ASV147)
Oceanospirillales_Endozoicomonadaceae_Kistimonas (ASV556)
Oceanospirillales_Litoricolaceae_Litoricola (ASV40)
Oceanospirillales_Marinomonadaceae_Marinomonas (ASV366)
Oceanospirillales_Marinomonadaceae_Marinomonas (ASV653)
Oceanospirillales_Pseudohongiellaceae_Pseudohongiella (ASV172)
Puniceispirillales_SAR116_clade (ASV16)
Puniceispirillales_SAR116_clade (ASV25)
Puniceispirillales_SAR116_clade (ASV39)
Puniceispirillales_SAR116_clade (ASV50)
Puniceispirillales_SAR116_clade (ASV79)
Puniceispirillales_SAR116_clade (ASV130)
Puniceispirillales_SAR116_clade (ASV151)
Rhodobacterales_Rhodobacteraceae (ASV22)
Rhodobacterales_Rhodobacteraceae (ASV36)
Rhodobacterales_Rhodobacteraceae (ASV73)
Rhodobacterales_Rhodobacteraceae_HIMB11 (ASV19)
Rhodobacterales_Rhodobacteraceae_Salinihabitans (ASV118)
Rhodospirillales_AEGEAN−169_marine_group (ASV21)
Rhodospirillales_AEGEAN−169_marine_group (ASV51)
Rickettsiales_S25−593 (ASV95)
SAR11_clade_Clade_I_Clade_Ia (ASV7)
SAR11_clade_Clade_I_Clade_Ia (ASV11)
SAR11_clade_Clade_I_Clade_Ia (ASV26)
SAR11_clade_Clade_I_Clade_Ib (ASV17)
SAR11_clade_Clade_I_Clade_Ib (ASV65)
SAR11_clade_Clade_II (ASV10)
SAR11_clade_Clade_III (ASV119)
SAR11_clade_Clade_IV (ASV41)
SAR86_clade (ASV23)
SAR86_clade (ASV28)
SAR86_clade (ASV42)
SAR86_clade (ASV48)
SAR86_clade (ASV52)
SAR86_clade (ASV63)
Sphingobacteriales_NS11−12_marine_group (ASV139)
Synechococcales_Cyanobiaceae_Prochlorococcus_MIT9313 (ASV8)
Synechococcales_Cyanobiaceae_Prochlorococcus_MIT9313 (ASV2)
Synechococcales_Cyanobiaceae_Synechococcus_CC9902 (ASV1)
Thiotrichales_Thiotrichaceae (ASV191)
Bacteroidales_Prolixibacteraceae_Draconibacterium (ASV1900)
Bdellovibrionales_Bdellovibrionaceae_OM27_clade (ASV216)
Bdellovibrionales_Bdellovibrionaceae_OM27_clade (ASV229)
Campylobacterales_Arcobacteraceae_Arcobacter (ASV6)
Campylobacterales_Arcobacteraceae_Arcobacter (ASV454)
Flavobacteriales (ASV316)
Micropepsales_Micropepsaceae_Micropepsis (ASV2079)
Oceanospirillales_Litoricolaceae_Litoricola (ASV15)
Oceanospirillales_Nitrincolaceae_Marinobacterium (ASV4)
Oceanospirillales_Nitrincolaceae_Marinobacterium (ASV33)
Oceanospirillales_Nitrincolaceae_Marinobacterium (ASV129)
PB19 (ASV569)
Rhodobacterales_Rhodobacteraceae (ASV184)
Rhodobacterales_Rhodobacteraceae (ASV190)
Rhodobacterales_Rhodobacteraceae_HIMB11 (ASV155)
Taxa
−10
−5
0
5
10
Coefficient

Figure 3-S1. (Next page) Bar chart of relative abundance of ASVs classified to the phylum level. Each site is represented by an individual chart. Bars are organized by sampling time point and tidal level on the x-axis. Colored bars each indicate a different phylum, with the dominant phyla numbered as followed: 1 = Bacteroidetes, 2 = Cyanobacteria, 3 = Epsilonbacteraeota, 4 = Proteobacteria, 5 = Verrumicrobia.

SUPPLEMENTARY INFORMATION

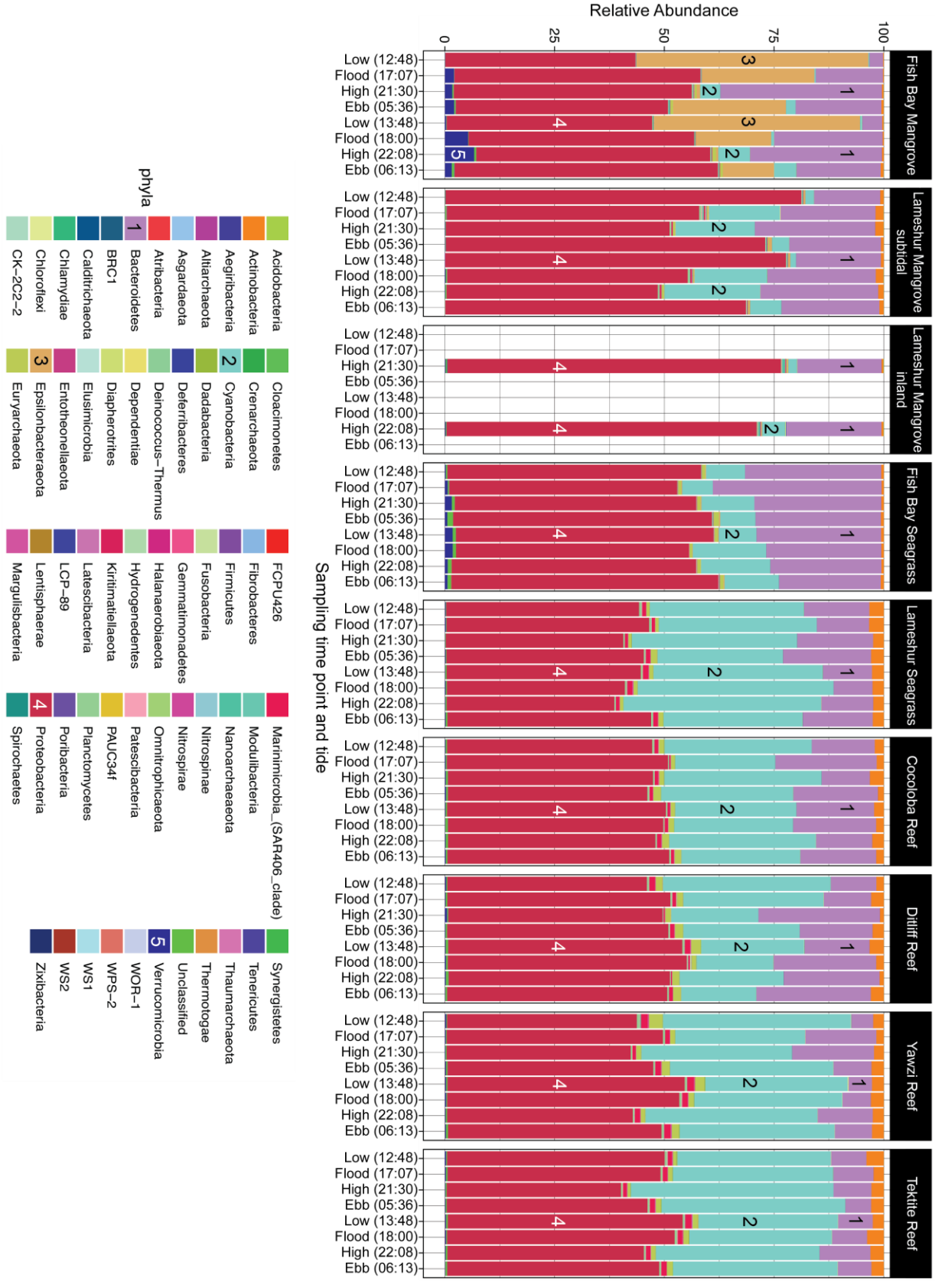

Table 3-S2. Pairwise Wilcoxon Rank Sum test for difference in Bray-Curtis dissimilarity values between sites. Benjamini-Hochberg adjusted p-values are reported in the table and significance below the 0.05 cutoff is indicated in bold.

Sites	Fish Bay Mangrove	Lameshur Mangrove*	Fish Bay Seagrass	Lameshur Seagrass	Cocoloba Reef	Ditliff Reef	Yawzi Reef
Lameshur Mangrove*	0.9805	-	-	-	-	-	-
Fish Bay Seagrass	**8.60×10^{-12}**	**1.90×10^{-12}**	-	-	-	-	-
Lameshur Seagrass	**3.20×10^{-10}**	**4.80×10^{-9}**	**4.90×10^{-6}**	-	-	-	-
Cocoloba Reef	**6.70×10^{-8}**	**6.60×10^{-7}**	**2.70×10^{-7}**	0.0626	-	-	-
Ditliff Reef	**0.0149**	**0.0134**	**1.00×10^{-12}**	**2.20×10^{-8}**	**6.40×10^{-5}**	-	-
Yawzi Reef	**3.50×10^{-6}**	**1.90×10^{-5}**	**6.70×10^{-8}**	**0.0024**	0.1819	**0.0068**	-
Tektite Reef	**7.80×10^{-10}**	**1.60×10^{-8}**	**2.80×10^{-7}**	0.3706	0.2842	**1.20×10^{-6}**	**0.0141**

*Lameshur mangrove subtidal site only

Chapter 4 - Microorganisms uniquely capture and predict stony coral tissue loss disease and hurricane disturbances on US Virgin Islands reefs

ABSTRACT

Caribbean reef ecosystems have declined over the past 50 years due to the cumulated impacts of numerous disturbances. Two disturbances that have recently impacted reefs of the US Virgin Islands (USVI) include hurricanes Irma and Maria in 2017 and the emergence of stony coral tissue loss disease in 2019-2020. Standard approaches to assess the impact of disturbances commonly involve measuring benthic reef composition, but rarely include assessments of microorganisms. However, bacterial and archaeal communities may be ideal targets for monitoring because they are the most abundant organisms on the reef, they respond to changes quickly due to fast growth rates and they are hypothesized to facilitate reef decline through microbialization. To identify the impacts of disturbance events on reef habitats, we examined eight reefs on St. John, USVI, over seven years (2016 – 2022) with a focus on microorganisms. We monitored algal and coral benthic cover as well as nutrient concentrations, microbial cell abundances and composition of microbial communities in the overlying water column. Over time and coincident with disturbances, we observed an increase in algal cover on the reefs, consistent with algal phase-shifts. The ongoing disease outbreak coincided with enriched organic nitrogen in reef water, but a loss of microbial community diversity and the numerically abundant primary producer, *Prochlorococcus*. By combining differential abundance tests and machine learning approaches, we identified microorganisms that were both changing in concert with and predictive of disturbance regimes on reefs. The more oligotrophic and autotrophic picocyanobacteria exhibited opposing dynamics to the more copiotrophic and heterotrophic Flavobacteriaceae, indicating both may be ideal targets in future reef monitoring programs. As disturbances impact reefs, the depletion of dominant primary producers and enrichment of heterotrophic lineages may be harbingers of reef decline and central to microbialization, one mechanism maintaining reef decline.

INTRODUCTION

Coral reef ecosystems in the Caribbean are mere ghosts compared to the habitats of 50 and more years ago. Hard coral, the keystone organisms that are responsible for building reefs, has declined by 20-30% in the Caribbean (Gardner *et al.*, 2003; Guest *et al.*, 2018). Anthropogenic and natural stressors including climate change, overfishing, disease, eutrophication, hurricanes, and disease contribute to these losses in coral cover, leaving space for algae to thrive (Hughes, 1994). Hurricanes frequently impact Caribbean coral reefs and severe hurricanes cause 17% losses in coral cover, which can take greater than eight years to regrow (Gardner *et al.*, 2005). Natural pressures like disease, which are common in the Caribbean, have completely restructured some reefs (Weil, 2004). More recently, the emergence of a multi-species stony coral tissue loss disease has spread across the Caribbean and is likely the most lethal recorded coral disease (Alvarez-Filip *et al.*, 2022). Repeated and ongoing stress events that target or remove stony corals leave space for algae to colonize and make it challenging for corals to settle and grow, reinforcing algal phase-shift phenomena on reefs.

The reefs of the United States Virgin Islands (USVI) are a natural laboratory to examine the impact of disturbance events on reefs. The reefs of the USVI are one of the longest-studied regions in the Caribbean, with the Territorial Coral Reef Monitoring Program (TCRMP) quantifying coral and fish abundances since 2002 (Ennis *et al.*, 2019), and over 30 years of research measuring the changing reef composition on the island of St. John (Edmunds, 2013, 2019). While coral cover on St. John is declining slowly overall, there are some reefs, such as Tektite, that could be “oasis” reefs that resists decline compared to other reefs (Guest *et al.*, 2018). Decades of disturbances such as hurricanes, bleaching, and coral disease have impacted the reefs, leaving them with lower coral cover than in the 1980’s, with no evidence of recovery (Rogers and Miller, 2006; Rogers *et al.*, 2008; Edmunds, 2013). More recently, these reefs were impacted by category five hurricanes, Irma and Maria, in September 2017. Despite being the most intense storms in over a century, the already coral-depauperate communities experienced little change (Edmunds, 2019). A few years later, stony coral tissue loss disease emerged on the reefs surrounding the islands, causing losses to coral that exceeded that of previous coral

bleaching events (Brandt *et al.*, 2021). Although these reefs have declined slowly over time, severe threats to USVI reefs have not abated, and may continue to threaten what little coral is remaining in these reef ecosystems.

Within the overlying water column of reef ecosystems reside the most abundant reef life: microorganisms. Bacteria and archaea are significant primary producers and consumers of organic matter in marine ecosystems, including coral reefs (Sorokin, 1973; Pomeroy, 1974; Chisholm *et al.*, 1988). In addition seawater microorganisms are also an important food source for corals (Sorokin, 1973; McNally *et al.*, 2017). As central players in organic matter recycling in reefs, the microbial community is highly responsive to natural environmental changes, including in coral cover (Glasl *et al.*, 2019; Apprill *et al.*, 2021), disease (Laas *et al.*, 2021), overall biogeography (Apprill *et al.*, 2021; Ma *et al.*, 2022a), and storm-based disturbances (Yeo *et al.*, 2013). As phase-shifts to increasingly algal-dominated reefs occur worldwide, reefs are hypothesized to undergo "microbialization" (Haas *et al.*, 2016). The microbialization hypothesis centers on the DDAM model (dissolved organic carbon, disease, algae, microorganism), in which algal dominance produces higher amounts of dissolved organic carbon, which promotes the growth of potentially pathogenic, copiotrophic microorganisms, contributing to coral disease and drawing down organic carbon, and reinforcing further growth of algae on reefs, creating a positive feedback loop that maintains algal dominance (Dinsdale *et al.*, 2008; Barott and Rohwer, 2012; Haas *et al.*, 2016). While spatial analyses of microbial communities across reefs of differing habitats are common, multi-year time series in reefs are rare but critical to evaluate ecosystem responses and potential microbialization following disturbance in reef ecosystems.

Microorganisms show promise as targets for reef monitoring programs because of their ability to respond to gradients in environmental conditions and their central role in reef functioning (Glasl *et al.*, 2017, 2018). Microorganisms reside in numerous habitats on reefs and relative to host-associated reef microbes, those in the seawater are more predictive of ecosystem-wide changes, such as temperature fluctuations (Glasl *et al.*, 2019). Microorganisms residing in coastal seawater habitats grow quickly, on the order of days, making them responsive to tidal and diurnal patterns (Kelly *et al.*, 2019; Becker *et al.*, 2020; Weber and

Apprill). They are also structured by yearly temperature patterns and driven by seasonality (Glasl *et al.*, 2019, 2020). On top of predictable changes in relation to environmental conditions, microorganisms within the seawater can easily be sampled non-invasively, and potentially even in an automated capacity. With established microbial baselines on short and yearly timescales in reef water and the relative ease of sampling, there is a need to identify specific microbial targets for monitoring in reef habitats.

In the present study, we monitored microorganisms in reefs in the United States Virgin Islands (USVI) over seven years to examine the impact of two major reef stressors: hurricanes and stony coral tissue loss disease. To understand the impact of these stressors on USVI reefs, we evaluated changes in the following components of the reef ecosystem over seven years: algal and coral benthic organisms, inorganic and organic nutrient concentrations in the overlying water column, and microbial cell abundance and community composition in the overlying water column. We additionally investigated individual microbial taxa that changed following hurricane and disease disturbances and used machine learning methods to identify microorganisms that are important for predicting disturbance events. As the hurricanes were a short-lived event compared to the stony coral tissue loss disease outbreak, we hypothesize the reef-wide impacts to be more pronounced from the disease outbreak. Additionally, we hypothesized that as disturbances impacted the reefs, heterotrophic lineages of microorganisms would become more abundant in agreement with the microbialization hypothesis (Barott and Rohwer, 2012; Haas *et al.*, 2016), but cyanobacteria such as *Prochlorococcus,* which have been suggested as signatures relevant for reef monitoring (Weber, González-Díaz, *et al.*, 2020), will decline over time.

METHODS

Reefs on the southern shore of St. John, United States Virgin Islands (USVI) were targeted for 11 opportunistic sampling events over six years from June 2016 to June 2022 (Figure 4-1). The reefs included (from west to east) Dittlif, Cocoloba, Joel's Shoal, Europa, Yawzi, Tektite, Booby Rock, and Ram Head, all of which are within the bounds of Virgin Islands National Park, except for Dittlif (Figure 4-1). Reef collections included surveys for benthic

composition, seawater for inorganic and organic nutrients, microbial abundances, microbial biomass for DNA and chlorophyll, and CTD casts for temperature and salinity. All collections occurred during daylight hours. Dates of seawater sampling events included June 10-12, 2016, October 28-29, 2016, March 25-28, 2017, July 26-30, 2017, November 27-30, 2017, April 11-13, 2018, November 5-9, 2018, August 6-10, 2020, January 17-24, 2021, October 20-25, 2021, and June 24-29, 2022. These sampling points surround two major stressors to St. John, USVI reefs: two category 5 hurricanes, Irma and Maria, which affected the reefs on September 6 and 19 ,2017, respectively, and stony coral tissue loss disease, a multi-species disease outbreak that began emerging around St. John, USVI between January-June, 2020. As of August 2020, the disease just began affecting all reefs in the study area, except Europa and Cocoloba. All reefs were impacted by the next sampling in January 2021.

Field collections. Benthic surveys were conducted via SCUBA using point intercept methods to understand the percent cover of organisms and substrates on each reefs. Surveys proceeded using four to six 10 m-long transects, with the underlying biological reef organisms or substrate recorded every 10 cm. Transects were collected yearly prior to the 2017 hurricane, then were collected at each field sampling event. Following the emergence of stony coral tissue loss disease in 2020, roving diver surveys to quantify that disease were conducted in January and October 2021. Disease surveys lasted thirty minutes within a 100 m^2 plot and the diver counted all apparently healthy and diseased coral colonies at the species level, when possible. At the conclusion of the survey, the area surveyed within the plot was estimated.

At each reef, measurements of temperature (ºC) and salinity (psu) were conducted using a CastAway CTD (SonTek, Xylem, San Diego, CA, USA). Next, water was collected from both surface and approximately within 1 m of reef depth (referred to as “benthic” depth) for organic nutrients, inorganic nutrients, microbial cell abundances, microbial biomass, and chlorophyll. Surface water collections were conducted directly off the sampling vessel, and for all benthic seawater collections prior to 2019, a groundwater pump (Mini-Monsoon 12V, Proactive Environmental Products, Bradenton, Florida, USA) was used. Beginning in August 2020, an 8L diver operated Niskin bottle was employed. Seawater for total organic carbon (TOC)

and total nitrogen (TN) was collected into 40 ml combusted borosilicate glass vials. Seawater for inorganic nutrients (phosphate, ammonium, silicate, nitrite plus nitrate), was collected in acid-clean 30 ml HDPE bottles (Nalgene, ThermoFisher Scientific, Waltham, MA, USA). Bottles for all collections were triple-rinsed with sample seawater prior to collection. Following collection, organic nutrient samples were fixed with 75 ul phosphoric acid and stored at room temperature until analysis. A 1.4 ml aliquot from the inorganic nutrient collection was placed into a cryovial for flow cytometry-based analysis for microbial cell abundances, then fixed with paraformaldehyde (1% final concentration, Electron Microscopy Sciences) in the dark for 20 minutes, then frozen in a liquid nitrogen dry shipper and stored at –80ºC until analysis. Bottles for inorganic nutrient analysis were kept frozen at –20ºC until analysis. Inorganic and organic nutrients and microbial cell abundances were collected in biological duplicates for the June and October 2016 sampling events, but not for further events. Duplicates from those events were averaged for comparison to all other timepoints, which were sampled in singlicate.

Seawater (4L) for chlorophyll (benthic depth only) and for microbial biomass was collected into acid-clean or bleach-clean, then triple seawater-rinsed Platy® water tank bags (Platypus, Cascade Designs, Seattle, WA, USA) or LDPE Nalgene bottles. Samples were kept in a cooler on ice until filtration within 6 hours of collection. Seawater was filtered for both microbial biomass and chlorophyll via peristalsis using a Masterflex L/S peristaltic pump (Cole-Parmer, Vernon Hills, IL, USA) through silicone tubing (L/S, platinum-cured, #96410-24 size, Cole-Parmer) and a 25 mm filter holder (Swinnex-25, Millipore Corporation) with either a 0.2 µm Supor filter (Pall, Port Washington, New York, USA) for microbial biomass or GF/F filter for chlorophyll. Seawater was filtered 2l at a time for technical duplicates. In some cases, the 0.2 µm would get clogged, so less than the 2l was filtered and the amount recorded. Prior to November 2018, the 4L chlorophyll sample was filtered through a single GF/F filter. For consistency with other environmental variables (nutrients and microbial abundances), any technical duplicates of chlorophyll (post-2018) were averaged to yield one variable for environmental analyses. All filters were placed in cryovials and frozen in a liquid nitrogen dry shipper or at –80ºC until analysis.

Temperature and precipitation. At each reef, HOBO loggers (Onset, Bourne, MA, USA) were deployed by divers at reef depth for near continuous assessments of temperature. In addition to monitoring at individual reef sites, we used data from the NOAA Lameshur Bay tidal and temperature monitoring station (ID 9751381) to fill gaps in our dataset when loggers were not deployed or failed. To test for any overall changes in average yearly temperatures over the course of the dataset, we used a linear regression through the averaged daily mean temperature in Celsius. In addition, we downloaded monthly precipitation (in millimeters) data from East End, St. John, US Virgin Islands, from the NOAA National Centers for Environmental Information (Lawrimore *et al.*, 2016). The dataset included 1972-2022, and we graphed the monthly precipitation from the duration of our study from 2016-2022.

Laboratory processing. Samples for organic nutrients were analyzed on a Shimadzu TOC-V_{CSH} TOC analyzer (Hansell and Carlson, 2001), using a TNM-1 module to generate non-purgeable total organic carbon (TOC) and total nitrogen (TN). The inorganic nutrient samples were analyzed at Oregon State University as described previously (Becker *et al.*, 2020), and used a Technicon AutoAnalyzer II (SEAL Analytical) and Alpkem RFA 300 Rapid Flow Analyzer to generate concentrations of ammonium, phosphate, silicate, nitrite, and nitrate plus nitrite. The microbial abundance samples were analyzed as described in Becker et al. (2020) at the University of Hawaii SOEST Flow Cytometry Facility. The facility used a Beckman-Coulter Altra flow cytometer (Beckman Coulter Life Sciences). The seawater samples were stained with Hoechst 33342 DNA stain and excited with 488 nm and UV wavelengths (Campbell and Vaulot, 1993; Monger and Landry, 1993). Signals were collected and then processed in FlowJo software (Tree Star) to generate populations and abundances (cells ml^{-1}) of *Prochlorococcus, Synechococcus,* eukaryotic phytoplankton ("picoeukaryotes"), and non-pigmented bacteria and archaea. Non-pigmented bacteria and archaea are mostly heterotrophic and referred to as "heterotrophic microbes" in this study (Monger and Landry, 1993; Marie *et al.*, 1997).

Chlorophyll was extracted with 90% acetone using standard methods (JGOFS, 1996). Briefly, filters were thawed and placed individually in 5 ml of 90% acetone and capped. If the filter was more colored, 10 ml of acetone was used. After a 24 hour extraction in the dark at

4°C, the tubes were vortexed and centrifuged and ~3 ml of solvent was measured on an AquaFluor fluorometer at 664 nm (Turner Designs handheld 800446) fitted with a red sensitive photomultiplier. Before and after analysis, blanks including air, 90% acetone, and a black standard were run. Readings volume-corrected and concentrations generated with a standard curve. Chlorophyll was also assessed via high-performance liquid chromatography for timepoints in 2016 to identify different specific pigments, and the chlorophyll a pigment values were used in the analysis.

DNA of duplicate 0.22 µm filters containing microbial biomass was extracted as described previously (Becker *et al.*, 2020) using a method that combines physical and chemical lysis with column purification (Santoro *et al.*, 2010). In addition to the seawater filters, DNA from 14 blank filters (without biomass) were extracted as extraction controls. Briefly, the filters were subjected to chemical lysis with a sucrose-EDTA and 10% SDS lysis buffer and physical lysis with a 15 bead-beating step. The DNeasy Blood and Tissue Kit (Qiagen) was then used to purify the lysate. Resulting DNA was diluted 1:100 in UV-sterile PCR-grade water in preparation for PCR. Single, barcoded PCR reactions per sample amplified the small subunit (SSU) ribosomal RNA (rRNA) gene of bacteria and archaea using primers 515FY and 806RB (Apprill *et al.*, 2015; Parada *et al.*, 2016). In addition to samples, genomic DNA from Microbial Mock Community B (even, low concentration), v5.1L, for 16S rRNA Gene Sequencing, HM-782D, was used as a sequencing control and PCR-grade water was used as a negative PCR control. PCR reactions (50 ul) contained the following: 2 µl DNA template, 0.5 µl of GoTaq DNA Polymerase (Promega), 1 µl each of forward and reverse primers at 10 µM, 1 µl of 10 mM deoxynucleoside triphosphate (dNTP) mix (Promega), 5 µl $MgCl_2$, 10 µl GoTaq 5X colorless flexi buffer (Promega), and 29.5 µl nuclease-free water. Reactions proceeded with: 95°C for 2 min; 28 cycles of 95°C for 20 s, 55°C for 15 s, and 72°C for 5 min; and finally 72°C for 10 min before holding at 4ºC. PCR products were all purified with the QIAquick 96 PCR purification kit (Qiagen) or MinElute PCR Purification Kit (Qiagen). Concentrations of purified barcoded PCR products was measured with the Qubit 2.0 fluorometer. Each barcoded sample was diluted to 1 ng/µl and pooled. Sequencing with Illumina MiSeq 2 x 250 bp was conducted at the Roy J. Carver Biotechnology Center at the

University of Illinois at Urbana-Champaign and the BioMicro center at Massachusetts Institute of Technology. All resulting fastq files were downloaded and used for further analysis.

Environmental data analysis. Data from point-intercept benthic survey transects were grouped into different benthic categories, including crustose coralline algae (CCA), cyanobacterial mats (CYAN), diseased coral, hard coral, macroalgae, *Ramicrusta*, soft coral, sponge, substrate (a combination of rubble, pavement, sand, and rock), turf algae, and other (a combination of *Millepora* and hydroids, zoanthids, and other invertebrates, dead coral, bleached coral, and eelgrass). Counts of each category were transformed to a percent and averaged over the 4-6 transects per reef at each timepoint. Those values were used for a principal component analysis to examine the change in overall benthic cover over time using the PCA function in *FactoMineR* (v2.6) and principal components 1 and 2 were visualized using *ggplot2* (v3.4.0) using a scatter plot and box plots separated by disturbance (Lê *et al.*, 2008; Wickham, 2016b). Permutational multivariate analysis of variance (PERMANOVA) tests were used to examine the effect of disturbance, reef site, and date on benthic composition using the adonis2 function and 999 permutations in *vegan* (v2.6.4) (Oksanen *et al.*, 2020). Disturbance is a variable that includes "historic" (2016-2017, 4 timepoints), which indicates the legacy impact of stressors on the reefs prior to the 2017 hurricanes, "hurricane" (2017-2018, 3 timepoints) to refer to the timepoints in which category 5 hurricanes Irma and Maria were recent, and finally "disease" (2020-2022, 4 timpoints) to refer to the presence of the ongoing stony coral tissue loss disease outbreak on the reefs. Europa and Cocoloba reefs did not show evidence of disease until January 2021, so these reefs had 4 hurricane timepoints and 3 disease timepoints, while all other reefs corresponded to the previously outlined number of timepoints.

To investigate the change in major algal and coral groups on reefs during the different disturbances, we used ANOVA or Kruskal-Wallis tests based on whether the assumptions of normality and homogeneity of variances were met (ANOVA) or not (Kruskal-Wallis). We calculated normality and homogeneity of variances tests using the functions shapiro_test and levene_test, respectively, from the R package *rstatix* (v0.7.1.999). Resulting p-values were evaluated as significant when $p < 0.05$, and post-hoc tests between all disturbance groups were

run using either Tukey's honest significant differences following ANOVA or Dunn's test following Kruskal-Wallis tests using the *rstatix* package. We reported significant pairwise relationships when the adjusted p-value < 0.05. We additionally examined the ratio between total algal cover on reefs (turf algae, macroalgae, and *Ramicrusta*) and total coral cover on reefs (hard and soft coral) to examine the extent of algal-coral phase shifts. *Ramicrusta* is a genus of peyssonnelid algal crusts containing many species that are spatially aggressive and likely invasive and detrimental to St. John reefs (Edmunds *et al.*, 2019). Crustose coralline algae was not included in total algae due to its beneficial role in coral settlement and because it comprised less than 1% of the benthic habitat. We regressed the two variables and graphed boxplots of algal: coral ratio across the three disturbances.

In addition to examining the benthic habitat, we analyzed the environmental parameters (inorganic and organic nutrients, chlorophyll, and microbial cell abundances) sampled from the benthic and surface waters overlying the reefs for changes coincident with the disturbance events. Prior to environmental analysis, we calculated total organic nitrogen (TON) by subtracting the concentration of inorganic nitrogen (ammonium and nitrite plus nitrate) from total nitrogen concentrations, and total nitrogen was removed from the analysis. Similarly, we calculated nitrate by subtracting nitrite from nitrite plus nitrate. Nitrite plus nitrate was removed from analysis. We also calculated the ratio of heterotrophic to photosynthetic cyanobacterial carbon biomass using the conversions: mixed population of heterotrophic microbes = 10 fg C cell^{-1} (Fukuda *et al.*, 1998), *Prochlorococcus* 30 fg C cell^{-1} (Cermak *et al.*, 2017), *Synechococcus* 100 fg C cell^{-1} (Bertilsson *et al.*, 2003). We first used t-tests or Wilcoxon tests based on assumptions of normality and homogeneity of variances (as described previously) to evaluate if surface and benthic waters had significantly different nutrients and cell abundances. Most parameters were not significantly different between surface and benthic waters and therefore surface and benthic samples were combined for tests evaluating changes across disturbances as described previously for the algal and coral cover.

Sequence and microbial community composition analysis. Microbial sequence reads were quality filtered, parsed into amplicon sequence variants (ASVs), dereplicated, filtered of

chimeras, and assigned taxonomic identities in the *DADA2* R package (v1.18.0) (Callahan *et al.*, 2016). In *DADA2*, parameters used for the filterAndTrim() function were chosen based on the quality profiles and were: truncLen = c(240, 200), truncQ = 2, maxN = 0, maxEE = c(1,1), rm.phix = TRUE, compress = TRUE, multithread = TRUE, verbose = TRUE. To ensure enough samples were used for learning error rates, the following parameter was added: nbases = 5000000000. Filtration and generation of ASVs caused loss of 19% ± 8% of sequence reads from samples, leaving 54,146 ± 11,228 sequence reads per sample that encompassed 36,404 total ASVs. ASVs and samples were further filtered to remove non-target mitochondrial and chloroplast sequences as well as any ASVs with no classification at the Kingdom level. Five samples contained fewer than 10,000 sequence reads and were removed prior to analysis. All DNA extraction controls (n = 14) contained fewer than 3,300 sequence reads and were used to identify potential contaminants in *decontam* (v1.18.0) using the prevalence method at a threshold of 0.2 chosen based on the distribution of the decontam score, *P* (Davis *et al.*, 2018). This left 33,362 ASVs within 375 reef samples. To reduce the number of low-abundance ASVs, the data were further filtered to retain ASVs with over five total counts across the dataset, which left 14,009 taxa. The low abundance-removed dataset was used for all ordination-based and differential abundance analyses. Any alpha diversity-based analyses were conducted using the data retaining the low-abundance ASVs.

We evaluated how microbial diversity changed in relation to disturbance, individual reefs, and seawater depth using analyses in R (v4.2.2). We first tested for a difference in microbial alpha diversity (specifically estimated richness) and beta diversity between surface and benthic waters to justify grouping them together or not. From this, we decided to group depths together for beta diversity analyses, but not alpha diversity (richness) analyses. We estimated microbial richness using the breakaway function with default parameters in the *breakaway* package (v4.8.4) (Willis and Bunge, 2015). We then tested for the effect of depth, disturbance and reef on estimated richness using the betta function and tested for the effect of disturbance with reef as a random effect using the betta_random function in *breakaway* (Willis *et al.*, 2017). Estimated richness was visualized using box and whisker plots in *ggplot2*. We analyzed microbial community composition by applying a centered-log-ratio transformation

using the transform function in the *microbiome* R package (v1.20.0) and calculated the Euclidean distance and visualized the communities using a principal component analysis. We used an adonis2 function in vegan (v2.6.4), which conducts a PERMANOVA test to examine the extent to which disturbance, reef, and disturbance nested within reef structured the microbial community composition (Oksanen *et al.*, 2020). Principal component analyses were visualized using *phyloseq* (v1.42.0) (McMurdie and Holmes, 2013).

We tested for differentially abundant taxa across disturbance groups using the R package *corncob* (v0.3.1) (Martin *et al.*, 2020). We subset the benthic seawater for the differential abundance tests as it was within one meter of the seafloor and therefore, we hypothesized that it might be more readily influenced by changes in the underlying reef habitat that occurred with disturbances. We tested the hypotheses that relative abundance of individual ASVs changed with respect to disturbance. Corncob models the relative abundances from an input count table and uses a logit-link function for mean and dispersion, and hypotheses were evaluated with the parametric Wald test. To test ASVs across the disturbance groups, we ran two separate tests with the "differentialTest" function in *corncob*. In the first, "historic" was used as the reference to evaluate changes following hurricanes and during the stony coral tissue loss disease outbreak. In the second, we removed the historic timepoint to test for changes in relative abundance of ASVs during the disease outbreak relative to the hurricane disturbance. In both tests, we controlled for the influence of reef site on the abundance of taxa due to the significant role reefs had in structuring reef seawater microbiomes (previous methods, Figure 4-S8). Differential ASV relative abundances were significant at a Benjamini-Hochberg false discovery rate corrected $p < 0.05$, and if the standard error of the resulting coefficient (also referred to as Estimate) did not pass through zero.

We used random forest models, a type of machine learning method, to classify reef samples into disturbance groups using the ASVs as predictor variables, and subsequently identify "important" ASVs that would contribute to the predictive ability of the seawater microbiome. Random forest models were run using the *randomforest* (v4.7.1.1) package in R (Liaw and Wiener, 2002). The model was trained using all benthic data samples (n = 178) with disturbance as the response variable. To decrease the sparsity of the ASV data used as

predictors in the model, we removed any ASV with a mean count across samples of 0.5, leaving 1,017 ASVs. Default parameters were used in the "randomForest" function addition to 'ntree' = 1000 and 'importance'=TRUE. The random forest algorithm output two measures of importance for each ASV used, mean decrease accuracy and mean decrease Gini in which higher values corresponded to higher importance of the values. We identified the top 50 ASVs with the highest mean decrease accuracy as the most important ASVs, because when removed, those ASVs led to the highest decrease in accuracy of the classification between disturbance groupings of the model. Therefore, they were most important for differentiating between disturbance groups. The out of bag error rate from the training of the random forest model was generated during training and then also generated during validation of the model. The model was validated using the surface seawater dataset using the "predict" function in R. The classification error was calculated by comparing the number of correctly predicted disturbance classification against the true disturbance using confusion matrices.

To identify taxa that both changed significantly across disturbances and were important in predicting disturbance in reef habitats, we compared the groups of taxa from both the differential abundance and random forests tests. We retained all ASV-level taxa that were shared between the results. The coefficients (*corncob*) and mean decrease accuracy scores (*randomforest*) were plotted using *ggplot2*. Additional box and whisker plots were generated of the relative abundance of each taxon across the disturbance groups to visualize the changes in taxa across disturbances.

RESULTS

Coral reefs on the southern shore of St. John varied in benthic composition at the start of the time series, with some reefs having more coral cover (hard and soft coral), including Tektite, Joel's Shoal, and Booby Rock, which had 25.6% - 35.2% coverage of coral, while other reefs, such as Cocoloba (7.9% coral cover) harbored much less coral cover (Figure 4-1a). Total algal coverage (crustose coralline algae, cyanobacterial mats, macroalgae, turf algae, and *Ramicrusta*) varied widely across reefs, from 4.4% at Joel's Shoal, to 57.8% at Tektite (Figure 4-1a). Over the next six years, the reefs experienced multiple disturbances, including hurricanes

Irma and Maria in September, 2017, and a multi-species stony coral tissue loss disease outbreak that emerged in 2020 and remained prevalent on the reefs through 2022 (Figure 4-2b). Coral disease surveys found prevalence of stony coral tissue loss disease on live coral during the outbreak in January 2021 was between 4.29% at Booby Rock and 17.28% at Yawzi and in October 2021 between 4.15% at Dittlif and 19.02% at Joel's Shoal (Figure 4-S1). Disease surveys were stopped after October 2021, but the disease was still present on reefs during June 2022.

Benthic composition of organisms such as coral and algae as well as other organisms and non-biological substrates changed significantly across disturbance regimes (PERMANOVA Disturbance, R^2=0.20556, F=8.9268, p<0.001, Figure 4-2a). In a principal component (PC) analysis of benthic composition, stony coral tissue loss disease-impacted reefs had an increase in PC 1 and 2, while reefs impacted by hurricanes responded differently and only increased on the PC 2 axis (Figure 4-2a). Benthic composition was also significantly different between reefs and over time (PERMANOVA, Reef, R^2=0.34489, F=4.8135, p<0.001; Date, R^2=0.19518, F=16.977, p<0.001) (Figure 4-2a). We investigated algae and coral cover on reefs and found that *Ramicrusta,* turf algae, and macroalgae significantly changed due to disturbance (ANOVA or Kruskal-Wallis $p < 0.05$; Figure 4-2b,c,d). *Ramicrusta* and turf algae were significantly elevated, but macroalgae was lowered following the disease outbreak (Tukey or Dunn post-hoc test, adjusted $p < 0.05$; Figure 4-2b,c,d). While hard and soft coral cover did not significantly change, median hard coral decreased during the disease outbreak (Kruskal-Wallis $p > 0.05$, Figure 4-S2). Relative to the immediate pre-disease cover (hurricane period), between 8.5-60% of coral cover was lost across the eight reefs (Figure 4-S2). Together, the ratio of total algal cover to total coral cover increased over the course of the time series, and was significantly elevated following the disease disturbance, but not the hurricane disturbance, relative to historic ratios (Kruskal-Wallis test and Dunn test, $p< 0.05$) (Figure 4-S3).

In the seawater column above the reefs, ammonium, total organic nitrogen (TON), and chlorophyll concentrations significantly increased during the disease outbreak (Kruskal-Wallis followed by Dunn test, $p < 0.05$) (Figure 4-3a,b,c). Silicate and phosphate concentrations significantly increased following the hurricane disturbance and decreased after the hurricane which was during the disease outbreak (Kruskal-Wallis followed by Dunn test, $p < 0.05$) (Figure

4-3d,e). Reef seawater concentrations of total organic carbon (TOC), nitrate, and nitrite did not significantly change across disturbances (ANOVA or Kruskal-Wallis, $p > 0.05$; Figure 4-S4). We additionally found that yearly averaged in situ reef temperatures stayed approximately the same over the course of seven years (linear regression, temperature ~ time, $p < 0.05$, Figure 4-S5).

Cell abundances of phototrophic microorganisms in surface and benthic wsaters above the reefs changed with disturbance. *Prochlorococcus* abundances were significantly lower following the disease outbreak relative to earlier timepoints, with a cumulative loss of 31.4-73.8% of historic abundances (Kruskal-Wallis followed by Dunn test, $p < 0.05$) (Figure 4-4a). Photosynthetic picoeukaryote abundances were also lowered following both disturbances relative to the historic timepoints (Kruskal-Wallis followed by Dunn test, $p < 0.05$) (Figure 4-4b). In contrast, *Synechococcus* and heterotrophic microbial (unpigmented bacteria and archaea) abundances did not significantly change with either disturbance (Kruskal-Wallis followed by Dunn test, $p > 0.05$) (Figure 4-S6). While heterotrophic microbes and *Synechococcus* were not significantly different, the median ratio of carbon biomass from heterotrophic microbial cells to photosynthetic picocyanobacterial cells (*Prochlorococcus* and *Synechococcus*) significantly increased following the disease outbreak, with the median ratios moving from below 1 prior to disease to above 1 during the disease outbreak (Kruskal-Wallis followed by Dunn test, $p > 0.05$)(Figure 4-4c). These changes were largely due to the decrease in *Prochlorococcus.*

Microbial community beta diversity in the seawater overlying reefs at benthic and surface changed significantly across hurricane and disease disturbances (Adonis2 test on Aitchison distance, $p < 0.001$, $R^2 = 0.06109$) (Figure 4-5a). Microbial community beta diversity was not significantly different by depth, so all beta diversity analyses incorporated both depths (Adonis2 test, $p > 0.05$) (Figure 4-S7a). In contrast, estimated microbial richness was significantly higher in benthic waters and as a result, alpha diversity was assessed separately for both depths (betta test for heterogeneity of total diversity $p < 0.001$) (Figure 4-S7b). Following the 2017 hurricanes, estimated microbial richness was elevated in surface and benthic reef depth waters, but this was not significant (betta test $p > 0.05$, benthic estimate 21.1, surface estimate 2.9) (Figure 4-5b,c). In contrast, richness was significantly lowered in both benthic and

surface reef waters during the stony coral tissue loss disease outbreak relative to the historic time period (benthic estimate –28.7, p = 0.001; surface estimate –12.1, p = 0.019) (Figure 4-5b,c). In addition to disturbance, microbial community beta diversity was significantly structured by reefs and disturbance nested within reefs (Adonis2 test $p < 0.001$; Reef R^2 = 0.04756; Reef/Disturbance R^2 = 0.10262) (Figure 4-S8a). Estimated microbial richness in both surface and benthic reef depth waters was significantly different across reefs and across disturbances within reef groups (betta test, global $p < 0.001$) (Figure 4-S8b,c).

To identify microbial taxa that were driving the observed changes in alpha and beta diversity across disturbances, we conducted differential abundance tests of ASV-level Bacteria and Archaea within the benthic depth seawater and found a total of 199 that were either significantly enriched or depleted across disturbance groups (Supplementary File 1, supplementary files can be accessed online at https://doi.org/10.6084/m9.figshare.22310434.v1). We also leveraged a Random Forest machine learning method to assess the predictive capability of benthic reef seawater ASVs to classify samples by disturbance regime. The out of bag error rate during training of the random forest model was 1.12%, with classification error of 4.44% of the hurricane disturbance and 0 for both historic and disease disturbance (Table 1). When the random forest model was validated using surface reef seawater, historic and disease disturbance groups were predicted with no error and the hurricane disturbance was predicted with 4.35% error (Table 1). To identify the ASVs that were most important to the classification accuracy of the model, we selected the top 50 ASVs with the highest mean decrease accuracy score, which is a measure the amount of classification accuracy the model loses when the ASV was removed (Supplementary File 2, accessed online).

We compared the significantly differentially abundant taxa across disturbances to the important taxa from the random forest classification and found 41 taxa that were shared between the two analyses (Figure 4-6). These 41 taxa spanned 10 different classes and included mostly Bacteria and two unclassified Marine Group II Archaea (Figure 4-6). The nine alphaproteobacteria ASVs included SAR11 clades I, II, and III, which were enriched during the disturbances, and SAR116, and an unclassified S25-593 Family of Rickettsiales (Figure 4-6,

Figure 4-S9). The majority of ASVs from Bacteroidia that were differentially abundant and important were enriched during the disease outbreak, and included NS4 and NS5 marine groups, and *Tenacibaculum,* as well as an unclassified Cryomorphaceae enriched during the hurricane disturbance (Figure 4-6, Figure 4-S10). Notably, the taxon with the highest mean decrease accuracy score from the random forest analysis was a Bacteroidia of the NS5 marine group (ASV100), which was depleted following the hurricane disturbance and enriched during the disease outbreak (Figure 4-6, Figure 4-S10). One Bdellovibionia (OM27 clade) and 11 Gammaproteobacteria were differentially abundant and important. Within Gammaproteobacteria, the SAR86 clade and *Litoricola* were enriched in both hurricane and disease disturbances, while *Pseudohongiella* and OM182 clades were enriched primarily following the hurricane disturbance only (Figure 4-6, Figure 4-S9). The remaining BD1-7 clade of Spongiibacteraceae, *Marinobacterium,* and unclassified Alteromonadaceae were most abundant during the disease outbreak (Figure 4-6, Figure 4-S9). Marine Group II archaea exhibited enrichment following the hurricanes, but their relative abundance was depleted during the disease outbreak (Figure 4-6, Figure 4-S9). Unclassified Marinimicrobia was enriched primarily during the hurricane disturbance and *Coraliomargarita* was enriched during the disease outbreak only (Figure 4-6, Figure 4-S9).

We identified several Cyanobacteria ASVs predictive of and differentially abundant across disturbances in reef waters (Figure 4-6, Figure 4-S11). Three *Synechococcus* CC9902 ASVs had greater relative abundances during the hurricane disturbance, but one ASV was significantly depleted in both disturbance groups (Figure 4-6, Figure 4-S11). The unclassified Cyanobiaceae ASV was enriched in both disturbance groups (Figure 4-6, Figure 4-S11). Both *Prochlorococcus* MIT9313 ASVs were significantly depleted during the disease outbreak, with relative abundance patterns consistent with the flow cytometry-based cell abundance findings (Figure 4-4a, Figure 4-6, Figure 4-S11).

DISCUSSION

We conducted seven years of coral reef monitoring focused on reef water microorganisms, nutrients, and the underlying habitat. US Virgin Islands (USVI) reefs have

declined over the past 30 years, and our data show recent changes in macro and micro-organisms coincident with two major disturbances: category five hurricanes in September 2017 and the multi-year stony coral tissue loss disease outbreak. Over time and with disturbances, while algal cover increased in the benthic habitat, nutrients and microorganisms in the overlying water column also changed significantly. The stony coral tissue loss disease outbreak coincided with depletion of dominant reef phototrophs, *Prochlorococcus*, which may be a potential indicaor of reef quality. In contrast, the increase in abundance of multiple lineages of heterotrophic microorganisms likely contributed to microbialization and reef decline. We found microbial communities were both sensitive to and predictive of disturbances, which lends support for their inclusion in programs that monitor increasingly threatened reef ecosystems.

In the face of two category five hurricanes and the ongoing stony coral tissue loss disease outbreak, the reefs changed substantially, with increases in the spatially aggressive encrusting alga, *Ramicrusta* (Edmunds *et al.*, 2019), and turf algae. Although hurricanes have caused losses in coral cover in the past, the 2017 Hurricanes, Irma and Maria, caused little change to reef benthic communities, similar to findings by Edmunds (2019). Instead, years-long persistence of stony coral tissue loss disease appears to have coincided with the greatest changes in reef habitats, such as lower cover of hard coral. Stony coral tissue loss disease is a particularly devastating disease, which affects over 20 species of hard coral, kills corals quickly, and can reach prevalence on a reef much higher than in recent history (Florida Keys National Marine Sanctuary, 2018; Meiling *et al.*, 2020; Brandt *et al.*, 2021). Over the course of the study, temperatures did not increase noticeably (Figure 4-S5), and the one bleaching event in 2019 caused limited mortality to corals, indicating that stony coral tissue loss disease was likely the main driver causing changes to USVI reefs (Ennis *et al.*, 2019). Beyond coral cover, we found significant increases in turf algae, which are often early colonizers to open space, including on newly dead corals, and may have proliferated as corals died off (Tâmega and Figueiredo, 2019). *Ramicrusta* increased following both disturbances, which aligns with reports that it is spatially aggressive, and promoting shifts to algal dominance on reefs (Edmunds *et al.*, 2019). As of the conclusion of the sampling in summer of 2022, the disease was ongoing, and we hypothesize

that hard coral and overall composition of the reef will continue to change as the disease continues to kill major reef builders.

Within the water column overlying the reefs, disturbances coincided with altered inorganic and organic nutrient regimes, with notable increases in nitrogen following disease emergence. Coral reefs reside in nutrient-poor waters and changes to nutrients may impact coral and reef ecosystem health (Szmant, 2002; Lapointe *et al.*, 2004). Increased organic nitrogen and decreased phosphate with disease disturbance mirrored the changes across highly protected, coral-rich reefs of Cuba compared to the less protected, coral-poor reefs of Florida, and perhaps is reflective of the changing reef composition that accompanies disease and coral-poor environments (Weber, González-Díaz, *et al.*, 2020). Organic nitrogen and carbon compounds are remineralized by heterotrophic microorganisms in reef seawater, and the excess ammonium following disease may be reflective of this process (Hopkinson *et al.*, 1987), or potentially from the degradation and dissolution of the sloughed diseased tissue. While the nitrogen compounds may reflect microbial activity within the reef habitat, heightened silicate in waters following the hurricane may reflect increased groundwater discharge from the hurricanes and other storm events in the fall, which often has heightened rainfall in the US Virgin Islands (Figure 4-S13)(Oehler *et al.*, 2019; Silbiger *et al.*, 2020).

The smallest photosynthesizers within the water column, *Prochlorococcus,* picoeukaryotes, and *Synechococcus* were sensitive to disturbances in reef habitats. *Prochlorococcus* was especially sensitive to disease, with 31.4-73.8% losses in abundance during the disease outbreak compared to the earliest time period. *Prochlorococcus* is known to be more sensitive to organic matter and nutrients than *Synechococcus*, and the observed enrichment of organic nitrogen may be contributing to these declines (Partensky *et al.*, 1999; Charpy *et al.*, 2012). Additionally, *Prochlorococcus* was associated with high quality and well-protected reefs in Cuba suggesting it may be an indicator of deteriorating reef quality resulting from stony coral tissue loss disease (Weber, González-Díaz, *et al.*, 2020). Interestingly, depletion of phototrophs corresponded with an increase in chlorophyll, which may be reflective of changing abundances of larger phytoplankton cell sizes not measured here. Seven individual Cyanobacteria were both significantly differentially abundant across disturbance regimes as

well as important for predicting disturbances. Hurricanes seemed to favor *Synechococcus* variants, which have been shown to increase following storm events (Chang *et al.*, 1996; Yeo *et al.*, 2013). In contrast, the stony coral tissue loss disease outbreak led to declines in *Prochlorococcus*, indicating differential sensitivities to disturbances across cyanobacteria. The sensitive responses of cyanobacteria to changes on Virgin Islands reefs lends support for including cyanobacteria in reef monitoring. Cyanobacteria also have a clear role in reef habitats. These numerically abundant organisms are dominant primary producers in reef habitats and carbon sources to grazing benthic organisms, such as coral (van Duyl *et al.*, 2002; Charpy *et al.*, 2012; McNally *et al.*, 2017).

Reef water microorganisms were sensitive to stony coral tissue loss disease, an ongoing and Caribbean-wide disturbance. Unlike hurricanes, which are intense and short-lived disturbances, the disease slowly moves reef to reef, targeting and removing the primary reef-builders. We found that heterotrophic reef water microbial taxa were significantly elevated during the disease. The enrichment of multiple generally copiotrophic Flavobacteriaceae, including NS4 and NS5 marine groups and *Tenacibaculum* may be reflective of the increasing algal cover or derived from the sloughing diseased tissue (Buchan *et al.*, 2014; Haas *et al.*, 2016; Huntley *et al.*, 2022). Within the Flavobacteriaceae, the NS5 marine group (ASV100) had the highest importance score, likely related to its significant depletion following the hurricane, but enrichment following the disease outbreak. The NS5 marine group comprises 35 species-level clusters that all have distinct ecological niches, temporal distribution, and are regularly found in Caribbean reef water (Becker *et al.*, 2020; Weber and Apprill, 2020; Weber, González-Díaz, *et al.*, 2020; Priest *et al.*, 2022). In a meta-analysis of stony coral tissue loss disease-impacted coral tissue, the NS5 marine group was enriched in unaffected tissue and mucus on diseased colonies, indicating it may even be an early indicator of disease within coral hosts (Rosales, Huebner, Evans, *et al.*, 2022). The recurrent association to disease, disturbances and deteriorating reef habitats warrants further investigation and monitoring of the NS5 marine group and other microorganisms within Flavobacteriaceae.

Other heterotrophic taxa enriched in disease included the Gammaproteobacteria *Marinobacterium*, Alteromonadaceae, and the BD1-7 clade of Spongiibacteraceae, as well as

the Verrucomicrobiae, *Coraliomargarita. Coraliomargarita* was originally isolated from seawater surrounding a coral and is also associated with stony coral tissue loss disease lesions (Yoon *et al.*, 2007; Huntley *et al.*, 2022). Alteromonadaceae are copiotrophs that grow off of coral- and algal-derived organic matter (Nelson *et al.*, 2013; Pedler *et al.*, 2014; McNally *et al.*, 2017; Quinlan *et al.*, 2019; Weber *et al.*, 2022). Copiotrophic lineages are predicted to increase in reef seawater as reefs deteriorate and become algal-dominated (reviewed in Nelson *et al.*, 2023). In contrast to this, we noted enrichment over time, particularly with disease, of the oligotrophic heterotrophs SAR11 and SAR86, which were some of the most abundant microorganisms in our dataset (Lauro *et al.*, 2009; Dupont *et al.*, 2012). These microorganisms are common in reef water and grow in response to coral and crustose coralline algae exudates (Apprill *et al.*, 2015; Quinlan *et al.*, 2019; Nelson *et al.*, 2023). Our heterotrophic microbial abundance analysis captured heterotrophs from both oligotrophic to copiotrophic life strategies; although the cell abundances of heterotrophs didn't change overall, the differential enrichment of specific groups likely has ecological implications in reef habitats. Coupled with the depletion of the major primary producer, *Prochlorococcus,* the ratio of bacterial and archaeal carbon biomass in the reef water transitioned from largely dominated by picocyanobacteria prior to disease, to dominated by heterotrophic microbial carbon. While many heterotrophic microorganisms were oligotrophs, many were also more copiotrophic, which increases the oxygen demand in reef water and may contribute to microbially-mediated deoxygenation, one potential mechanism of reef decline (Johnson *et al.*, 2021; Nelson *et al.*, 2023).

By leveraging seven years of monitoring microorganisms in reef habitats, we both generated microbial baselines in a historically impacted reef system and demonstrated the capacity of reef water microorganisms to predict disturbance regimes with low classification error. In increasingly coral-depauperate reefs, microorganisms emerge as an ideal candidate for reef monitoring. They are impacted by the organic matter exuded by algal and coral organisms on reefs, and therefore may change as the underlying composition of a reef changes (Nelson *et al.*, 2013; Weber *et al.*, 2022). Additionally, they are directly involved in stony coral tissue loss disease, and likely many other coral diseases (Ushijima *et al.*, 2020; Vega Thurber *et al.*, 2020).

In the present study, photosynthetic cyanobacteria, particularly *Prochlorococcus,* decreased during the disease disturbances on reefs, and was important for predicting disturbances. As reefs experience increased algal growth and future disturbances, incorporating these dominant primary producers into microbialization assessments considers an abundant and important functional component of reef microbial communities. Additionally, the NS5 marine group of Flavobacteriaceae had the highest importance score and was significantly differentially abundant between disturbances. As a result, these and other Flavobacteriaceae with more copiotrophic lifestyles may be ideal heterotrophic microorganisms for reef monitoring. With seven years of data, we provide novel insights into the dynamics of microbes in disturbance-impacted reefs, providing baseline data for other reef ecosystems. Additionally, by demonstrating the capability for reef water microorganisms to predict disturbances, we urge for further inclusion of microorganisms such as picocyanobacteria and Flavobacteriaceae into future reef monitoring programs.

ACKNOWLEDGEMENTS

We thank the numerous people that have assisted with sample collection and field support, including Paul Caiger, Justin Suca, Alexis Earl, Jessica Dehn, Ian Jones, Rod Catanach, Kathy Catanach, Ashlee Lillis, Kalina Grabb, Naomi Huntley, Seth Cones, Justin Ossolinski, Nadège Aoki, and Kayla Caymitte. We also thank people that assisted with sample and data processing and organization, including Emily Peacock, Yan Jia, Nathan Formel, and Jeff Coogan. We'd like to thank the crew of the R/V Walton Smith, the Virgin Islands Environmental Resource Station, and the University of Virgin Islands for logistical support. This research was supported by National Science Foundation (OCE-1536782, OCE-1736288), NOAA OAR Cooperative Institutes (no. NA19OAR4320074) and Academic Programs Office at WHOI for summer and fall undergraduate research support. The research was conducted under US Virgin Islands National Park Service permits VIIS-2016-SCI-0018, VIIS-2017-SCI-0019, VIIS-2018-SCI-0010, VIIS-2018-SCI-0024, VIIS-2019-SCI-0008, VIIS-2020-SCI-0010, VIIS-2021-SCI-0002, and VIIS-2022-SCI-0005.

DATA AVAILABILITY

All sequence data are uploaded to the NCBI Sequence Read Archive under BioProject accession number PRJNA936592. Project environmental data and sample-specific sequence accession numbers are uploaded to BCO-DMO under project 659919. All code and scripts for reproducing the analyses presented are publicly available on GitHub at https://github.com/CynthiaBecker/USVI-timeseries. Supplementary Files 1 and 2 (Excel tables) can be accessed via figshare online at https://doi.org/10.6084/m9.figshare.22310434.v1

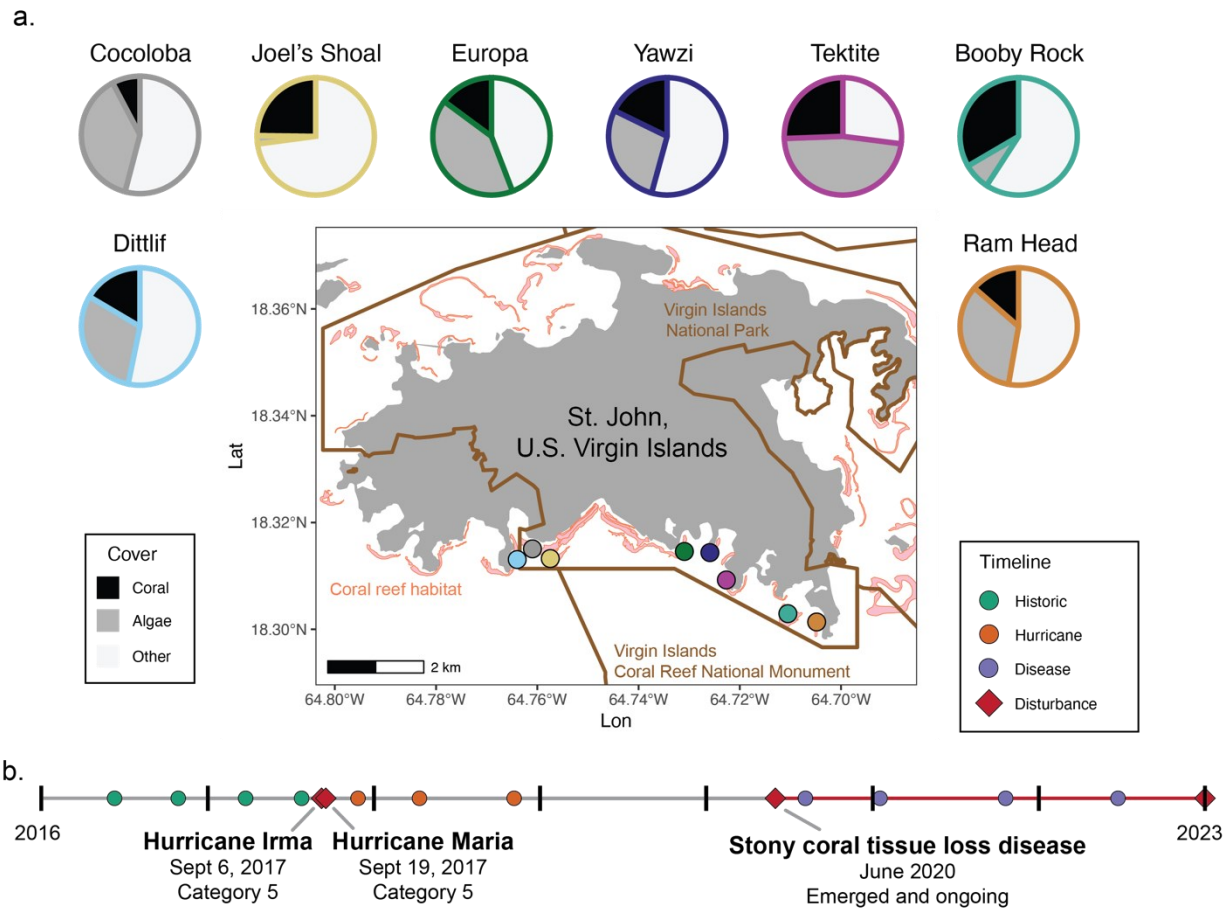

Figure 4-1. St. John, US Virgin Islands reefs and timeline.
Eight reefs with varying benthic cover in St. John, US Virgin Islands, were sampled from 2016 through 2022. A) The eight reefs included (from west to east) Dittlif, Cocoloba, Joel's Shoal, Europa, Yawzi, Tektite, Booby Rock, and Ram Head. Dittlif is the only reef just outside the boundary of Virgin Islands National Park (brown). At the beginning of the time series (June 2016) the cover (a) of benthic habitats at each reef varied in percent cover of hard and soft coral (black) and algae (gray). The algal cover included macroalgae, and turf algae. The remaining cover ("Other", light gray) included cyanobacterial mats, sponges, crustose coralline algae, non-biological substrate, invertebrates and the hydroid, fire coral. B) "Historic" sampling events (2016-2017, green) precede two major impacts: category five hurricanes, Irma and Maria, in September 2017, and stony coral tissue loss disease emergence in 2020. Hurricane-impacted events are those in the year following the hurricane (2017-2018, orange) and disease-impacted sampling events (2020-2022, purple) are those during active stony coral tissue loss outbreaks.

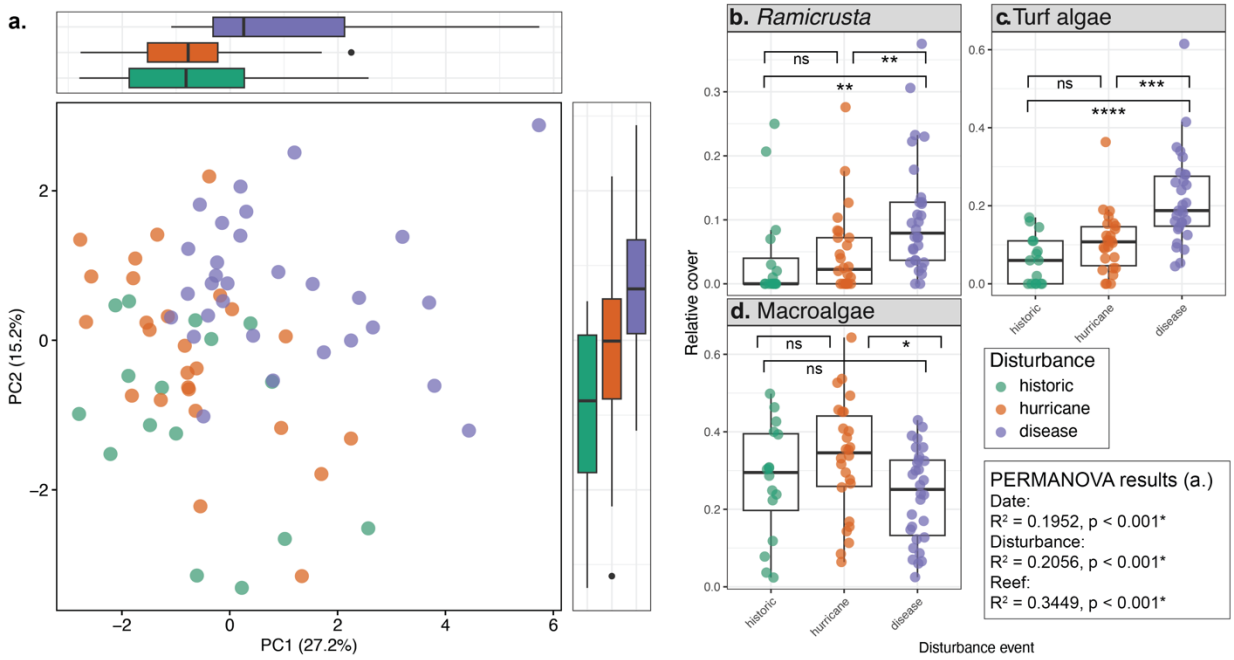

Figure 4-2. Benthic composition.

Benthic composition at eight reefs significantly changed with disturbances in St. John, U.S. Virgin Islands (a. PERMANOVA $p < 0.001$; b-d. ANOVA or Kruskal-Wallis $p < 0.05$). Principal component analysis (a) of habitat cover at individual reefs is colored by the three categories of disturbance: historic (2016-2017, green), hurricane (2017-2018, orange), and disease (2020-2022, purple). Boxplots adjacent to the PCA display distributions of principal components 1 (top) and 2 (right) grouped by disturbance. Results of permutational analysis of variance (PERMANOVA, 999 permutations) for date, disturbance, and reef are displayed on the right. Reef benthos components that significantly increased or decreased following disturbances included (b) *Ramicrusta* (Kruskal-Wallis, $p < 0.001$), (c) turf algae (Kruskal-Wallis, $p < 0.001$), and (d) macroalgae (ANOVA, $p = 0.038$). In b-d, significant pairwise tests from Tukey and Dunn post-hoc tests are displayed with brackets and asterisks indicating significance levels of adjusted p-values: ns = not significant, *$p < 0.05$, **$p < 0.01$, ***$p < 0.001$, ****$p < 0.0001$

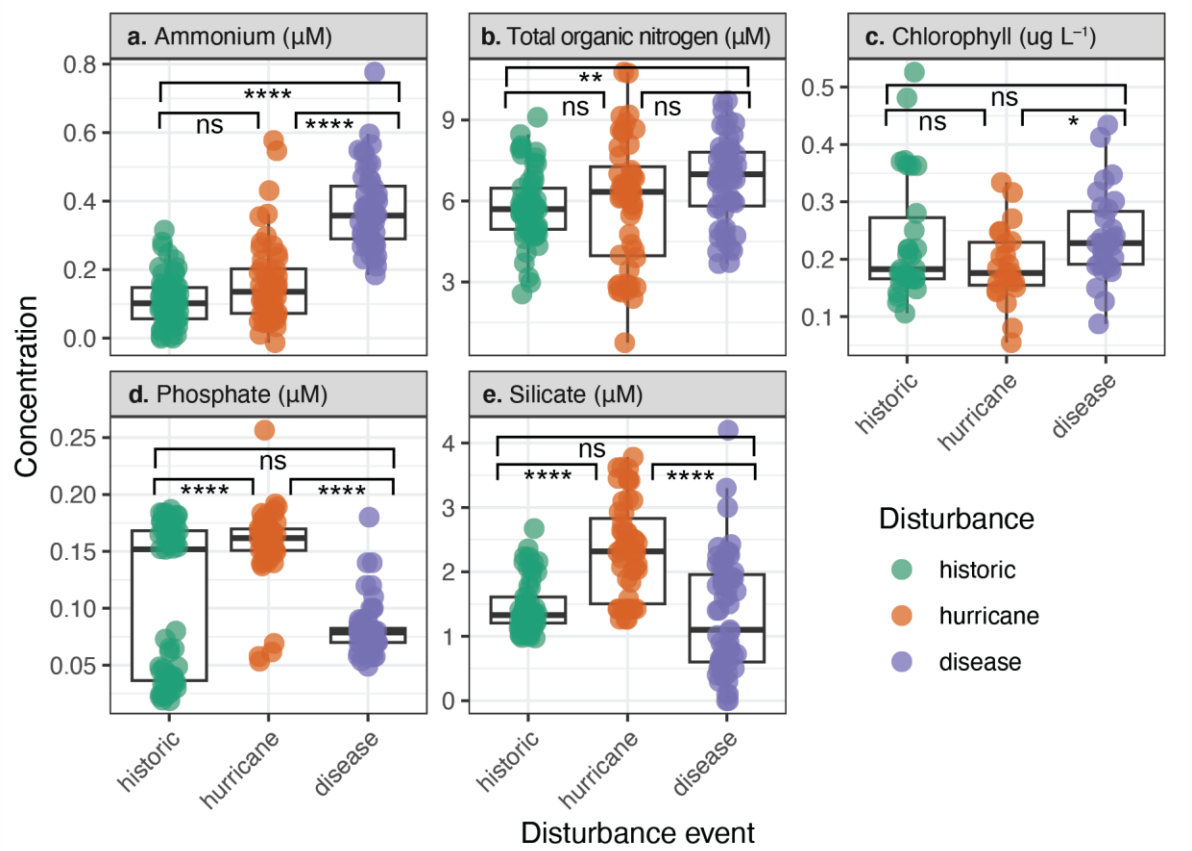

Figure 4-3. Reef water nutrient concentrations

Nutrient concentrations from both benthic and surface waters significantly changed with disturbance events in the US Virgin Islands (Kruskal-Wallis, $p < 0.05$). Nutrients and pigments that changed between historic (green), hurricane (orange), and disease (purple) time periods included (a) ammonium (Kruskal-Wallis, $p < 0.0001$), (b) total organic nitrogen (Kruskal-Wallis, $p = 0.0028$), (c) chlorophyll (Kruskal-Wallis, $p = 0.033$), (d) phosphate (Kruskal-Wallis, $p < 0.0001$), and (e) silicate (Kruskal-Wallis, $p < 0.0001$). Significant pairwise tests from Dunn post-hoc tests are displayed with brackets and asterisks indicating significance levels of adjusted p-values: ns = not significant, *$p < 0.05$, **$p < 0.01$, ***$p < 0.001$, ****$p < 0.0001$

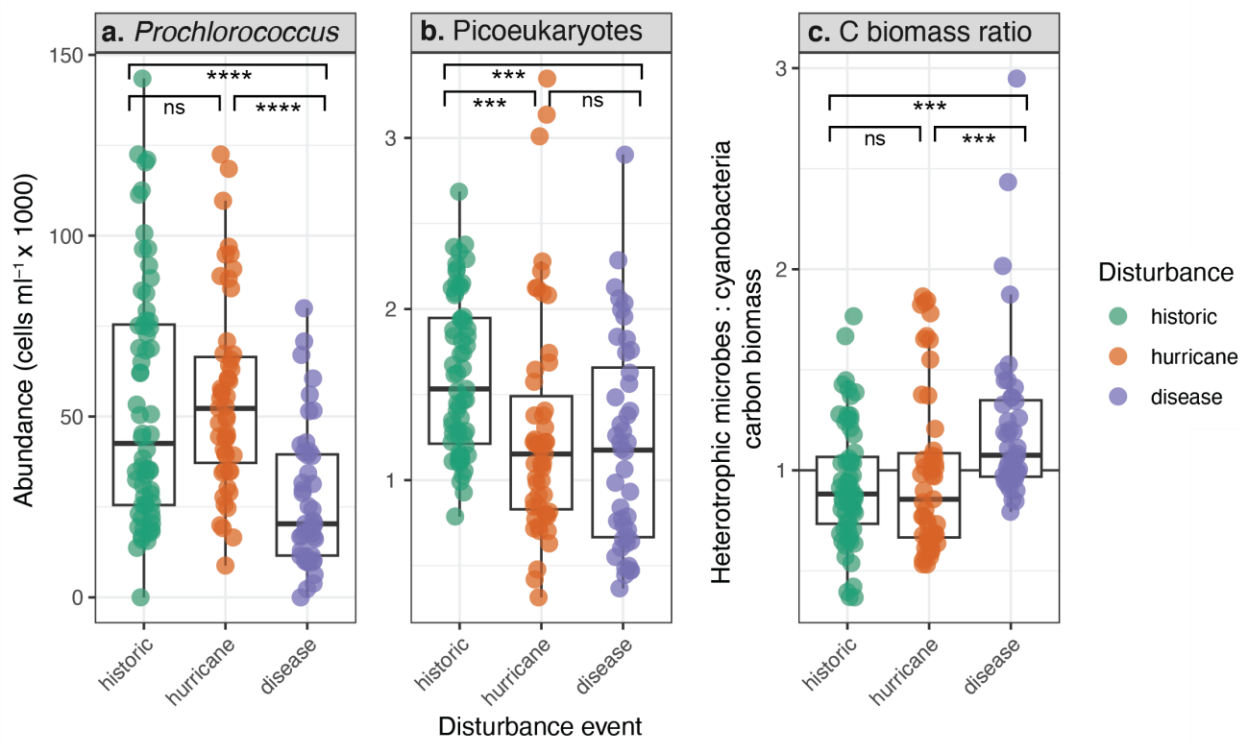

Figure 4-4. Reef water cell abundances

Photosynthetic (a) *Prochlorococcus* and (b) picoeukaryote abundances in the seawater column overlying reefs were depleted significantly during and following disturbances in the US Virgin Islands (Kruskal-Wallis, $p < 0.0001$). After converting from cell abundances to carbon biomass, the ratio of heterotrophic microbial carbon biomass to *Prochlorococcus* and *Synechococcus* carbon biomass significantly increased during the disease outbreak (Kruskal-Wallis, $p < 0.0001$). Significant pairwise tests from Dunn post-hoc tests are displayed with brackets and asterisks indicating significance levels of adjusted p-values: ns = not significant, *$p < 0.05$, **$p < 0.01$, ***$p < 0.001$, ****$p < 0.0001$

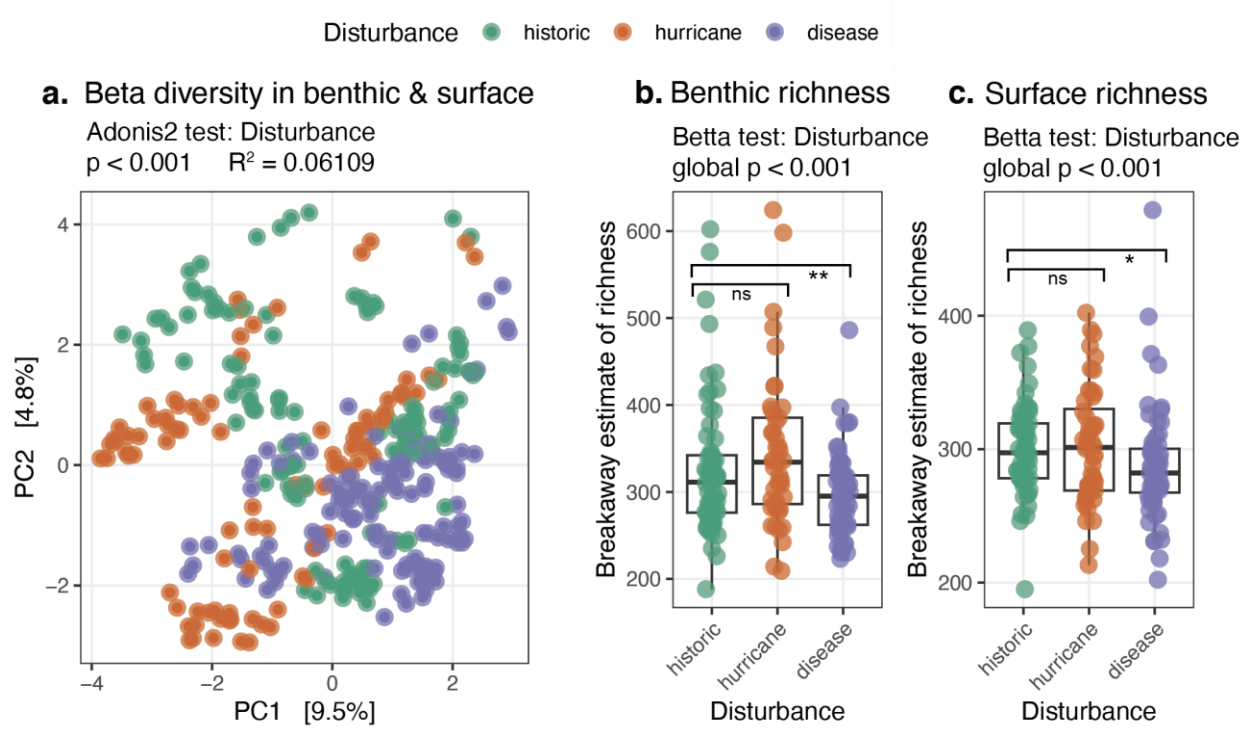

Figure 4-5. Diversity of seawater microbial communities

Benthic and surface seawater microbial alpha and beta diversity changed significantly with disturbance events. a) Principal component analysis of surface and benthic microbial community beta diversity (Aitchison distance on centered log-ratio transformed data) significantly differed across disturbance events (PERMANOVA test, 999 permutations, $p < 0.001$). Estimated richness (alpha diversity metric) significantly increased and decreased with disturbance events (betta test for heterogeneity of total diversity, global $p < 0.001$) in both (b) benthic and (c) surface waters. Asterisks denote significant changes in disturbance time periods relative to historic samplings. ns = not significant, *p < 0.05, **p < 0.01

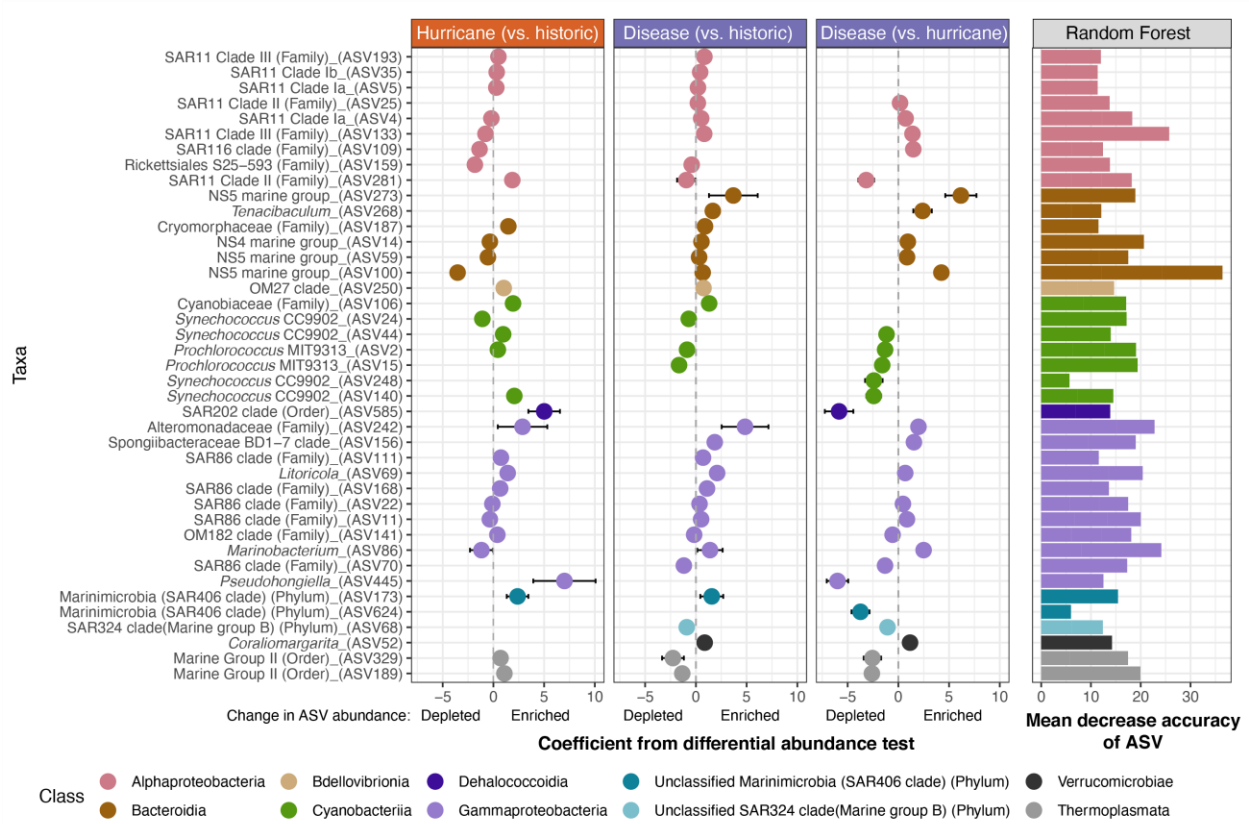

Figure 4-6. Differentially abundant and predictive taxa

Microbial taxa that were both significantly differentially abundant and predictive of disturbance groups. First three panels show significantly differentially abundant taxa evaluated using tests in corncob that were significant at a Benjamini-Hochberg false discovery rate corrected $p < 0.05$. The x-axis coefficient relates to enrichment (positive) or depletion (negative) of the ASV modeled relative abundance during the disturbance (hurricane or disease) relative to the baseline time frame (either "vs. historic" or "vs. hurricane"). In the case where an ASV does not have a point on one of the panels indicates that the ASV was not significantly differentially abundant between the two time periods. For each of the taxa, the fourth panel displays an output from the random forest model, the mean decrease accuracy. This parameter shows how much accuracy the random forest model loses if that taxon were removed from the analysis. In this case, a higher value indicates a greater importance of the ASV in the classification of disturbance.

Table 4-1. Random forest classification error

Training data - benthic seawater	Historic	Hurricane	Disease	Percent classification error
Historic	65	0	0	0.00 %
Hurricane	2	43	0	4.44 %
Disease	0	0	68	0.00 %
Validation data - surface seawater	Historic	Hurricane	Disease	Percent classification error
Historic	61	0	0	0.00 %
Hurricane	4	44	0	4.35 %
Disease	0	0	62	0.00 %

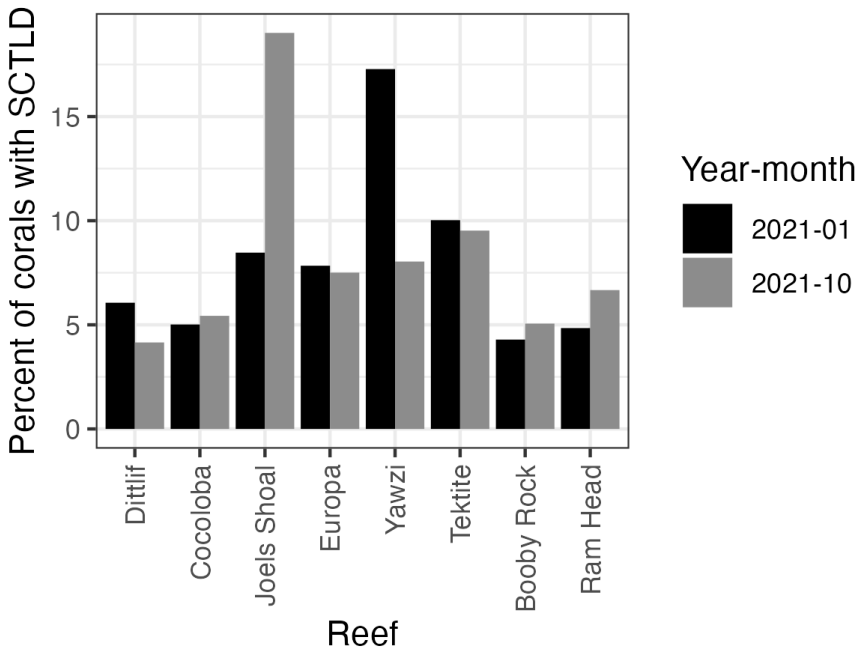

Figure 4-S1. Prevalence of stony coral tissue loss disease (SCTLD) varied across reefs in January and October, 2021 (black and gray, respectively). Prevalence of SCTLD is shown as the percent of live corals showing active disease lesions during 30-minute roving diver surveys.

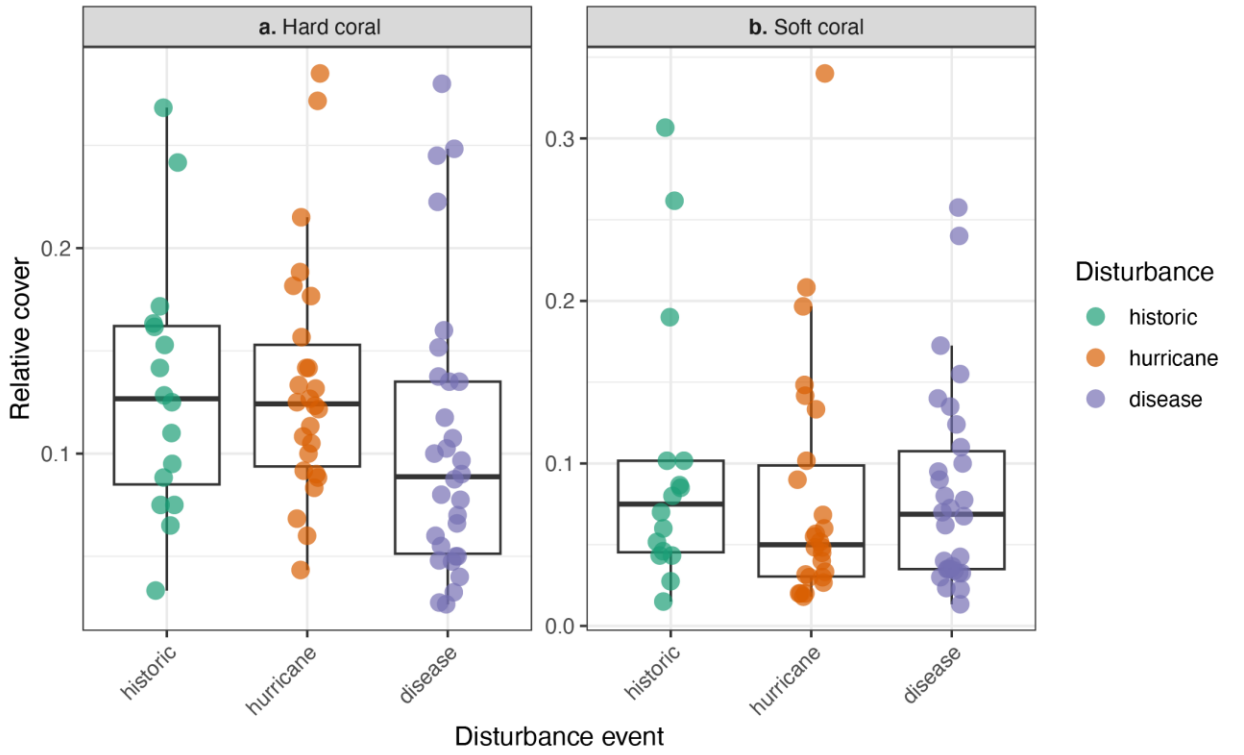

Figure 4-S2. Relative cover of hard and soft coral did not significantly change across disturbance time frames (a. Hard coral Kruskal-Wallis p = 0.0611; b. Soft coral Kruskal-Wallis p = 0.477). While overall not significant, median hard coral decreased during the disease outbreak.

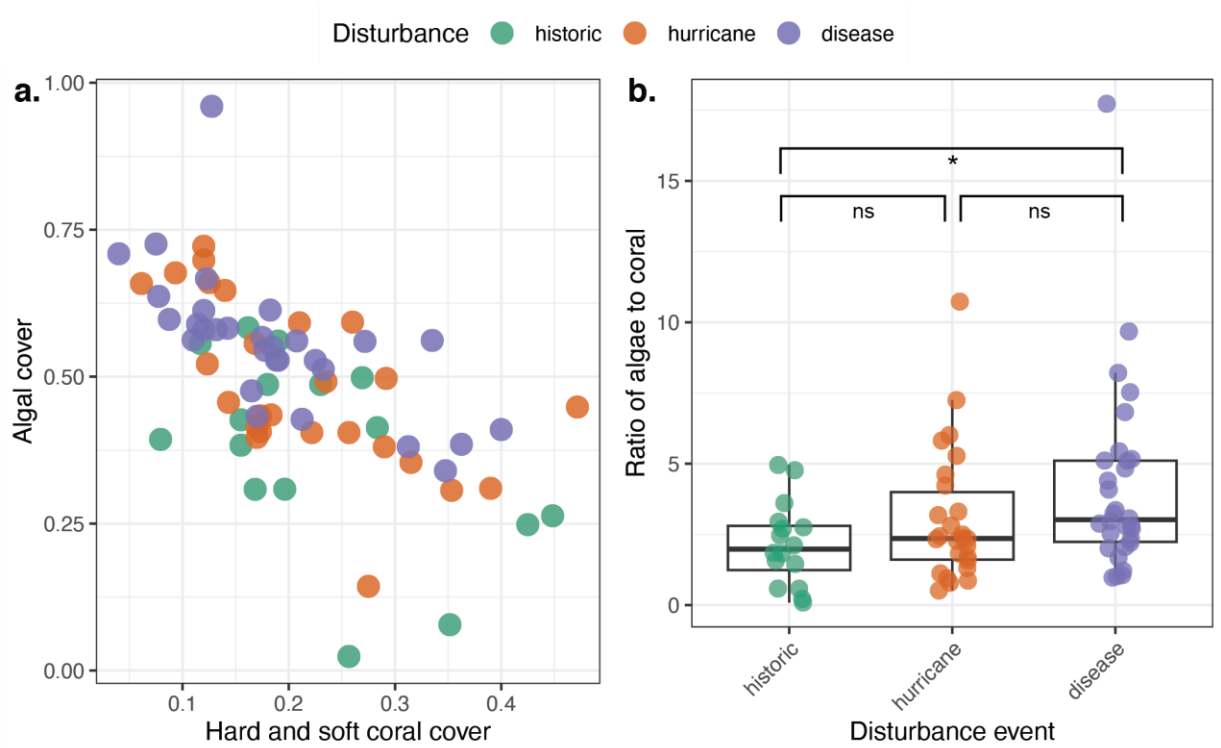

Figure 4-S3. Coral-algal phase shifts are becoming more pronounced as disturbance impacts US Virgin Islands reefs. a) Scatter plot displays the relationship between relative cover of hard and soft coral and the total algal cover on reefs, which can also be distilled as the (b) ratio between algae and coral on the reefs, which is significantly elevated during the disease outbreak relative to historic disturbances (Kruskal-Wallis p = 0.033). Significant pairwise tests from Dunn post-hoc tests are displayed with brackets and asterisks indicating significance levels of adjusted p-values: ns = not significant, *p < 0.05

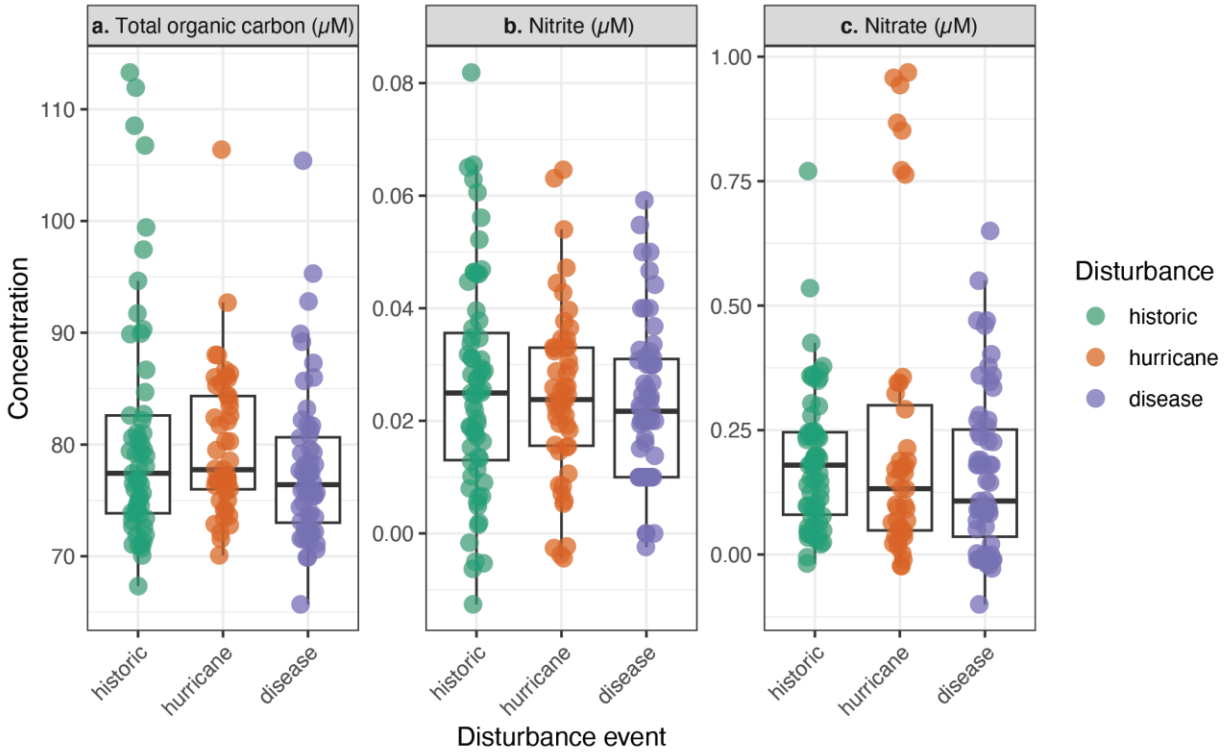

Figure 4-S4. Concentrations of organic and inorganic nutrients that did not significantly change across disturbances include (a) total organic carbon (Kruskal-Wallis p=0.152), (b) nitrite (ANOVA p=0.633) and (c) nitrate (Kruskal-Wallis p=0.341) did not significantly change with disturbances over seven years in US Virgin Islands reefs.

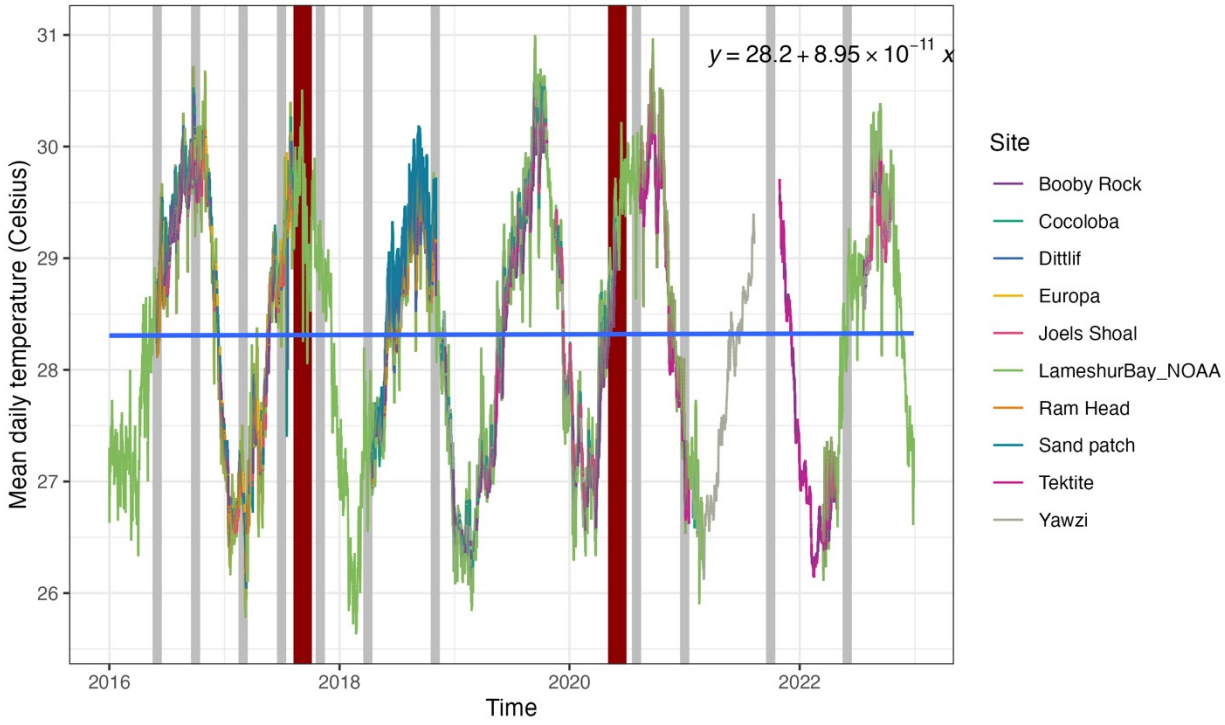

Figure 4-S5. Temperature from in situ loggers at reefs and in Lameshur Bay, US Virgin Islands, over seven years shows average temperature remained static over the course of the study. Trend line is the result of a linear regression (lm(temperature ~ time), $p < 0.05$) and the equation of the line is provided as an inset. Red vertical lines indicate the disturbance events. Gray vertical lines indicate sampling events before and after both disturbances.

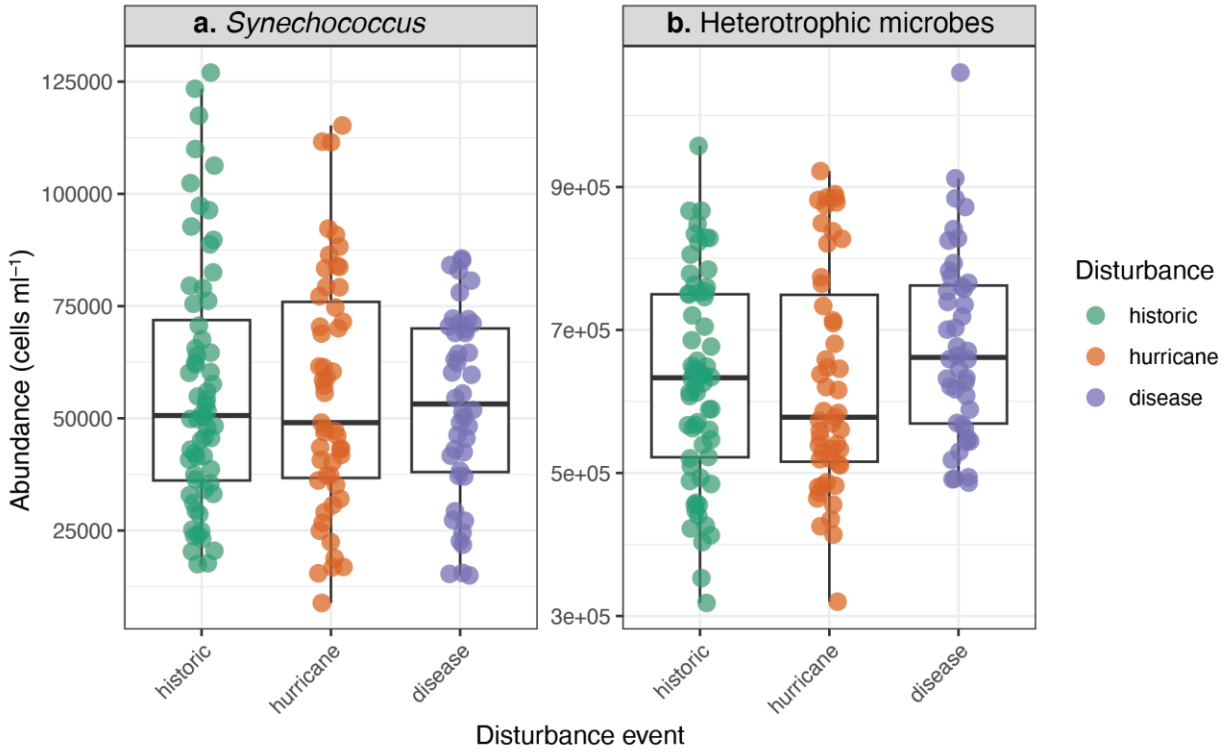

Figure 4-S6. Reef seawater abundances (cells ml^{-1}) that did not differ across disturbances included (a) *Synechococcus* (Kruskal-Wallis p = 0.984) and (b) heterotrophic microbes (Kruskal-Wallis p = 0.119).

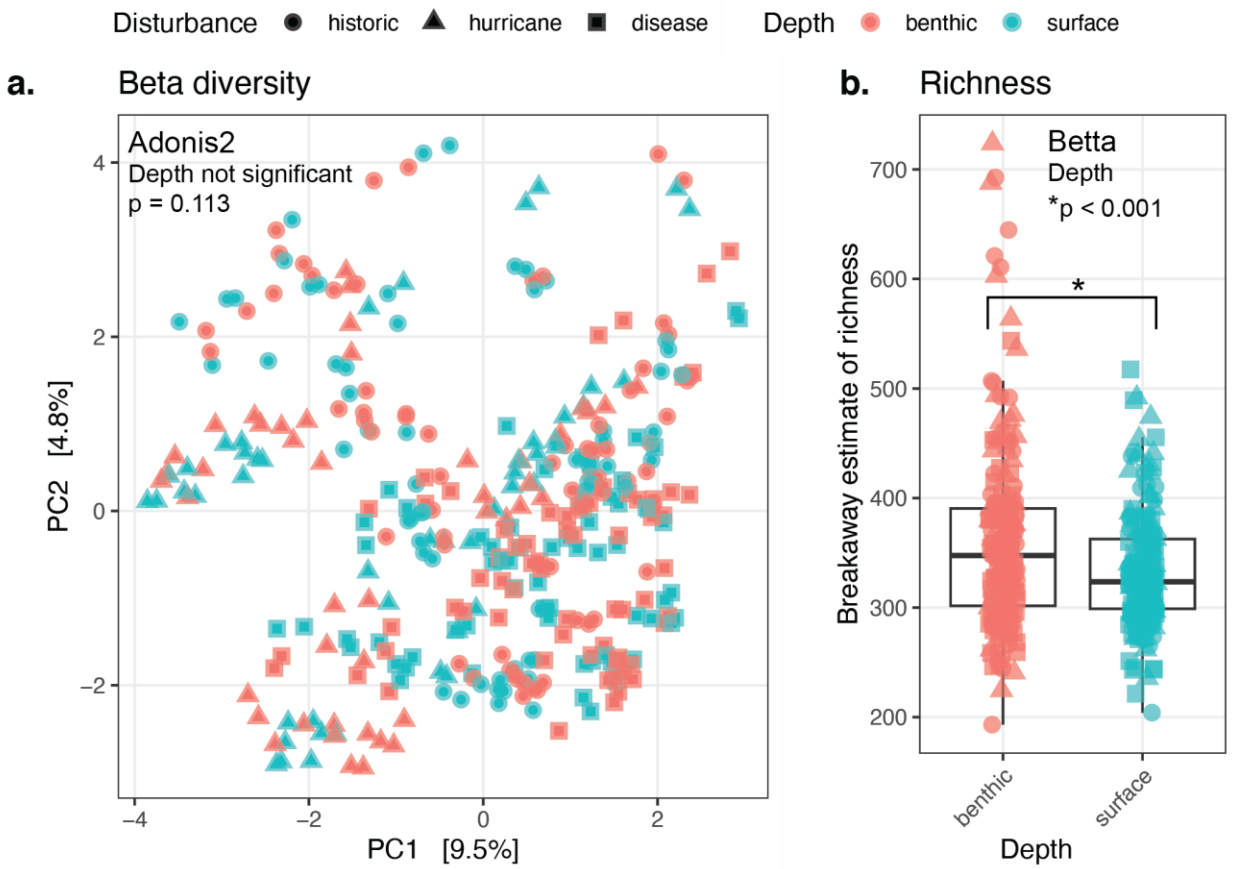

Figure 4-S7. Surface and benthic microbial community composition and richness. a) Principal component analysis of microbial community beta diversity in reef waters was not significantly different by depth (Aitchison distance on centered log-ratio transformed data, Adonis2 test $p > 0.05$). b) Estimated richness in reef waters was significantly elevated at benthic depths (breakaway estimate of richness, betta test for heterogeneity of total diversity, $p < 0.001$). Points are shaped based on disturbance event.

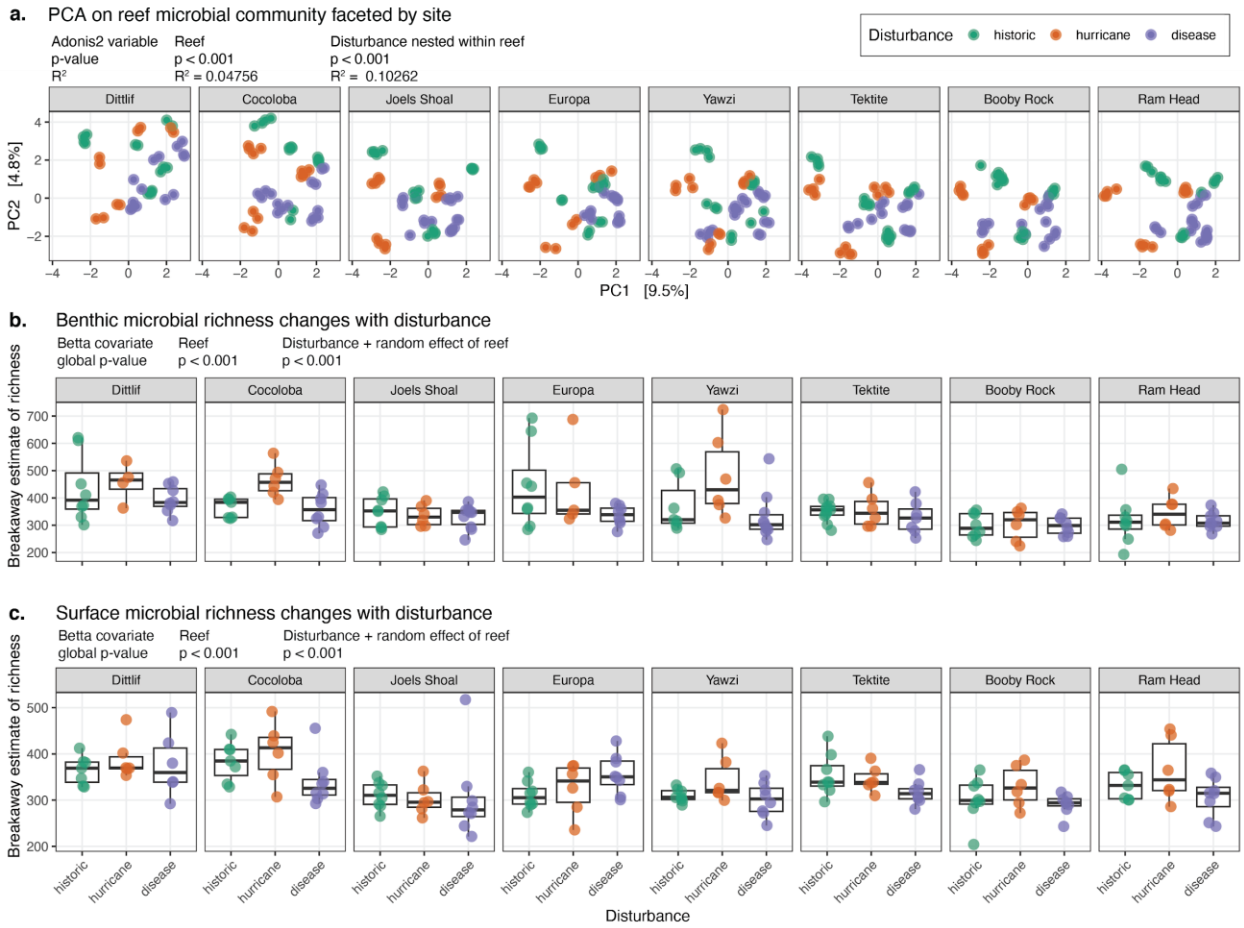

Figure 4-S8. Reef seawater microbial community beta diversity and richness was influenced by reefs and disturbance events. a) Principal component analysis of benthic and surface microbial community beta diversity calculated using Aitchison distance on centered log-ratio transformed data significantly changed across reefs and by disturbance nested within reefs (Adonis2 test, 999 permutations, $p < 0.001$). b) Benthic reef water and (c) surface reef water microbial estimated richness (alpha diversity metric) significantly changed across reefs and by disturbance with reef as a random effect (betta test for heterogeneity of total diversity, global $p < 0.001$). All graphs are faceted by reef, ordered by geographic orientation (east to west) and colored by disturbance event.

Figure 4-S9. Taxa that significantly differed across disturbance groups and were important for disturbance classifications. All taxa are shown except the Bacteroidia and Cyanobacteria, which are shown in separate graphs. Box and whisker plots display the relative abundance of the ASV-level taxa displayed in Figure 6 in the main text that were significantly differentially abundant across disturbances (corncob analysis, Benjamini-Hochberg false discovery rate corrected $p < 0.05$) and evaluated as important for random forest classification (among the top 50 taxa with the highest mean decrease accuracy). Brackets show the results of the pairwise differential abundance tests: ns = not significant, *adjusted $p < 0.05$. The top headings are colored by Phylum or Class groups as in Figure 6 in the main text.

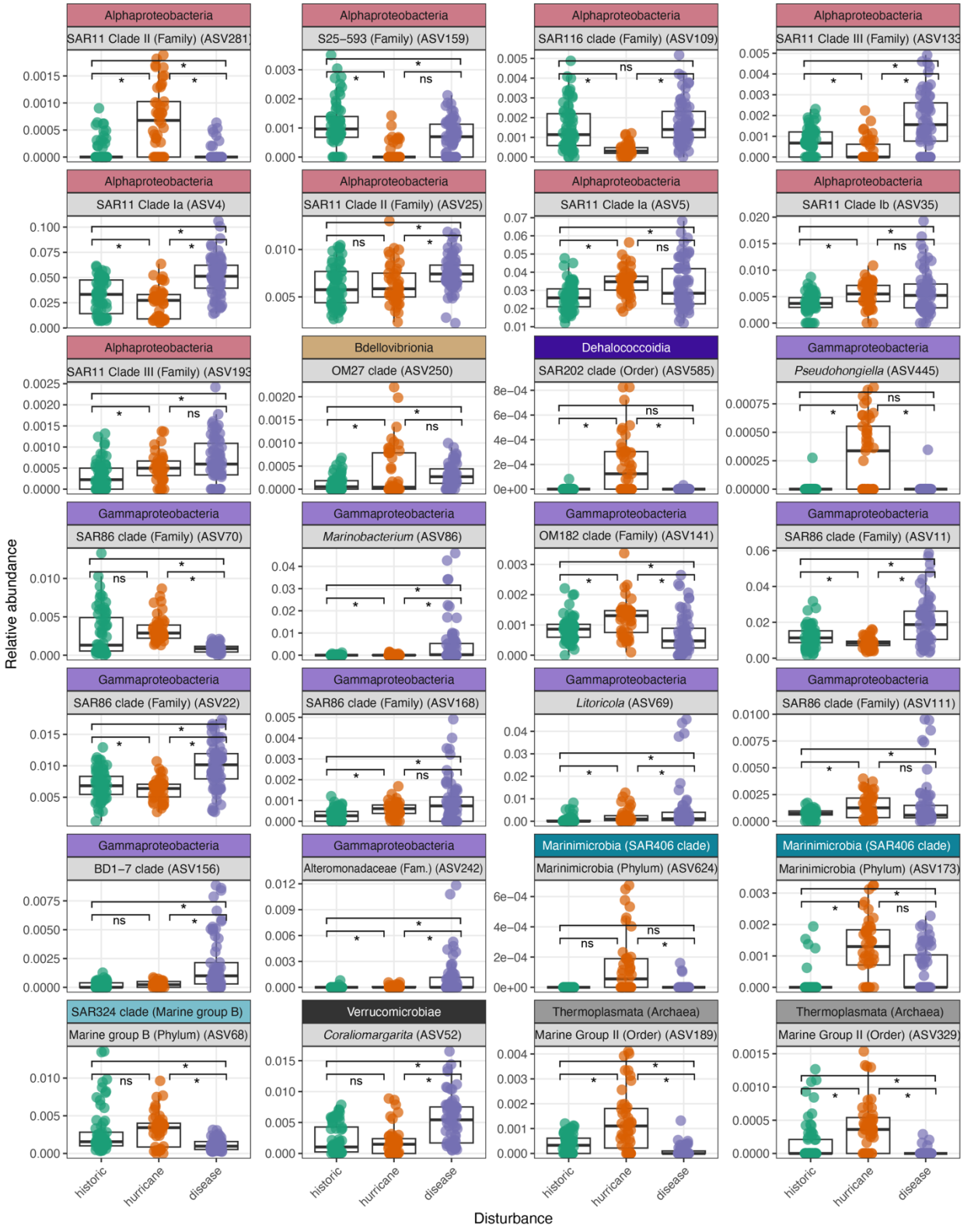
Alphaproteobacteria
SAR11 Clade II (Family) (ASV281)
Alphaproteobacteria
S25−593 (Family) (ASV159)
Alphaproteobacteria
SAR116 clade (Family) (ASV109)
Alphaproteobacteria
SAR11 Clade III (Family) (ASV133)
Alphaproteobacteria
SAR11 Clade Ia (ASV4)
Alphaproteobacteria
SAR11 Clade II (Family) (ASV25)
Alphaproteobacteria
SAR11 Clade Ia (ASV5)
Alphaproteobacteria
SAR11 Clade Ib (ASV35)
Alphaproteobacteria
SAR11 Clade III (Family) (ASV193)
Bdellovibrionia
OM27 clade (ASV250)
Dehalococcoidia
SAR202 clade (Order) (ASV585)
Gammaproteobacteria
Pseudohongiella (ASV445)
Gammaproteobacteria
SAR86 clade (Family) (ASV70)
Gammaproteobacteria
Marinobacterium (ASV86)
Gammaproteobacteria
OM182 clade (Family) (ASV141)
Gammaproteobacteria
SAR86 clade (Family) (ASV11)
Gammaproteobacteria
SAR86 clade (Family) (ASV22)
Gammaproteobacteria
SAR86 clade (Family) (ASV168)
Gammaproteobacteria
Litoricola (ASV69)
Gammaproteobacteria
SAR86 clade (Family) (ASV111)
Gammaproteobacteria
BD1−7 clade (ASV156)
Gammaproteobacteria
Alteromonadaceae (Fam.) (ASV242)
Marinimicrobia (SAR406 clade)
Marinimicrobia (Phylum) (ASV624)
Marinimicrobia (SAR406 clade)
Marinimicrobia (Phylum) (ASV173)
SAR324 clade (Marine group B)
Marine group B (Phylum) (ASV68)
Verrucomicrobiae
Coraliomargarita (ASV52)
Thermoplasmata (Archaea)
Marine Group II (Order) (ASV189)
Thermoplasmata (Archaea)
Marine Group II (Order) (ASV329)
Relative abundance
historic
hurricane
disease
Disturbance

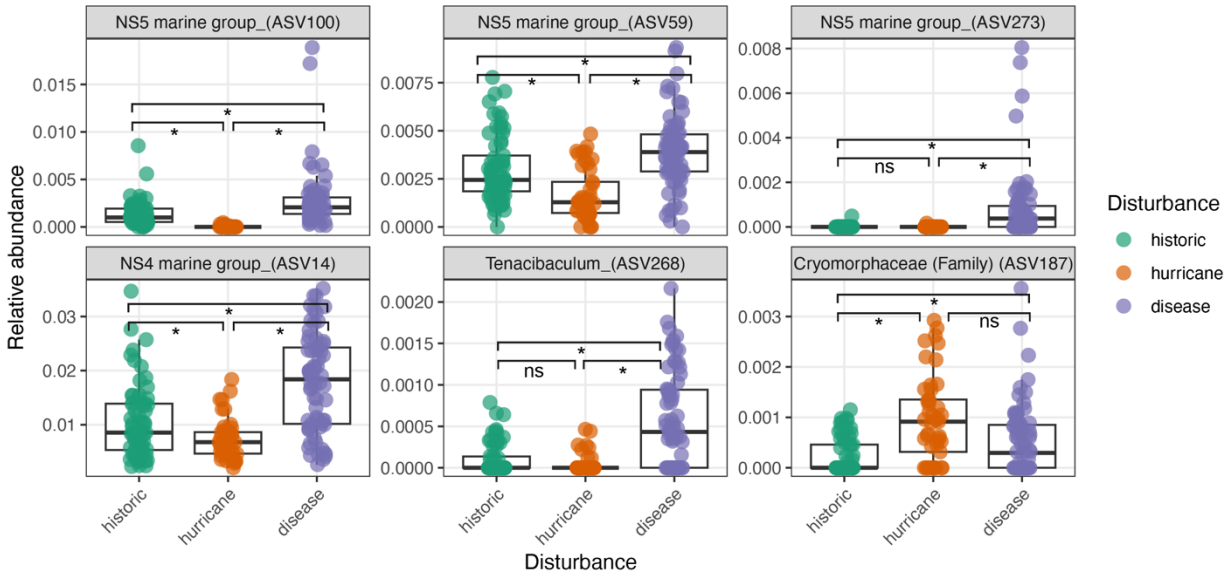

Figure 4-S10. Bacteroidia taxa were more abundant during the disease outbreak, except for Cryomorphaceae, which was more abundant during the hurricane time period. Box and whisker plots display the relative abundance of the six ASV-level taxa belonging to the class Bacteroidia that were significantly differentially abundant across disturbances (corncob analysis, Benjamini-Hochberg false discovery rate corrected $p < 0.05$) and evaluated as important for random forest classification (among the top 50 taxa with the highest mean decrease accuracy). Brackets show the results of the pairwise differential abundance tests: ns = not significant, *adjusted $p < 0.05$. Labels are at the genus level, except for Cryomorphaceae, which is Family-level.

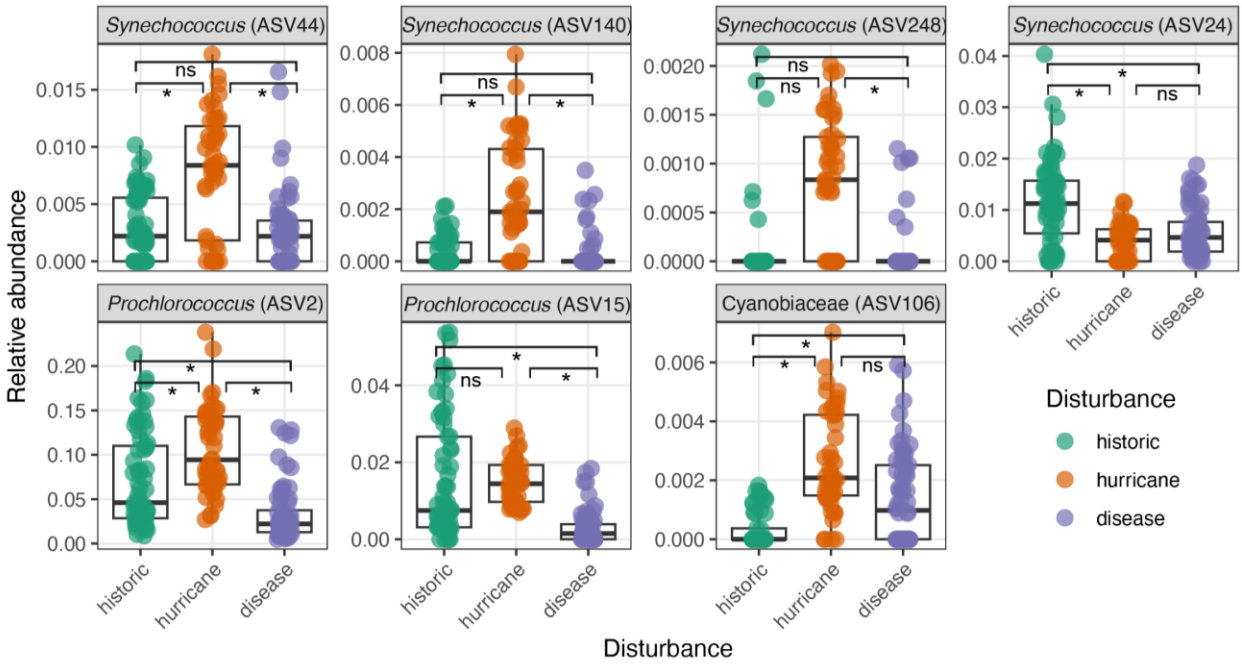

Figure 4-S11. Cyanobacteria were generally elevated during the hurricane time period, but depleted during the stony coral tissue loss disease outbreak, except for one *Synechococcus*, which was depleted during both disturbances. Box and whisker plots display the relative abundance of the six ASV-level taxa belonging to the class Bacteroidia that were significantly differentially abundant across disturbances (corncob analysis, Benjamini-Hochberg false discovery rate corrected $p < 0.05$) and evaluated as important for random forest classification (among the top 50 taxa with the highest mean decrease accuracy). Brackets show the results of the pairwise differential abundance tests: ns = not significant, *adjusted $p < 0.05$. Labels are at the genus level, except for Cyanobiaceae, which is Family-level.

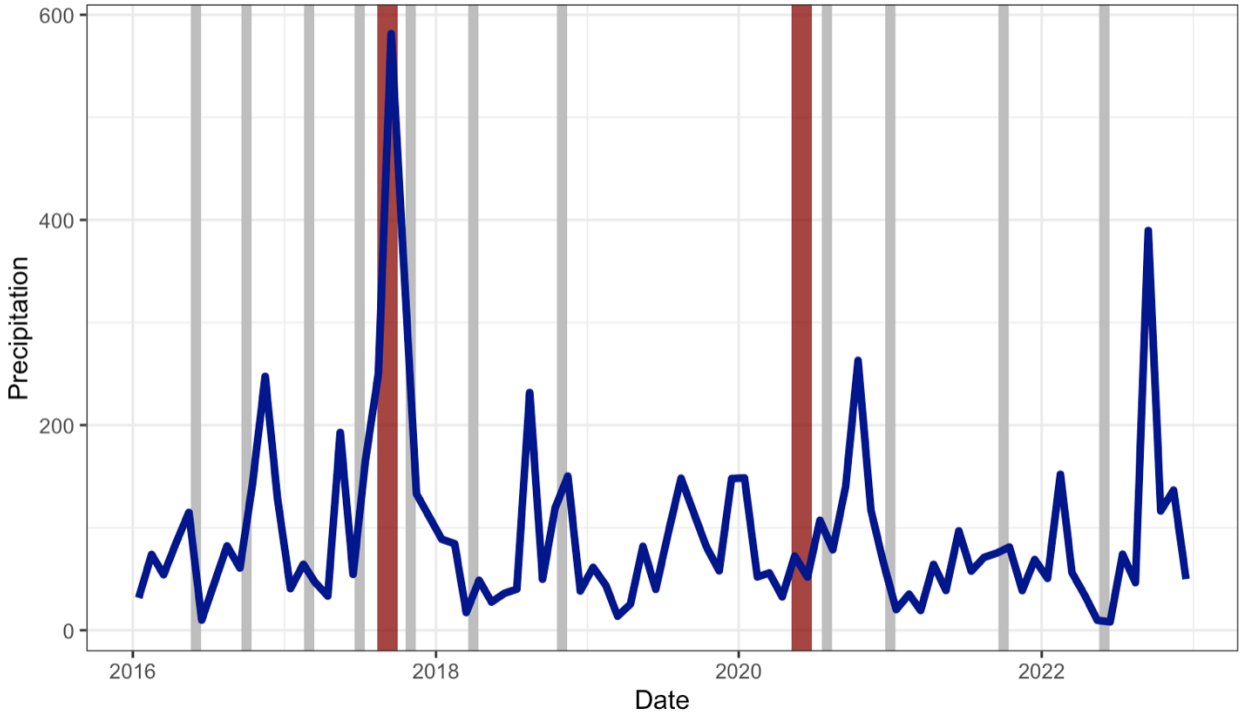

Figure 4-S12. Monthly precipitation (millimeters) at East End on St. John, US Virgin Islands from 2016-2022. The data are recorded and compiled by NOAA and were retrieved from the National Centers for Environmental Information global summary of the month (GSOM), version 1 tool. The data shown are from East End on St. John, US Virgin Islands (station VQC00672551).

Chapter 5 - Microorganisms and dissolved metabolites distinguish Florida's Coral Reef habitats[3]

[3] This chapter was submitted to *PNAS Nexus* as:

Becker CC, Weber L, Zgliczynski B, Sullivan C, Sandin S, Clark AS, Muller E, Kido Soule M, Longnecker K, Kujawinski EB, Apprill A. Microorganisms and dissolved metabolites distinguish Florida's Coral Reef habitats.

CCB, LW, BZ, SS, EM, ASC, EBK, and AA conceived and designed the sampling scheme. CCB, LW, BZ, CS, ASC, and EM collected the data. ASC and EM processed and contributed disease data. BZ, CS, and SS processed and contributed benthic photomosaic data. LW, MCKS, and KL processed and contributed metabolomic data. CCB and LW processed and contributed microbiome data. CCB performed the analysis and wrote the manuscript. All authors provided helpful comments and edits on the manuscript.

ABSTRACT

As coral reef ecosystems experience unprecedented change, effective monitoring of reef features supports management, conservation, and intervention efforts. ‘Omics techniques show promise in quantifying key components of reef ecosystems, dissolved metabolites and microorganisms, that may serve as invisible sensors for reef health. Dissolved metabolites are released by reef organisms and transferred among microorganisms, acting as chemical currencies, and contributing to nutrient cycling and signaling on reefs. Here we applied four ‘omics techniques (taxonomic microbiome via amplicon sequencing, functional microbiome via shotgun metagenomics, targeted metabolomics and untargeted metabolomics) to waters overlying Florida’s Coral Reef, as well as microbiome profiling on individual coral colonies from these reefs to understand how microbes and dissolved metabolites reflect biogeographical, benthic and nutrient properties of this 500-km barrier reef. We show that the microbial and metabolite ‘omics approaches both differentiated reef habitats based on geographic zone. Further, seawater microbiome profiling and targeted metabolomics were significantly related to more reef habitat characteristics, such as amount of hard and soft coral, compared to metagenomic sequencing and untargeted metabolomics. Across five coral species, microbiomes were also significantly related to reef zone, followed by species and disease status, suggesting that the geographic water circulation patterns in Florida also impact the microbiomes of reef builders. A combination of differential abundance and indicator species analyses revealed metabolite and microbial signatures of specific reef zones, which demonstrates the utility of these techniques to provide new insights into reef microbial and metabolite features that reflect broader ecosystem processes.

Significance

Microorganisms and the dissolved metabolites they process are central to the functioning of ocean ecosystems. These ‘invisible’ ocean features are poorly understood in biodiverse and productive coral reef ecosystems, where they contribute to nutrient cycling and signaling cues among reef organisms. This study demonstrates that reef water microbes and metabolites successfully distinguish reef habitats, including geographical, reef compositional and

environmental features, and together they provide novel insights into reef ecosystem characteristics. Microbes and dissolved metabolites offer a new means to examine reef features and have applications for conservation, monitoring, and restoration efforts in these changing ecosystems.

INTRODUCTION

Coral reefs, one of the most biodiverse and economically valuable ocean ecosystems, are declining worldwide due to the interaction of climate change and other human pressures. Documentation of this decline primarily focuses on hard coral cover, a metric that represents the percentage of benthic habitat these keystone species encompass. By this metric, reefs have seen significant coral cover loss over the past 50 years, including 20 – 30% in Caribbean reefs (Gardner *et al.*, 2003; Guest *et al.*, 2018), 50% in the Great Barrier Reef (De'ath *et al.*, 2012), and as high as 92% in Florida's Coral Reef (Dustan, 2003; Alevizon and Porter, 2015; McClenachan *et al.*, 2017). Many significant efforts are in place to protect coral reefs (Mora *et al.*, 2006; Selig and Bruno, 2010; Topor *et al.*, 2019) and restore endangered corals (van Woesik *et al.*, 2021; Vardi *et al.*, 2021), and these efforts do not always incorporate the innumerable components of coral reefs that interact to create the most biodiverse ocean ecosystem.

Central to the success of reef ecosystems are the invisible microbial and chemical dynamics that play a major role in reef processes, such as settlement (Vermeij *et al.*, 2009; Lecchini and Nakamura, 2013; Sneed *et al.*, 2014) and coral growth and health (Sullivan *et al.*, 1983; Pawlik *et al.*, 2007; Bourne *et al.*, 2016; Andersson *et al.*, 2021; Wada *et al.*, 2022). Detrimental microbial and chemical dynamics may even be central to reef decline, as exemplified by the microbialization hypothesis, in which algal-exuded dissolved organic carbon promotes growth of pathogenic microorganisms, which in turn threaten corals and other reef organisms (Haas *et al.*, 2016). Although microorganisms and chemicals are emerging as critical components for the success or failure of reefs, monitoring programs generally do not incorporate these parameters, due to the lack of scientific evidence documenting their utility as well as the high levels of cost and expertise needed to evaluate them. Therefore, integrative

studies that employ a suite of chemical and microbial comparisons are critical for understanding how these parameters may differentiate reef habitats.

Reef microorganisms and dissolved chemicals, or metabolites, are well-poised to serve as sensors of reef health (Glasl *et al.*, 2017; Wegley Kelly *et al.*, 2021). The production of dissolved metabolites within reef seawater is species-specific, with corals producing diverse nitrogen and phosphorus-based compounds and macroalgae yielding prenol lipids, steroids (Wegley Kelly *et al.*, 2022b) and organic compounds enriched in neutral sugars (Nelson *et al.*, 2013). These species-specific signals collectively make up the metabolome signature of a reef, which differs from open ocean waters (Weber, Armenteros, *et al.*, 2020). In seawater overlying a reef, microorganisms are a primary consumer of metabolites, and while certain lineages of microorganisms are enriched in response to species-specific benthic exudates (Nelson *et al.*, 2013; Nakajima *et al.*, 2018; Ochsenkühn *et al.*, 2018), we are only beginning to understand which individual metabolites may be responsible for such enrichment (Weber *et al.*, 2022). Studies have documented relationships between reef microbial composition and reef parameters, including hard coral cover (Kelly *et al.*, 2014; Apprill *et al.*, 2021), temperature (Glasl *et al.*, 2019; Laas *et al.*, 2021), chlorophyll (Glasl *et al.*, 2019), organic carbon (Laas *et al.*, 2021), biogeography (Apprill *et al.*, 2021; Ma *et al.*, 2022b), and reef protection (Weber, González-Díaz, *et al.*, 2020). To date, most investigations study either metabolites or microbes in isolation (Haas *et al.*, 2016; Weber, Armenteros, *et al.*, 2020; Wegley Kelly *et al.*, 2022b). A direct comparison of reef water metabolites and microorganisms is needed to inform the individual or collective value of these factors within reef habitats.

Florida's Coral Reef (FCR) is an ideal environment for examining reef microbial and metabolic characteristics within the context of broader reef processes. Decades of research have demonstrated biogeographic reef zones partitioning the system, largely driven by reef hydrography, with the Gulf of Mexico loop current and meandering Florida Current producing many gyres and eddies (Lee *et al.*, 1995; Fratantoni *et al.*, 1998; Kourafalou and Kang, 2012). These currents interact with tidal mixing from Florida Bay, especially in the Lower and Middle Keys, but less so in the Upper Keys, which are more isolated from Florida Bay water, contributing to zonal patterns of nearshore nutrients and organic matter (Briceño and Boyer,

2018). For example, the Upper, Middle, and Lower Keys zones vary, and are distinct from more offshore reef zones, such as the Marquesas and Dry Tortugas, in terms of, but not limited to, total organic carbon, nutrients, and turbidity (Briceño *et al.*, 2013). Geological evidence also reflects these regional patterns, with historical reef accretion and present day coral calcification rates higher in the remote Dry Tortugas zone compared to other zones within the Florida Keys (Toth *et al.*, 2018; Kuffner *et al.*, 2020). Presently, FCR coral communities are facing the highly contagious stony coral tissue loss disease (SCTLD), a devastating disease that has already led to the regional extinction of a coral (Muller *et al.*, 2020; Neely *et al.*, 2021). This, along with climate pressures, are leading to increased homogenization on the reefs (Burman *et al.*, 2012), though some zonation within the benthic community persists (Murdoch and Aronson, 1999; van Woesik *et al.*, 2020). Relative to these well-studied features of FCR, microorganisms and metabolites have received little attention (Yamashita *et al.*, 2013; Weber, González-Díaz, *et al.*, 2020).

To better understand the metabolite and microbial landscape of FCR and the potential utility of these invisible sensors to reef health, we leveraged a cruise of opportunity on OceanX's M/V *Alucia* during June 2019 to study 85 reefs dispersed along the 500-km reef tract. We examined if and how reef water microbes and metabolites differentiate each reef within the context of geography, reef benthos, disease and environmental parameters, using four 'omics approaches (taxonomic microbiome via amplicon sequencing, functional microbiome via shotgun metagenomics, targeted metabolomics and untargeted metabolomics). We also conducted microbiome profiling via amplicon sequencing of near-coral seawater and coral hosts. Our results demonstrate that microbes and metabolites successfully distinguish between individual reefs according to biogeochemical zones and that their combined use provides novel insights into reef ecosystem parameters that may benefit monitoring, conservation, and restoration activities in these important ecosystems.

METHODS

Study area and sampling. We sampled coral reef benthic environments during a research cruise aboard the M/V *Alucia* between June 5 – 19, 2019 (Figure 5-1, Supplementary File 1, supplementary files are accessible online at https://doi.org/10.6084/m9.figshare.22310434.v1). We targeted up to 85 reefs that were separated into eight zones (between 8-14 reefs per zone). At 85 reefs, 30 minute roving diver surveys were used to measure the prevalence of stony coral tissue loss disease (SCTLD). Within a 100 m^2 plot, high-resolution imagery for benthic composition was captured on 45 reefs. We collected 30-40 ml of seawater via SCUBA at all 85 reefs at reef depth for inorganic nutrients and organic carbon and total nitrogen. Inorganic nutrient samples were frozen after 1.4 ml subsamples were removed and fixed with paraformaldehyde (1% final concentration) to quantify cell abundances. Organic carbon and total nitrogen samples were acidified and kept at room temperature or 4°C until analysis. At 13 reefs, we collected triplicate 1.7 l seawater samples for metabolomics analysis (targeted and untargeted) via SCUBA. The seawater was pre-filtered (0.1 µm) to remove microbial biomass and acidified before low molecular weight organic metabolites were concentrated using solid-phase extraction (SPE) cartridges. At 27 reefs (including the 13 sampled for metabolomics), we collected two 4 l benthic seawater samples. We filtered 2 l at a time using a 0.2 µm filter (microbiome analysis) or GF/F filter (chlorophyll analysis). Filters and SPE cartridges were frozen at −80°C for analysis at WHOI.

On 11 reefs with active SCTLD, we collected coral tissue with 10-ml Luer-Slip syringes and near-coral seawater with 60-ml Luer-Lok™ syringes from separate apparently healthy and SCTLD-afflicted coral colonies. We targeted the following coral species: *Colpophyllia natans, Dichocoenia stokesii, Montastraea cavernosa, Orbicella faveolata,* and *Pseudodiploria strigosa.* The seawater was hand-filtered (0.2 µm) and all samples (filters and coral tissue) were frozen at −80°C until analysis at WHOI. Further details are included in the SI Methods.

Benthic and seawater environmental sample processing. Photomosaics at 45 reefs were analyzed for benthic composition as described in Fox et al. (2019). The number of diseased and apparently healthy coral colonies were counted and used to generate a proportion of colonies

at each reef with SCTLD. Samples collected for quantifying microbial cell abundances were processed at the University of Hawaii, as described previously (Becker *et al.*, 2020). Non-pigmented prokaryotes were used as a proxy for heterotrophic bacterial and archaeal cells (Monger and Landry, 1993; Marie *et al.*, 1997), referred to as "heterotrophic microbes". Non-purgeable total organic carbon (TOC), total nitrogen (TN), and inorganic nutrients (phosphate, ammonium, silicate, nitrite and nitrate) were analyzed as described previously (Weber, González-Díaz, *et al.*, 2020). Total organic nitrogen (TON) was calculated by subtracting ammonium and nitrite plus nitrate from TN. Chlorophyll analysis involved a 24-hour 90% acetone extraction, followed by fluorometric analysis. See SI Methods for further details.

Metabolomic and microbiome laboratory processing. SPE cartridges were processed following the methods in Weber et al. (2020). For untargeted metabolite analysis, eluted and resuspended extracts were measured using an ultrahigh performance liquid chromatography system (Vanquish UHPLC) coupled with an Orbitrap Fusion Lumos Tribrid mass spectrometer that was run in both positive and negative ion modes (See SI methods). Processing the untargeted data using XCMS (SI methods), resulted in a final chemical feature table with unique mass-to-charge ratios and retention times for each feature as well as the corresponding peak intensity for that feature across samples. To prepare the untargeted metabolomic data for statistical analyses, data were filtered of blank-associated features and features with low coefficient of variation across samples, and then normalized to seawater volume, keeping 1428 (negative ion mode) and 2759 (positive ion mode) features. Extracts for targeted metabolomics were analyzed using UHPLC (Accela Open Autosampler and Accela 1250 Pump) coupled with a heated electrospray ionization source (H-ESI) and a triple stage quadrupole mass spectrometer (TSQ Vantage) that was operated in selective reaction monitoring mode. Targeted compounds included a range of environmentally relevant vitamins, amino acids, and other metabolites that have been detected in marine microorganisms, their culture media, and reef seawater (Fiore *et al.*, 2015, 2017; Kido Soule *et al.*, 2015). After conversion of instrument files, final concentrations were corrected for limit of detection and extraction efficiency (Johnson *et al.*, 2017). See SI Methods for further details.

We extracted DNA from 0.2 µm filters used for 1.7 l seawater collections and 4 control blank filters using PowerBiofilm kits (Qiagen, Germantown, MD, USA) following manufacturer protocols. The resulting DNA was used as the template for both 16S rRNA gene sequencing of bacteria and archaea as well as shotgun sequencing. For 16S rRNA gene sequencing for the taxonomic microbiome, we followed methods previously reported (Becker *et al.*, 2020) and sequenced 2 x 250 bp on an Illumina MiSeq. A library for shotgun metagenomics (functional microbiome) was prepared using the Illumina DNA Prep following manufacturer protocols. Samples were sequenced 2 x 150 bp on a P3 flow cell on an Illumina NextSeq 2000. See SI methods for library preparation details.

To expedite the turnaround time between sample collection and taxonomic microbiome results for disease diagnostics, we performed on-ship processing and 2 x 150 bp sequencing on the Illumina iSeq100 system for near-coral seawater samples from five reefs from June 9-10, 2019. All remaining coral and near-coral seawater samples were processed at WHOI. On-ship and at-WHOI methods followed in-the-field microbiome preparation protocols described previously (Becker *et al.*, 2021) and are detailed further in the SI methods.

Bioinformatics. Sequence reads from the Illumina MiSeq and iSeq runs were separately run through the DADA2 pipeline to generate amplicon sequence variants (ASVs) (v1.18.0)(Callahan *et al.*, 2016). We removed mitochondrial and chloroplast ASVs and filtered out low-abundant ASVs (average count < 0.5). DNA extraction and PCR controls were removed for data analysis. ASVs were given a unique number, and sequences associated with the IDs were saved.

Shotgun sequencing on the Illumina NextSeq yielded 13,592,782 ± 3,357,010 paired-end sequence reads per reef seawater microbial community sample. Due to sequencing errors, 6 reefs were singulars, while all others had duplicate sequence samples. We quality filtered the sequence reads and co-assembled them with MegaHit (v1.2.9)(Li *et al.*, 2015), as this assembler has been shown to generate more genes that could be successfully annotated in complex environments such as ocean and soil samples compared to MetaSPAdes (Quince *et al.*, 2017). We annotated the assembly and calculated gene abundances. We kept only genes with known Clusters of Orthologous Genes (COG) identifiers and further filtered to remove low-abundance

genes, leaving 103,665 genes. All resultant gene and taxa data tables were transformed to relative abundance and log transformed after adding a pseudocount of 1. See SI Methods for detailed bioinformatic packages, parameters, and links to scripts.

Statistical analysis. Benthic cover, organic and inorganic nutrients, cell abundances, and disease prevalence data were measured from 45 reefs (benthic cover) or 85 reefs (all other parameters) in FCR across eight zones. We used a Kruskal-Wallis test in R (v4.0.3) to compare changes across zones with a Bonferroni-corrected *p* value to account for multiple comparisons (Figure 5-2). We followed with a Wilcoxon rank sum test for pairwise comparisons (significant at $p < 0.05$ after a Benjamini-Hochberg FDR adjustment) (Supplementary File 2, accessible online). To examine the changes in benthic composition across Florida's Coral Reef, we conducted a principal component analysis, followed by a permutational multivariate analysis of variance (PERMANOVA) test by zone. Wilcoxon rank sum tests were used to compare environmental variables at Dry Tortugas National Park to all other zones. Additional linear regressions were conducted between environmental variables.

A distance-based redundancy analysis (dbRDA) was calculated to evaluate how geography (zone) and environmental conditions (TOC, heterotrophic microbes, *Prochlorococcus, Synechococcus,* picoeukaryotes, hard coral, algae, soft coral, and sponge) explained changes in metabolomes and microbiomes. dbRDAs were calculated for each dataset with either gower (targeted metabolomes) or Bray-Curtis (other 'omic datasets) dissimilarities. Significance of individual environmental variables within the analysis was evaluated with an ANOVA using the parameter by = "terms".

To test for metabolites that changed across zones, sites in Zones 2 & 3 as well as Zones 5 & 6 were grouped to ensure each zone had more than one reef. Kruskal-Wallis or ANOVA tests were used to evaluate significantly changing metabolites across zones (Bonferroni-corrected $p < 7.246\times10^{-5}$ and 3.378×10^{-5} for negative and positive metabolites, respectively), followed by pairwise Wilcoxon rank sum tests between zones (FDR-adjusted $p < 0.05$). The 56 untargeted features were z-score standardized for visualization. Model II ordinary least squares linear

regressions were used to relate average relative abundance of MTA source and sink genes in seawater metagenomes to dissolved concentration of MTA.

To identify seawater taxa and functional microbiome indicators of FCR, we used the multi-level pattern analysis, multipatt() function in the R package indicspecies (v1.7.12). Indicators were reported if they had a positive predictor value (A) over 0.6, sensitivity (B) over 0.6 and had a $p < 0.05$. Indicator ASVs and functional genes were visualized with heatmaps and summarized in Supplementary File 3, accessible online.

Coral and near-coral seawater taxonomic microbiome beta diversity was calculated with Bray-Curtis dissimilarity and visualized with principal coordinates analysis. A PERMANOVA test was used to identify the influence of zone, disease, and coral species on microbiome composition. Apparently healthy coral microbiomes were subset from the larger dataset for differential abundance analysis to test which ASVs significantly changed by zone and controlling for the effect of species using corncob (Martin *et al.*, 2020). All statistical tests are detailed further in the SI methods.

RESULTS

This comparative 'omics study was conducted over 15 days in June 2019 along Florida's Coral Reef (FCR). At 13 geographically dispersed reefs, we collected seawater (1.7 l in biological triplicates) from within 0.5 m of the reef benthos for both targeted and untargeted metabolome analyses (Figure 5-1a). At 27 reefs, including the 13 examined for metabolomics, we collected benthic seawater (2 l in duplicate) for taxonomic (bacteria and archaea 16S ribosomal RNA gene) and functional (shotgun metagenome) microbiome analyses and chlorophyll (Figure 5-1a). Given the active stony coral tissue loss disease (SCTLD) outbreak, we also targeted apparently healthy and diseased coral tissue and near-coral seawater within 1-3 cm from the coral for taxonomic microbiome (16S rRNA gene) analysis (11 reefs). To comprehensively assess the reef habitat, at 85 reefs (Figure 5-2a) we measured prevalence of (SCTLD), nutrients (total organic carbon (TOC), total organic nitrogen (TON), inorganic nutrients), and abundances of microbial functional groups (*Prochlorococcus, Synechococcus,*

picoeukaryotes, and heterotrophic microbes (unpigmented bacteria and archaea)), from reef depth waters (Figure 5-2a). Of the 85 reefs, high-resolution photomosaics were taken at 45 reefs to examine the composition of benthic organisms (Figure 5-S4). Detailed methods and information on these data sets can be found in the SI Methods.

Four high-resolution 'omic data sets were produced from the benthic seawater samples. The reef water taxonomic microbiome (27 reefs) approach yielded 43,118 ± 6,834 sequences per sample and 468 total amplicon sequence variants (ASVs, similar to microbial species-level designations (Callahan *et al.*, 2017)), with 110-191 ASVs per sample (see methods). The functional microbiome (metagenomics, 27 reefs) effort produced 13.6 ± 3.4 M paired end reads per sample, which were assembled into contigs, annotated and mapped to 592,912 bacterial gene annotations. Targeted metabolomics (13 reefs) was applied to the reef water, with samples analyzed via ultrahigh performance liquid chromatography coupled to a heated electrospray ionization source and triple stage quadrupole mass spectrometer. This approach quantified 39 environmentally relevant dissolved metabolites in the samples. The untargeted metabolomics approach analyzed extracts via ultrahigh performance liquid chromatography system coupled to an Orbitrap Fusion Lumos Tribrid mass spectrometer and ionized chemical features in two modes, positive and negative (see SI methods). After removing features associated with blanks and with low variance across samples, 2,759 features remained in the positive ion mode dataset and 1,428 features remained in the negative ion mode dataset.

Microorganism and metabolite compositions reflect zonal habitat patterns

Analysis of seawater 'omics datasets (taxonomic and functional microbiome, and targeted and untargeted metabolome) via ordinations revealed significant clustering of all data types according to biogeographic reef zone (depicted via colors in Figure 5-1). A distance-based redundancy analysis (dbRDA) followed by an analysis of variance (ANOVA) revealed that biogeographic reef zone was the most significant parameter in structuring the composition of seawater 'omics datasets (Table 5-1, Pseudo-F values indicate significance). For untargeted metabolomes with triplicate biological replication per reef, reef structured the chemical

composition to a greater extent than zone, which contained multiple reefs, though both were significant (Figure 5-S1, PERMANOVA results in Table 5-S1).

We further demonstrated that benthic, geographic, and environmental parameters significantly structured the seawater microbiome and metabolome compositions (PERMANOVA for dbRDA with Bray-Curtis dissimilarity, $p<0.05$, Figure 5-1, Table 5-1). Reef zone and *Prochlorococcus* abundance structured all 'omics data types. TOC, heterotrophic microbes, and *Synechococcus* explained changes in the microbiome as well as in the targeted and negative mode untargeted metabolome (Figure 5-1, Table 5-1). Significant structuring by other parameters varied by 'omics data type, with the targeted metabolome significantly structured by all tested parameters (Figure 5-1, Table 5-1).

Dry Tortugas National Park (Zone 8) was distinctly clustered from Zones 1-7 in seawater taxonomic and functional microbiomes (Figure 5-1b,c). Environmental parameters were also different at Dry Tortugas, which harbored significantly lower prevalence of SCTLD, seawater TOC, heterotrophic microbial abundances, ratio of heterotrophic microbes: photosynthetic microbes, and cover of turf algae compared to Zone 1-7. In contrast, *Synechococcus* abundances were higher at Zone 8 compared to other zones (Wilcoxon rank sum test with Bonferroni-corrected $p < 0.001667$; Figure 5-S3).

Targeted metabolomes and taxonomic microbiomes were both significantly explained by compositional differences in the benthos (hard coral, sponge, etc.) (Figure 5-1b,d, Table 5-1). Unlike reef seawater 'omics data, benthic reef composition was not significantly structured by zone (PERMANOVA on principal components analysis, Figure 5-S4b). Individual tests of zonal changes in hard coral and algal cover, common metrics used to assess reef quality, changed slightly, but were not significantly different (Kruskal-Wallis rank sum test with Bonferroni-corrected $p > 0.00192$; Figure 5-S5). Instead of zone, distance to shore and percent cover of algae were both significantly negatively correlated with coral cover (linear regression, $p < 0.05$; Figure 5-S6, 5-S7).

Zonal changes were evident in many environmental parameters measured at 85 reefs across eight zones (Kruskal-Wallis test with Bonferroni-corrected $p < 0.00192$, Figure 5-2). The ratio of heterotrophic microbes: photosynthetic microbes, TOC concentrations, and

heterotrophic microbial abundances all increased northeastward across reefs from Zone 8 to Zone 1 (Figure 5-2c,d,e). SCTLD prevalence generally peaked in Zones 4-6 (Figure 5-2b), zones that also had high silicate concentrations (Figure 5-2i). Across zones, abundances of *Prochlorococcus* had a parabolic distribution while *Synechococcus* and picoeukaryote abundances were higher in Dry Tortugas, then increased from the Marquesas Zone 7 to Zone 1 (Figure 5-2f,g,h). Chlorophyll *a* and inorganic nitrogen and phosphorus concentrations shifted with zone, but these trends were not significant (Kruskal-Wallis test with Bonferroni-corrected $p > 0.00192$, Figure 5-S2).

Reef seawater metabolites driven by Florida's Coral Reef zone

To evaluate which metabolites may be signatures of reef zones, we conducted ANOVA or Kruskal-Wallis tests on targeted and untargeted (positive and negative ion modes) metabolites. Two of the 39 targeted metabolites in reef seawater changed across reef zones: 5'-methylthioadenosine (MTA) and taurocholic acid (Kruskal-Wallis test with Bonferroni-corrected $p < 0.00128$, Figure 5-3a,b). Taurocholic acid median concentrations were variable across zones, while MTA concentrations generally increased as sampling moved northeast (Figure 5-3a,b). Additionally, the extracellular seawater concentration of MTA was positively related to the relative abundance of microbial genes found in seawater metagenomes that use MTA (sinks - MTA phosphorylase, MTA/S-adenosylhomocysteine (SAM) nucleosidase, and MTA/SAM deaminase) and produce MTA (sources - polyamine aminopropyltransferase and Isovaleryl-homoserine lactone synthase) (Model II ordinary least squares linear regression $p < 0.001$, 999 permutations, Figure 5-S8). Within the untargeted metabolome datasets, 33 of the 2,759 features in negative ion mode and 23 of the 1,428 features in positive ion mode differed across zones (Kruskal-Wallis test with Bonferroni-corrected $p < 7.246\times10^{-5}$ and $p < 3.378\times10^{-5}$ for negative and positive metabolites, respectively) (Figure 5-3c,d).

Reef seawater microbiome indicators of Florida's Coral Reef zone

We identified microbial ASVs and functional genes diagnostic of individual reef zones via indicator value analysis (indicspecies R package, specificity ≥ 0.6, sensitivity ≥ 0.6, $p < 0.05$, see

SI methods) (Figure 5-4). Of the 468 seawater ASVs, 24 were diagnostic of one of the reef zones (summarized in Supplementary File 3, accessible online), with most representing Dry Tortugas (Zone 8), including *Alcanivorax*, *Coxiella*, *Synechococcus*, *Fluviicola*, and the Families Cryomorphaceae and PS1 clade of Parvibaculales (Figure 5-4a, Supplementary File 3, accessible online). Zones 1 and 3 also harbored several indicator taxa, including SAR11 and SAR116 clades, the NS5 marine group and the PS1 clade of Parvibaculales in Zone 1 and the SAR116 clade, Pirellulaceae, *Propionigenium, Coxiella,* and *Turmeriella* (Figure 5-4a) in Zone 3.

Functional microbial genes were abundance-filtered to 103,665 genes (see methods), and of these, 324 were diagnostic of a reef zone (Figure 5-4b). All genes and their respective pathways are summarized in Supplementary File 3. Like the taxonomic microbiome, the highest number of indicator genes were for Dry Tortugas National Park (Zone 8, n = 127). Some of these genes were involved in biosynthetic pathways unique to Zone 8, including arginine, cysteine, folate, glutamine, isoprenoid, serine, and ubiquinone biosynthesis. Additionally, genes from two types of ATP synthases (FoF1 and A/V) and 66 genes with unknown pathways were Zone 8 indicators (Figure 5-4b, Supplementary File 3). Zone 3 in the Upper Keys also had many functional indicators (119), including some involved in asparagine, biotin, heme, lipoate, lysine, menaquinone, and nicotinamide adenine dinucleotide (NAD) biosynthesis pathways. Additionally, 75 of the 119 Zone 3 indicator genes were from unknown pathways encoded for proteins such as a flagellar basal body protein, nitrate reductase, phosphate import protein, zinc metalloprotease, and a type II secretion system protein, among others (Figure 5-4b, Supplementary File 3). Zone 1 had 55 indicator genes, including a Lipid A biosynthesis gene, as well as 30 indicator genes of unknown pathways (Figure 5-4b, Supplementary File 3).

Coral host-associated microbiomes driven by reef habitat

To examine if reef seawater zonal patterns are reflected in the corals, we applied the most cost-effective 'omics technique, taxonomic microbiome profiling, to corals and near-coral seawater collected within five reef zones (11 reefs). We collected samples from five coral species (*Colpophyllia natans, Dichocoenia stokesii, Montastraea cavernosa, Orbicella faveolata, Pseudodiploria strigosa*) that were either apparently healthy or showing active SCTLD lesions,

and this resulted in 116,942 ± 59,302 sequences per sample and a total of 3,020 ASVs after filtering (see SI methods). Within coral-associated microbiomes, zone significantly structured the microbial community composition, reflective of microbial patterns in overlying seawater microbiomes (Figure 5-5a, Figure 5-1b). Coral species and disease state was also significant (PERMANOVA on Bray-Curtis dissimilarity, $p < 0.05$, Figure 5-5a). Near-coral seawater taxonomic microbiomes were significantly structured by zone and coral species, but not disease state (PERMANOVA, Figure 5-5b).

We next identified specific microbial taxa that may be related to the biogeographic environment. We conducted a differential abundance test by zone and identified 12 ASVs that significantly differed in apparently healthy colonies (false discovery rate (FDR) adjusted $p < 0.05$, Figure 5-5c). The ASVs that differed included two Clostridiaceae bacteria, which varied in abundance by zone. Several other ASVs also had variable abundances relative to Zone 3 (Upper Keys, chosen as the reference zone because it had the highest ratio of heterotrophs: autotrophs and highest organic carbon), including *Alteromonas*, *Paramoritella*, Rickettsiales S25-593, *Balneola*, and *Acinetobacter.* The Pirellulaceae Family and SAR11 Clade III microbes were depleted at all zones relative to Zone 3, while *Rubritalea,* Desulfocapsaceae and Sandaracinaceae were enriched in all zones relative to Zone 3 (Figure 5-5c).

DISCUSSION

We present a comprehensive ‘omics analysis of microorganisms and dissolved metabolites spanning hundreds of kilometers of Florida’s Coral Reef (FCR), which has suffered over the past 50 years from numerous natural and anthropogenic stressors. Following comparative analyses of these ‘omic datasets, we demonstrate that reef water metabolites and microorgansisms as well as coral-associated microbes distinguish between biogeographically distributed reef habitats. Further, taxonomic microbiomes and targeted metabolomics methods were related to underlying benthic organisms and environmental features. These data provide novel insights into reef ecosystem parameters which inform reef ecosystem-level functioning and may be a useful tool for tracking restoration and conservation activities in coral reef ecosystems.

The biogeographic zone emerged as the strongest driver of microbiome and metabolome composition from individual reefs in Florida compared to other habitat and environmental features. These differential patterns, as well as emergent habitat and environmental features, are summarized in Supplementary Figure 5-S9. For example, 'omics signatures in Zones 1 and 8 were often opposing and distinct. Indeed, Dry Tortugas National Park (Zone 8) emerged as a unique habitat, containing low levels of 5'-methylthioadenosine (MTA), a distinct microbial community with low abundances of heterotrophic microbes, and high numbers of functional and taxonomic microbial indicators, including *Synechococcus* and *Alcanivorax,* compared to Zone 1, North Key Largo and Biscayne Bay (Supplementary Figure 5-S9). Within the Upper to Lower Keys and Marquesas, seawater signatures were likewise distinct, and these zonal signatures were even captured within apparently healthy coral host-associated microbial taxa that shifted across reef zones.

These zonal changes agree with the established importance of biogeography for microorganisms in reef seawater (Kelly *et al.*, 2014; Apprill *et al.*, 2021; Ma *et al.*, 2022b). While microbiome studies abound, understanding of biogeographic signatures of reef metabolites is still in its infancy. Similar to our findings, Yamashita and colleagues found significant shifts in optical properties of seawater DOM across regions in FCR, largely attributed to differences in anthropogenic and terrestrial influences (2013). In contrast, a study of the high-quality reefs in the Cuban Jardines de la Reina archipelago using the same mass spectrometry-based methods as the present paper did not find a strong biogeographic signature (Weber, Armenteros, *et al.*, 2020). These differences could be related to variation in anthropogenic influence, hydrogeography, and overall quality between the two reef systems, the FCR and Jardines de la Reina (Weber, González-Díaz, *et al.*, 2020). As reef metabolomics (both targeted and untargeted approaches) begin to gain traction in reef ecology (Wegley Kelly *et al.*, 2021), we anticipate future analyses of dissolved reef metabolites will provide insight into the mechanisms and consequences of such metabolomic and microbial biogeography.

Environmental features of FCR habitats, which changed zonally, explained some of the variation in microbiomes and metabolomes. The abundance of heterotrophic microbes and the degree to which they outnumbered their photosynthetic counterparts (*Prochlorococcus* and

Synechococcus) significantly increased northeast along FCR, suggesting the northern region may be more heterotrophic, or the types of autotrophs could be shifting to different phytoplankton groups. Additionally, high total organic carbon (TOC) concentrations and heterotrophic microbial abundances have been previously documented on Floridian reefs (Weber, González-Díaz, *et al.*, 2020), and were especially high near North Key Largo and Biscayne Bay. The increased heterotrophic microbes and TOC in that region explained metabolomic and microbiome compositions of Zone 1 (Figure 5-1) and was further validated by the five indicator microbes for North Key Largo and Biscayne Bay, which are all known heterotrophs (SAR116, SAR11, NS5 marine group, Parvibaculales) (Figure 5-5). Interestingly, SAR11 clade 1a ASVs were indicators for Zone 1, while clades Ib and II were indicative of Zone 7, likely reflecting physiological adaptations to the different oceanographic influences of the two regions, or potentially the differing anthropogenic influences between the regions (Carlson *et al.*, 2009). At the western end of FCR, at Dry Tortugas National Park (Zone 8), concurrence in the microbial patterns emerged, where *Synechococcus* cells were most abundant and related to microbiome composition. Strain CC9902 was also a microbial indicator for that zone. Fundamental differences in coral growth (Kuffner *et al.*, 2020) and nutrient (inorganic and organic) regimes exist between Dry Tortugas, a more offshore environment, and the nearshore North Key Largo/Biscayne Bay area (Briceño *et al.*, 2013), which supports the stark microbial community differences between these habitats.

Total organic carbon significantly changed across FCR, but TOC is a single value that does not capture the complex dynamics of thousands of low-molecular-weight dissolved and particulate compounds. After using both targeted and untargeted approaches, we found that dissolved targeted metabolites related well to the benthic and biogeochemical habitats, while the dissolved untargeted metabolome (in both positive and negative ion modes) related to only a few tested biogeochemical parameters. Within the untargeted metabolome (positive and negative ion modes), 56 total metabolites shifted across reef zones, in patterns that varied broadly from the concentration of TOC. Two metabolites from the targeted metabolomics analysis, taurocholic acid and 5'-methylthioadenosine (MTA), changed significantly across the zones in FCR. Taurocholic acid is a bile salt, which is released and used as an olfactory cue by

fishes, and the varied concentrations may reflect differences in fish communities (Buchinger *et al.*, 2014), though we did not measure fish biomass or diversity in this study. MTA, a sulfur-containing metabolite, is more concentrated in water overlying reefs compared to deeper, off-reef waters (Weber, Armenteros, *et al.*, 2020) and is cycled by reef sponges (Fiore *et al.*, 2017). Concentrations of MTA in the Marquesas and the Dry Tortugas National Park were similar to the off-reef water measured by Weber et al. (2020), perhaps due to the similar open-ocean hydrodynamic regimes. MTA is cycled by several pathways intracellularly, and microbial proteins involved in these pathways were encoded for in the seawater metagenomes, including proteins that produce MTA (polyamine aminopropyltransferase, COG0421, EC 2.5.1.16, EC 2.5.1.104; Isovaleryl-homoserine lactone synthase, COG3916, EC 2.3.1.228), and proteins that use MTA (MTA phosphorylase, COG0005, EC 2.4.2.28; MTA/SAM nucleosidase, COG0775, EC 3.2.2.9; MTA/SAM deaminase, COG0402, EC 3.5.4.28). In the present study, the negative relationship between decreasing MTA concentrations and increasing abundances of genes for proteins that use MTA followed an expected pattern, but the opposite correlation was true for proteins that produce MTA (Figure 5-S10). While we measured extracellular MTA concentrations, our genetic data did not identify any removal pathways from cells (i.e. transporters), and instead identified intracellular proteins found in many Bacteria and Archaea for recycling MTA so that it does not accumulate in cells and inhibit other cellular pathways (Parveen and Cornell, 2011; Sauter *et al.*, 2013). Ultimately, given the presence of MTA and MTA cycling genes in reef seawater metagenomes, further experimental research on this and other metabolites in reef habitats is warranted.

FCR has been impacted by a yearslong highly contagious stony coral tissue loss disease (SCTLD) outbreak (Precht *et al.*, 2016; Muller *et al.*, 2020). After sampling apparently healthy and diseased tissue across five zones and five coral species, surprisingly, reef zone was a stronger driver of coral microbiome structure than species and disease, which are known to impact coral microbiomes (Hernandez-Agreda *et al.*, 2018; Becker *et al.*, 2021). Geography is increasingly important to coral microbiome signatures, showing temporal stability (Epstein *et al.*, 2019) that extends for years in aquaria-raised corals (Williams *et al.*, 2022). Within the overall changes, we identified 12 microorganisms from multiple species of apparently healthy

corals that shifted across reef zones regardless of species. Many of these microbes frequently associate with corals, including *Paramoritella* (Hosoya *et al.*, 2009)*, Acinetobacter* (Pereira *et al.*, 2017; Yang *et al.*, 2020)*, Alteromonas* (Raina *et al.*, 2009)*, Balneola* (Ziegler, 2016)*,* and *Rubritalea* (Water *et al.*, 2020)*.* Given the strong influence of zones on host microbiomes, further studies on microbiomes associated with coral diseases should consider and control for regional changes in microbial communities.

The zonal structure of the coral microbiome is consistent with the changes we observed in seawater biogeochemistry, but contrasts with the muted changes in benthic organism assemblages across reef zones that we found using photomosaics. Hard coral cover is a common metric for identifying reef quality and even reef "oases" (Guest *et al.*, 2018). Historically, coral cover was variable across FCR and highest at Dry Tortugas (Murdoch and Aronson, 1999), a pattern only moderately recapitulated by our findings (Figure 5-S5). Instead, we observed a stronger trend of higher hard coral cover at nearshore reefs compared with those further offshore, which may offer a more turbid refuge that shields against increased light and temperature (van Woesik *et al.*, 2020). Presently, we measured hard coral cover on reefs of 10% on average, a steep decline from ~50% coral cover in the late 1970s in the Caribbean (Gardner *et al.*, 2003). As coral reefs continue to degrade and as restoration works to rebuild such reefs, implementing 'omics in addition to coral cover may help capture reef ecosystem changes. While some programs monitor specific groups of microorganisms of public health interest (Seruge *et al.*, 2019), expanding to multiple 'omics strategies focused on reef quality may shed light into potential mechanisms leading to the reef's condition.

While the benthic community changed minimally over the eight zones we studied, the microorganisms, metabolites, and organic nutrients we measured within the overlying water column differed across the zones. For example, at one end of Florida's Coral Reef, Dry Tortugas National Park, the waters harbored increased *Synechococcus,* lowered heterotrophic microbes and more diverse microbial taxonomic and biosynthetic pathways indicative of the region (Figure 5-6). At the northeastern end of our study area, North Key Largo and Biscayne Bay harbored low abundances of *Prochlorococcus,* increased heterotrophic microorganisms, lipid biosynthesis, and less diverse microbial indicator taxa (Figure 5-6). Metabolite and nutrient

signatures were also distinct between the two regions (Figure 5-6). These seawater-bound features are connected through benthic-pelagic coupling with the underlying reef habitat which varies across reef regions, and are likely influenced by anthropogenic impacts like development and population density (Kelly *et al.*, 2014; Ziegler, 2016), though that was not measured here.

Metabolome and microbiome analyses have the potential to revolutionize our understanding of reef processes and energetics, but our understanding of the current data and their implications is limited, and their inclusion into monitoring programs and research studies comes with significant challenges. Metabolomics alone requires specialized equipment and expertise from sampling to mass spectrometric analysis, and access to and use of such mass spectrometry facilities can be costly and analytically and computationally challenging. To begin, monitoring targeted compounds, like MTA, could offer an initial glimpse into reef processes. Targeted metabolomics utilizes authentic standards to quantify each metabolite and is adaptable and comparable between mass spectrometry facilities. Microbiome analyses are even more developed and accessible, with more facilities and at a lower cost than metabolomics. Characterizing taxonomic microbiomes (via 16S rRNA gene sequencing) is more cost-effective compared to shotgun metagenomic sequencing and is even adaptable to in-the-field use (Apprill, 2019; Becker *et al.*, 2021). Given the significant associations and indicators of the taxonomic microbiome with reef zones, benthic organisms, and environmental features in this dataset, characterizing taxonomic microbiomes could be highly informative if added in a time-series context to existing monitoring programs for understanding reef dynamics.

In conclusion, this novel ‘omics dataset of reef microorganisms and metabolites enhances our understanding of the chemical and microbial habitat within FCR. Further, it provides insights into specific compounds (e.g. MTA) and microbial indicators for focus in follow-up experimental studies to better understand the reef ecosystem under stress and in the context of restoration efforts. With the apparent diagnostic value of many of these parameters, we recommend incorporating targeted metabolite and microbiome measurements into programs that monitor, mitigate, and rebuild reefs into the future. Further work linking metabolite patterns to habitat characteristics and microbial metabolisms are also needed to elucidate the mechanisms behind patterns we observed, and how these features may

contribute to reef decline or growth. While metabolomics and microbial analyses probe the smallest components of a reef, they also reflect larger habitat patterns in reef environments, warranting further inclusion of these techniques in studying and monitoring Earth's most biodiverse ocean ecosystem.

ACKNOWLEDGEMENTS

We thank the crew of the M/V *Alucia* for diving and sampling support. We thank Katey Lesneski, Sam Clements, Clinton Edwards, and Hanna Koch for sampling assistance, Carolyn Miller for support with preparing iSeq 100 protocols for on-ship sequencing, and Gretchen Swarr for assistance with metabolomics sample processing. We thank the National Park Service, the Florida Fish and Wildlife Conservation Commission, the Florida Department of Environmental Conservation, the NOAA Coral Reef Conservation Program, Les Kauffman, Arthur Gleason, and Mote Marine Laboratory for assistance with reef site selection. This work was supported by the Dalio Foundation (now "OceanX"), The Tiffany Foundation and the National Science Foundation (OCE-1736288) (to AA) and NOAA OAR Cooperative Institutes award to AA and EBK (#NA19OAR4320074). Corals and seawater were collected under Dry Tortugas National Park permit, DRTO-2019-SCI-0010, Florida Keys National Marine Sanctuary permit, FKNMS-2019-046, John Pennekamp Coral Reef State Park permit, 05131925, and Biscayne National Park permit: BISC-2018-SCI-0029.

DATA AVAILABILITY

Metabolomic data files are uploaded to MetaboLights database and currently in curation under accession MTBLS6574. All sequence data (metagenomic and 16S rRNA) are uploaded to the NCBI Sequence Read Archive under BioProject numbers PRJNA910824 and PRJNA742384. Environmental data and metabolite and sequence data accessions can be accessed within BCO-DMO project 746196 under dataset 890979. Code for reproducing statistical analyses and main figures in the manuscript are uploaded to https://github.com/CynthiaBecker/FL-reef-omics.

Supplementary files (3 total) are accessible online via figshare at

https://doi.org/10.6084/m9.figshare.22310434.v1

FIGURES AND TABLES

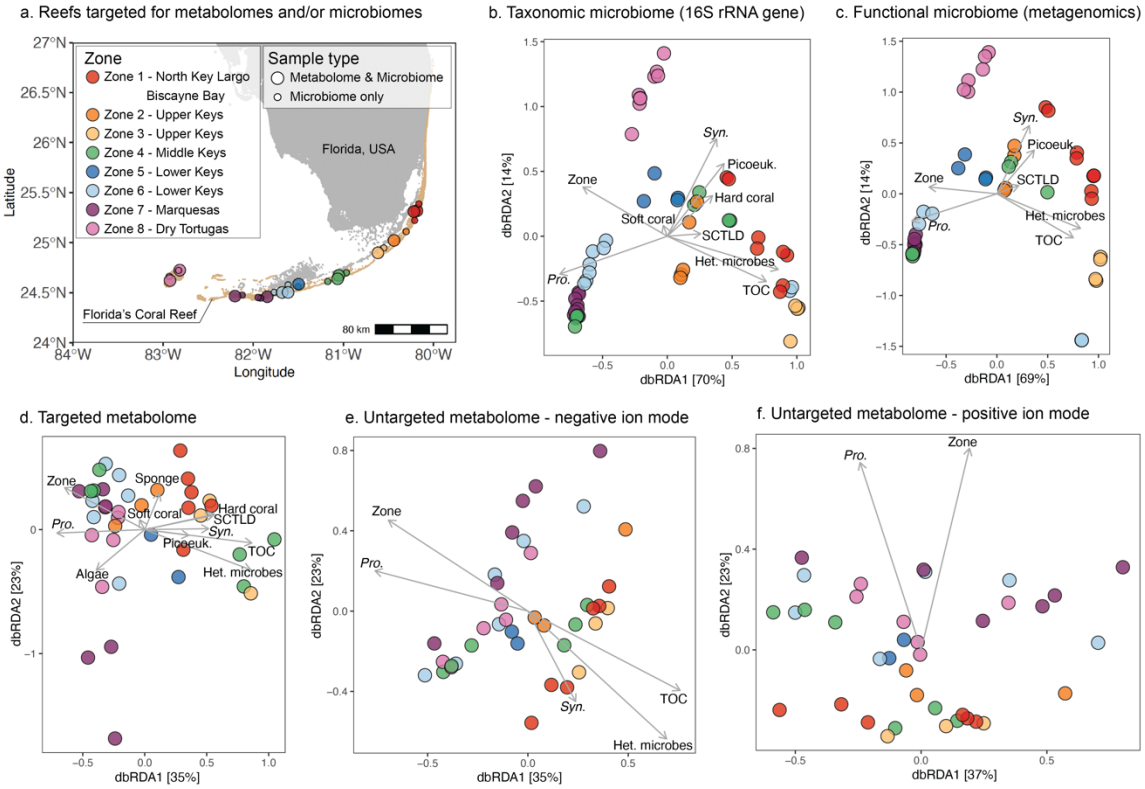

Figure 5-1. Microbiome and metabolome distance-based redundancy analyses
Distance-based redundancy analysis (dbRDA) reveals seawater microbiomes and metabolomes are significantly explained by Florida's Coral Reef biogeography and measured reef microbial and environmental parameters (ANOVA on dbRDA model, $p < 0.05$). a) Map of 27 coral reefs (out of 85 reefs visited in total) sampled across 8 color-coded zones for either both seawater metabolomes and microbiomes (13 reefs) or only seawater microbiomes (27 reefs total) during June 2019. The dbRDA include (b) reef water taxonomic microbiome via 16S rRNA gene sequencing of Bacteria and Archaea, (c) functional microbiome via shotgun metagenomics, (d) targeted metabolomes, (e) untargeted metabolomes that ionized in negative mode, and (f) untargeted metabolomes that ionized in positive mode. *Syn*. = *Synechococcus*, *Pro*. = *Prochlorococcus*, Picoeuk. = picoeukaryotes, SCTLD = stony coral tissue loss disease, TOC = total organic carbon, Het. microbes = heterotrophic microbes.

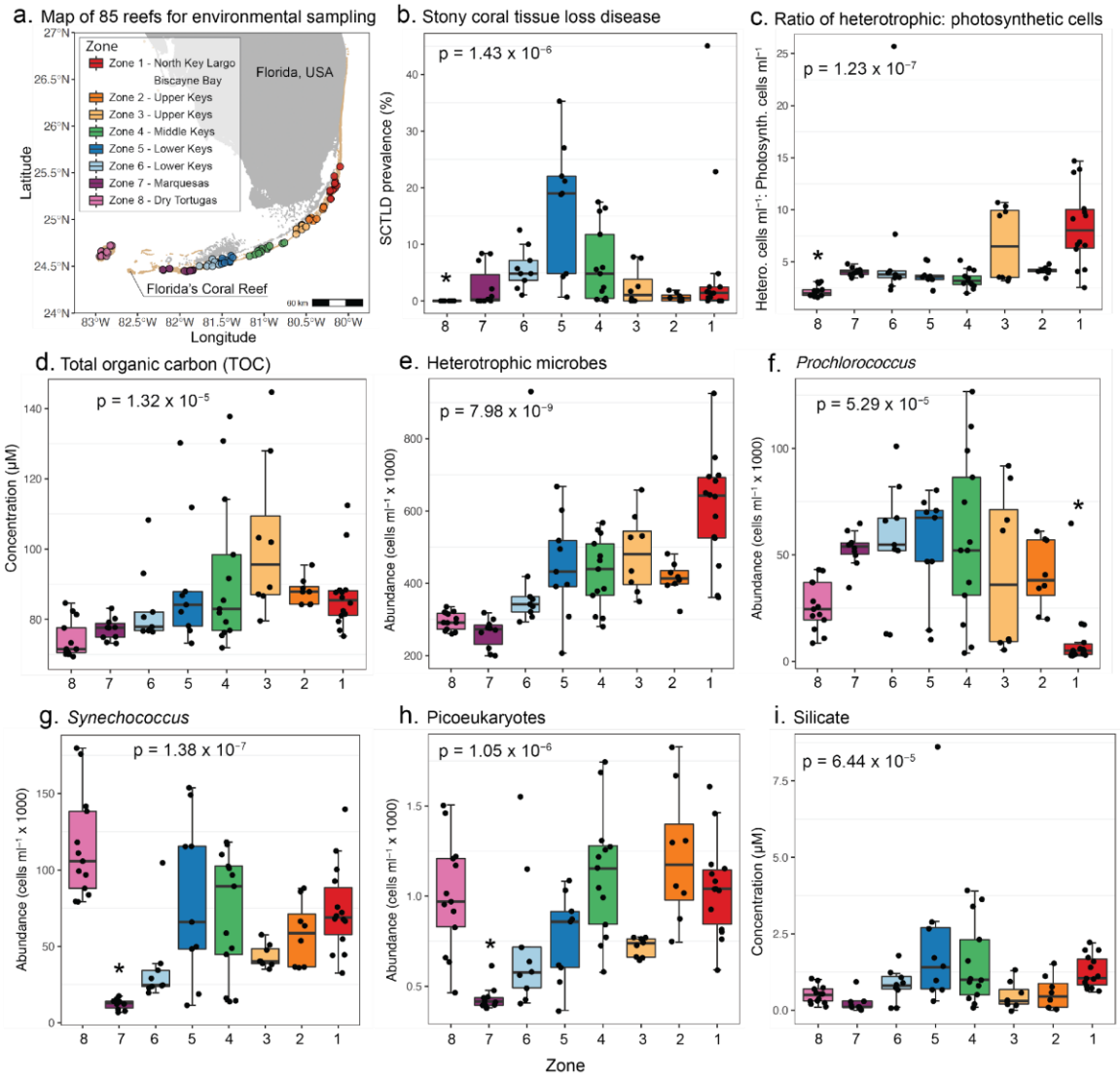

Figure 5-2. Zonal changes in environmental parameters

Zones in Florida's Coral Reef (FCR) have significantly different disease prevalence, microbial abundances and organic carbon and silicate concentrations. a) Map of all 85 reefs sampled for environmental variables are colored by zone and placed above FCR (tan). Environmental variables that changed significantly by zone include b) stony coral tissue loss disease prevalence (percent of live coral), (c) ratio of heterotrophic to photosynthetic microbial cells, (d) total organic carbon concentration, (e) heterotrophic microbial abundances (unpigmented bacteria and archaea), (f) *Prochlorococcus* abundances, (g) *Synechococcus* abundances, (h) picoeukaryote abundances, and (i) silicate concentration was significantly different between FCR zones as a result of a Kruskal-Wallis test and less than the Bonferroni-corrected p-value of 0.00192. Asterisks denote the zone was significantly different than all other zones tested in the pairwise Wilcoxon rank sum test (Benjamini-Hochberg adjusted $p<0.05$).

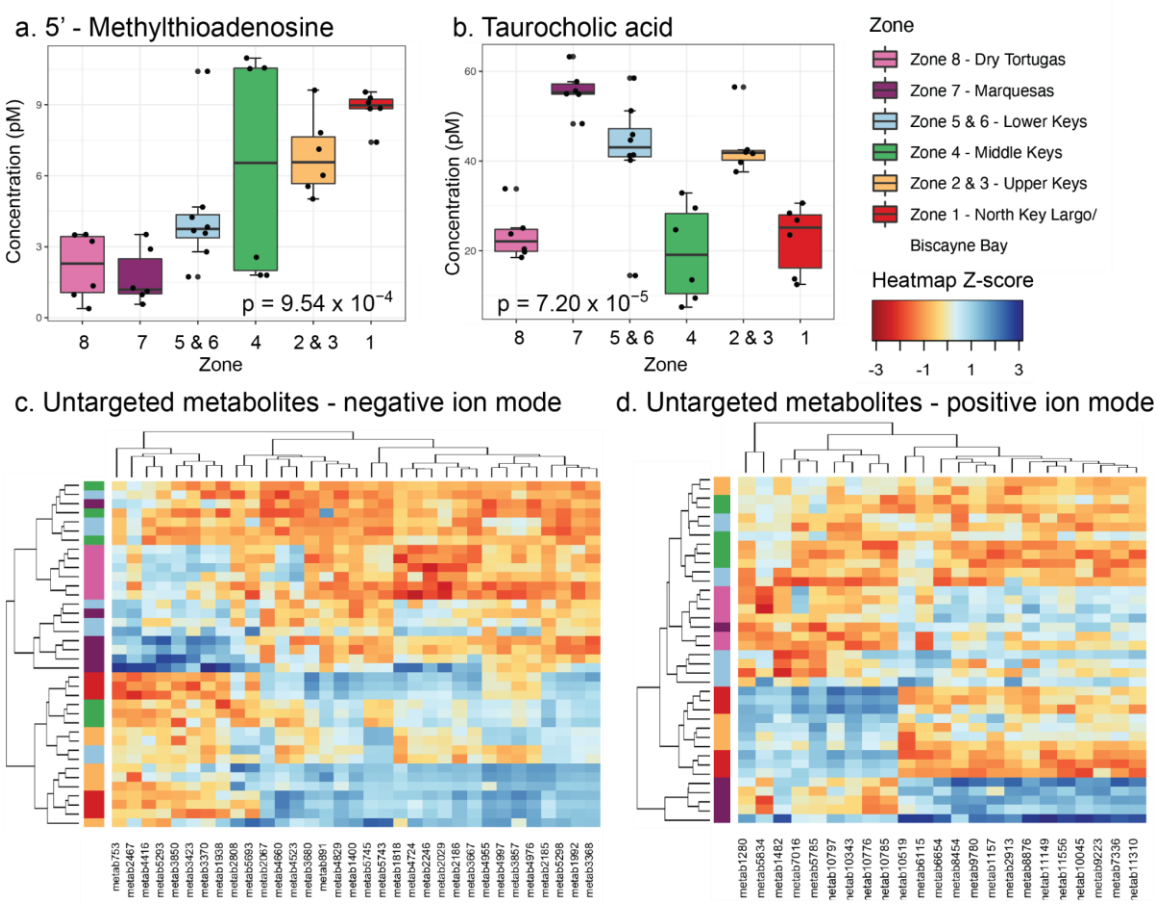

Figure 5-3. Zonal changes in metabolites

Zones in Florida's Coral Reef (FCR) harbor significantly different concentrations of dissolved metabolites (a) 5'-methylthioadenosine (MTA) and (b) taurocholic acid. Concentrations were significantly different between FCR zones (Kruskal-Wallis test, Bonferroni-corrected $p < 0.00128$). Heatmaps of z-score standardized feature peak intensities depict untargeted metabolites that ionized in (c) negative or (d) positive ion modes that were significantly different across zones (ANOVA or Kruskal-Wallis test, significant at Bonferroni-corrected *p*, See SI Methods). Colors to the left of the heatmap indicate reef zone. Adjacent zones 5 & 6 in the Lower Keys and zones 2 & 3 in the Upper Keys were combined to ensure at least 2 reefs were within each group for statistical tests.

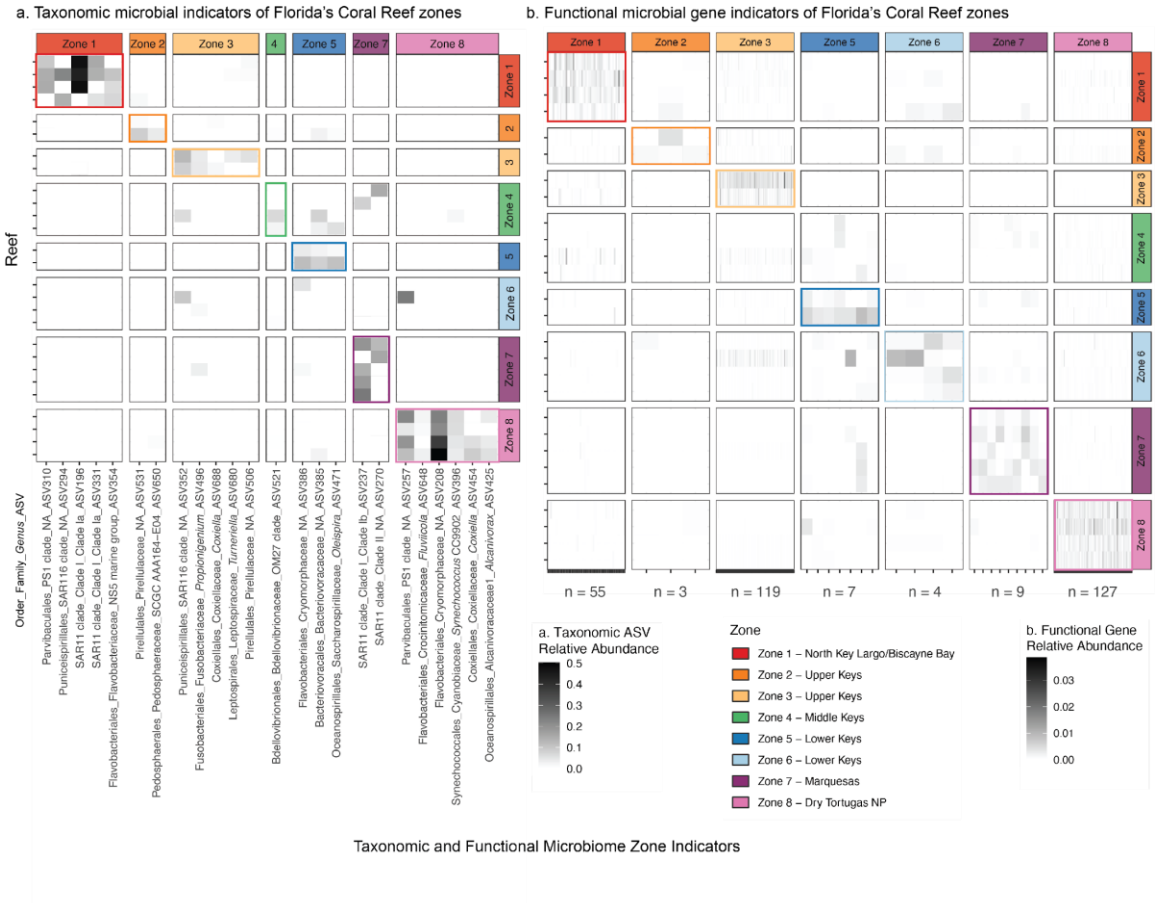

Figure 5-4. Indicator microbial taxa and functional genes

Indicator microbial taxa and functional genes across Florida's Coral Reef zones. a) Relative abundance across all reefs of amplicon sequence variants (ASVs) diagnostic of individual reef zones, and ASV identifier on the x-axis. b) Relative abundance across all reefs of bacterial functional genes diagnostic of individual reef zones. Number of functional genes indicative in each grouping labeled on x axis, with full summary of genes in Supplementary File 3. All indicator taxa and functional genes determined by indicator value analysis (A ≥ 0.6, B ≥ 0.6, $p <$ 0.05). Taxa and functional genes are grouped by the associated zone they are indicative of, which is boxed in the zone color within the heatmaps.

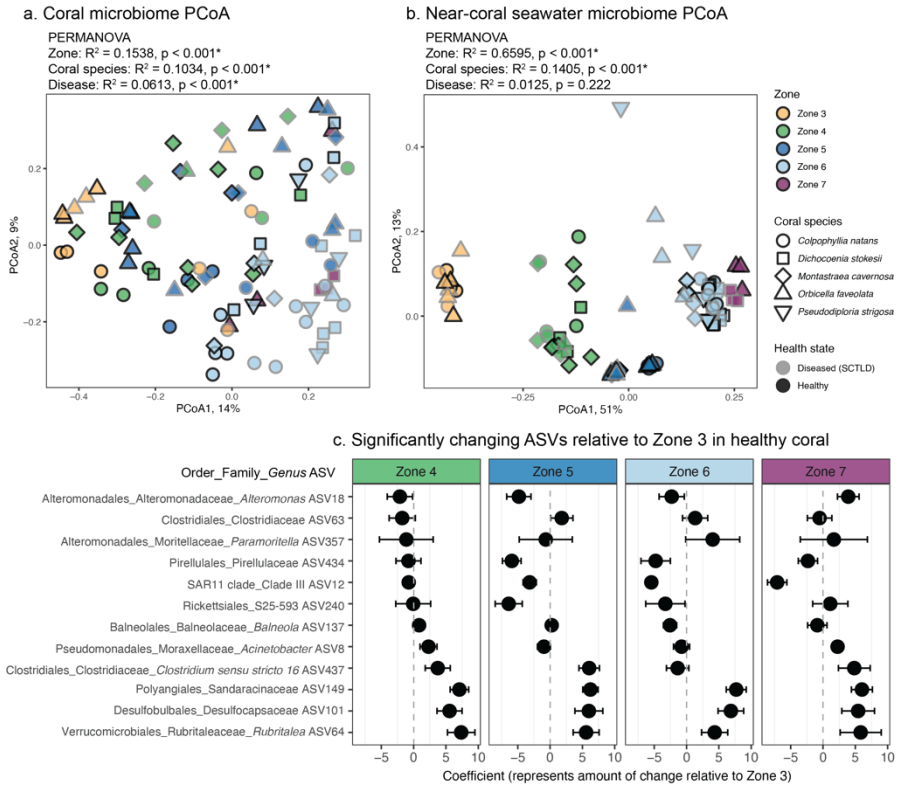

Figure 5-5. Coral and near-coral seawater microbiomes

Coral and near-coral seawater taxonomic microbiomes are influenced by biogeography. Principal coordinates analysis (PCoA) of (a) coral and (b) near-coral seawater taxonomic microbiome beta diversity (Bray-Curtis dissimilarity). Results from a permutational analysis of variance (PERMANOVA) displayed above each graph indicate coral microbiomes are significantly different across zones, coral species, and between apparently healthy and diseased corals, while near-coral seawater microbiomes are significantly different across zones and coral species ($p < 0.05$). Symbols are outlined with black (healthy) or gray (diseased) to indicate healthy state. C) 12 amplicon sequence variants (ASVs) significantly differed relative to zone 3, within apparently healthy coral microbiomes as identified by differential abundance tests (Benjamini-Hochberg adjusted $p < 0.05$, see SI methods).

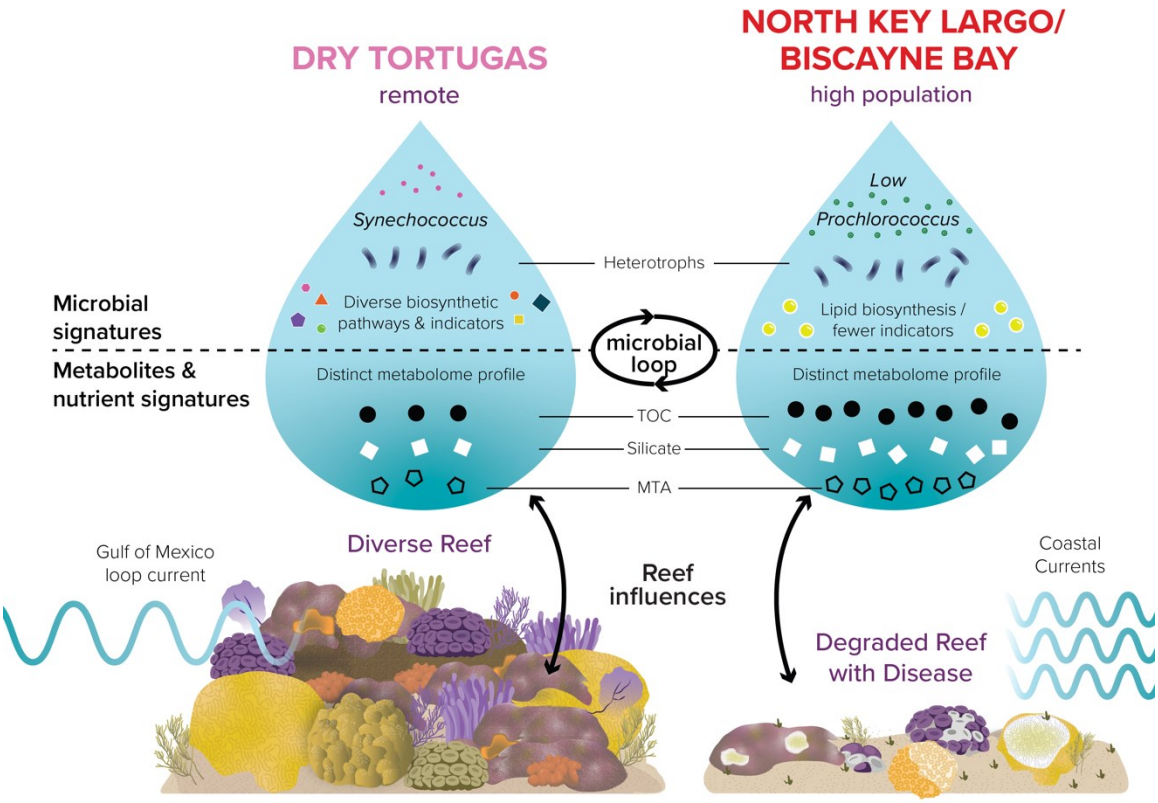

Figure 5-6. 'Omics signatures

Conceptual diagram of how differential seawater 'omics signatures depict ocean environment and ecosystem conditions in two contrasting Florida's Coral Reef habitats, Dry Tortugas (Zone 8) and North Key Largo/Biscayne Bay (Zone 1). Metabolites and microorganisms that are measured by 'omics and other approaches are connected via the microbial loop. Within two different habitats, the 'omics signatures become unique as they are influenced by reef habitat, and likely by parameters not examined here, such as prevailing water currents and human population density. While habitat conditions influenced seawater 'omics, next steps include experimental investigations into the mechanisms related to these signatures and determining if these can serve as diagnostic tools for reefs.

Table 5-1. Reef benthic and environmental characteristics significantly explained reef seawater 'omics

	Microbiome				Metabolome					
	Taxonomic (16S rRNA)		Functional (metagenomics)		Targeted		Untargeted negative		Untargeted positive	
PERMANOVA* term	F†	p-value	F†	p-value	F†	p-value	F†	p-value	F†	p-value
Zone	93.0	**0.001**	61.2	**0.001**	6.09	**0.001**	5.87	**0.002**	3.36	**0.010**
Prochlorococcus	47.2	**0.001**	32.9	**0.001**	3.04	**0.002**	4.20	**0.003**	4.05	**0.008**
Total organic carbon	57.6	**0.001**	38.6	**0.001**	2.84	**0.001**	2.20	**0.038**	1.35	0.192
Heterotrophic microbes	32.9	**0.001**	18.6	**0.001**	3.16	**0.001**	2.18	**0.038**	1.78	0.089
Synechococcus	20.1	**0.001**	12.0	**0.001**	1.95	**0.033**	2.35	**0.036**	2.03	0.067
SCTLD prevalence	5.27	**0.006**	3.22	**0.027**	3.45	**0.002**	1.54	0.142	0.95	0.392
Picoeukaryotes	4.38	**0.019**	3.69	**0.029**	2.25	**0.012**	1.17	0.243	0.96	0.366
Soft coral	3.04	**0.040**	2.70	0.060	2.68	**0.003**	1.34	0.190	1.20	0.285
Hard coral	4.08	**0.027**	2.32	0.089	1.91	**0.034**	1.32	0.220	0.90	0.415
Sponge	2.77	0.054	2.43	0.078	1.94	**0.026**	0.67	0.701	0.81	0.500
Algae (fleshy and turf)	1.13	0.299	1.50	0.192	2.12	**0.023**	1.56	0.129	1.25	0.222

Bold indicates significant at $p < 0.05$. †Pseudo-F value indicates overall significance of the term (higher is more significant). *PERMANOVA is a permutational ANOVA for distance-based redundancy analysis (dbRDA) using 999 permutations.

SUPPLEMENTARY INFORMATION

SI Methods

1. Study Area.

We sampled coral reef environments during a research cruise aboard the M/V *Alucia* between June 3 – 20, 2019. During this time, we conducted surveys and sampled biogeochemical seawater parameters at 85 reefs across 8 zones in Florida's Coral Reef (FCR), from the North Key Largo/Biscayne Bay area, designated as Zone 1, to the Dry Tortugas National Park (Zone 8) (Figure 5-1, Supplementary File 1, accessible online at https://doi.org/10.6084/m9.figshare.22310434.v1). We selected reefs based on input from the Florida Fish and Wildlife Conservation Commission, Florida Department of Environmental Protection, National Park Service, NOAA Coral Reef Conservation Program and Mote Marine Laboratory, with a focus on reefs that were part of long-term monitoring programs (e.g., Coral Reef Evaluation and Monitoring Project, CREMP).

2. Sample Collection and Ship-board Processing.

We conducted diver-based surveys to evaluate the prevalence of stony coral tissue loss disease (SCTLD) at each of the 85 reefs (Figure 5-1, Supplementary File 1). At each reef, one diver performed a 30-minute roving diver survey to determine the richness of scleractinian species, the presence or absence of stony coral tissue loss disease (SCTLD), and the size of all observed coral colonies. The diver assigned coral colonies to four size classes, based on diameter/length: <10cm, 10–25cm, 25–50cm, >50cm. Each diver estimated the area (m^2) surveyed. Prevalence of SCTLD was calculated as the percent of all coral colonies exhibiting disease symptoms.

Large area imagery for benthic surveys was collected in plots ($100m^2$) at 45 individual reefs using the protocol established in Edwards et. al (2017)(Supplementary File 1). Three dimensional model processing was performed using Agisoft Metashape (formerly Agisoft Photoscan Pro) and Viscore as described previously in Fox et al (2019).

We collected discrete seawater samples at all 85 reefs to measure inorganic nutrient (phosphate, ammonium, silicate, nitrite plus nitrate) concentrations, total organic carbon (TOC)

and total nitrogen (TN) concentrations, and cell abundances (heterotrophic microbes [unpigmented bacteria and archaea], *Prochlorococcus, Synechococcus,* and picoeukaryotes) (Supplementary File 1). We collected samples via SCUBA with acid-washed and combusted 40 ml borosilicate glass vials for TOC and TN collections and 30 ml acid-washed square bottles (HDPE, Nalgene, ThermoFisher Scientific, Waltham, MA, USA) for nutrient collections, and filled both vials while at reef depth. Samples were kept on ice in a cooler for less than 4 hr prior to processing. Once on board the M/V *Alucia*, we processed all samples. We added 75 µl phosphoric acid to the 40 ml glass vials to fix the samples for TOC and TN and kept these samples at room temperature or 4°C until laboratory analysis. We removed 1.4 ml seawater from the nutrient bottles, mixed the seawater with 8% paraformaldehyde (1% final concentration, Electron Microscopy Sciences), fixed it in the dark for 20 minutes at 4°C, then froze it at −80°C. We capped the 30 ml inorganic nutrient bottles and placed them at −80°C until analysis.

We collected seawater for targeted and untargeted metabolomic analyses at 13 reefs across the 8 zones of FCR (summarized in Supplementary File 1). At each reef, we collected seawater in 1.7 l Niskin bottles via SCUBA at three distinct locations on the reef for biological replication. These Niskin bottles were kept in a cooler for less than 4 hr prior to processing on the M/V *Alucia*. Once back on board the M/V *Alucia*, we transferred seawater from the Niskin bottles into acid-washed 2l polycarbonate bottles using acid-washed PharMed BPT tubing (Masterflex, Cole-Parmer, Vernon Hills, IL, USA). These water samples were processed as described previously by Weber et al. (Weber, Armenteros, *et al.*, 2020). Briefly, we prefiltered the seawater through a 47 mm 0.1 µm pore size polytetrafluoroethylene filter (Omnipore, EMD Millipore Corporation, Billerica, MA, USA) to remove all microbial biomass via peristalsis and placed the filtered seawater directly into a second acid-washed 2 l polycarbonate bottle. We acidified this filtrate with 2 ml OPTIMA-grade 12 M hydrochloric acid to reach a pH of 2-3 prior to solid phase extraction (SPE). We used SPE to concentrate metabolites (primarily low molecular weight dissolved organic matter) from the filtered seawater. We used a Waters vacuum manifold to slowly pass the seawater through 1 g/6 cc SPE cartridges (Bond Elut PPL; Agilent, Santa Clara, CA, United States) pre-conditioned with HPLC-grade methanol and

weighed bottles with seawater prior to and following SPE to calculate the volume of seawater filtered. SPE cartridges were wrapped in combusted aluminum foil and frozen to −80°C prior to analysis at the Woods Hole Oceanographic Institution.

We collected seawater for microbial biomass and chlorophyll analysis at 27 reefs across the 8 zones of FCR (summarized in Supplementary File 1). At each reef, we employed a groundwater pump (Mini-Monsoon 12V, Proactive Environmental Products, Bradenton, Florida, USA) to pump seawater from just above the reef benthos into acid-washed or 10% bleach-rinsed 4 l LDPE bottles (Nalgene). Samples were kept in a cooler on ice until processing less than 4 hr following collection. Once back on board the M/V *Alucia*, we used peristalsis to filter 2 l of seawater to obtain duplicates from each reef through a 0.2 µm Supor filter (Pall, Port Washington, New York, USA) for microbial biomass housed in a 25 mm filter holder (Swinnex-25, Millipore Corporation), as described previously (Becker *et al.*, 2020). Chlorophyll samples were obtained by filtering 2 l of seawater in duplicate with the same peristalsis setup, but using a GF/F filter. We placed filters (GF/F or 0.2 µm) into 2 ml cryovials and froze them at −80°C prior to further processing at the Woods Hole Oceanographic Institution.

On reefs with active stony coral tissue loss disease, we collected coral tissue and near-coral seawater samples from apparently healthy and actively diseased coral colonies. We aimed to only sample reefs where at least three healthy colonies were present in addition to at least three diseased colonies for reef-level replication. We identified 11 reefs across Zones 3-7 that met the above criteria and collected coral tissue samples from the following species: *Colpophyllia natans, Dichocoenia stokesii, Montastraea cavernosa, Orbicella faveolata,* and *Pseudodiploria strigosa.* Corals were sampled as found, with some apparently healthy colonies targeted first, and some diseased colonies targeted first, depending on reef conditions and presence of suitable colonies to sample. For each colony, collection proceeded on near-coral seawater followed by coral tissue as described previously (Becker *et al.*, 2021). We collected near-coral seawater via 60-ml Luer-Lok™ syringes within 1-5 cm of the lesion margin on colonies with active SCTLD or 1-5 cm above apparently healthy colonies. Following the near-coral seawater collections, we collected tissue from colonies with active SCTLD and from apparently healthy colonies using 10 ml Luer-Slip syringes. We collected tissue samples from

along the lesion margin (i.e., between the apparently unaffected tissue and the bleached and sloughing tissue) of diseased colonies. On apparently healthy colonies (i.e., colonies without any indication of disease or other affliction), an area of the apparently healthy tissue was sampled at random. Syringes were immediately placed into individual Whirl-Pak bags to contain any mucus and tissue leaking from the syringe. Following the collections, all tissue and near-coral seawater syringe samples were placed on ice prior to processing. We transferred samples of coral tissue and mucus into 15 ml conical tubes that were transferred from ice into storage at −80°C until analysis. We attached filter holders containing 25 mm 0.2 µm Supor filters to the 60 ml Luer-Lok™ syringes and depressed them by hand to capture microbial biomass on the filters. We placed the filters into labeled 2 ml cryovials and transferred them to a −80°C freezer until analysis.

3. Benthic reef composition analysis.

Benthic composition analysis was conducted using the imagery generated from 45 reefs. We followed the Viscore and Visual Point Intercept methods with the exception that an additional 500 points were sampled per plot, resulting in 2500 stratified random points per plot, similar to methods previously reported (Fox *et al.*, 2019). Each point was designated to highest taxonomic resolution, with points landing on coral designated to genus. Points were aggregated into 14 functional groups for benthic composition analysis of each plot.

4. Flow cytometry, organic nutrient, inorganic nutrient, and chlorophyll analyses for water quality.

Flow cytometry samples were processed and analyzed by the University of Hawaii SOEST Flow Cytometry Facility as described previously (Becker *et al.*, 2020). Briefly, each sample was stained with Hoechst 33342 DNA stain and excited with both 488 nm (1W) and UV (~350 nm, 200 mW) lasers co-linearly on a Beckman-Coulter Altra flow cytometer (Beckman Coulter Life Sciences). Signals of forward and side scatter and fluorescence were analyzed to distinguish populations and abundances (cells ml^{-1}) of four cell types: *Prochlorococcus, Synechococcus,* eukaryotic picophytoplankton (picoeukaryotes), and non-pigmented bacteria. Non-pigmented prokaryotes were used as a proxy for heterotrophic bacterial and archaeal cells (Monger and

Landry, 1993; Marie *et al.*, 1997), and are referred to as "heterotrophic microbes" in the manuscript.

Non-purgeable total organic carbon (TOC) samples and total nitrogen (TN) samples were analyzed with a Shimadzu TOC-V_{CSH} TOC analyzer (Hansell and Carlson, 2001) using a TNM-1 module. We shipped inorganic nutrient samples to Oregon State University for analysis of phosphate, ammonium, silicate, nitrite and nitrate, as in Apprill and Rappé (Apprill and Rappé, 2011). Briefly, samples were run on a Technicon AutoAnalyzer II (SEAL Analytical) and an Alpkem RFA 300 Rapid Flow Analyzer to generate nutrient concentrations (µM). We determined total organic nitrogen (TON) concentrations by subtracting concentrations of inorganic nitrogen (ammonium and nitrite plus nitrate) from total nitrogen.

Chlorophyll was extracted with acetone using standard methods (JGOFS, 1996). Filters were thawed individually and immediately placed in a glass test tube with 5 ml or 10 ml of 90% acetone, with 10 ml used in the case the filter appeared particularly dark, and capped. The filters were left to extract for 24 hours in the dark at 4°C. After the extraction, the tubes were vortexed and centrifuged to concentrate any particulate matter at the bottom of the tube. Prior to analysis, blanks including air, 90% acetone, and a black standard were run on an AquaFluor fluorometer (Turner Designs handheld 800446) fitted with a red sensitive photomultiplier. Approximately 3 ml of solvent was analyzed on the fluorometer at wavelength of 664 nm, followed by acidifying the sample with two drops of 10% hydrochloric acid, then measuring again to assess phaeopigment concentration. Readings were corrected for the volume filtered and concentration of chlorophyll was measured by referencing a standard curve.

5. Targeted and untargeted metabolomic laboratory processing and mass spectrometry.

We eluted dissolved organic matter (DOM) from the SPE cartridges and prepared samples for analyses as outlined by Weber and colleagues (Weber, Armenteros, *et al.*, 2020). To summarize, 4 bed-volumes of 0.01 M HCl were added to the cartridges to remove salt. The cartridges were then dried for five minutes and eluted into combusted glass vials using 6 ml of 100% methanol. Extracts were frozen at –20ºC until they were dried down using a vacuum centrifuge. Extracts were then resuspended with a 95:5 (v/v) MilliQ water: acetonitrile (ACN) solution with deuterated biotin (final concentration 0.05 mg ml^{-1}) (200 µl total) and vortexed. A pooled

sample was made for all mass spectrometry runs by combining equal volume aliquots from all extracts into one vial. The pooled sample was injected throughout both analytical runs to monitor instrument drift and run quality. After preparation, all extracts were stored at −20ºC until analysis. For targeted metabolomics, 100 µl aliquots of each extract were placed in separate vials with combusted glass inserts. For the untargeted metabolomics analysis, 300 µl of the deuterated biotin standard and water: ACN solution was used to dilute a 25 µl aliquot of each extract. Untargeted metabolite analysis was performed using an ultrahigh performance liquid chromatography system (Vanquish UHPLC, Thermo ScientificTM) coupled with an Orbitrap Fusion Lumos Tribid mass spectrometer (Thermo ScientificTM). A Vanguard pre-column and Waters Acquity HSS T3 column (2.1 mm × 100 mm, 1.8 µm), was used for chromatographic separation at 40ºC. The column was eluted at 0.5 ml min^{-1} with the following solvents: A) 0.1% formic acid in water and B) 0.1% formic acid in ACN. The chromatographic gradient was: 1% B for 1 min, 15% B for 1 – 3 min, 50% B for 3 – 6 min, 95% B for 6 – 9 min, and 95% B for 10 min. Between injections, the column was washed and re-equilibrated with 1% B for 2 min. Individual autosampler injections (5 µl each) were made for negative and positive ion mode analyses. In negative ion mode, the electrospray voltage was set to 2600 V. Settings for source gases were 55 (sheath), 20 (auxiliary), and 1 (sweep) in arbitrary units. The temperatures of the heated capillary and vaporizer were 350ºC and 400ºC, respectively. MS data were collected in the Orbitrap analyzer with a mass resolution of 120,000 FWHM at *m/z* 200. The automatic gain control (AGC) target was 4e5, with a 50 sec maximum injection time, and a scan range of 100 – 1000 *m/z*. Data dependent MS/MS spectra were collected at 7,500 resolution in the Orbitrap analyzer. Parent ions were isolated with a 1 *m/z* width in the quadrupole, and fragmented with a HCD (higher energy collisional dissociation) energy of 35%. All data were collected in profile mode. Samples were run in a random order and after every seven samples, a pooled sample was run. Raw data files from the instrument were converted into mzML files using msConvert and then processed using XCMS (Smith *et al.*, 2006; Chambers *et al.*, 2012). Peak-picking was performed with the CentWave algorithm and a Gaussian fit with the following parameters: noise = 10000, peak-width = 3 – 15, ppm = 15, prefilter = c(2,168.600), integrate = 2, mzdiff = −0.005, snthresh = 10. Retention times were then adjusted using Orbiwarp and

correspondence between the peaks was conducted. The coefficient of variation across the eight untargeted pooled sample features was 0.044, demonstrating good agreement between the pooled samples, and the pooled samples were removed from further analyses. In the untargeted analysis, only MS1 features were analyzed, and were defined as unique combinations of mass-to-charge ratios (*m/z*) and retention times (RT). This analysis yielded a table of MS1 features (*m/z* x RT) and their peak intensities across each sample.

Extracts prepared for targeted metabolomics were run on a triple stage quadrupole mass spectrometer (TSQ Vantage, Thermo Fisher Scientific™) using UHPLC (Accela Open Autosampler and Accela 1250 Pump, Thermo Scientific™) coupled to a heated electrospray ionization source (H-ESI) and operated in selective reaction monitoring (SRM) mode. The same chromatography column, conditions, gradient, and flow rates were used for targeted analyses as those described for untargeted analyses. Separate autosampler injections of 5 µl each were made for positive and negative modes. Additionally, as with the untargeted analysis, samples were run in a random order and pooled samples were run every seven samples. SRM parameters were optimized for each compound using a standard as described in Kido Soule et al. (Kido Soule *et al.*, 2015) and two SRM transitions (precursor – product ion pairs) were monitored for quantification and confirmation. Target metabolites included compounds found in central carbon metabolism and metabolites that are environmentally relevant in marine habitats or are produced by marine microorganisms (Fiore *et al.*, 2015, 2017; Kido Soule *et al.*, 2015). The resulting XCalibur raw files (MS/MS data) were converted into mzML files using msConvert (Chambers *et al.*, 2012) and processed with the open-source program El-MAVEN (v.774)(Agrawal *et al.*, 2019). Using El-MAVEN, 8-point calibration curves based on integrated peak area were generated for each compound. Environmental concentrations of metabolites were determined by dividing each concentration by the original sample collection volume. Next, metabolites that passed the limits of detection and quantification for the UPLC-MS/MS analysis (Kido Soule, Longnecker, Swarr, unpublished) were corrected for extraction efficiency based on published data for each metabolite in seawater (Johnson *et al.*, 2017).

To prepare the untargeted metabolomic data for statistical analyses, data from mass spectrometry runs in both positive and negative ion modes were filtered and normalized using

blank correction, low coefficient of variation filtration, and seawater volume normalization. First, for the blank correction, metabolite features were kept if they exhibited an average fold change greater than 1 across all samples compared to the blanks. This removed 11% and 9% of metabolite features from negative and positive ion mode data, respectively. Second, metabolite peak intensities with a low coefficient of variation (CV) across samples were removed to maintain only the metabolites with more variable peak intensities. Overall, the CV of metabolite peak intensities was low across samples so a cutoff at the third quartile removed metabolites with a CV below 0.081 (Negative mode) or 0.079 (Positive mode). The remaining peak intensities from metabolite features (1,428 from negative mode and 2,759 from positive mode) were normalized to volume of seawater. These procedures yielded tables of filtered MS1 features (*m/z* x retention time) and their normalized peak intensities across each sample.

6. DNA extraction and sequencing for 16S rRNA and shotgun metagenomes

We extracted DNA from 25 mm filters used for 2 l seawater collections using Qiagen PowerBiofilm kits (Qiagen, Germantown, MD, USA). To begin, we added the filter directly to the bead tube, then proceeded with the extraction following manufacturer protocols. We also included four DNA extraction controls by extracting DNA from unused filters. Resulting DNA from these extractions were used as the template for both 16S rRNA gene sequencing and shotgun metagenomic sequencing.

For 16S rRNA gene sequencing of bacteria and archaea, we included 2 µl of template DNA into a 50 µl (total volume) PCR reaction. We added a PCR negative control by including one PCR reaction with 2 µl of PCR grade H_2O instead of DNA. Earth Microbiome Project primers, 515F (Parada *et al.*, 2016) and 806R (Apprill *et al.*, 2015), were used to amplify the V4 region of the small subunit (SSU) rRNA gene in bacteria and archaea and included sample-specific barcodes with an 8 bp barcode, 10 bp pad, and 2 bp link, similar to Kozich et al. (Kozich *et al.*, 2013). The 50 µl reactions were diluted in UV-sterilized nuclease-free water and contained 2.5 units of GoTaq DNA Polymerase (Promega, Madison, WI, USA), barcoded primers at 0.2 µM, 0.2 mM dNTP mix (Promega), 2.5 mM $MgCl_2$, and 1X colorless GoTaq flexi buffer (Promega). The reactions were run on a Bio-Rad Thermocycler using the following criteria: denaturation at 95°C for 2 min; 28 cycles at 95°C for 20 s, 55°C for 15 s, and 72°C for 5 min; and extension at 72°C for

10 min. We used gel electrophoresis to verify successful amplification using 5 µl of product on a 1% agarose-Tris-borate-EDTA (TBE) gel stained with SYBR Safe gel stain (Invitrogen, ThermoFisher Scientific). We used the QIAquick 96 PCR Purification Kit (Qiagen) with the QIAvac 96 (Qiagen) and vacuum pressure to purify the remaining 45 µl of PCR products following manufacturer's protocols. We applied the HS dsDNA assay on the Qubit 2.0 fluorometer (ThermoFisher Scientific) to quantify the DNA concentrations then converted to nM assuming an average library size of 450 bp, and average molar mass of DNA nucleotides of 660 g/mol. We diluted individual barcoded PCR products to 10 nM, pooled all samples, and shipped the pooled, ready-to-run library to the Georgia Genomics and Bioinformatics Core at the University of Georgia for sequencing on an Illumina MiSeq using paired-end 250 bp sequencing.

We prepared a library for shotgun metagenomic sequencing following the Illumina DNA Prep Reference Guide (Illumina, San Diego, CA, USA, Document # 1000000025416 v09 June 2020). DNA input for all samples was between 100-500 ng. Concentrations of the four DNA extraction control samples were below detection, so we included 30 ul of each in the procedure and processed them in the same way as all seawater samples. We used IDT for Illumina DNA/RNA UD Indexes Set A, Tagmentation (Illumina, 96 samples, Cat # 20027213), to apply sample-specific indices. Following the procedure, we eluted samples in 30 µl resuspension buffer. To verify successful processing, we used a fluorometric assay (HS dsDNA) on a Qubit 2.0 fluorometer to measure DNA concentrations of a subset of samples. All final concentrations were greater than 4 ng/µl, and therefore deemed sufficient for pooling. All samples were pooled, and the final concentration was 5.30 ng/µl. The final library was run at the Georgia Genomics and Bioinformatics Core at the University of Georgia on an Illumina NextSeq 2000 with the P3 flow cell and paired-end 150 bp sequencing.

7. On-ship near-coral seawater sample processing and sequencing

To expedite the turnaround time between sample collection and sample processing, we performed on-ship DNA extraction, PCR, and sequencing with the Illumina iSeq 100 System on near-coral seawater samples following methods for in-the-field microbiome preparation described previously (Becker *et al.*, 2021). Seawater samples targeted for on-ship sequencing included those sampled from 5 reefs over two days (June 9-10, 2019).

8. DNA extraction and sequencing of near-coral seawater and coral microbiomes

All processing of near-coral seawater and coral tissue slurries proceeded as described previously to identify bacteria and archaea within each environment (Becker *et al.*, 2021). Briefly, we extracted DNA from all seawater and tissue samples using the DNeasy PowerBiofilm kit (Qiagen). PCR occurred in a two-stage procedure. In stage one, we used Earth Microbiome Project primers, 515F (Parada *et al.*, 2016) and 806R (Apprill *et al.*, 2015), to amplify the V4 region of the small subunit (SSU) ribosomal RNA gene of bacteria and archaea. In stage two, we attached unique index primers to each sample using the Nextera XT v2 set A kit (Illumina). For PCR that occurred at the Woods Hole Oceanographic Institution, we used larger benchtop centrifuges (Eppendorf 5418) and thermocyclers (Bio-Rad), rather than the small and portable versions used on the M/V *Alucia*. Following purification of stage two PCR products, we diluted and pooled samples such that we included approximately 40 samples. Seawater and tissue samples were randomized across all library pools. Pooled libraries were diluted to approximately 90 pM, and a 10% PhiX Control v3 (Illumina) spike-in was added to increase base diversity. All libraries were run on the Illumina iSeq 100 System (Illumina) with the i1 cartridge pack, over a total of 6 sequencing runs.

9. Benthic survey, disease survey, and water quality data analysis.

Benthic cover, organic and inorganic nutrients, cell abundances, and disease prevalence data were measured from 45 reefs (benthic cover) or 85 reefs (all other parameters) in FCR across eight zones. To evaluate which environmental parameters changed significantly across reef zones, we conducted a Kruskal-Wallis test in R (v4.0.3) and evaluated significance of the results against a Bonferroni-corrected p-value to account for multiple comparisons (Figure 5-2). For significant environmental variables, we followed up with a pairwise Wilcoxon rank sum test to investigate which zones were significantly different from other zones at a p-value < 0.05 after a Benjamini-Hochberg false discovery rate adjustment (Supplementary File 2).

To examine the changes in benthic composition across FCR, we conducted a principal component analysis (PCA) in R and visualized the PCA using the function “fviz_pca” and displayed the strength of each benthic component with the PCA. We used the package *vegan*

and function adonis() to conduct a PERMANOVA test by zone using the formula adonis(benthic_data ~ zone, data = metadata, method = “eu”).

To identify environmental conditions that were significantly different at Dry Tortugas National Park (Zone 8) compared to all other reefs and zones in FCR combined, we conducted a Wilcoxon Rank Sum test and the results were deemed significant at a Bonferroni corrected p-value less than 0.001667 (Figure 5-S3). Additional linear regressions were conducted to individually evaluate the influence the relationship between hard coral cover and algal cover using lm(hard coral ~ algae) (Figure 5-S7), and the effect of distance to shore on hard coral cover using lm(hard coral ~ distance to shore) (Figure 5-S6).

10. Targeted Metabolomics analysis.

Targeted metabolites were corrected for extraction efficiency and converted to picomolar (pM) concentrations prior to analysis (see above). The metabolites were grouped by Zone, except the two zones in the upper keys (Zones 2 & 3) and the zones in the lower keys (Zone 5 & 6) that were combined to ensure at least two reefs (n = 3 per reef) were in each group for statistical tests. To evaluate how the 39 quantified metabolites related to the environmental conditions in FCR, we conducted a distance-based redundancy analysis (dbRDA) using the *vegan* (v2.5-7) package (Oksanen *et al.*, 2020). Further dbRDA details are below. The gower distance metric for the dbRDA was chosen because it yielded the highest value after comparing several distance metrics with the “rankindex” function in the *vegan* R package. As with the environmental parameters, we identified targeted metabolites that significantly changed with zone by conducting a Kruskal-Wallis test in R (v4.0.3) and evaluated significance of the results against a Bonferroni-corrected p-value to account for multiple comparisons (Figure 5-3). For significant metabolites, we followed up with a pairwise Wilcoxon rank sum test to investigate which zones were significantly different from other zones at a p-value < 0.05 after a Benjamini-Hochberg false discovery rate adjustment (Supplementary File 2).

11. 16S rRNA sequence analysis to generate amplicon sequence variants.

Sequence reads from the Illumina MiSeq run were inspected for quality, trimmed, filtered, and amplicon sequence variants (ASVs) were generated using the *DADA2* R package (v1.18.0) (Callahan *et al.*, 2016). We used default filtering parameters and trimming parameters were

trimLeft = c(20,20) and truncLen=c(240,200) based on when quality profiles began to drop below a quality score of around 30. For data generated by the Illumina iSeq (near coral seawater and coral microbiomes), we used the parameters trimLeft=20 and truncLen=125 and only forward reads were used due to lack of overlap between forward and reverse reads. For MiSeq-generated data, we also merged forward and reverse reads, removed chimeras and assigned the taxonomy of ASVs in DADA2. For taxonomic assignment, we used the SILVA SSU rRNA database (v138) and assigned species, when possible (Quast *et al.*, 2012). We removed any ASVs that classified as mitochondria and chloroplasts, and filtered out ASVs with an average count of 0.5 across samples to remove low abundant taxa. We also removed DNA extraction controls and PCR controls for data analysis. Additionally, ASVs were given a unique number identifier for tractability in the manuscript. This ASV generation and filtering from *DADA2* yielded two tables of ASVs (one for seawater microbiomes from MiSeq sequencing and one for near-coral seawater and coral microbiomes from the iSeq) and their counts across samples were transformed to relative abundances and log transformed after a pseudo count addition of 1 for further data analysis.

12. Shotgun metagenomic analysis to generate bacterial functional data.

Shotgun sequencing on the Illumina NextSeq yielded 13,592,781.7 ± 3,357,010.1 paired-end sequence reads per reef seawater microbial community sample. Due to sequencing errors, 6 of the reef samples had single samples, while the other 21 had duplicate sequence samples. We inspected read quality using FastQC (0.11.9) running default parameters. FastQC results showed high quality sequences. Based on the FastQC output, we trimmed forward and reverse reads with Trimmomatic (v0.39) using the parameters “SLIDINGWINDOW:4:20” and “MINLEN:50” to trim reads if quality dropped below 25 over 4 bases and to remove any reads with fewer than 50 bp, respectively. This retained approximately 94.16% ± 0.37% of sequence reads per sample. Trimmed paired-end reads were then used as input for a metagenome co-assembly of all samples using MegaHit (v1.2.9)(Li *et al.*, 2015). We chose MegaHit as the assembler as it has been shown to generate more genes that could be successfully annotated compared to MetaSPAdes in complex environments such as ocean and soil samples (20). MegaHit parameters included --min-contig-len 500 --continue -t 60. We further filtered the output

metagenome assembly using seqkit (v0.16.1) to retain only contigs greater than 1000 bp. We used Quast (v5.0.2) to measure assembly statistics. The filtered metagenome assembly had an N50 of 2,742 and contained 1,041,682 contigs.

To obtain functional annotations of the metagenome assembly, we used Prokka (v1.14.6). With the functional annotations, the .ffn file containing nucleotide sequences of each annotated gene was input into Salmon (v3.7.4) for read mapping of short reads to the functional annotations to generate abundances of each functional gene at each reef. This yielded a table of sequence counts of each annotated gene across the 27 samples. We retained the 592,973 genes with Clusters of Orthologous Genes (COG) identifiers. We additionally included pathway information for the relevant COG IDs by downloading the latest COG database FTP from https://ftp.ncbi.nih.gov/pub/COG/COG2020/data/ and using the cog-20.def.tab document.

To prepare the abundance matrix for statistical analysis, we filtered out low-abundance genes with an average count of < 0.5 across the samples, transformed the gene counts to relative abundances, and log transformed after adding a pseudocount of 1.

13. Comparative 'omic data analysis.

To evaluate how the composition of metabolite features, taxonomic microbial communities, and microbial functional genes changed across different reefs, we calculated Bray-Curtis dissimilarity across different reefs using the function vegdist() in *vegan* (v2.5-7) and then calculated principal coordinates with the function cmdscale() in R (Oksanen *et al.*, 2020). The resulting principal coordinates were plotted using *ggplot2* (v3.3.3) (Wickham, 2016b). To test the influence of zone, Dry Tortugas versus all other zones combined, disease prevalence, and sampling date on the compositions of metabolites or microbial genomic data, we used the adonis() function in *vegan*.

A distance-based redundancy analysis (dbRDA) was calculated to evaluate the significant association between sample metadata (zone) and environmental variables (TOC, heterotrophic microbes, *Prochlorococcus, Synechococcus,* picoeukaryotes, stony coral tissue loss disease prevalence, hard coral, algae (fleshy macroalgae and turf algae), soft coral, and sponge) and the relative abundances of ASVs. We calculated the dbRDA with Bray-Curtis dissimilarity using the

capscale() function in *vegan*. The model formula was as follows: “capscale(OmicsDataFrame ~ Zone + SCTLD + TOC + Het. microbes + Prochlorococcus + Synechococcus + picoeukaryotes + hard coral + algae + soft coral + sponge, EnvironmentalVariables_Dataframe, distance = "bray", na.action = na.exclude). Note for the targeted metabolomics analysis, distance= “gower” was used. We evaluated the significance of the response variables (environmental variables and metadata) using an analysis of variance (ANOVA) with the parameter by = “terms”. Response variables were evaluated as significant when $p < 0.05$ and they were plotted onto the ordination with *ggplot2*.

To identify significant untargeted metabolites that changed with FCR zones, an ANOVA or Kruskal-Wallis test was used based on the normality of the data, tested with a Shapiro-Wilk test. Metabolite features in both negative and positive ion modes were assumed significant following $p < 0.05$ that was Bonferroni-corrected based on the number of metabolite features. The resulting 56 untargeted features were z-score standardized and visualized with a heatmap using the “heatmap.2” function in the R package *gplots* (v3.1.3).

To identify taxa and functional microbiome indicators of FCR, we used the multi-level pattern analysis, multipatt() function in the R package *indicspecies* (v1.7.12). The function implemented the “IndVal.g” function and microbiome taxa or functional genes were identified as indicators if they had a positive predictor value (A) over 0.6, sensitivity (B) over 0.6 and were significant at a $p < 0.05$. Tiled heatmaps were generated in *ggplot2* to visualize all indicator ASVs and functional genes, with a summary of all results presented in Supplementary File 3.

To evaluate the abundance of genes for source and sink proteins of 5’-methylthioadenosine (MTA), we manually filtered the full list of annotated genes (prior to low abundance filtering) to search for genes encoding proteins that use MTA (sinks - MTA/S-adenosylhomocysteine (SAM) deaminase, COG0402, EC 3.5.4.28; MTA/SAM nucleosidase, COG0775, EC 3.2.2.9; MTA phosphorylase, COG0005, EC 2.4.2.28) and genes encoding proteins that produce MTA (sources – polyamine aminopropyltransferase, COG0421, EC 2.5.1.16, EC 2.5.1.104; Isovaleryl-homoserine lactone synthase, COG3916, EC 2.3.1.228; S-adenosylmethionine:diacylglycerol 3-amino-3-carboxypropyl transferase, COG5379). The relative abundance of all source and sink genes encoding these proteins was added up by

sample and averaged across technical duplicates. Then, a model II simple linear regression using the ordinary least squares (OLS) method was used to relate the square-root transformed concentration of MTA biological triplicates at each reef to the relative abundance (averaged over technical duplicates) of source and sink genes at that reef. The regression was computed using the *lmodel2* (v1.7.3) package in R. The OLS method was used as the MTA concentration failed normality tests (Shapiro-Wilk test $p > 0.05$). Permuted 1-tailed p-values were computed using 999 permutations.

14. Near-coral seawater and coral microbiome analyses.

Near coral seawater and coral taxonomic microbiome beta diversity was calculated with Bray-Curtis dissimilarity and visualized with principal coordinates analysis using the R packages *vegan* and *ggplot2*. The significant influence of zone, disease, and coral species on microbiome composition was tested with the adonis() function in *vegan* (v2.5-7) using 999 permutations and the resulting R^2, F, and p-values were reported to assess the significance of the relationships. Healthy coral taxonomic microbiomes were subset for differential abundance analysis to test which ASVs significantly changed by reef zone using the R package *corncob* (Martin *et al.*, 2020). Zone 3 was used as the reference zone as it was the most northeast region and the test was run in *corncob*, which models relative abundance of ASV raw counts with a logit-link for mean and dispersion. Differential abundance of coral ASVs were modeled as a linear function of reef zone. We tested the hypotheses that relative abundance of an ASV changed significantly with respect to reef zone using the parametric Wald test. Significantly changing ASV relative abundances were assessed at a Benjamini-Hochberg false discovery rate corrected p-value of 0.05.

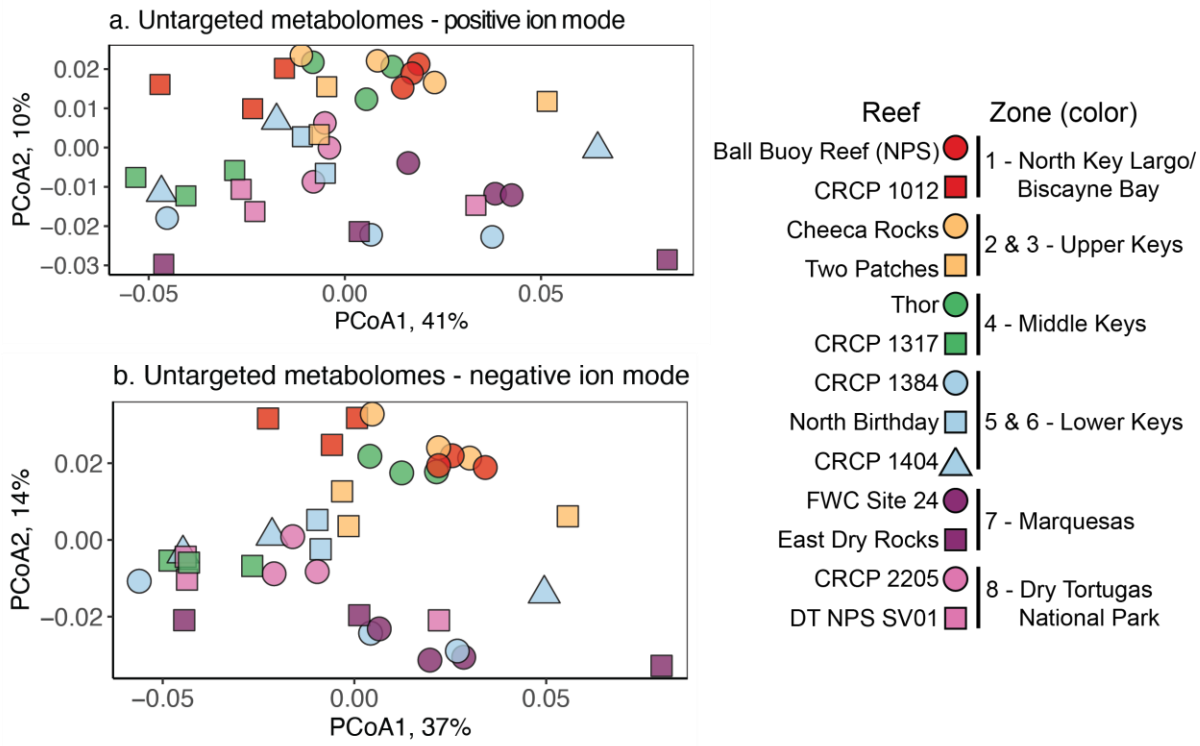

Figure 5-S1. Principal coordinates analysis (PCoA) of untargeted metabolite composition for metabolites that ionized in (a) positive mode and (b) negative mode, displayed according to reef zone (color) and site (symbol). Negative mode revealed the most structuring by individual reef, then by reef zone (color) (PERMANOVA $p < 0.001$ – Table S1).

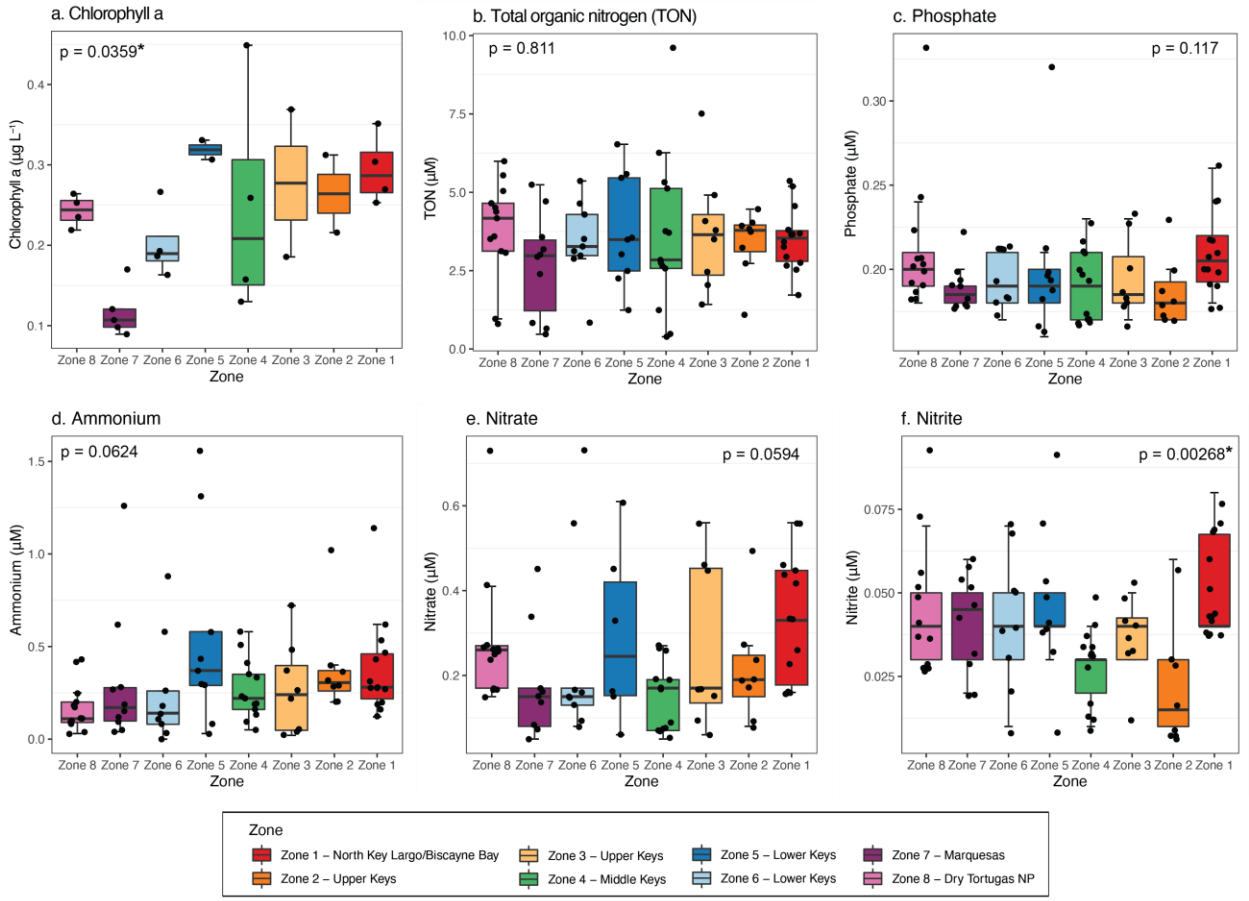

Figure 5-S2. Concentration of chlorophyll a and micronutrients across 85 reefs in Florida's Coral Reef did not change significantly by zone via Kruskal-Wallis test (Bonferroni corrected $p > 0.00192$). Box and whisker plots depict the center line, representing the median. Boxes extend from the 1st to 3rd quartiles and the whiskers extend 1.5 x interquartile range. * = $p < 0.05$, but not smaller than Bonferroni-corrected p

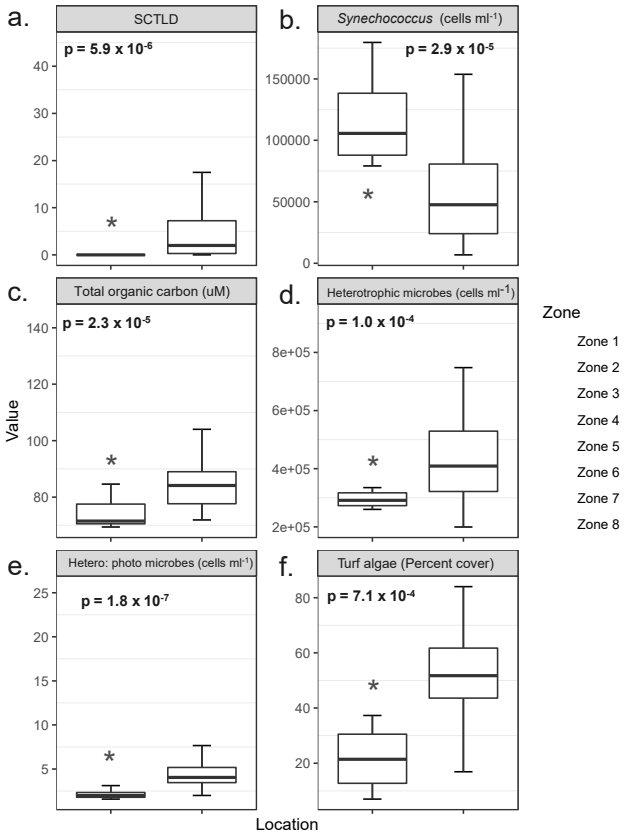

Figure 5-S3. Environmental parameters that were significantly different (Bonferroni-corrected $p < 0.001667$) at Dry Tortugas National Park (Zone 8, pink) reefs compared to reefs in Zones 1-7 (all other colors)(p-values result from Wilcoxon Rank Sum test). Parameters included (a) stony coral tissue loss disease (SCTLD) prevalence, (b) abundances of *Synechococcus*, (c) concentrations of total organic carbon, (d) abundances of heterotrophic microbes, (e) the ratio of heterotrophic: photosynthetic microbes, and (f) turf algal cover. * = significantly different at Bonferroni-corrected $p < 0.001667$

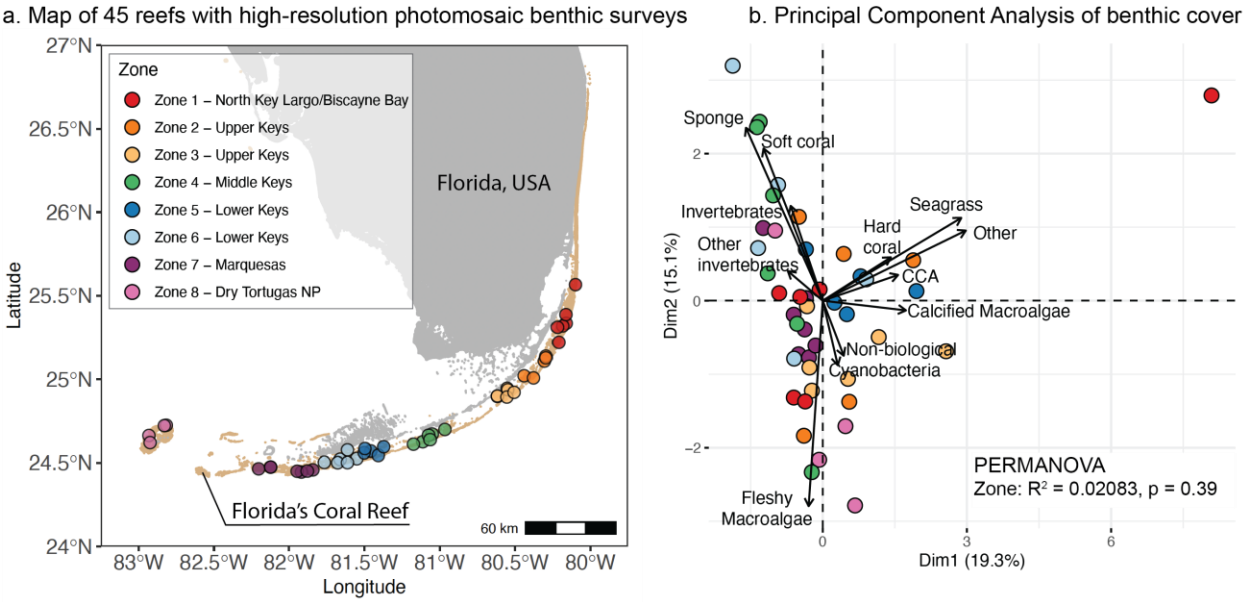

Figure 5-S4. a) Reefs (45) sampled for high-resolution photomosaics of 100 m^2 plots of reef were analyzed for coverage of benthic organisms, which did not change significantly by reef zone as seen by (b) principal components analysis of coral benthic cover (PERMANOVA results of zone on PCA of benthic cover was not significant, p = 0.39).

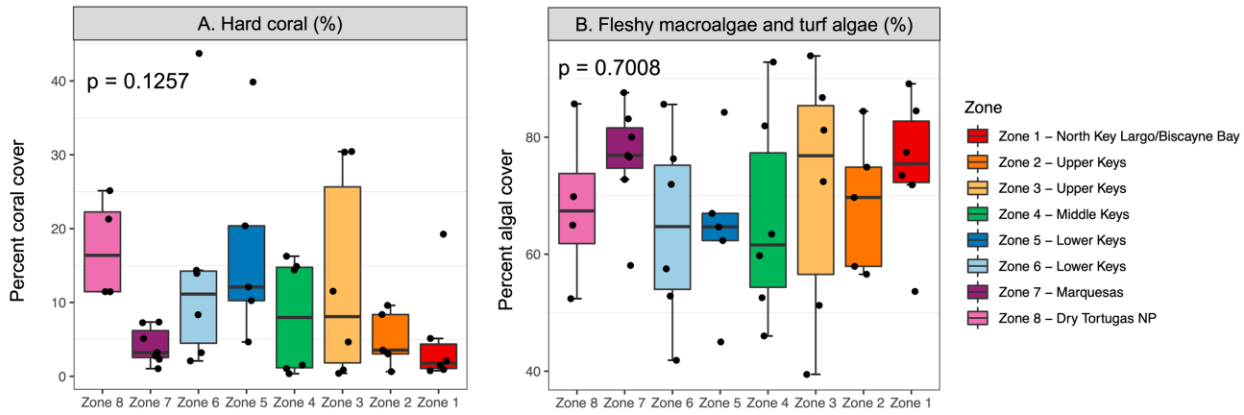

Figure 5-S5. Benthic hard coral (a) and algal (b) coverage do not significantly change by zone via Kruskal-Wallis test (Bonferroni-corrected $p > 0.00192$). Benthic cover was measured at 45 reefs across 8 different zones represented by different colors (Figure S4a). Box and whisker plots depict the center line, representing the median. Boxes extend from the 1st to 3rd quartiles and the whiskers extend 1.5 x interquartile range. Further analyses of all other individual benthic components (graphs not shown) did not significantly differ by Florida's Coral Reef zones (Kruskal-Wallis test, Bonferroni-corrected $p > 0.00192$).

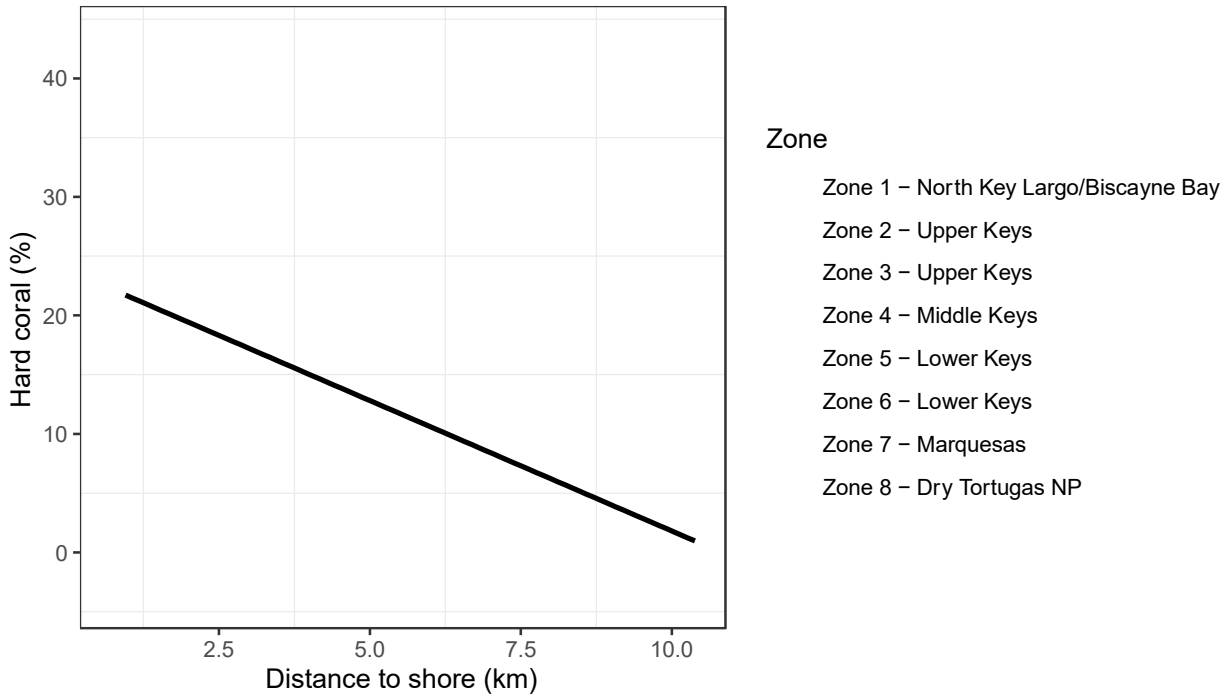

Figure 5-S6. Hard coral coverage on Florida's Coral Reefs significantly decreases as distance from shore increases (linear regression, $p < 0.05$). Points are colored by zone. Shaded area indicates standard error. Black line is the line of best fit following a linear regression.

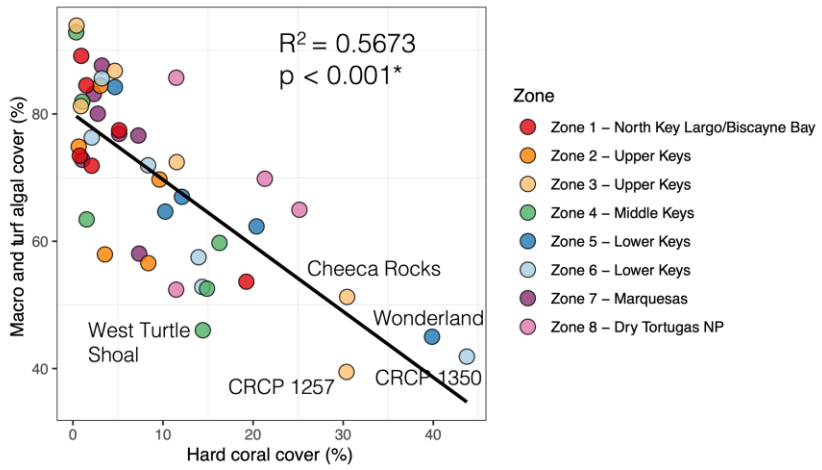

Figure 5-S7. Linear regression shows increasing hard coral coverage significantly correlates with decreasing algal coverage ($p < 0.001$, $R^2 = 0.5673$). Reefs with the combination of highest hard coral cover and lowest algal cover (defined as both fleshy macroalgae and turf algae combined) are labeled.

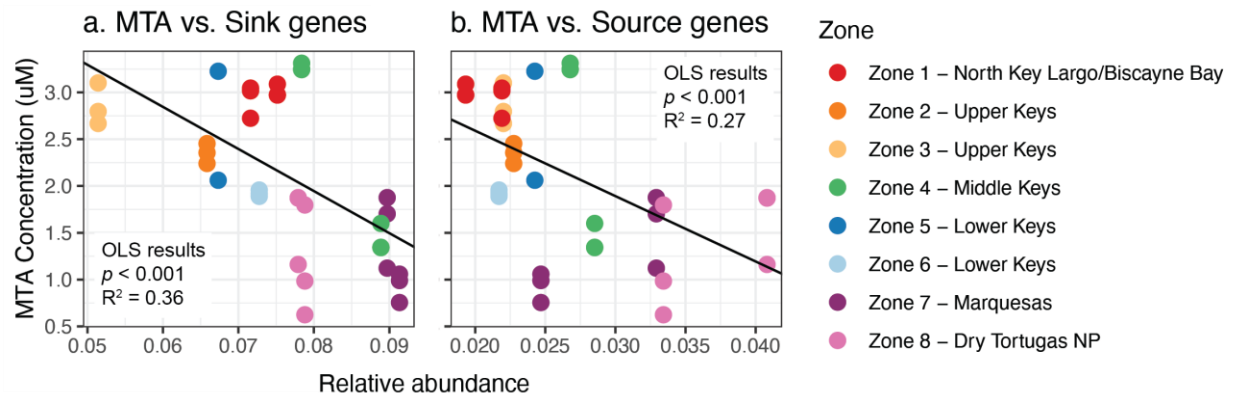

Figure 5-S8. Abundance of genes that consume (sink, a) and produce (source, b) MTA are significantly negatively correlated with extracellular concentration of MTA. Correlation is with a model II ordinary least squares (OLS) regression. MTA concentration shown is the square root of the original concentration. Sink genes found in the seawater metagenomes include MTA phosphorylase (COG0005, EC 2.4.2.28), MTA/SAM nucleosidase (COG0775, EC 3.2.2.9), and MTA/SAM deaminase (COG0402, EC 3.5.4.28). Source genes found in the seawater metagenomes include polyamine aminopropyltransferase (COG0421, EC 2.5.1.16, EC 2.5.1.104) and Isovaleryl-homoserine lactone synthase (COG3916, EC 2.3.1.228). MTA = 5'-methylthioadenosine. SAM = S-adenosylhomocysteine. Relative abundances of source and sink genes were averaged between technical replicates for each reef. Concentrations shown are from separate biological triplicates from a reef. The resulting *p* value displayed is from a 1-tailed parametric test using 999 permutations.

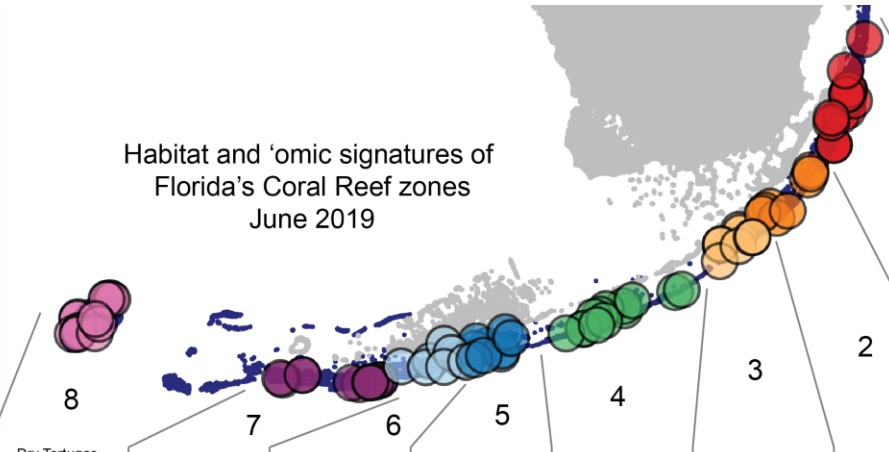

Zone	Dry Tortugas National Park	Marquesas	Lower Keys	Lower Keys	Middle Keys	Upper Keys	Upper Keys	North Key Largo/ Biscayne Bay
Seawater metabolome	Low taurocholic acid Low MTA Distinct untargeted metabolome	High taurocholic acid Low MTA Distinct untargeted metabolome	High taurocholic acid Untargeted metabolome similar to Zones 7 & 8		Low taurocholic acid	High taurocholic acid Untargeted metabolome similar to Zone 1 and 4		Low taurocholic acid High MTA Distinct targeted metabolome
Seawater microbiome	High *Synechococcus* Low het. microbes Distinct community Most indicator taxa and functions	Low *Synechococcus* Low het. microbes Low picoeukaryotes SAR11	Abundances intermediate to Zone 7 & 5 Few to no indicator taxa and functions	*Oleispira* indicator	OM27 clade No indicator functions	High Het. microbes Low picoeuk. & *Syn.* Distinct community Many indicator taxa and functions	High picoeuk. Few indicator taxa and functions	High hetero:photo High het. microbes Low *Prochlorococcus* Many indicator taxa and functions
Coral microbiome	N/A	Enriched taxa: *Alteromonas* *Paramoritella* Rickettsiales	Enriched taxa: *Paramoritella* Clostridiaceae	Enriched taxa: Clostridiaceae *Clostridium*	Enriched taxa: *Balneola* *Acinetobacter* *Clostridium*	Enriched taxa: Pirellulaceae SAR11	N/A	N/A
Habitat features	Low TOC Low Silicate Low turf algae High hard coral No disease	Low TOC Low silicate Low hard coral High algal cover Low disease	Low TOC High sponge High soft coral Moderate disease	High silicate High hard coral High CCA High disease	High silicate Moderate disease	High TOC Low silicate Nearshore high hard coral Low diseae	High TOC Low silicate Low hard coral Low disease	High TOC High silicate Low hard coral High algae Low disease

Figure 5-S9. Signatures of individual Florida's Coral Reef zones determined through water sampling for inorganic and organic nutrients, photomosaic analysis of benthic cover, metabolomic, metagenomic, and microbiome analyses within seawater and coral hosts. High and low refers to values relative to other reef zones. N/A indicates data are not available. MTA = 5'-methylthioadenosine, het. microbes = heterotrophic microbes, hetero:photo = heterotrophic microbes: photosynthetic microbes, TOC = total organic carbon, CCA = crustose coralline algae.

Table 5-S1. PERMANOVA results from untargeted metabolomics analysis.

Variable	Untargeted metabolomes - positive ion mode		Untargeted metabolomes - negative ion mode	
PERMANOVA variable	p-value	R^2	p-value	R^2
Reef	**0.006**	0.441	**<0.001**	0.516
Zone	**0.023**	0.217	**<0.001**	0.277

Chapter 6 - Conclusions

Microorganisms in coral reefs are central to organismal fitness, reef biogeochemical cycling, and overall productivity. Within coral hosts, they contribute to nutrient transformations as endosymbionts and help defend against infection. Seawater-bound microorganisms, particularly bacteria and archaea, play important roles through remineralization of dissolved organic matter on reefs and as a link between dissolved organic matter and higher trophic levels, such as corals, which directly feed on microorganisms. Beyond nutrient transformations, microorganisms are implicated in reef ecological processes like settlement on suitable reefs, competition, and chemical signaling. As important members for reef success, they are also implicated in reef decline. Microorganisms are directly or indirectly implicated in numerous coral and other reef organism diseases. The proliferation of heterotrophic microorganisms on more degraded reefs consumes dissolved organic matter and draws down oxygen in reef waters, potentially contributing to reef deoxygenation, which suffocates corals and prevents coral-depauperate reefs from rebounding to a coral-rich state. In this dissertation, my goal was to understand the dynamics of microbial and metabolite diversity on coral reefs in the face of various changes. This included analyses of microorganisms over temporal (tide, interannual disturbances), spatial (biogeography), and reef health gradients, as well as an analysis of metabolites in a spatial study. Together, by furthering the field's understanding of the dynamics of microorganisms and metabolites in reef habitats across these gradients, my research has laid the groundwork for future work that elucidates mechanisms by which microorganisms and metabolites contribute to reef change and incorporates these parameters into monitoring programs.

My dissertation constitutes important and novel contributions to reef microbial and disease ecology, but the work does not end with this thesis. In this conclusion, I outline key targets of future research and ideas for how the coral reef field could leverage the immense and untapped potential of microorganisms for monitoring reef health. In two of my thesis chapters, I documented microbial dynamics over multiple time scales ranging from 48 hours to seven years in the US Virgin Islands (USVI) (Chapter 3-4) (Becker *et al.*, 2020). This research demonstrates the significant value of time-series-based research, and I urge researchers and

reef managers to prioritize implementing microbial components in time-series contexts whenever possible. A major theme of my research involved identifying microbial and metabolite signatures, or bioindicators, of gradients (e.g., zones in Florida's Coral Reef, disease in coral hosts, disturbance in a reef ecosystem) (Chapters 2, 4, 5). These characteristics were all identified by leveraging field-based research, and a key next step will be moving from the environment into an experimental system that integrates multiple 'omics techniques to test hypotheses regarding how specific signatures of microbes and metabolites contribute to reef health. During my graduate tenure, stony coral tissue loss disease (SCTLD) spread throughout my study areas. This devastated some of the important reef habitats I studied, but also afforded opportunities to contribute new knowledge to the interdisciplinary and multi-institution efforts aimed at understanding and combating that disease. I developed a faster sequencing-based method for characterizing microbiomes of corals impacted by SCTLD and contributed the first work on microbiome bioindicators of disease outside Florida (Chapter 2) (Becker *et al.*, 2021). As SCTLD continues to ravage reefs throughout the Caribbean and marine diseases emerge every year, a program that centralizes and streamlines initial surveys of microbial bioindicators would assist scientists and managers in the Caribbean by identifying targets quickly and efficiently, enabling local managers to focus on interventions and potential treatments.

In the following conclusion, I will elaborate on three next steps for coral reef microbial ecology that build upon the research I conducted during my graduate career:

1. Incorporate microbial ecology into multi-year existing and future coral reef time-series.
2. Prioritize experiments that test hypotheses about the role of microorganisms and metabolites in reef health.
3. Centralize and streamline survey-based investigations into microbial bioindicators of coral reef and marine diseases.

A place for microbial ecology in long-term reef monitoring

Reef monitoring over long timescales is commonplace in coral reef ecology. Some examples include the time-series reef studies that are part of NSF-funded programs and include a Long

Term Research in Environmental Biology (LTREB) project in St. John, USVI, and a Long-Term Ecological Research (LTER) project in Moorea that have both been ongoing for decades, providing datasets on habitat change and coral recruitment in these habitats. Additionally, monitoring programs exist worldwide and within the Caribbean that are run by local scientists and stakeholders. For example, in the USVI, the Territorial Coral Reef Monitoring Program (TCRMP) regularly assesses disease and habitat quality on USVI reefs. There are also programs to monitor the water quality in coastal reef environments, such as the Water Quality Monitoring Project within the Florida Keys National Marine Sanctuary, which regularly samples for nutrients, turbidity, and chlorophyll. These time series, along with innumerable ones around the world I have not listed, provide essential context for the current outlook of coral reefs as well as information on the major natural and anthropogenic stressors that harm reef environments.

While time series have produced essential knowledge of the status of and impacts to coral reefs, few time series exist in reef research that incorporate microbial community sampling. Research studies in reef habitats over the course of 1-3 days, including the tidal-based study in this dissertation (Chapter 3), have all documented significant diurnal patterns in reef ecosystems, but these are isolated sampling efforts (Kelly *et al.*, 2019; Becker *et al.*, 2020; Weber and Apprill, 2020). Over seasonal timescales, other studies have demonstrated variation in reef water microorganisms (Yeo *et al.*, 2013; Glasl *et al.*, 2019, 2020). Few studies extend microbial sampling in reef habitats beyond a single year, and to my knowledge my research on changes to microorganisms in USVI reefs over seven years and in concert with disturbances (Chapter 4) is the longest study of its kind in reef habitats. As such, Chapter 4 contributes important knowledge of interannual variability of microorganisms and indicators of disturbance to the field of reef microbial ecology.

Some established water quality monitoring programs do incorporate microorganisms in coastal reef habitats, but they are motivated by human health concerns. In Hawaii and the US Virgin Islands, for example, these programs monitor bacteria such as fecal coliform bacteria and enterococci that cause gastrointestinal diseases in humans (USVI Integrated Water Quality Monitoring & Assessment Report, 2016; Seruge *et al.*, 2019). While some coral diseases are

associated with bacteria that originate in wastewater (i.e., *Serratia marcescens*), this covers only one facet of coral reef health: coral disease (Patterson *et al.*, 2002). In my time-series research, I identified multiple indicators of reef disease at the ecosystem-wide level (Chapter 4), and even bioindicators of disease within coral hosts (Becker *et al.*, 2021). Reef microorganisms in the seawater are impacted by multiple organisms and environmental conditions in the reef habitat, and thus represent the cumulative impacts of change on reefs, rather than simply one disease. Given these findings, microorganisms are ideal targets for monitoring reef-wide changes, a concept that has gained traction in recent years (Glasl *et al.*, 2017). By incorporating microbial analyses directly motivated by association to reef health and quality, we will begin to center ecosystem health over human health in programs that monitor reef waters.

Incorporation of microorganisms for reef health monitoring comes with many options. In my thesis research alone, I combined flow cytometry data, 16S rRNA-based studies, and metagenomics. Beyond this, cultivation-based work and microscopy are also viable methods for monitoring microorganisms. Within my thesis research, patterns emerged within many chapters that justify flow cytometry- and microscopy-based methods as a first step toward including microbes in reef monitoring. These would enable the capture of both naturally pigmented and non-pigmented groups of microorganisms. Picocyanobacteria, especially *Prochlorococcus*, were associated with the multi-year SCTLD disease outbreak (Chapter 4), exhibited diurnal variability (Chapter 3, Becker *et al.*, 2020), and significantly differed across zones in Florida's Coral Reef (Chapter 5). Additionally, heterotrophic bacteria and archaea significantly increased northeastward across the zones of Florida's Coral Reef (Chapter 5). These two components of reef seawater microbiomes encompass major functional groups. Picocyanobacteria are the most numerically dominant primary producers in reef water and heterotrophic microbes recycle and remineralize organic matter produced on the reef, making them central to reef carbon cycling. Additionally, although they are numerically less dominant, flow cytometry and microscropy methods would even capture picoeukaryotes, which can vary with disturbance (Chapter 4) and biogeography (Chapter 5). Inclusion of flow cytometry and microscopy methods would enable the quantification of ecologically relevant microorganisms in reef habitats.

In addition to ecological relevance, flow cytometry and microscopy are relatively straight forward and quantitative. Flow cytometry requires small volumes of water (~2 ml) and relies on one instrument, a flow cytometer, and specialized stains for enumeration. Microscopy might be even easier. It also requires one main instrument, a microscope, with high-enough resolution to capture the 0.2 μm-size picocyanobacteria. In addition to using stains for the non-pigmented microorganisms, microscopy has the additional flexibility—with specially-designed probes—of targeting specific taxonomic groups. Relative to the intensity of lab work, sequencing, and computationally complex analytical needs of microbial sequence data, flow cytometry and microscopy outputs can be processed more easily and generate a single number, making analysis much easier. Ultimately, adding flow cytometry to reef monitoring programs would ensure the addition of microbial functional groups already implicated in reef ecosystem health to monitoring programs. Microorganisms are critical to add to these programs because they are the link between nutrients and organic matter monitored by water quality programs and the changing coral habitat captured by existing reef monitoring programs.

Experiments: the link between pattern and mechanism

My thesis research relied on field-based sampling, which enabled me to interface directly with the relevant ecological conditions facing reefs and microorganisms but provided little opportunity for examining mechanisms behind the patterns I found. The research I conducted as part of my thesis is an important component of reef research. With it, I identified numerous new patterns that could be targets for future experimentation. As I think about the future of coral reef microbial ecology, it is my hope that we as scientists prioritize experimentation. Experimental research exists that demonstrates links between benthic organisms like coral and algae, exuded metabolites, and reef water microorganisms (Nelson *et al.*, 2013; Quinlan *et al.*, 2019; Weber *et al.*, 2022), but they are far outnumbered by correlative research that identifies associations between environmental conditions and microorganisms or metabolites (e.g., Chapters 2-5). In this section, I will outline exciting opportunities for experimentation that directly build off patterns I observed in my thesis.

One of the most exciting findings of my dissertation research was the decline of *Prochlorococcus* and some strains of *Synechococcus* in disease-wrought reefs of the USVI (Chapter 4). While I also found these groups to exhibit diurnal variability (Becker *et al.*, 2020), during the longer time series these were always sampled during the daytime. The coordinated decline during each disease sampling event relative to pre-disease makes me confident these patterns are related to the degradation of the reefs because of SCTLD. These groups are globally distributed in open ocean and coastal marine waters, but the association between these groups and reef degradation is novel. Experiments from Caribbean reefs have shown that *Prochlorococcus* grows off common sea fan exudates (Weber *et al.*, 2022) and corals graze on *Synechococcus* (McNally *et al.*, 2017). With few existing studies, further investigation into picocyanobacterial ecology in coral reefs could answer the following outstanding questions from my research: (1) How much primary productivity do *Prochlorococcus* and *Synechococcus* contribute to reef habitats relative to coral endosymbiont algae and benthic algae, (2) How do dissolved nutrients from diseased coral tissue directly impact growth of picocyanobacteria, and (3) How does the presence of algae like *Ramicrusta* and turf algae, which increased on disease-impacted reefs, impact picocyanobacteria? Continued experimentation that defines the role of picocyanobacteria in reef systems will enable scientists such as myself to better define how and why observed patterns in picocyanobacteria exist. Furthermore, it will elevate interpretations of patterns that are captured both in scientific studies and as part of future monitoring programs that incorporate microorganisms.

Another example of where experimentation is needed is in the pattern of change in metabolites on reefs. In my research, 5'-methylthioadenosine (MTA) and taurocholic acid concentrations changed significantly across the zones of Florida's Coral Reef (Chapter 5). These patterns may be related to the reef habitats or even the microbial community. Within the metagenomes of reef water, I identified the presence of source and sink genes for MTA that encoded for intracellular proteins, yet we measured extracellular concentrations of MTA (Chapter 5). Subsequent experimental incubation-based studies with fish and corals or growth experiments with natural reef microbial communities spiked with these compounds are needed to further define source and sink dynamics of these compounds. An emphasis on experiments

that integrate metabolomic methods with flow cytometry or metagenomic methods to identify microorganisms will further link ecological interactions between metabolites, microorganisms, and the reef.

Beyond the two targeted metabolites identified in Chapter 5 as differing across reef habitats, the targeted metabolome was significantly related to the most reef habitat features. As metabolomics gains traction in reef research, expanding the library of targeted metabolite standards for examination in reef and environmental habitats is urgently needed. For example, a new method that expands the recoverability of amine and alcohol containing compounds, generally nitrogen-containing organic molecules, by targeted metabolomics could be applied to reefs (Widner *et al.*, 2021). The enrichment of total organic nitrogen during the multi-year disease outbreak in the USVI reefs (Chapter 4) might be a signature of reef decline in other areas. Research that focuses on methods development to expand the library of detectable biomolecules and metabolites in reef habitats will lend insight into a critical component of reefs, metabolites, which are a major link between reef macro- and micro-organisms.

Expanded recovery of compounds by new metabolomic methods like this could be essential for not only identifying patterns associated with reef disease, or zones, as in my own research, but would be ideal for experiments. One emergent threat to reefs I documented is *Ramicrusta,* the invasive encrusting algal group that was increasing in cover on St. John reefs (Chapter 4). This spatially aggressive alga is impacting reefs across the Caribbean (Eckrich and Engel, 2013; Edmunds *et al.*, 2019). Additionally, coral larvae are killed by it and unable to settle on it (Stockton and Edmunds, 2021; Cayemitte *et al.*, 2023). While my own research could identify microbial patterns associated with the change in cover of *Ramicrusta,* experimentation is needed to identify how and why that algal group is recently so successful on Caribbean reefs. The alga exudes caffeine, which may be part of its success as this metabolite deters herbivores and pathogens in land plants, but more work is needed (Weber *et al.*, 2022). Experimentation that identifies how the metabolites both on its surface biofilm and exuded by *Ramicrusta* differ from native and beneficial crustose coralline algae could shed further light into its success. Furthermore, examining how the suite of these metabolites select for specific lineages of microorganisms in reef water and on its surface biofilm will allow for mechanistic

understandings into how the alga kills coral larvae (Cayemitte *et al.*, 2023) and the reef-wide repercussions of the invasion of *Ramicrusta* algae in the Caribbean. Importantly, the experiments would incorporate microbiome analyses as well as targeted metabolomics, particularly using a method to identify more nitrogen-containing compounds. As methods and resources expand for analyzing microbiomes, integrative and experimental studies combining multi-'omic approaches like the one I just outlined are urgently needed to examine the how metabolites and microorganisms may be implicated in ecological changes, such as with invasive species on reefs. Expanding research to experimental contexts is an important step forward in interpreting emerging microbial and metabolomic patterns associated with change and stress on reefs.

Scaling up disease microbial bioindicators

A central theme of my dissertation was the impact of SCTLD within coral hosts and at the ecosystem-wide level. In Chapter 2, I sped up the microbiome processing timeline to 10 days and conducted all microbiome processing in the field. This level of on-site speed and capacity is novel for SCTLD. Additionally, I identified microbial bioindicators of SCTLD. Four of these bioindicators were exact sequence matches to the two previous studies on this disease. My emphasis on open access to sequence data analysis on GitHub and data deposits on NCBI enabled these bioindicators and data to be easily incorporated into other studies on SCTLD (Evans *et al.*, 2022; Rosales *et al.*, 2023). As research continues with this disease, efforts that hasten pipelines and facilitate ease of data sharing are essential.

My research on SCTLD involved a small-scale study localized to one area, but SCTLD is a Caribbean-wide problem. Beyond SCTLD, other reef and marine diseases impact reefs and can restructure the ecosystem, such as with die-offs of *Diadema* sea urchins that are important algal grazers (Mumby *et al.*, 2006; Levitan *et al.*, 2023). Recent findings determined *Diadema* die-offs were caused by a ciliate, and sequencing-based analyses helped identify the pathogen (Hewson *et al.*, 2023). To address the scourge of SCTLD and other marine diseases, I imagine a space in which we could scale up the rapid sequencing pipeline and analytical workflow I presented in Chapter 2 to both generate and analyze data more easily across the Caribbean.

This would facilitate streamlined monitoring and diagnoses of marine diseases and ultimately enable reef managers to combat devastating disease outbreaks that further threaten these already coral-depauperate ecosystems.

Scaling up the rapid sequencing pipeline would require significant funds and international scientific coordination, but I imagine a scale-up that would enable Caribbean nations to submit samples to sequencing core facilities designed for reef research. I imagine 5-10 core facilities dispersed throughout the Caribbean that are specialized in microbiome-based analyses. These core facilities would ideally be established at universities or public health labs, which may already have sequencing capacity growing as a result of the needs of COVID-19 variant sequencing (PAHO, 2022). The reef scientists and managers that directly interface with the reef could take samples with representative images of the coral or other reef organism and send a small sample, ideally on dry ice, to the core facility. The scientists in the core facility could provide regular training workshops on how to collect the samples and quickly preserve them. Additionally, the facility would need to provide recommendations on sample shipping boxes for successful transport of the reef samples. With many nations and islands dispersed across the Caribbean, there would be challenges. International shipping customs and permitting make it challenging to quickly send delicate reef samples. Additionally, the limited availability of dry ice and liquid nitrogen for preserving samples in many Caribbean small island nations and territories may make it difficult to control sample preservation conditions prior to processing. Despite these challenges, the goal of conducting quicker and easier processing of samples would enable the inclusion of samples from multiple nations. As it stands, most publications on SCTLD are from Florida. While this is the location of coral “patient zero” for SCTLD, this area has significant scientific, managerial, and funding support for coral reef disease research relative to many other parts of the Caribbean. Combating this coral pandemic cannot happen from one nation and area. Establishment of core facilities that conduct the sample processing and sequencing would enable the examination of disease from multiple areas, ensuring diverse scientists, managers, and nations are represented in the analysis of reef diseases.

Core facilities would produce enormous amounts of data, creating analytical challenges associated with this ‘big data’. To circumvent this, a central function of the core facilities would

be for data analysis. I imagine this would come in two parts. First, a packaged pipeline targeted at bioindicator identification would enable the core facility scientists to quickly generate targeted results that would be more easily interpreted by a reef manager than raw .fastq files directly from the sequencing machine. This pipeline would be modeled after the set of analyses conducted in Chapter 2 that are already accessible from my GitHub page and would add in comparisons of bioindicators to previous research. The second key product would be a database. There are numerous databases of genetic sequences (i.e., antibiotic resistance genes database), and a "marine disease bioindicator" database would be useful for ease of analysis. The key identifier of the database would be the genetic sequence from the 16S rRNA-based bioindicator analysis. The metadata associated with it would be the coral species it was associated with (or other marine animal), the disease diagnosis, and any other sampling metadata (i.e. lat/lon, reef name, date of collection). This database would need to be regularly updated and released at least every six months to accommodate the suite of new associations as diseases emerge and research continues. These releases would be accessible to managers around the world that may be interested in reef or marine diseases outside the Caribbean. Altogether, a centralized and regularly updated database of bioindicator sequences from marine diseases in addition to a packaged pipeline would enable managers and local scientists that may be less familiar with microbiome analyses to easily interpret and relate their data to existing research.

Taken together, the scaling up of my research from Chapter 2 would constitute a major step forward in the capacity of Caribbean reef scientists to incorporate sequencing and microbiome-based analyses into their research. But beyond this, we still have a problem: most reef diseases, including SCTLD, have no known pathogen. As we continue to identify pathogens or opportunists in disease, moving toward a quicker, cheaper, and specific assay for marine diseases is urgently needed. With a targeted culprit and pathogen genome, we could create qPCR-based assays for the marine pathogen, like how qPCR assays are used to track covid infections in wastewater, a messy and complex environment like marine systems (Larsen and Wigginton, 2020). Moving even further, we could design an immunoassay-based rapid test for these pathogens, like one already produced for detecting *Vibrio coralliilyticus* co-infections

associated with SCTLD (Ushijima *et al.*, 2020), and similar to the ones familiar to all of us for quickly testing if our cold is COVID-19. Finally, with these pathogens identified, treatments would be possible and more specific. As research on marine diseases such as SCTLD continues to grow and expand, taking every possible measure to speed up and streamline the scientific procedures currently in place are sure to get us closer to what reefs truly need, a solution.

Final thoughts

Collectively, my work contributes detailed inventories of microorganisms and metabolites associated with reef dynamics, demonstrating their potential utility for reef monitoring. But the exciting work of microbial and chemical ecology on coral reefs does not end here. The sensitive and predictive nature of microorganisms to short and long temporal scales make them ideal candidates for inclusion into existing monitoring programs and it is my hope that scientists will prioritize microbial time-series samplings in the future. Moving from the environmental reef system into an experimental context is another top priority. Through carefully designed experiments that integrate measurements of metabolites as well as microorganisms, scientists will better capture the mechanisms and implications of the signatures of microbes and metabolites that I documented in my thesis work. Beyond natural patterns and signatures present on reefs, coral reefs face numerous disturbances, like disease. Disease, particularly stony coral tissue loss disease, permeated multiple chapters of my thesis. As reef managers and scientists look to save coral reefs from imminent degradation, centralized and streamlined workflows for identifying potential pathogens for marine diseases would facilitate targeted solutions and intervention strategies that aim to curb the plague of disease on coral reefs. As reefs worldwide face anthropogenic and natural disturbances beyond coral disease, I see a world in which microorganisms and metabolites take center stage as ideal candidates for understanding and monitoring these important ecosystems.

Bibliography

Aburto-Oropeza, O., Ezcurra, E., Danemann, G., Valdez, V., Murray, J., and Sala, E. (2008) Mangroves in the Gulf of California increase fishery yields. *Proceedings of the National Academy of Sciences* **105**: 10456–10459.

Aeby, G.S., Ushijima, B., Campbell, J.E., Jones, S., Williams, G.J., Meyer, J.L., et al. (2019) Pathogenesis of a tissue loss disease affecting multiple species of corals along the Florida Reef Tract. *Front Mar Sci* **6**: 678.

Agrawal, S., Kumar, S., Sehgal, R., George, S., Gupta, R., Poddar, S., et al. (2019) El-MAVEN: A Fast, Robust, and User-Friendly Mass Spectrometry Data Processing Engine for Metabolomics. In *High-Throughput Metabolomics*. Methods in Molecular Biology. D'Alessandro, A. (ed). New York, NY: Springer New York, pp. 301–321.

Ainsworth, T.D., Fordyce, A.J., and Camp, E.F. (2017) The Other Microeukaryotes of the Coral Reef Microbiome. *Trends in Microbiology* **25**: 980–991.

Ainsworth, T.D., Heron, S.F., Ortiz, J.C., Mumby, P.J., Grech, A., Ogawa, D., et al. (2016) Climate change disables coral bleaching protection on the Great Barrier Reef. *Science* **352**: 338–342.

Alevizon, W.S. and Porter, J.W. (2015) Coral loss and fish guild stability on a Caribbean coral reef: 1974–2000. *Environ Biol Fish* **98**: 1035–1045.

Alfaro-Espinoza, G. and Ullrich, M.S. (2014) *Marinobacterium mangrovicola* sp. nov., a marine nitrogen-fixing bacterium isolated from mangrove roots of *Rhizophora mangle*. *Int J Syst Evol Micr* **64**: 3988–3993.

Alongi, D.M. (1987) Intertidal zonation and seasonality of meiobenthos in tropical mangrove estuaries. *Mar Biol* **95**: 447–458.

Alvarez-Filip, L., González-Barrios, F.J., Pérez-Cervantes, E., Molina-Hernández, A., and Estrada-Saldívar, N. (2022) Stony coral tissue loss disease decimated Caribbean coral populations and reshaped reef functionality. *Commun Biol* **5**: 440.

Andersson, E.R., Day, R.D., Work, T.M., Anderson, P.E., Woodley, C.M., and Schock, T.B. (2021) Identifying metabolic alterations associated with coral growth anomalies using 1H NMR metabolomics. *Coral Reefs* **40**: 1195–1209.

Apprill, A. (2019) On-site sequencing speeds up and re-directs field-based microbiology. *Env Microbiol Rep* **11**: 45–47.

Apprill, A., Holm, H., Santoro, A., Becker, C., Neave, M., Hughen, K., et al. (2021) Microbial ecology of coral-dominated reefs in the Federated States of Micronesia. *Aquat Microb Ecol* **86**: 115–136.

Apprill, A., McNally, S., Parsons, R., and Weber, L. (2015) Minor revision to V4 region SSU rRNA 806R gene primer greatly increases detection of SAR11 bacterioplankton. *Aquat Microb Ecol* **75**: 129–137.

Apprill, A. and Rappé, M. (2011) Response of the microbial community to coral spawning in lagoon and reef flat environments of Hawaii, USA. *Aquat Microb Ecol* **62**: 251–266.

Apprill, A., Weber, L.G., and Santoro, A.E. (2016) Distinguishing between microbial habitats unravels ecological complexity in coral microbiomes. *mSystems* **1**: 1–18.

Armstrong, F., Stearns, C., and Strickland, J. (1967) The measurement of upwelling and subsequent biological processes by means of the Technicon AutoAnalyzer and associated equipment. *Deep-Sea Res* **14**: 381–389.

Aronson, R.B. and Precht, W.F. (2001) White-band disease and the changing face of Caribbean coral reefs. In *The Ecology and Etiology of Newly Emerging Marine Diseases*. Porter, J.W. (ed). Dordrecht: Springer Netherlands, pp. 25–38.

Azam, F., Fenchel, T., Field, J., Gray, J., Meyer-Reil, L., and Thingstad, F. (1983) The Ecological Role of Water-Column Microbes in the Sea. *Mar Ecol Prog Ser* **10**: 257–263.

Baedke, J., Fábregas-Tejeda, A., and Nieves Delgado, A. (2020) The holobiont concept before Margulis. *J Exp Zool (Mol Dev Evol)* **334**: 149–155.

Barott, K.L. and Rohwer, F.L. (2012) Unseen players shape benthic competition on coral reefs. *Trends Microbiol* **20**: 621–628.

Becker, C., Hughen, K., Mincer, T., Ossolinski, J., Weber, L., and Apprill, A. (2017) Impact of prawn farming effluent on coral reef water nutrients and microorganisms. *Aquaculture Environment Interactions* **9**: 331–346.

Becker, C., Weber, L., Suca, J.J., Llopiz, J.K., Mooney, T.A., and Apprill, A. (2020) Microbial and nutrient dynamics in mangrove, reef, and seagrass waters over tidal and diurnal time scales. *Aquat Microb Ecol* **85**: 101–119.

Becker, C.C., Brandt, M., Miller, C.A., and Apprill, A. (2021) Microbial bioindicators of Stony Coral Tissue Loss Disease identified in corals and overlying waters using a rapid field-based sequencing approach. *Environ Microbiol* 1462-2920.15718.

Ben-Haim, Y., Thompson, F.L., Thompson, C.C., Cnockaert, M.C., Hoste, B., Swings, J., and Rosenberg, E. (2003) *Vibrio coralliilyticus* sp. nov., a temperature-dependent pathogen of the coral *Pocillopora damicornis*. *Int J Syst Evol Micr* **53**: 309–315.

Berger, S.A., Krompass, D., and Stamatakis, A. (2011) Performance, Accuracy, and Web Server for Evolutionary Placement of Short Sequence Reads under Maximum Likelihood. *Systematic Biology* **60**: 291–302.

Bernhardt, H. and Wilhelms, A. (1967) The continuous determination of low-level iron, soluble phosphate and total phosphate with the Autoanalyzer. *Technicon Symp* **1**: 385–389.

Bertilsson, S., Berglund, O., Karl, D.M., and Chisholm, S.W. (2003) Elemental composition of marine *Prochlorococcus* and *Synechococcus* : Implications for the ecological stoichiometry of the sea. *Limnol Oceanogr* **48**: 1721–1731.

Binder, B.J. and DuRand, M.D. (2002) Diel cycles in surface waters of the equatorial Pacific. *Deep Sea Research Part II: Topical Studies in Oceanography* **49**: 2601–2617.

Blake, E.S., Landsea, C.W., and Gibney, E.J. (2011) The deadliest, costliest, and most intense United States tropical cyclones from 1851 to 2010 (and other frequently requested hurricane facts), Miami, Florida: National Weather Service National Hurricane Center.

Blanchot, J., Andre, J.-M., Navarette, C., and Neveux, J. (1997) Picophytoplankton dynamics in the equatorial Pacific: diel cycling from flow-cytometer observations. *Comptes Rendus de l'Académie des Sciences* **320**: 7.

Blum, L. and Mills, A. (1991) Microbial growth and activity during the initial stages of seagrass decomposition. *Mar Ecol Prog Ser* **70**: 73–82.

Boehm, A.B. and Weisberg, S.B. (2005) Tidal Forcing of Enterococci at Marine Recreational Beaches at Fortnightly and Semidiurnal Frequencies. *Environ Sci Technol* **39**: 5575–5583.

Bourne, D.G., Morrow, K.M., and Webster, N.S. (2016) Insights into the Coral Microbiome: Underpinning the Health and Resilience of Reef Ecosystems. *Annual Review of Microbiology* **70**: 317–340.

Bourne, D.G. and Webster, N.S. (2013) Coral reef bacterial communities. In *The Prokaryotes: Prokaryotic communities and ecophysiology*. Rosenberg, E., DeLong, E.F., Lory, S., Stackebrandt, E., and Thompson, F. (eds). Berlin, Heidelberg: Springer Berlin Heidelberg, pp. 163–187.

Bouvier, T.C. and del Giorgio, P.A. (2002) Compositional changes in free-living bacterial communities along a salinity gradient in two temperate estuaries. *Limnol Oceanogr* **47**: 453–470.

Brander, L.M., Van Beukering, P., and Cesar, H.S.J. (2007) The recreational value of coral reefs: A meta-analysis. *Ecological Economics* **63**: 209–218.

Brandt, M.E., Ennis, R.S., Meiling, S.S., Townsend, J., Cobleigh, K., Glahn, A., et al. (2021) The Emergence and Initial Impact of Stony Coral Tissue Loss Disease (SCTLD) in the United States Virgin Islands. *Front Mar Sci* **8**: 715329.

Briceño, H.O. and Boyer, J.N. (2018) 2017 Annual Report of the Water Quality Monitoring Project for the Water Quality Protection Program of the Florida Keys National Marine Sanctuary.

Briceño, H.O., Boyer, J.N., Castro, J., and Harlem, P. (2013) Biogeochemical classification of South Florida's estuarine and coastal waters. *Marine Pollution Bulletin* 18.

Bruckner, A.W. (2015) History of Coral Disease Research. In *Diseases of Coral*. Woodley, C.M., Downs, C.A., Bruckner, A.W., Porter, J.W., and Galloway, S.B. (eds). Hoboken, NJ: John Wiley & Sons, Inc, pp. 52–84.

Bruckner, A.W. (2002) Life-Saving Products from Coral Reefs. *Issues in Science and Technology* **18**: 39–44.

Bruno, J.F., Sweatman, H., Precht, W.F., Selig, E.R., and Schutte, V.G.W. (2009) Assessing evidence of phase shifts from coral to macroalgal dominance on coral reefs. *Ecology* **90**: 1478–1484.

Buchan, A., LeCleir, G.R., Gulvik, C.A., and González, J.M. (2014) Master recyclers: features and functions of bacteria associated with phytoplankton blooms. *Nat Rev Microbiol* **12**: 686–698.

Buchinger, T.J., Li, W., and Johnson, N.S. (2014) Bile Salts as Semiochemicals in Fish. *Chemical Senses* **39**: 647–654.

Bulan, D.E., Wilantho, A., Krainara, P., Viyakarn, V., Chavanich, S., and Somboonna, N. (2018) Spatial and seasonal variability of reef bacterial communities in the upper Gulf of Thailand. *Front Mar Sci* **5**: 441.

Bunse, C. and Pinhassi, J. (2017) Marine bacterioplankton seasonal succession dynamics. *Trends in Microbiology* **25**: 494–505.

Burge, C.A., Kim, C.J.S., Lyles, J.M., and Harvell, C.D. (2013) Special Issue Oceans and Humans Health: The Ecology of Marine Opportunists. *Microb Ecol* **65**: 869–879.

Burman, S., Aronson, R., and van Woesik, R. (2012) Biotic homogenization of coral assemblages along the Florida reef tract. *Mar Ecol Prog Ser* **467**: 89–96.

Callahan, B.J., McMurdie, P.J., and Holmes, S.P. (2017) Exact sequence variants should replace operational taxonomic units in marker-gene data analysis. *ISME J* **11**: 2639–2643.

Callahan, B.J., McMurdie, P.J., Rosen, M.J., Han, A.W., Johnson, A.J.A., and Holmes, S.P. (2016) DADA2: High-resolution sample inference from Illumina amplicon data. *Nat Methods* **13**: 581–583.

Campbell, B.J. and Kirchman, D.L. (2013) Bacterial diversity, community structure and potential growth rates along an estuarine salinity gradient. *ISME J* **7**: 210–220.

Campbell, L. and Vaulot, D. (1993) Photosynthetic picoplankton community structure in the subtropical North Pacific Ocean near Hawaii (station ALOHA). *Deep Sea Research Part I: Oceanographic Research Papers* **40**: 2043–2060.

Carlson, C.A., Morris, R., Parsons, R., Treusch, A.H., Giovannoni, S.J., and Vergin, K. (2009) Seasonal dynamics of SAR11 populations in the euphotic and mesopelagic zones of the northwestern Sargasso Sea. *ISME J* **3**: 283–295.

Carpenter, R.C. (1988) Mass mortality of a Caribbean sea urchin: Immediate effects on community metabolism and other herbivores. *Proc Natl Acad Sci USA* **85**: 511–514.

Cayemitte, K., Aoki, N., Ferguson, S.R., Mooney, T.A., and Apprill, A. (2023) Ramicrusta invasive alga causes mortality in Caribbean coral larvae. *Front Mar Sci* **10**: 1158947.

Cermak, N., Becker, J.W., Knudsen, S.M., Chisholm, S.W., Manalis, S.R., and Polz, M.F. (2017) Direct single-cell biomass estimates for marine bacteria via Archimedes' principle. *ISME J* **11**: 825–828.

Chambers, M.C., Maclean, B., Burke, R., Amodei, D., Ruderman, D.L., Neumann, S., et al. (2012) A cross-platform toolkit for mass spectrometry and proteomics. *Nat Biotechnol* **30**: 918–920.

Chang, J., Chung, C., and Gong, G. (1996) Influences of cyclones on chlorophyll a concentration and Synechococcus abundance in a subtropical western Pacific coastal ecosystem. *Mar Ecol Prog Ser* **140**: 199–205.

Charpy, L., Casareto, B.E., Langlade, M.J., and Suzuki, Y. (2012) Cyanobacteria in Coral Reef Ecosystems: A Review. *Journal of Marine Biology* **2012**: 1–9.

Chen, Q., Zhao, Q., Li, J., Jian, S., and Ren, H. (2016) Mangrove succession enriches the sediment microbial community in South China. *Sci Rep* **6**: 27468.

Chen, W.-C., Tseng, W.-N., Hsieh, J.-L., Wang, Y.-S., and Wang, S.-L. (2010) Biodegradation and microbial community changes upon shrimp shell wastes amended in mangrove river sediment. *Journal of Environmental Science and Health, Part B* **45**: 473–477.

Chen, X., Wei, W., Wang, J., Li, H., Sun, J., Ma, R., et al. (2019) Tide driven microbial dynamics through virus-host interactions in the estuarine ecosystem. *Water Research* **160**: 118–129.

Chen, Y.-H., Yang, S.-H., Tandon, K., Lu, C.-Y., Chen, H.-J., Shih, C.-J., and Tang, S.-L. (2019) A genomic view of coral-associated *Prosthecochloris* and a companion sulfate-reducing bacterium, bioRxiv.

Chiappone, M., Rutten, L.M., Swanson, D.W., and Miller, S.L. (2008) Population status of the urchin Diadema antillarum in the Florida Keys 25 years after the Caribbean mass mortality. *Proceedings of the 11th International Coral Reef Symposium* **18**: 6.

Chiarello, M., Auguet, J.-C., Bettarel, Y., Bouvier, C., Claverie, T., Graham, N.A.J., et al. (2018) Skin microbiome of coral reef fish is highly variable and driven by host phylogeny and diet. *Microbiome* **6**:.

Chisholm, S.W., Olson, R.J., Zettler, E.R., Goericke, R., Waterbury, J.B., and Welschmeyer, N.A. (1988) A novel free-living prochlorophyte abundant in the oceanic euphotic zone. *Nature* **334**: 340–343.

Choi, D.H., Park, K.-T., An, S.M., Lee, K., Cho, J.-C., Lee, J.-H., et al. (2015) Pyrosequencing revealed SAR116 clade as dominant dddP-containing bacteria in oligotrophic NW Pacific Ocean. *PLoS ONE* **10**: e0116271.

Clark, A.S., Williams, S.D., Maxwell, K., Rosales, S.M., Huebner, L.K., Landsberg, J.H., et al. (2021) Characterization of the Microbiome of Corals with Stony Coral Tissue Loss Disease along Florida's Coral Reef. *Microorganisms* **9**: 2181.

Collado, L. and Figueras, M.J. (2011) Taxonomy, Epidemiology, and Clinical Relevance of the Genus Arcobacter. *Clin Microbiol Rev* **24**: 174–192.

Davis, G.E. (1982) A century of natural change in coral distribution at the Dry Tortugas: a comparison of reef maps from 1881 and 1976. *Bull Mar Sci* **32**: 608–623.

Davis, N.M., Proctor, D.M., Holmes, S.P., Relman, D.A., and Callahan, B.J. (2018) Simple statistical identification and removal of contaminant sequences in marker-gene and metagenomics data. *Microbiome* **6**: 226.

De'ath, G., Fabricius, K.E., Sweatman, H., and Puotinen, M. (2012) The 27–year decline of coral cover on the Great Barrier Reef and its causes. *Proc Natl Acad Sci USA* **109**: 17995–17999.

Deutsch, J.M., Jaiyesimi, O.A., Pitts, K.A., Houk, J., Ushijima, B., Walker, B.K., et al. (2021) Metabolomics of Healthy and Stony Coral Tissue Loss Disease Affected Montastraea cavernosa Corals. *Front Mar Sci* **8**: 714778.

Dinsdale, E.A., Pantos, O., Smriga, S., Edwards, R.A., Angly, F., Wegley, L., et al. (2008) Microbial ecology of four coral atolls in the northern line islands. *PLoS ONE* **3**: e1584.

Dittmar, T. and Lara, R.J. (2001) Driving forces behind nutrient and organic matter dynamics in a mangrove tidal creek in North Brazil. *Estuarine, Coastal and Shelf Science* **52**: 249–259.

Dobbelaere, T., Holstein, D.M., Muller, E.M., Gramer, L.J., McEachron, L., Williams, S.D., and Hanert, E. (2022) Connecting the Dots: Transmission of Stony Coral Tissue Loss Disease From the Marquesas to the Dry Tortugas. *Front Mar Sci* **9**: 778938.

Dobbelaere, T., Muller, E.M., Gramer, L.J., Holstein, D.M., and Hanert, E. (2020) Coupled Epidemio-Hydrodynamic Modeling to Understand the Spread of a Deadly Coral Disease in Florida. *Front Mar Sci* **7**: 591881.

Donato, D.C., Kauffman, J.B., Murdiyarso, D., Kurnianto, S., Stidham, M., and Kanninen, M. (2011) Mangroves among the most carbon-rich forests in the tropics. *Nature Geosci* **4**: 293–297.

Du, Z.-J., Wang, Y., Dunlap, C., Rooney, A.P., and Chen, G.-J. (2014) *Draconibacterium orientale* gen. nov., sp. nov., isolated from two distinct marine environments, and proposal of *Draconibacteriaceae* fam. nov. *International Journal of Systematic and Evolutionary Microbiology* **64**: 1690–1696.

Duarte, C.M. and Cebrián, J. (1996) The fate of marine autotrophic production. *Limnol Oceanogr* **41**: 1758–1766.

Duke, N.C., Meynecke, J.-O., Dittmann, S., Ellison, A.M., Anger, K., Berger, U., et al. (2007) A world without mangroves? *Science* **317**: 41–42.

Dupont, C.L., Rusch, D.B., Yooseph, S., Lombardo, M.-J., Alexander Richter, R., Valas, R., et al. (2012) Genomic insights to SAR86, an abundant and uncultivated marine bacterial lineage. *ISME J* **6**: 1186–1199.

Dustan, P. (2003) Ecological Perspective: The Decline of Carysfort Reef, Key Largo, Florida 1975-2000.

van Duyl, F., Gast, G., Steinhoff, W., Kloff, S., Veldhuis, M., and Bak, R. (2002) Factors influencing the short-term variation in phytoplankton composition and biomass in coral reef waters. *Coral Reefs* **21**: 293–306.

Eckrich, C.E. and Engel, M.S. (2013) Coral overgrowth by an encrusting red alga (Ramicrusta sp.): a threat to Caribbean reefs? *Coral Reefs* **32**: 81–84.

Eddy, T.D., Lam, V.W.Y., Reygondeau, G., Cisneros-Montemayor, A.M., Greer, K., Palomares, M.L.D., et al. (2021) Global decline in capacity of coral reefs to provide ecosystem services. *One Earth* **4**: 1278–1285.

Edmunds, P.J. (2013) Decadal-scale changes in the community structure of coral reefs of St. John, US Virgin Islands. *Marine Ecology Progress Series* **489**: 107–123.

Edmunds, P.J. (2019) Three decades of degradation lead to diminished impacts of severe hurricanes on Caribbean reefs. *Ecology* **100**: e02587.

Edmunds, P.J. and Smith, T.B. (2022) Spatial variation in the dynamics and synchrony of coral reef communities in the US Virgin Islands. *Mar Biol* **169**: 60.

Edmunds, P.J., Zimmermann, S.A., and Bramanti, L. (2019) A spatially aggressive peyssonnelid algal crust (PAC) threatens shallow coral reefs in St. John, US Virgin Islands. *Coral Reefs* **38**: 1329–1341.

Edwards, C.B., Eynaud, Y., Williams, G.J., Pedersen, N.E., Zgliczynski, B.J., Gleason, A.C.R., et al. (2017) Large-area imaging reveals biologically driven non-random spatial patterns of corals at a remote reef. *Coral Reefs* **36**: 1291–1305.

Egan, S. and Gardiner, M. (2016) Microbial Dysbiosis: Rethinking Disease in Marine Ecosystems. *Front Microbiol* **7**:.

Ennis, R., Kadison, E., Heidmann, S., Brandt, M.E., Henderson, L., and Smith, T. (2019) The United States Virgin Islands Territorial Coral Reef Monitoring Program. 2019 Annual Report.

Epstein, H.E., Smith, H.A., Cantin, N.E., Mocellin, V.J.L., Torda, G., and van Oppen, M.J.H. (2019) Temporal Variation in the Microbiome of Acropora Coral Species Does Not Reflect Seasonality. *Front Microbiol* **10**: 1775.

Evans, J.S., Paul, V.J., and Kellogg, C.A. (2022) Biofilms as potential reservoirs of stony coral tissue loss disease. *Front Mar Sci* **9**: 1009407.

Fabricius, K. and Klumpp, D. (1995) Widespread mixotrophy in reef-inhabiting soft corals:the influence of depth, and colony expansion and contraction on photosynthesis. *Mar Ecol Prog Ser* **125**: 195–204.

Field, C.B., Behrenfeld, M., Renderson, J., and Falkowski, P. (1998) Primary production of the biosphere: integrating terrestrial and oceanic components. *Science* **281**: 237–240.

Fiore, C.L., Freeman, C.J., and Kujawinski, E.B. (2017) Sponge exhalent seawater contains a unique chemical profile of dissolved organic matter. *PeerJ* **5**: e2870.

Fiore, C.L., Longnecker, K., Kido Soule, M.C., and Kujawinski, E.B. (2015) Release of ecologically relevant metabolites by the cyanobacterium *S ynechococcus elongatus* CCMP 1631: Metabolomics of *Synechococcus*. *Environ Microbiol* **17**: 3949–3963.

Florida Keys National Marine Sanctuary (2018) Case Definition: Stony Coral Tissue Loss Disease (SCTLD).

Fox, M.D., Carter, A.L., Edwards, C.B., Takeshita, Y., Johnson, M.D., Petrovic, V., et al. (2019) Limited coral mortality following acute thermal stress and widespread bleaching on Palmyra Atoll, central Pacific. *Coral Reefs* **38**: 701–712.

Fratantoni, P.S., Lee, T.N., Podesta, G.P., and Muller-Karger, F. (1998) The influence of Loop Current perturbations on the formation and evolution of Tortugas eddies in the southern Straits of Florida. *J Geophys Res* **103**: 24759–24779.

Fuhrman, J.A., Hewson, I., Schwalbach, M.S., Steele, J.A., Brown, M.V., and Naeem, S. (2006) Annually reoccurring bacterial communities are predictable from ocean conditions. *Proceedings of the National Academy of Sciences* **103**: 13104–13109.

Fukuda, R., Ogawa, H., Nagata, T., and Koike, I. (1998) Direct Determination of Carbon and Nitrogen Contents of Natural Bacterial Assemblages in Marine Environments. *Appl Environ Microbiol* **64**: 3352–3358.

Gardner, T.A., Côté, I.M., Gill, J.A., Grant, A., and Watkinson, A.R. (2005) Hurricanes and Caribbean coral reefs: impacts, recovery patterns, and role in long-term decline. *Ecology* **86**: 174–184.

Gardner, T.A., Côté, I.M., Gill, J.A., Grant, A., and Watkinson, A.R. (2003) Long-term region-wide declines in Caribbean corals. *Science* **301**: 958–960.

Garren, M. and Azam, F. (2012) Corals shed bacteria as a potential mechanism of resilience to organic matter enrichment. *ISME J* **6**: 1159–1165.

Gast, G., Wiegman, S., Wieringa, E., van Duyl, F., and Bak, R. (1998) Bacteria in coral reef water types: removal of cells, stimulation of growth and mineralization. *Mar Ecol Prog Ser* **167**: 37–45.

Gilbert, J.A., Field, D., Swift, P., Newbold, L., Oliver, A., Smyth, T., et al. (2009) The seasonal structure of microbial communities in the Western English Channel. *Environmental Microbiology* **11**: 3132–3139.

Glasl, B., Bourne, D.G., Frade, P.R., Thomas, T., Schaffelke, B., and Webster, N.S. (2019) Microbial indicators of environmental perturbations in coral reef ecosystems. *Microbiome* **7**: 94.

Glasl, B., Bourne, D.G., Frade, P.R., and Webster, N.S. (2018) Establishing microbial baselines to identify indicators of coral reef health. *Microbiology Australia*.

Glasl, B., Herndl, G.J., and Frade, P.R. (2016) The microbiome of coral surface mucus has a key role in mediating holobiont health and survival upon disturbance. *ISME J* **10**: 2280–2292.

Glasl, B., Robbins, S., Frade, P.R., Marangon, E., Laffy, P.W., Bourne, D.G., and Webster, N.S. (2020) Comparative genome-centric analysis reveals seasonal variation in the function of coral reef microbiomes. *ISME J*.

Glasl, B., Webster, N.S., and Bourne, D.G. (2017) Microbial indicators as a diagnostic tool for assessing water quality and climate stress in coral reef ecosystems. *Marine Biology* **164**:.

Gong, B., Cao, H., Peng, C., Perčulija, V., Tong, G., Fang, H., et al. (2019) High-throughput sequencing and analysis of microbial communities in the mangrove swamps along the coast of Beibu Gulf in Guangxi, China. *Sci Rep* **9**: 9377.

Grafeld, S., Oleson, K.L.L., Teneva, L., and Kittinger, J.N. (2017) Follow that fish: Uncovering the hidden blue economy in coral reef fisheries. *PLoS ONE* **12**: e0182104.

Green, E.P. and Bruckner, A.W. (2000) The signicance of coral disease epizootiology for coral reef conservation. *Biological Conservation* 15.

Grimes, D.J., Stemmler, J., Hada, H., May, E.B., Maneval, D., Hetrick, F.M., et al. (1984) *vibrio* species associated with mortality of sharks held in captivity. *Microbial Ecology* **10**: 271–282.

Guest, J.R., Edmunds, P.J., Gates, R.D., Kuffner, I.B., Andersson, A.J., Barnes, B.B., et al. (2018) A framework for identifying and characterising coral reef "oases" against a backdrop of degradation. *Journal of Applied Ecology*.

Gwak, J.-H., Kim, S.-J., Jung, M.-Y., Kim, J.-G., Roh, S.W., Yim, K.J., et al. (2015) *Draconibacterium filum* sp. nov., a new species of the genus of *Draconibacterium* from sediment of the east coast of the Korean Peninsula. *Antonie van Leeuwenhoek* **107**: 1049–1056.

Haas, A.F., Fairoz, M.F.M., Kelly, L.W., Nelson, C.E., Dinsdale, E.A., Edwards, R.A., et al. (2016) Global microbialization of coral reefs. *Nat Microbiol* **1**: 16042.

Haas, A.F., Nelson, C.E., Rohwer, F., Wegley-Kelly, L., Quistad, S.D., Carlson, C.A., et al. (2013) Influence of coral and algal exudates on microbially mediated reef metabolism. *PeerJ* **1**: e108.

Haas, A.F., Nelson, C.E., Wegley Kelly, L., Carlson, C.A., Rohwer, F., Leichter, J.J., et al. (2011) Effects of coral reef benthic primary producers on dissolved organic carbon and microbial activity. *PLoS ONE* **6**: e27973.

Hansell, D.A. and Carlson, C.A. (2001) Biogeochemistry of total organic carbon and nitrogen in the Sargasso Sea: control by convective overturn. *Deep Sea Research Part II: Topical Studies in Oceanography* **48**: 1649–1667.

Harbison, A.B., Price, L.E., Flythe, M.D., and Bräuer, S.L. (2017) *Micropepsis pineolensis* gen. nov., sp. nov., a mildly acidophilic alphaproteobacterium isolated from a poor fen, and proposal of Micropepsaceae fam. nov. within Micropepsales ord. nov. *International Journal of Systematic and Evolutionary Microbiology* **67**: 839–844.

Hernandez-Agreda, A., Leggat, W., Bongaerts, P., Herrera, C., and Ainsworth, T.D. (2018) Rethinking the Coral Microbiome: Simplicity Exists within a Diverse Microbial Biosphere. *mBio* **9**: e00812-18, /mbio/9/5/mBio.00812-18.atom.

Hewson, I., Ritchie, I.T., Evans, J.S., Altera, A., Behringer, D., Bowman, E., et al. (2023) A scuticociliate causes mass mortality of *Diadema antillarum* in the Caribbean Sea. *Sci Adv* **9**: eadg3200.

Hodge, J.D., Barry, D., Haase, E., O'Reily, R., Smith, H., Towle, E., and Wright, J. (2001) Fish Bay management plan for Fish Bay watershed, St. John, United States Virgin Islands, Department of Planning and Natural Resources.

Hoegh-Guldberg, O., Mumby, P.J., Hooten, A.J., Steneck, R.S., Greenfield, P., Gomez, E., et al. (2007) Coral reefs under rapid climate change and ocean acidification. *Science* **318**: 1737–1742.

Hopkinson, C.S., Sherr, B.F., and Ducklow, H.W. (1987) Microbial regeneration of ammonium in the water column of Davies Reef, Australia. *Marine Ecology Progress Series* **41**: 147–153.
Hosoya, S., Suzuki, S., Adachi, K., Matsuda, S., and Kasai, H. (2009) Paramoritella alkaliphila gen. nov., sp. nov., a member of the family Moritellaceae isolated in the Republic of Palau. *International Journal of Systematic and Evolutionary Microbiology* 6.
Huggett, M.J. and Apprill, A. (2019) Coral microbiome database: Integration of sequences reveals high diversity and relatedness of coral-associated microbes. *Env Microbiol Rep* **11**: 372–385.
Hughes, T.P. (1994) Catastrophes, Phase Shifts, and Large-Scale Degradation of a Caribbean Coral Reef. *Science* **265**: 1547–1551.
Hughes, T.P., Anderson, K.D., Connolly, S.R., Heron, S.F., Kerry, J.T., Lough, J.M., et al. (2018) Spatial and temporal patterns of mass bleaching of corals in the Anthropocene. *Science* **359**: 80–83.
Huntley, N., Brandt, M.E., Becker, C.C., Miller, C.A., Meiling, S.S., Correa, A.M.S., et al. (2022) Experimental transmission of Stony Coral Tissue Loss Disease results in differential microbial responses within coral mucus and tissue. *ISME COMMUN* **2**: 46.
Illumina, Inc. (2020) iSeq 100 Sequencing System Specification Sheet.
Iwanowicz, D.D., Schill, W.B., Woodley, C.M., Bruckner, A., Neely, K., and Briggs, K.M. (2020) Exploring the Stony Coral Tissue Loss Disease Bacterial Pathobiome, Microbiology.
Jackson, J.B.C. (2001) Historical overfishing and the recent collapse of coastal ecosystems. *Science* **293**: 629–637.
JGOFS (1996) Protocols for the joint global ocean flux study (JGOFS) core measurements (Report 19), Bergen, Norway: IOC SCOR.
Johnson, M.D., Scott, J.J., Leray, M., Lucey, N., Bravo, L.M.R., Wied, W.L., and Altieri, A.H. (2021) Rapid ecosystem-scale consequences of acute deoxygenation on a Caribbean coral reef. *Nat Commun* **12**: 4522.
Johnson, W.M., Kido Soule, M.C., and Kujawinski, E.B. (2017) Extraction efficiency and quantification of dissolved metabolites in targeted marine metabolomics. *Limnol Oceanogr Methods* **15**: 417–428.
Katoh, K. (2002) MAFFT: a novel method for rapid multiple sequence alignment based on fast Fourier transform. *Nucleic Acids Res* **30**: 3059–3066.
Kelly, L.W., Nelson, C.E., Haas, A.F., Naliboff, D.S., Calhoun, S., Carlson, C.A., et al. (2019) Diel population and functional synchrony of microbial communities on coral reefs. *Nat Commun* **10**: 1691.
Kelly, L.W., Williams, G.J., Barott, K.L., Carlson, C.A., Dinsdale, E.A., Edwards, R.A., et al. (2014) Local genomic adaptation of coral reef-associated microbiomes to gradients of natural variability and anthropogenic stressors. *Proceedings of the National Academy of Sciences* **111**: 10227–10232.
Kido Soule, M.C., Longnecker, K., Johnson, W.M., and Kujawinski, E.B. (2015) Environmental metabolomics: Analytical strategies. *Marine Chemistry* **177**: 374–387.
Kim, H. and Ducklow, H.W. (2016) A Decadal (2002–2014) analysis for dynamics of heterotrophic bacteria in an Antarctic coastal ecosystem: variability and physical and biogeochemical forcings. *Frontiers in Marine Science* **3**:.

Kim, Y., Jeon, J., Kwak, M.S., Kim, G.H., Koh, I., and Rho, M. (2018) Photosynthetic functions of *Synechococcus* in the ocean microbiomes of diverse salinity and seasons. *PLoS ONE* **13**: e0190266.

Kirchman, D., Peterson, B., and Juers, D. (1984) Bacterial growth and tidal variation in bacterial abundance in the Great Sippewissett Salt Marsh. *Mar Ecol Prog Ser* **19**: 247–259.

Kourafalou, V.H. and Kang, H. (2012) Florida Current meandering and evolution of cyclonic eddies along the Florida Keys Reef Tract: Are they interconnected?: FLORIDA CURRENT AND CYCLONIC EDDIES. *J Geophys Res* **117**: n/a-n/a.

Kozich, J.J., Westcott, S.L., Baxter, N.T., Highlander, S.K., and Schloss, P.D. (2013) Development of a Dual-Index Sequencing Strategy and Curation Pipeline for Analyzing Amplicon Sequence Data on the MiSeq Illumina Sequencing Platform. *Applied and Environmental Microbiology* **79**: 9.

Kramer, P.R., Roth, L., and Lang, J. (2021) Map of Stony Coral Tissue Loss Disease Outbreak in the Caribbean. *AGRRA*.

Kuffner, I.B., Stathakopoulos, A., Toth, L.T., and Bartlett, L.A. (2020) Reestablishing a stepping-stone population of the threatened elkhorn coral Acropora palmata to aid regional recovery. *Endang Species Res* **43**: 461–473.

Kujawinski, E.B. (2011) The Impact of Microbial Metabolism on Marine Dissolved Organic Matter. *Annu Rev Mar Sci* **3**: 567–599.

Laas, P., Ugarelli, K., Absten, M., Boyer, B., Briceño, H., and Stingl, U. (2021) Composition of Prokaryotic and Eukaryotic Microbial Communities in Waters around the Florida Reef Tract. 15.

Landsberg, J.H. (2020) Stony Coral Tissue Loss Disease in Florida Is Associated With Disruption of Host–Zooxanthellae Physiology. *Frontiers in Marine Science* **7**: 24.

Lapointe, B.E., Barile, P.J., and Matzie, W.R. (2004) Anthropogenic nutrient enrichment of seagrass and coral reef communities in the Lower Florida Keys: discrimination of local versus regional nitrogen sources. *Journal of Experimental Marine Biology and Ecology* **308**: 23–58.

Larsen, D.A. and Wigginton, K.R. (2020) Tracking COVID-19 with wastewater. *Nat Biotechnol* **38**: 1151–1153.

Lauro, F.M., McDougald, D., Thomas, T., Williams, T.J., Egan, S., Rice, S., et al. (2009) The genomic basis of trophic strategy in marine bacteria. *Proc Natl Acad Sci USA* **106**: 15527–15533.

Lawrimore, J., Ray, R., Applequist, S., Korzeniewski, B., and Menne, M.J. (2016) Global Summary of the Month (GSOM), Version 1 [EAST END, VI US, VQC00672551.csv].

Lê, S., Josse, J., and Husson, F. (2008) **FactoMineR** : An *R* Package for Multivariate Analysis. *J Stat Soft* **25**:.

Lecchini, D. and Nakamura, Y. (2013) Use of chemical cues by coral reef animal larvae for habitat selection. *Aquat Biol* **19**: 231–238.

Lee, R. and Joye, S. (2006) Seasonal patterns of nitrogen fixation and denitrification in oceanic mangrove habitats. *Mar Ecol Prog Ser* **307**: 127–141.

Lee, T.N., Leaman, K., Williams, E., Berger, T., and Atkinson, L. (1995) Florida Current meanders and gyre formation in the southern Straits of Florida. *J Geophys Res* **100**: 8607.

Letunic, I. and Bork, P. (2016) Interactive tree of life (iTOL) v3: an online tool for the display and annotation of phylogenetic and other trees. *Nucleic Acids Res* **44**: W242–W245.
Leung, J.Y.S. (2015) Habitat heterogeneity affects ecological functions of macrobenthic communities in a mangrove: Implication for the impact of restoration and afforestation. *Global Ecology and Conservation* **4**: 423–433.
Levitan, D.R., Best, R.M., and Edmunds, P.J. (2023) Sea urchin mass mortalities 40 y apart further threaten Caribbean coral reefs. *Proc Natl Acad Sci USA* **120**: e2218901120.
Li, D., Liu, C.-M., Luo, R., Sadakane, K., and Lam, T.-W. (2015) MEGAHIT: an ultra-fast single-node solution for large and complex metagenomics assembly via succinct *de Bruijn* graph. *Bioinformatics* **31**: 1674–1676.
Liaw, A. and Wiener, M. (2002) Classification and regression by randomForest. **2**: 6.
Lindh, M.V., Lefébure, R., Degerman, R., Lundin, D., Andersson, A., and Pinhassi, J. (2015) Consequences of increased terrestrial dissolved organic matter and temperature on bacterioplankton community composition during a Baltic Sea mesocosm experiment. *Ambio* **44**: 402–412.
Liu, J., Peng, M., and Li, Y. (2012) Phylogenetic diversity of nitrogen-fixing bacteria and the *nifH* gene from mangrove rhizosphere soil. *Can J Microbiol* **58**: 531–539.
Liu, M., Huang, Z., Zhao, Q., and Shao, Z. (2019) *Cohaesibacter intestini* sp. nov., isolated from the intestine of abalone, *Haliotis discus hannai*. *Int J Syst Evol Microbiol* **69**: 3202–3206.
Liu, P.-Y., Wu, W.-K., Chen, C.-C., Panyod, S., Sheen, L.-Y., and Wu, M.-S. (2020) Evaluation of Compatibility of 16S rRNA V3V4 and V4 Amplicon Libraries for Clinical Microbiome Profiling, Microbiology.
Lu, X., Sun, S., Zhang, Y.-Q., Hollibaugh, J.T., and Mou, X. (2015) Temporal and vertical distributions of bacterioplankton at the Gray's Reef National Marine Sanctuary. *Appl Environ Microbiol* **81**: 910–917.
Ludwig, W. (2004) ARB: a software environment for sequence data. *Nucleic Acids Res* **32**: 1363–1371.
Luna, G.M., Bongiorni, L., Gili, C., Biavasco, F., and Danovaro, R. (2010) *Vibrio harveyi* as a causative agent of the White Syndrome in tropical stony corals. *Env Microbiol Rep* **2**: 120–127.
Ma, L., Becker, C., Weber, L., Sullivan, C., Zgliczynski, B., Sandin, S., et al. (2022a) Biogeography of reef water microbes from within-reef to global scales. *Aquat Microb Ecol* **88**: 81–94.
Ma, L., Becker, C., Weber, L., Sullivan, C., Zgliczynski, B., Sandin, S., et al. (2022b) Biogeography of reef water microbes from within-reef to global scales. *Aquat Microb Ecol* **88**: 81–94.
MacKnight, N.J., Cobleigh, K., Lasseigne, D., Chaves-Fonnegra, A., Gutting, A., Dimos, B., et al. (2021) Microbial dysbiosis reflects disease resistance in diverse coral species. *Commun Biol* **4**: 679.
Manzello, D.P. (2015) Rapid Recent Warming of Coral Reefs in the Florida Keys. *Sci Rep* **5**: 16762.
Margulis, L. (1991) Symbiogenesis and symbionticism. *Symbiosis as a source of evolutionary innovation: Speciation and morphogenesis* **10**:.
Marie, D., Partensky, F., Jacquet, S., and Vaulot, D. (1997) Enumeration and cell cycle analysis of natural populations of marine picoplankton by flow cytometry using the nucleic acid stain SYBR green I. *Applied and Environmental Microbiology* **63**: 8.

Martin, B.D., Witten, D., and Willis, A.D. (2020) Modeling microbial abundances and dysbiosis with beta-binomial regression. *Ann Appl Stat* **14**: 94–115.
McClenachan, L., O'Connor, G., Neal, B.P., Pandolfi, J.M., and Jackson, J.B.C. (2017) Ghost reefs: Nautical charts document large spatial scale of coral reef loss over 240 years. *Sci Adv* **3**: e1603155.
McMurdie, P.J. and Holmes, S. (2013) phyloseq: An R Package for Reproducible Interactive Analysis and Graphics of Microbiome Census Data. *PLoS ONE* **8**: e61217.
McNally, S.P., Parsons, R.J., Santoro, A.E., and Apprill, A. (2017) Multifaceted impacts of the stony coral *Porites astreoides* on picoplankton abundance and community composition: Corals impact reef picoplankton. *Limnology and Oceanography* **62**: 217–234.
McWilliams, J.P., Côté, I.M., Gill, J.A., Sutherland, W.J., and Watkinson, A.R. (2005) Accelerating impacts of temperature-induced coral bleaching in the Caribbean. *Ecology* **86**: 2055–2060.
Meiling, S., Muller, E.M., Smith, T.B., and Brandt, M.E. (2020) 3D Photogrammetry Reveals Dynamics of Stony Coral Tissue Loss Disease (SCTLD) Lesion Progression Across a Thermal Stress Event. *Front Mar Sci* **7**: 597643.
Meiling, S.S., Muller, E.M., Lasseigne, D., Rossin, A., Veglia, A.J., MacKnight, N., et al. (2021) Variable Species Responses to Experimental Stony Coral Tissue Loss Disease (SCTLD) Exposure. *Front Mar Sci* **8**: 670829.
Mera, H. and Bourne, D.G. (2018) Disentangling causation: complex roles of coral-associated microorganisms in disease: Disentangling coral disease causation. *Environ Microbiol* **20**: 431–449.
Meyer, J.L., Castellanos-Gell, J., Aeby, G.S., Häse, C.C., Ushijima, B., and Paul, V.J. (2019) Microbial community shifts associated with the ongoing stony coral tissue loss disease outbreak on the Florida Reef Tract. *Front Microbiol* **10**: 2244.
Miller, J., Muller, E., Rogers, C., Waara, R., Atkinson, A., Whelan, K.R.T., et al. (2009) Coral disease following massive bleaching in 2005 causes 60% decline in coral cover on reefs in the US Virgin Islands. *Coral Reefs* **28**: 925–937.
Miller, M.A., Pfeiffer, W., and Schwartz, T. (2010) Creating the cipres science gateway for inference of large phylogenetic trees. 1–8.
Monger, B.C. and Landry, M.R. (1993) Flow cytometric analysis of marine bacteria with Hoechst 33342. *Appl Environ Microbiol* **59**: 905–911.
Mora, C., Andrèfouët, S., Costello, M.J., Kranenburg, C., Rollo, A., Veron, J., et al. (2006) Coral Reefs and the Global Network of Marine Protected Areas. *Science* **312**: 1750–1751.
Moran, M.A. (2015) The global ocean microbiome. *Science* **350**: 8455–8455.
Moriarty, D.J.W., Boon, P.I., Hansen, J.A., Hunt, W.G., Poiner, I.R., Pollard, P.C., et al. (1985) Microbial biomass and productivity in seagrass beds. *Geomicrobiology Journal* **4**: 21–51.
Moriarty, D.J.W. and Pollard, P.C. (1982) Diel variation of bacterial productivity in seagrass (Zostera capricorni) beds measured by rate of thymidine incorporation into DNA. *Marine Biology* **72**: 165–173.
Muller, E.M., Sartor, C., Alcaraz, N.I., and van Woesik, R. (2020) Spatial epidemiology of the Stony-Coral-Tissue-Loss Disease in Florida. *Front Mar Sci* **7**: 163.

Mumby, P.J., Hedley, J.D., Zychaluk, K., Harborne, A.R., and Blackwell, P.G. (2006) Revisiting the catastrophic die-off of the urchin Diadema antillarum on Caribbean coral reefs: Fresh insights on resilience from a simulation model. *Ecological Modelling* **196**: 131–148.
Murdoch, T.J.T. and Aronson, R.B. (1999) Scale-dependent spatial variability of coral assemblages along the Florida Reef Tract. *Coral Reefs* **18**: 341–351.
Nakajima, R., Haas, A.F., Silveira, C.B., Kelly, E.L.A., Smith, J.E., Sandin, S., et al. (2018) Release of dissolved and particulate organic matter by the soft coral Lobophytum and subsequent microbial degradation. *Journal of Experimental Marine Biology and Ecology* **504**: 53–60.
Neave, M.J., Rachmawati, R., Xun, L., Michell, C.T., Bourne, D.G., Apprill, A., and Voolstra, C.R. (2017) Differential specificity between closely related corals and abundant *Endozoicomonas* endosymbionts across global scales. *ISME J* **11**: 186–200.
Needham, D.M. and Fuhrman, J.A. (2016) Pronounced daily succession of phytoplankton, archaea and bacteria following a spring bloom. *Nat Microbiol* **1**: 16005.
Neely, K.L., Lewis, C.L., Lunz, K.S., and Kabay, L. (2021) Rapid Population Decline of the Pillar Coral Dendrogyra cylindrus Along the Florida Reef Tract. *Front Mar Sci* **8**: 656515.
Neely, K.L., Macaulay, K.A., Hower, E.K., and Dobler, M.A. (2020) Effectiveness of topical antibiotics in treating corals affected by Stony Coral Tissue Loss Disease. *PeerJ* **8**: e9289.
Nelson, C.E., Alldredge, A.L., McCliment, E.A., Amaral-Zettler, L.A., and Carlson, C.A. (2011) Depleted dissolved organic carbon and distinct bacterial communities in the water column of a rapid-flushing coral reef ecosystem. *ISME J* **5**: 1374–1387.
Nelson, C.E., Goldberg, S.J., Kelly, L.W., Haas, A.F., Smith, J.E., Rohwer, F., and Carlson, C.A. (2013) Coral and macroalgal exudates vary in neutral sugar composition and differentially enrich reef bacterioplankton lineages. *ISME J* **7**: 962–979.
Nelson, C.E., Wegley Kelly, L., and Haas, A.F. (2023) Microbial Interactions with Dissolved Organic Matter Are Central to Coral Reef Ecosystem Function and Resilience. *Annu Rev Mar Sci* **15**: annurev-marine-042121-080917.
Neubauer, S.C., Piehler, M.F., Smyth, A.R., and Franklin, R.B. (2019) Saltwater intrusion modifies microbial community structure and decreases denitrification in tidal freshwater marshes. *Ecosystems* **22**: 912–928.
Noonan, K.R. and Childress, M.J. (2020) Association of butterflyfishes and stony coral tissue loss disease in the Florida Keys. *Coral Reefs* **39**: 1581–1590.
Norström, A., Nyström, M., Lokrantz, J., and Folke, C. (2009) Alternative states on coral reefs: beyond coral–macroalgal phase shifts. *Mar Ecol Prog Ser* **376**: 295–306.
Ochsenkühn, M.A., Schmitt-Kopplin, P., Harir, M., and Amin, S.A. (2018) Coral metabolite gradients affect microbial community structures and act as a disease cue. *Commun Biol* **1**: 184.
Oehler, T., Tamborski, J., Rahman, S., Moosdorf, N., Ahrens, J., Mori, C., et al. (2019) DSi as a Tracer for Submarine Groundwater Discharge. *Front Mar Sci* **6**: 563.
Oksanen, J., Blanchet, F.G., Friendly, M., Kindt, R., Legendre, P., McGlinn, D., et al. (2020) vegan: community ecology package. *R package version 25-7*.
PAHO (2022) Capacity for genomic sequencing grows in Latin America and Caribbean with training and equipment provided by PAHO.

Parada, A.E., Needham, D.M., and Fuhrman, J.A. (2016) Every base matters: assessing small subunit rRNA primers for marine microbiomes with mock communities, time series and global field samples. *Environ Microbiol* **18**: 1403–1414.

Park, S., Jung, Y.-T., Kim, S., and Yoon, J.-H. (2016) *Marinobacterium aestuariivivens* sp. nov., isolated from a tidal flat. *International Journal of Systematic and Evolutionary Microbiology* **66**: 1718–1723.

Partensky, F., Blanchot, J., and Vaulot, D. (1999) Differential distribution and ecology of *Prochlorococcus* and *Synechococcus* in oceanic waters: a review. In *Bulletin de l'Institud océanographique*. Monaco.

Parveen, N. and Cornell, K.A. (2011) Methylthioadenosine/S-adenosylhomocysteine nucleosidase, a critical enzyme for bacterial metabolism: Involvement of MTA/SAH nucleosidase in bacterial metabolism. *Molecular Microbiology* **79**: 7–20.

Patterson, K.L., Porter, J.W., Ritchie, K.B., Polson, S.W., Mueller, E., Peters, E.C., et al. (2002) The etiology of white pox, a lethal disease of the Caribbean elkhorn coral, *Acropora palmata*. *Proc Natl Acad Sci USA* **99**: 8725–8730.

Pawlik, J.R., Steindler, L., Henkel, T.P., Beer, S., and Ilan, M. (2007) Chemical warfare on coral reefs: Sponge metabolites differentially affect coral symbiosis in situ. *Limnol Oceanogr* **52**: 907–911.

Pedersen, K., Verdonck, L., Austin, B., Austin, D.A., Blanch, A.R., Grimont, P.A.D., et al. (1998) Taxonomic evidence that *Vibrio carchariae* Grimes et al, 1985 is a junior synonym of *Vibrio harveyi* (Johnson and Shunk 1936) Baumann et al. 1981. *Int J Syst Bacteriol* **48**: 749–758.

Pedler, B.E., Aluwihare, L.I., and Azam, F. (2014) Single bacterial strain capable of significant contribution to carbon cycling in the surface ocean. *Proc Natl Acad Sci USA* **111**: 7202–7207.

Peduzzi, P. and Herndl, G. (1991) Decomposition and significance of sea-grass leaf litter (*Cymodocea nodosa*) for the microbial food web in coastal waters (Gulf of Trieste, Northern Adriatic Sea). *Mar Ecol Prog Ser* **71**: 163–174.

Peixoto, R.S., Rosado, P.M., Leite, D.C. de A., Rosado, A.S., and Bourne, D.G. (2017) Beneficial Microorganisms for Corals (BMC): Proposed Mechanisms for Coral Health and Resilience. *Frontiers in Microbiology* **8**:.

Pereira, A., Soares, M.C., Santos, T., Poças, A., Pérez-Losada, M., Apprill, A., et al. (2022) Reef Location and Client Diversity Influence the Skin Microbiome of the Caribbean Cleaner Goby Elacatinus evelynae. *Microb Ecol*.

Pereira, L.B., Palermo, B.R.Z., Carlos, C., and Ottoboni, L.M.M. (2017) Diversity and antimicrobial activity of bacteria isolated from different Brazilian coral species. 8.

Pernice, M., Raina, J.-B., Rädecker, N., Cárdenas, A., Pogoreutz, C., and Voolstra, C.R. (2020) Down to the bone: the role of overlooked endolithic microbiomes in reef coral health. *ISME J* **14**: 325–334.

Peterson, C.H. (1991) Intertidal Zonation of Marine Invertebrates in Sand and Mud. *American Scientist* **79**: 236–249.

Pita, L., Rix, L., Slaby, B.M., Franke, A., and Hentschel, U. (2018) The sponge holobiont in a changing ocean: from microbes to ecosystems. *Microbiome* **6**: 46.

Plaisance, L., Caley, M.J., Brainard, R.E., and Knowlton, N. (2011) The Diversity of Coral Reefs: What Are We Missing? *PLoS ONE* **6**: e25026.

Pohlner, M., Dlugosch, L., Wemheuer, B., Mills, H., Engelen, B., and Reese, B.K. (2019) The majority of active Rhodobacteraceae in marine sediments belong to uncultured genera: a molecular approach to link their distribution to environmental conditions. *Front Microbiol* **10**: 659.

Polónia, A.R.M., Cleary, D.F.R., Freitas, R., Coelho, F.J.R. da C., de Voogd, N.J., and Gomes, N.C.M. (2016) Comparison of archaeal and bacterial communities in two sponge species and seawater from an Indonesian coral reef environment. *Marine Genomics* **29**: 69–80.

Pomeroy, L.R. (1974) The Ocean's Food Web, A Changing Paradigm. *BioScience* **24**: 499–504.

Precht, W.F., Gintert, B.E., Robbart, M.L., Fura, R., and van Woesik, R. (2016) Unprecedented disease-related coral mortality in southeastern Florida. *Sci Rep* **6**: 31374.

Priest, T., Heins, A., Harder, J., Amann, R., and Fuchs, B.M. (2022) Niche partitioning of the ubiquitous and ecologically relevant NS5 marine group. *ISME J* **16**: 1570–1582.

Qu, L., Lai, Q., Zhu, F., Hong, X., Sun, X., and Shao, Z. (2011) *Cohaesibacter marisflavi* sp. nov., isolated from sediment of a seawater pond used for sea cucumber culture, and emended description of the genus *Cohaesibacter*. *Int J Syst Evol Microbiol* **61**: 762–766.

Quast, C., Pruesse, E., Yilmaz, P., Gerken, J., Schweer, T., Yarza, P., et al. (2012) The SILVA ribosomal RNA gene database project: improved data processing and web-based tools. *Nucleic Acids Res* **41**: D590–D596.

Quince, C., Walker, A.W., Simpson, J.T., Loman, N.J., and Segata, N. (2017) Shotgun metagenomics, from sampling to analysis. *Nat Biotechnol* **35**: 833–844.

Quinlan, Z.A., Ritson-Williams, R., Carroll, B.J., Carlson, C.A., and Nelson, C.E. (2019) Species-specific differences in the microbiomes and organic exudates of crustose coralline algae influence bacterioplankton communities. *Front Microbiol* **10**: 2397.

Raina, J.-B., Tapiolas, D., Willis, B.L., and Bourne, D.G. (2009) Coral-Associated Bacteria and Their Role in the Biogeochemical Cycling of Sulfur. *APPL ENVIRON MICROBIOL* **75**: 10.

Reaka-Kudla, M.L. (1997) The global biodiversity of coral reefs: a comparison with rain forests. In *Biodiversity II: Understanding and protecting our biological resources*. The National Academy of Sciences, pp. 83–108.

Reef, R., Feller, I.C., and Lovelock, C.E. (2010) Nutrition of mangroves. *Tree Physiology* **30**: 1148–1160.

Reguero, B.G., Storlazzi, C.D., Gibbs, A.E., Shope, J.B., Cole, A.D., Cumming, K.A., and Beck, M.W. (2021) The value of US coral reefs for flood risk reduction. *Nat Sustain* **4**: 688–698.

Ren, H., Ma, H., Li, H., Huang, L., and Luo, Y. (2019) *Acidimangrovimonas sediminis* gen. nov., sp. nov., isolated from mangrove sediment and reclassification of *Defluviimonas indica* as *Acidimangrovimonas indica* comb. nov. and *Defluviimonas pyrenivorans* as *Acidimangrovimonas pyrenivorans* comb. nov. *International Journal of Systematic and Evolutionary Microbiology,* **69**: 2445–2451.

Rogers, C. and Miller, J. (2006) Permanent phase shifts or reversible declines in coral cover? Lack of recovery of two coral reefs inSt. John, US Virgin Islands. *Mar Ecol Prog Ser* **306**: 103–114.

Rogers, C.S., Miller, J., Muller, E.M., Edmunds, P., Nemeth, R.S., Beets, J.P., et al. (2008) Ecology of Coral Reefs in the US Virgin Islands. In *Coral Reefs of the USA*. Riegl, B.M. and Dodge, R.E. (eds). Dordrecht: Springer Netherlands, pp. 303–373.

Rohwer, F., Seguritan, V., Azam, F., and Knowlton, N. (2002) Diversity and distribution of coral-associated bacteria. *Mar Ecol Prog Ser* **243**: 1–10.

Rosales, S.M., Clark, A.S., Huebner, L.K., Ruzicka, R.R., and Muller, E.M. (2020) *Rhodobacterales* and *Rhizobiales* are associated with stony coral tissue loss disease and its suspected sources of transmission. *Front Microbiol* **11**: 681.

Rosales, S.M., Huebner, L.K., Clark, A.S., McMinds, R., Ruzicka, R.R., and Muller, E.M. (2022) Bacterial Metabolic Potential and Micro-Eukaryotes Enriched in Stony Coral Tissue Loss Disease Lesions. *Front Mar Sci* **8**: 776859.

Rosales, S.M., Huebner, L.K., Evans, J.S., Apprill, A., Baker, A.C., Becker, C.C., et al. (2023) A meta-analysis of the stony coral tissue loss disease microbiome finds key bacteria in unaffected and lesion tissue in diseased colonies. *ISME COMMUN* **3**: 19.

Rosales, S.M., Huebner, L.K., Evans, J.S., Apprill, A., Baker, A.C., Bellantuono, A.J., et al. (2022) A meta-analysis of the stony coral tissue loss disease microbiome finds key bacteria in lesions and unaffected tissue of diseased colonies, Microbiology.

Rosenau, N.A., Gignoux-Wolfsohn, S., Everett, R.A., Miller, A.W., Minton, M.S., and Ruiz, G.M. (2021) Considering Commercial Vessels as Potential Vectors of Stony Coral Tissue Loss Disease. *Front Mar Sci* **8**: 709764.

Sánchez-Carrillo, S., Sánchez-Andrés, R., Alatorre, L.C., Angeler, D.G., Álvarez-Cobelas, M., and Arreola-Lizárraga, J.A. (2009) Nutrient fluxes in a semi-arid microtidal mangrove wetland in the Gulf of California. *Estuarine, Coastal and Shelf Science* **82**: 654–662.

Santoro, A.E., Casciotti, K.L., and Francis, C.A. (2010) Activity, abundance and diversity of nitrifying archaea and bacteria in the central California Current: Nitrification in the central California Current. *Environmental Microbiology* **12**: 1989–2006.

Sasi Jyothsna, T.S., Rahul, K., Ramaprasad, E.V.V., Sasikala, C., and Ramana, C.V. (2013) *Arcobacter anaerophilus* sp. nov., isolated from an estuarine sediment and emended description of the genus *Arcobacter*. *Int J Syst Evol Micr* **63**: 4619–4625.

Sauter, M., Moffatt, B., Saechao, M.C., Hell, R., and Wirtz, M. (2013) Methionine salvage and *S* -adenosylmethionine: essential links between sulfur, ethylene and polyamine biosynthesis. *Biochemical Journal* **451**: 145–154.

Selig, E.R. and Bruno, J.F. (2010) A Global Analysis of the Effectiveness of Marine Protected Areas in Preventing Coral Loss. *PLoS ONE* **5**: e9278.

Seruge, J., Wong, M., Noble, R.T., Blackwood, A.D., Moravcik, P.S., and Kirs, M. (2019) Application of a rapid qPCR method for enterococci for beach water quality monitoring purposes in Hawaii: Loss of DNA during the extraction protocol due to coral sands. *Marine Pollution Bulletin* **149**: 110631.

Silbiger, N.J., Donahue, M.J., and Lubarsky, K. (2020) Submarine groundwater discharge alters coral reef ecosystem metabolism. *Proc R Soc B* **287**: 20202743.

Silveira, C.B., Gregoracci, G.B., Coutinho, F.H., Silva, G.G.Z., Haggerty, J.M., de Oliveira, L.S., et al. (2017) Bacterial community associated with the reef coral *Mussismilia braziliensis's* momentum boundary layer over a diel cycle. *Front Microbiol* **8**: 784.

Silveira, C.B. and Rohwer, F.L. (2016) Piggyback-the-Winner in host-associated microbial communities. *npj Biofilms Microbiomes* **2**: 16010.

Small, A., Adey, W.H., and Spoon, D. (1998) Are current estimates of coral reef biodiversity too low? The view through the window of a microcosm. *Atoll Research Bulletin* **458**: 1–20.

Smith, C.A., Want, E.J., O'Maille, G., Abagyan, R., and Siuzdak, G. (2006) XCMS: Processing Mass Spectrometry Data for Metabolite Profiling Using Nonlinear Peak Alignment, Matching, and Identification. *Anal Chem* **78**: 779–787.

Sneed, J.M., Sharp, K.H., Ritchie, K.B., and Paul, V.J. (2014) The chemical cue tetrabromopyrrole from a biofilm bacterium induces settlement of multiple Caribbean corals. *Proceedings of the Royal Society B: Biological Sciences* **281**: 20133086–20133086.

Soffer, N., Brandt, M.E., Correa, A.M., Smith, T.B., and Thurber, R.V. (2014) Potential role of viruses in white plague coral disease. *ISME J* **8**: 271–283.

Sorokin, Y.I. (1973) Trophical Role of Bacteria in the Ecosystem of the Coral Reef. *Nature* **242**: 415–417.

Stackebrandt, E. and Goebel, B.M. (1994) Taxonomic Note: A Place for DNA-DNA Reassociation and 16S rRNA Sequence Analysis in the Present Species Definition in Bacteriology. *International Journal of Systematic and Evolutionary Microbiology* **44**: 846–849.

Stamatakis, A. (2014) RAxML version 8: a tool for phylogenetic analysis and post-analysis of large phylogenies. *Bioinformatics* **30**: 1312–1313.

Stat, M., Carter, D., and Hoeghguldberg, O. (2006) The evolutionary history of Symbiodinium and scleractinian hosts—Symbiosis, diversity, and the effect of climate change. *Perspectives in Plant Ecology, Evolution and Systematics* **8**: 23–43.

Stockton, L. and Edmunds, P.J. (2021) Spatially aggressive peyssonnelid algal crusts (PAC) constrain coral recruitment to Diadema grazing halos on a shallow Caribbean reef. *Journal of Experimental Marine Biology and Ecology* **541**: 151569.

Studivan, M.S., Baptist, M., Molina, V., Riley, S., First, M., Soderberg, N., et al. (2022) Transmission of stony coral tissue loss disease (SCTLD) in simulated ballast water confirms the potential for ship-born spread, In Review.

Sullivan, B., Faulkner, D.J., and Webb, L. (1983) Siphonodictidine, a Metabolite of the Burrowing Sponge *Siphonodictyon* sp. That Inhibits Coral Growth. *Science* **221**: 1175–1176.

Sun, F., Zhang, X., Zhang, Q., Liu, F., Zhang, J., and Gong, J. (2015) Seagrass (*Zostera marina*) colonization promotes the accumulation of diazotrophic bacteria and alters the relative abundances of specific bacterial lineages involved in benthic carbon and sulfur cycling. *Appl Environ Microbiol* **81**: 6901–6914.

Sutton, D.C. and Besant, P.J. (1994) Ecology and characteristics of bdellovibrios from three tropical marine habitats. *Marine Biology* **119**: 313–320.

Sweatman, H. (1988) Field evidence that settling coral reef fish larvae detect resident fishes using dissolved chemical cues. *Journal of Experimental Marine Biology and Ecology* **124**: 163–174.

Sweet, M., Croquer, A., and Bythell, J. (2010) Temporal and spatial patterns in waterborne bacterial communities of an island reef system. *Aquat Microb Ecol* **61**: 1–11.

Sweet, M.J., Croquer, A., and Bythell, J.C. (2011) Bacterial assemblages differ between compartments within the coral holobiont. *Coral Reefs* **30**: 39–52.

Szmant, A.M. (2002) Nutrient Enrichment on Coral Reefs: Is It a Major Cause of Coral Reef Decline? *Estuaries* **25**: 743–766.

Tâmega, F.T.S. and Figueiredo, M.A.O. (2019) Colonization, Growth and Productivity of Crustose Coralline Algae in Sunlit Reefs in the Atlantic Southernmost Coral Reef. *Front Mar Sci* **6**: 81.

Thingstad, T.F. (2000) Elements of a theory for the mechanisms controlling abundance, diversity, and biogeochemical role of lytic bacterial viruses in aquatic systems. *Limnol Oceanogr* **45**: 1320–1328.

Thome, P.E., Rivera-Ortega, J., Rodríguez-Villalobos, J.C., Cerqueda-García, D., Guzmán-Urieta, E.O., García-Maldonado, J.Q., et al. (2021) Local dynamics of a white syndrome outbreak and changes in the microbial community associated with colonies of the scleractinian brain coral *Pseudodiploria strigosa*. *PeerJ* **9**: e10695.

Thurber, R.V., Payet, J.P., Thurber, A.R., and Correa, A.M.S. (2017) Virus–host interactions and their roles in coral reef health and disease. *Nat Rev Microbiol* **15**: 205–216.

Titus, K., O'Connell, L., Matthee, K., and Childress, M. (2022) The Influence of Foureye Butterflyfish (Chaetodon capistratus) and Symbiodiniaceae on the Transmission of Stony Coral Tissue Loss Disease. *Front Mar Sci* **9**: 800423.

Toledo, G., Bashan, Y., and Soeldner, A. (1995) Cyanobacteria and black mangroves in Northwestern Mexico: colonization, and diurnal and seasonal nitrogen fixation on aerial roots. *Can J Microbiol* **41**: 999–1011.

Topor, Z.M., Rasher, D.B., Duffy, J.E., and Brandl, S.J. (2019) Marine protected areas enhance coral reef functioning by promoting fish biodiversity. *CONSERVATION LETTERS* **12**:.

Toth, L.T., Kuffner, I.B., Stathakopoulos, A., and Shinn, E.A. (2018) A 3,000-year lag between the geological and ecological shutdown of Florida's coral reefs. *Glob Change Biol* **24**: 5471–5483.

Tremblay, P., Grover, R., Maguer, J.F., Legendre, L., and Ferrier-Pagès, C. (2012) Autotrophic carbon budget in coral tissue: a new 13C-based model of photosynthate translocation. *Journal of Experimental Biology* **215**: 1384–1393.

Tsounis, G. and Edmunds, P.J. (2017) Three decades of coral reef community dynamics in St. John, USVI : a contrast of scleractinians and octocorals. *Ecosphere* **8**:.

Ugarelli, K., Chakrabarti, S., Laas, P., and Stingl, U. (2017) The seagrass holobiont and Its microbiome. *Microorganisms* **5**: 81.

Ugarelli, K., Laas, P., and Stingl, U. (2018) The microbial communities of leaves and roots associated with turtle grass (*Thalassia testudinum*) and manatee grass (*Syringodium filliforme*) are distinct from seawater and sediment communities, but are similar between species and sampling sites. *Microorganisms* **7**: 4.

US Environmental Protection Agency (1983) Nitrogen, ammonia. Method 350.1 (colorimetric, automated, phenate). In *Methods for chemical analysis of water and wastes*. Cincinnati, OH: USEPA, p. 350.1-1-350.1–4.

Ushijima, B., Meyer, J.L., Thompson, S., Pitts, K., Marusich, M.F., Tittl, J., et al. (2020) Disease Diagnostics and Potential Coinfections by <i>Vibrio coralliilyticus<i/> During an Ongoing Coral Disease Outbreak in Florida. *Front Microbiol* **11**: 569354.

Ushijima, B., Smith, A., Aeby, G.S., and Callahan, S.M. (2012) *vibrio owensii* induces the tissue loss disease *Montipora* white syndrome in the Hawaiian reef coral *Montipora capitata*. *PLoS ONE* **7**: e46717.

USVI Integrated Water Quality Monitoring & Assessment Report (2016) Department of Planning & Natural Resources Division of Environmental Protection.

Vanwonterghem, I. and Webster, N.S. (2020) Coral Reef Microorganisms in a Changing Climate. *iScience* **23**: 100972.

Vardi, T., Hoot, W.C., Levy, J., Shaver, E., Winters, R.S., Banaszak, A.T., et al. (2021) Six priorities to advance the science and practice of coral reef restoration worldwide. *Restor Ecol* **29**:.

Vaulot, D. and Marie, D. (1999) Diel variability of photosynthetic picoplankton in the equatorial Pacific. *J Geophys Res* **104**: 3297–3310.

Vega Thurber, R., Mydlarz, L.D., Brandt, M., Harvell, D., Weil, E., Raymundo, L., et al. (2020) Deciphering coral disease dynamics: Integrating host, microbiome, and the changing environment. *Front Ecol Evol* **8**: 575927.

Veglia, A.J., Beavers, K., Van Buren, E.W., Meiling, S.S., Muller, E.M., Smith, T.B., et al. (2022) Alphaflexivirus Genomes in Stony Coral Tissue Loss Disease-Affected, Disease-Exposed, and Disease-Unexposed Coral Colonies in the U.S. Virgin Islands. *Microbiol Resour Announc* **11**: e01199-21.

Vermeij, M.J.A., Smith, J.E., Smith, C.M., Vega Thurber, R., and Sandin, S.A. (2009) Survival and settlement success of coral planulae: independent and synergistic effects of macroalgae and microbes. *Oecologia* **159**: 325–336.

VI-CDAC (2021) Virgin Islands Coral Disease. *Stony Coral Tissue Loss Disease in the US Virgin Islands*.

Viehman, S., Mills, D., Meichel, G., and Richardson, L. (2006) Culture and identification of *Desulfovibrio* spp. from corals infected by black band disease on Dominican and Florida Keys reefs. *Dis Aquat Org* **69**: 119–127.

Wada, N., Hsu, M.-T., Tandon, K., Hsiao, S.S.-Y., Chen, H.-J., Chen, Y.-H., et al. (2022) High-resolution spatial and genomic characterization of coral-associated microbial aggregates in the coral *Stylophora pistillata*. *Sci Adv* **8**: eabo2431.

Walker, B.K., Turner, N.R., Noren, H.K.G., Buckley, S.F., and Pitts, K.A. (2021) Optimizing Stony Coral Tissue Loss Disease (SCTLD) Intervention Treatments on Montastraea cavernosa in an Endemic Zone. *Front Mar Sci* **8**: 666224.

Walsh, K., Haggerty, J.M., Doane, M.P., Hansen, J.J., Morris, M.M., Moreira, A.P.B., et al. (2017) Aura-biomes are present in the water layer above coral reef benthic macro-organisms. *PeerJ* **5**: e3666.

Walton, C.J., Hayes, N.K., and Gilliam, D.S. (2018) Impacts of a regional, multi-year, multi-species coral disease outbreak in southeast Florida. *Front Mar Sci* **5**: 323.

Wang, Q., Garrity, G.M., Tiedje, J.M., and Cole, J.R. (2007) Naïve Bayesian Classifier for Rapid Assignment of rRNA Sequences into the New Bacterial Taxonomy. *AEM* **73**: 5261–5267.

Wang, Y., Sheng, H.-F., He, Y., Wu, J.-Y., Jiang, Y.-X., Tam, N.F.-Y., and Zhou, H.-W. (2012) Comparison of the levels of bacterial diversity in freshwater, intertidal wetland, and marine sediments by using millions of illumina tags. *Appl Environ Microbiol* **78**: 8264–8271.

Water, J.A.J.M. van de, Coppari, M., Enrichetti, F., Ferrier-Pagès, C., and Bo, M. (2020) Local Conditions Influence the Prokaryotic Communities Associated With the Mesophotic Black Coral Antipathella subpinnata. *Frontiers in Microbiology* **11**: 20.

Weber, L. and Apprill, A. (2020) Diel, daily, and spatial variation of coral reef seawater microbial communities. *PLoS ONE* **15**: e0229442.

Weber, L. and Apprill, A. Diel, daily and spatial variation of coral reef seawater microbial communities. *PLoS One* **In press**:

Weber, L., Armenteros, M., Kido Soule, M., Longnecker, K., Kujawinski, E.B., and Apprill, A. (2020) Extracellular Reef Metabolites Across the Protected Jardines de la Reina, Cuba Reef System. *Front Mar Sci* **7**: 582161.

Weber, L., Gonzalez-Díaz, P., Armenteros, M., and Apprill, A. (2019) The coral ecosphere: A unique coral reef habitat that fosters coral-microbial interactions. *Limnol Oceanogr* **9999**: 1–16.

Weber, L., González-Díaz, P., Armenteros, M., Ferrer, V.M., Bretos, F., Bartels, E., et al. (2020) Microbial signatures of protected and impacted Northern Caribbean reefs: changes from Cuba to the Florida Keys. *Environ Microbiol* **22**: 499–519.

Weber, L., Soule, M.K., Longnecker, K., Becker, C.C., Huntley, N., Kujawinski, E.B., and Apprill, A. (2022) Benthic exometabolites and their ecological significance on threatened Caribbean coral reefs. *ISME COMMUN* **2**: 101.

Webster, N.S. and Taylor, M.W. (2012) Marine sponges and their microbial symbionts: love and other relationships: Marine sponge microbiology. *Environmental Microbiology* **14**: 335–346.

Wegley Kelly, L., Nelson, C.E., Aluwihare, L.I., Arts, M.G.I., Dorrestein, P.C., Koester, I., et al. (2021) Molecular Commerce on Coral Reefs: Using Metabolomics to Reveal Biochemical Exchanges Underlying Holobiont Biology and the Ecology of Coastal Ecosystems. *Front Mar Sci* **8**: 630799.

Wegley Kelly, L., Nelson, C.E., Petras, D., Koester, I., Quinlan, Z.A., Arts, M.G.I., et al. (2022a) Distinguishing the molecular diversity, nutrient content, and energetic potential of exometabolomes produced by macroalgae and reef-building corals. *Proc Natl Acad Sci USA* **119**: e2110283119.

Wegley Kelly, L., Nelson, C.E., Petras, D., Koester, I., Quinlan, Z.A., Arts, M.G.I., et al. (2022b) Distinguishing the molecular diversity, nutrient content, and energetic potential of exometabolomes produced by macroalgae and reef-building corals. *Proc Natl Acad Sci USA* **119**: e2110283119.

Weil, E. (2004) Coral Reef Diseases in the Wider Caribbean. In *Coral Health and Disease*. Rosenberg, E. and Loya, Y. (eds). Berlin, Heidelberg: Springer Berlin Heidelberg, pp. 35–68.

Weisse, T. (2016) Functional ecology of aquatic phagotrophic protists – Concepts, limitations, and perspectives. *European Journal of Protistology*.

Wickham, H. (2016a) ggplot2: elegant graphics for data analysis, Springer.

Wickham, H. (2016b) ggplot2: Elegant Graphics for Data Analysis, 2nd ed. 2016. Cham: Springer International Publishing : Imprint: Springer.

Widner, B., Kido Soule, M.C., Ferrer-González, F.X., Moran, M.A., and Kujawinski, E.B. (2021) Quantification of Amine- and Alcohol-Containing Metabolites in Saline Samples Using

Pre-extraction Benzoyl Chloride Derivatization and Ultrahigh Performance Liquid Chromatography Tandem Mass Spectrometry (UHPLC MS/MS). *Anal Chem* **93**: 4809–4817.

Williams, D.E. and Miller, M.W. (2012) Attributing mortality among drivers of population decline in Acropora palmata in the Florida Keys (USA). *Coral Reefs* **31**: 369–382.

Williams, S.D., Klinges, J.G., Zinman, S., Clark, A.S., Bartels, E., Villoch Diaz Maurino, M., and Muller, E.M. (2022) Geographically driven differences in microbiomes of *Acropora cervicornis* originating from different regions of Florida's Coral Reef. *PeerJ* **10**: e13574.

Willis, A. and Bunge, J. (2015) Estimating diversity via frequency ratios: Estimating Diversity via Ratios. *Biom* **71**: 1042–1049.

Willis, A., Bunge, J., and Whitman, T. (2017) Improved detection of changes in species richness in high diversity microbial communities. *J R Stat Soc C* **66**: 963–977.

van Woesik, R., Banister, R.B., Bartels, E., Gilliam, D.S., Goergen, E.A., Lustic, C., et al. (2021) Differential survival of nursery-reared *Acropora cervicornis* outplants along the Florida reef tract. *Restor Ecol* **29**:.

van Woesik, R., Roth, L.M., Brown, E.J., McCaffrey, K.R., and Roth, J.R. (2020) Niche space of corals along the Florida reef tract. *PLoS ONE* **15**: e0231104.

Work, T.M., Weatherby, T.M., Landsberg, J.H., Kiryu, Y., Cook, S.M., and Peters, E.C. (2021) Viral-Like Particles Are Associated With Endosymbiont Pathology in Florida Corals Affected by Stony Coral Tissue Loss Disease. *Front Mar Sci* **8**: 750658.

Yamashita, Y., Boyer, J.N., and Jaffé, R. (2013) Evaluating the distribution of terrestrial dissolved organic matter in a complex coastal ecosystem using fluorescence spectroscopy. *Continental Shelf Research* **66**: 136–144.

Yang, S.-H., Tseng, C.-H., Lo, H.-P., Chen, H.-J., Shiu, J.-H., Lai, H.-C., et al. (2020) Locality Effect of Coral-Associated Bacterial Community in the Kuroshio Current From Taiwan to Japan. *Frontiers in Ecology and Evolution* **8**: 11.

Yeo, S.K., Huggett, M.J., Eiler, A., and Rappé, M.S. (2013) Coastal Bacterioplankton Community Dynamics in Response to a Natural Disturbance. *PLoS ONE* **8**: e56207.

Yoon, J., Yasumoto-Hirose, M., Katsuta, A., Sekiguchi, H., Matsuda, S., Kasai, H., and Yokota, A. (2007) Coraliomargarita akajimensis gen. nov., sp. nov., a novel member of the phylum 'Verrucomicrobia' isolated from seawater in Japan. *International Journal of Systematic and Evolutionary Microbiology* **57**: 959–963.

Yu, Z., Cao, Y., Zhou, G., Yin, J., and Qiu, J. (2018) *Mangrovicoccus ximenensis* gen. nov., sp. nov., isolated from mangrove forest sediment. *International Journal of Systematic and Evolutionary Microbiology* **68**: 2172–2177.

Yun, J., Deng, Y., and Zhang, H. (2017) Anthropogenic protection alters the microbiome in intertidal mangrove wetlands in Hainan Island. *Appl Microbiol Biotechnol* **101**: 6241–6252.

Ziegler, M. (2016) Coral microbial community dynamics in response to anthropogenic impacts near a major city in the central Red Sea. *Marine Pollution Bulletin* 12.

ZoBell, C.E. (1946) Marine microbiology, a monograph on hydrobacteriology, Waltham, Mass.: Chronica botanica company.